FUNCTIONALIZED POLYTHIOPHENE-COATED MAGNETIC NANOPARTICLES FOR SOLID-PHASE EXTRACTION OF PHTHALATES

SITI NOR ATIKA BINTI BAHARIN

FACULTY OF SCIENCE
UNIVERSITY OF MALAYA
KUALA LUMPUR

2016

FUNCTIONALIZED POLYTHIOPHENE-COATED MAGNETIC NANOPARTICLES FOR SOLID-PHASE EXTRACTION OF PHTHALATES

SITI NOR ATIKA BINTI BAHARIN

THESIS SUBMITTED IN FULFILMENT OF THE REQUIREMENTS FOR THE DEGREE OF DOCTOR OF PHILOSOPHY

FACULTY OF SCIENCE
UNIVERSITY OF MALAYA
KUALA LUMPUR

2016

UNIVERSITY OF MALAYA

ORIGINAL LITERARY WORK DECLARATION

Name of Candidate: **Siti Nor Atika binti Baharin**

Registration/Matric No: **SHC 120020**

Name of Degree: **Doctor of Philosophy**

Functionalized Polythiophene-Coated Magnetic Nanoparticles for Solid-Phase Extraction of Phthalates

Field of Study: **Polymer Chemistry**

I do solemnly and sincerely declare that:

(1) I am the sole author/writer of this Work;
(2) This Work is original;
(3) Any use of any work in which copyright exists was done by way of fair dealing and for permitted purposes and any excerpt or extract from, or reference to or reproduction of any copyright work has been disclosed expressly and sufficiently and the title of the Work and its authorship have been acknowledged in this Work;
(4) I do not have any actual knowledge nor do I ought reasonably to know that the making of this work constitutes an infringement of any copyright work;
(5) I hereby assign all and every rights in the copyright to this Work to the University of Malaya ("UM"), who henceforth shall be owner of the copyright in this Work and that any reproduction or use in any form or by any means whatsoever is prohibited without the written consent of UM having been first had and obtained;
(6) I am fully aware that if in the course of making this Work I have infringed any copyright whether intentionally or otherwise, I may be subject to legal action or any other action as may be determined by UM.

Candidate's Signature Date:

Subscribed and solemnly declared before,

Witness's Signature Date:

Name:

Designation:

ABSTRACT

Polythiophene, poly(3-hexylthiophene), poly(N-phenyl-1-(2-thienyl)methanimine) and poly(phenyl-(4-(6-thiophen-3-yl-hexyloxy)-benzylidine)amine) were successfully coated on the surface of Fe_3O_4 magnetic nanoparticles (MNP). Two of the functionalized monomers, N-phenyl-1-(2-thienyl)methanimine and phenyl(4-(6-thiophen-3-yl-hexyloxy)-benzylidine)amine were successfully synthesized. Characterization by FT-IR, TGA, XRD, VSM and BET confirmed the coating has taken place. Further characterization of MNP coated poly(phenyl-(4-(6-thiophen-3-yl-hexyloxy)-benzylidine)amine) (P3TArH) was conducted using TEM and FESEM. Among those nanocomposites, MNP coated P3TArH has shown higher determination capabilities of phthalates. The adsorption behaviour of di(2-ethylhexyl) phthalate (DEHP) onto the MNP coated P3TArH showed fast kinetics, occurred heterogenously on the adsorption sites and exothermic. The activation energy determined found was -40.6 kJ mol^{-1} K^{-1}, indicated the process is physisorption. The successful synthesised magnetic nanoparticles were further optimized for magnetic solid-phase extraction (MSPE) of environmental samples. Separation and determination of the extracted phthalates namely dimethyl phthalate (DMP), diethyl phthalate (DEP), dipropyl phthalate (DPP), dibutyl phthalate (DBP), butyl benzyl phthalate (BBP), dicyclohexyl phthalate (DCP), di(2-ethylhexyl) phthalate (DEHP) and di-n-octyl phthalate (DNOP) were conducted by gas chromatography-flame ionization detector (GC-FID). The best working conditions were as follows; sample at pH 7, 30 min extraction time, ethyl acetate as elution solvent, 500 µL elution solvent volumes, 10 min desorption time, 10 mg adsorbent dosage, 20 mL sample loading volume and 15 g L^{-1} concentration of NaCl. Under the optimized conditions, the analytical performances were determined with linear range

of 0.1-50 µg L^{-1} and limit of detection at 0.054-0.468 µg L^{-1} for all the studied analytes. The intra-day (n=7) and inter-day (n=3) relative standard deviations, RSD (%) of three replicates each demonstrated in the range of 3.7-4.9 and 3.0-5.0 respectively. The steadiness and reusability studies suggested that the MNP@P3TArH could be used up to five cycles. The proposed method was executed to analysis of real water samples namely commercial bottled mineral waters and fresh milk and recoveries in the range of 68-101 % and relative standard deviation (RSD %) lower than 7.7 % were attained.

ABSTRAK

Politiofena, poli(3-hexiltiofena), poli(N-fenil-1-(2-tienil)metanimina) dan poli(fenil-[4-(6-tiofena-3-il-heksilloksi)-benzilidina]amina) telah berjaya disalut pada permukaan nanopartikel magnet Fe_3O_4 (MNP). Dua daripada pemfungsian monomer, N-fenil-1-(2-tienil)metanimina dan fenil-[4-(6-tiofena-3-il-heksilloksi)-benzilidina] amina telah berjaya disintesis. Analisis oleh FT-IR, TGA, XRD, VSM dan BET mengesahkan proses salutan telah berlaku. Analisis lanjut MNP bersalut poli(fenil-[4-(6-tiofena-3-il-heksilloksi)-benzilidina]-amina) (P3TArH) dilakukan menggunakan TEM dan FESEM. Antara semua nanokomposit, MNP bersalut P3TArH mempunyai keupayaan yang lebih tinggi dalam mengesahkan kehadiran ftalat. Kelakuan penjerapan di(2-etilhexil) ftalat (DEHP) ke MNP bersalut P3TArH menunjukkan kinetik yang cepat, berlaku secara heterogen pada tapak penjerapan dan eksotermik. Tenaga pengaktifan ditentukan adalah -40.6 kJ mol^{-1} K^{-1}, menunjukkan proses penjerapan ini adalah penjerapan fizikal. Nanokomposit yang berjaya disintesis juga telah dioptimumkan untuk magnet pengekstrakan fasa pepejal (MSPE) sampel alam sekitar. Pemisahan dan penentuan ftalat diekstrak iaitu dimetil ftalat (DMP), dietil ftalat (DEP), dipropil ftalat (DPP), dibutil ftalat (DBP), butil benzil ftalat (BBP), disiklohexil ftalat (DCP), di(2-etilhexil) ftalat (DEHP) dan di-n-oktil ftalat (DNOP) telah dijalankan oleh gas kromatografi pengesan api pengionan (GC-FID). Hasil yang yang terbaik adalah seperti berikut; sampel pada pH 7, 30 min masa pengekstrakan, etil asetat sebagai pelarut, 500 µl jumlah pelarut, 10 min masa nyahserap, 10 mg jisim penjerap, 20 mL isipadu sampel dan 15 g L^{-1} kepekatan natrium klorida (NaCl). Di bawah keadaan yang dioptimumkan, persembahan analisis telah ditentukan dengan linear 0.1-50 µg L^{-1} dan had pengesanan di 0.054-0.468 µg L^{-1} untuk semua analit dikaji. Analisis antara hari (n=7) dan hari yang sama

(n=3) sisihan piawai relative, RSD (%) daripada tiga replikasi setiap menunjukkan masing-masing dalam julat 3.7-4.9 dan 3.0-5.0. Kajian keunggulan dan boleh digunapakai mencadangkan bahawa MNP@P3TArH boleh digunakan sehingga lima kali. Kaedah yang dicadangkan dilaksanakan analisis sampel air sebenar iaitu komersial air mineral dan susu segar. Peratus pengambilan semula adalah dalam lingkungan 68-101 % dan sisihan piawai relatif yang lebih rendah daripada 7.7 % telah dicapai.

ACKNOWLEDGEMENTS

This thesis would not have been possible without the opportunity given to me by the University of Malaya and the inspiration and constant support bestowed to me by the following people: First of all, I would like to express my gratitude to my supervisor Dr. Norazilawati Muhamad Sarih and my co-supervisor Associate Prof. Dr. Sharifah Mohamad for their supervision, advice and guidance. I appreciate all their contributions of time, ideas, and support to make my Ph.D. program productive and exciting.

I would also like to thank Department of Chemistry for providing me conducive facilities, University of Malaya for PPP Grant (PG044-2012B), Ministry of Higher Education for High Impact Research Grant (HIR/MOHE/SC/F0031) and Foundation Research Grant Scheme (FRGS/MOHE/ FP031-2014B). I also acknowledge Ministry of Higher Education of Malaysia and Universiti Teknologi MARA Malaysia (UITM) for fellowship funding.

I would like to thank my lab members and staffs of Department of Chemistry for their kind supports. Words fail me to express my appreciation to my husband and children, whose love and encouragement allowed me to finish this journey. Finally, I would like to thank all of my family for their support, especially my parents and my parents-in-law.

TABLE OF CONTENTS

LIST OF FIGURES

LIST OF TABLES

LIST OF SYMBOLS AND ABBREVIATIONS

AOP	:	Advanced oxidation process
Al_2O_3	:	Alumiunium(III) oxide
APTEOS	:	3-aminopropyltriethoxysilane
APTS	:	p-aminophenyltrimethoxysilane
AsFs	:	Arsenenothious fluoride
ATSDR	:	US Agency for Toxic Substances and Disease Registry
BBP	:	Butyl benzyl phthalate
BET	:	Brunauer-Emmet-Teller
Br_2	:	Bromine
CEMNP	:	Carbon-encapsulated metal nanoparticle
CPC	:	Cetylpyridinium chloride
CTAB	:	Cetyltrimethylammonium bromide
CVD	:	Chemical vapour deposition
DBP	:	Dibutyl phthalate
DCP	:	Dicyclohexyl phthalate
DEHA	:	Di-2-ethyl hexyl adipate
DEHP	:	Di(2-ethylhexyl) phthalate
DEP	:	Diethyl phthalate
DES	:	Diethyl sulfosuccinate
DIBP	:	Di-iso-butyl-phthalate
DIDP	:	Di-isodecyl phthalate
DINP	:	Di-isononyl phthalate
DMP	:	Dimethyl phthalate
DNHP	:	Di-*n*-hexyl-phthalate

DNOP	:	Di-*n*-octyl Phthalate
DODMAC	:	Dioctadecyldimethylammonium chloride
DPP	:	Dipropyl phthalate
ECMO	:	Extracorporal membrane oxygenation
EDTA	:	Ethylene diamine tetraacetic acid
EFSA	:	European Food Safety Authority
Fe_3O_4	:	Iron(III) oxide
FESEM	:	Field emission scanning electron micrsocope
FT-IR	:	Fourier transform infra-red
GC-FID	:	Gas chromatography flame ionizer detection
HPLC	:	High performance liquid chromatography
I_2	:	Iodine
LDR	:	Linear dynamic range
LLE	:	Liquid-liquid extraction
LOD	:	Limit of detection
LOQ	:	Limit of quantitation
MIP	:	Molecular imprinting polymer
MNP	:	Magnetic nanoparticles
MOF	:	Metal organic frame work
MPTES	:	Mercaptopropyltrimethoxysilane
MSPE	:	Magnetic solid-phase extraction
MWCNT	:	Multi-walled carbon nanotube
NLO	:	Nonlinear optical devices
OFET	:	Field effect transducer
OLED	:	Organic light emitting diodes
PAH	:	Polyaromatic hydrocarbon

PCMS	:	Polychloromethylstyrene
PET	:	Polyethylene terephthalate
PVC	:	Polyvinyl chloride
PVP	:	Polyvinylpyrrolid
SDS	:	Sodium dodecyl sulphate
SIO_2	:	Silica
SPE	:	Solid-phase extraction
TEM	:	Transmission electron microscope
USEPA	:	United State Environmental Protection Agency
UV	:	Ultra-violet
VSM	:	Vibrating solid sample

LIST OF APPENDICES

CHAPTER 1: INTRODUCTION

1.1 Background of Study

Phthalates or phthalate esters which belong to non-halogenated esters of phthalic acid are used as plasticizers for nitrocellulose since it was first recognized in 1880, replacing camphor (Franck & Stadelhofer, 1988). Nowadays, phthalates can be found in many different matrices in our environment and are widely utilized in the PVC industries as a plasticizer for floors, hoses, cables (building materials), toys and medical appliances (Jones-Lepp *et al*., 2000). Other consumer-based products utilizing phthalates are as a component in inks, adhesive materials, lacquers, sealing and packing materials, materials for treating surfaces, solvents and fixing agents in fragrances, as well as additives in cosmetics (Serôdio & Nogueira, 2006; Wypych, 2004; Yuan *et al*., 2008).

Phthalates become emerging pollutants and harmful to humans, especially children, since they are not chemically bound in plastics and could be leached out into the environment (Serodio & Nogueira, 2006). Thus, the usage of phthalates in the production of toys, baby bottles and pacifiers is banned in many countries (Sathyanarayana *et al.*, 2008). Exposure to phthalates over long-term periods could result in health issues, for example potential carcinogenic effects or critical impact on the hormonal systems, since they own lipophilic properties, which make them easily stored in fatty tissues (Foster, 2006; Latini *et al*., 2004; Ohtani *et al*., 2000; Pitter, 2009). The higher molecular weight of phthalates, such as DEHP, DBP and DNOP often leads to serious health illnesses and is alleged to be carcinogenic and lethal to liver and kidneys, as well as reproductive organs (Gomez-Hens & Aguilar-Caballos, 2003; Swan *et al.*, 2005). In Malaysia, due to the awareness of the migration of phthalates from food packaging, baby bottles and pacifiers, a regulation has been proposed, which

in stated in Law of Malaysia (1985) under Food Regulation, which regulated plastic materials, and articles shall be examined in agreement with Standard Malaysia (2014) in MS 2234: "Plastic Materials and Articles Intended to Come into Contact with Food", which clarified the specific migration limits as follows; 1.5 mg kg^{-1} for DEHP, 0.3 mg kg^{-1} for DBP, 30 mg kg^{-1} for BBP and 9.0 mg kg^{-1} for DIDP.

Recently, phthalates have been found in polyethylene terephthalate (PET) bottles which may lead to many serious consequences, since the PET bottles are widely used as containers for mineral water, milk and soft drinks. The existence of phthalates in PET bottles may be explained through several possibilities: the type of raw materials, the chemicals or processes involved in bottle manufacturing, the practice of the use of PET bottles, as well as cross contamination in the bottling plant and cap resins (Amiridou & Voutsa, 2011; Bach *et al.*, 2012; Leivadara *et al.*, 2008; Liu *et al.*, 2008; Schmid *et al.*, 2008; Wu *et al.*, 2012). Studies conducted by Plotan *et al.* and Wagner *et al.* reported that in most of the inspected PET-bottled water samples, endocrine disruptor activity was found (Plotan *et al.*, 2013; Wagner & Oehlmann, 2009).

Given the unlimited toxic effects arising from these materials, much research have been conducted to find a solution to eliminate its contamination of the environment (Chen & Chung, 2006; Julinová & Slavík, 2012). However, the determination of phthalates in environmental samples is challenging due to their trace amounts and the intervention of an intricate matrix (Yuan *et al.*, 2002). Therefore, a sample preparation step for the extraction and preconcentration of the analytes is required (Lopez-Jimenez *et al.*, 2005). Solid phase extraction (SPE) is one of the established and popular methods for sample enrichment prior to analysis using high performance liquid chromatography (HPLC) and gas chromatography (GC) (Farahani *et*

al., 2008; Kerienė *et al.*, 2011; Ling *et al.*, 2007). The advantages of SPE over liquid-liquid extraction (LLE) are its simplicity, rapidness, that the adsorbent is recyclable, the steadiness, low cost, high enrichment factors and low usage of organic solvents (Tahmasebi & Yamini, 2014). Numerous types of sorbents were synthesized and used for the determination of plasticizers, for example an octadecyl packed column (C18), α-cyclodextrin functionalized chitosan, poly(styrene–divinylbenzene) polymers and zeolitic imidazolate (Holadova & Hajslova, 1995; Khan *et al.*, 2015; Kvistad *et al.*, 1998). The selection of adsorbent plays an important role in SPE, since it can determine the efficiency, anti-interference ability and selectivity of the method for the targeted analytes (Raoov *et al.*, 2014).

Magnetic nanoparticles (MNPs), especially iron oxides, have become one of the most useful materials in numerous applications since their discovery, for example magnetic fluids, catalysis, magnetic resonance imaging and environmental disciplines (Farrukh *et al.*, 2013; Li *et al.*, 2005; Lin *et al.*, 2012). In the application for the removal of pollutants from the environment, the nano-sized particles provide a high surface area to volume ratio, which enhances adsorption capacity and efficiency (Shahabuddin *et al.*, 2016). Moreover, the distinct feature of MNPs is their rapid response to an external magnetic field. This special property, called superparamagnetism, does not preserve magnetism after the elimination of an external field. Thus, it helps to isolate the adsorbents from an aqueous solution in a complex matrix without the need for centrifugation or filtration and can be referred to as magnetic solid-phase extraction (MSPE) (Li *et al.*, 2010; Xie *et al.*, 2014). Due to the simplicity of the technique, much research has been published on utilizing Fe_3O_4 as the adsorbent for MSPE in water samples, for example determining antimicrobial residue, heavy metals, non-steroidal anti-inflammatory drugs and pesticides (Aguilar-Arteaga *et al.*, 2010; Fayazi *et al.*, 2016; Ibarra *et al.*, 2014; Mehdinia *et al.*, 2016).

However, the smaller the particle size, the more it becomes unstable, which initiates particle accumulation. Moreover, metal oxide may be oxidize easily and reduce its magnetism properties. Therefore, an appropriate surface functionalization can be done, which can be tailored to the specific targeted analyte. The strategy to protect the magnetic core can be either by organic or inorganic compounds, for example Al_2O_3, SiO_2, surfactants, alkyl carboxylates and polymeric coatings (Ballesteros-Gomez & Rubio, 2009; Faraji *et al.*, 2010; Sun *et al.*, 2010; Zhai *et al.*, 2010). Recently, research articles reported on the utilization of conducting polymers as a coating agent of the MNPs (Gao *et al.*, 2011; Tahmasebi *et al.*, 2012; Zhao *et al.*, 2013). These nanocomposites have multifunctional and diverse properties, which may enhance the surface functionalization and protect the magnetic core from environmental agitation. Moreover, it may reduce aggregation and disperse the nanoparticles' core shell distribution within the suspension media (Shin & Jang, 2007). Herein, we prepared a modified polythiophene containing an additional aromatic ring and aliphatic sides on the surface of Fe_3O_4 magnetic nanoparticles (MNPs) to investigate its performance as a magnetic solid phase extraction of phthalates, as shown in Figure 1.1. Thus, in this work, the sorbent was further tested for real aqueous samples, including commercial mineral water and commercial fresh milk which were kept in a PET bottle.

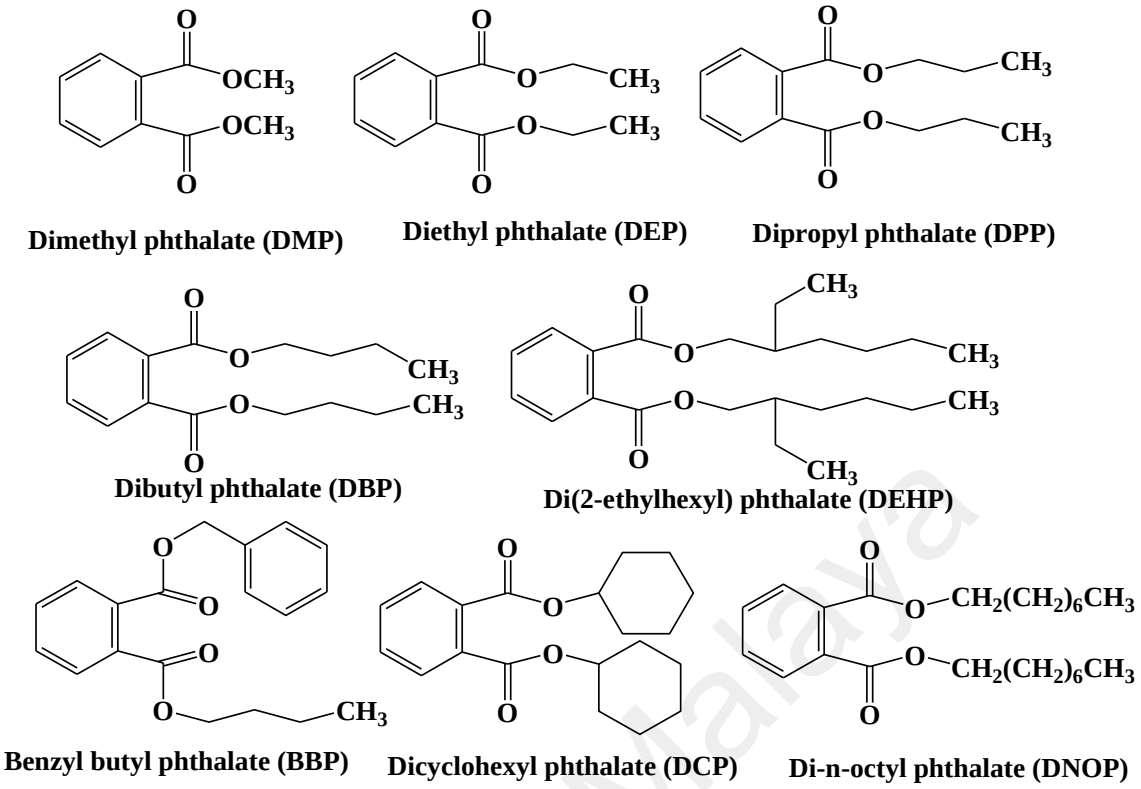

Figure 1.1: Phthalates used in this study

1.2 Objectives of Study

In this study, four objectives were achieved as follows:

a) Synthesis and characterization of magnetic nanoparticles (MNP) coated functionalized polythiophene nanocomposites,

b) Adsorption studies of di(2-ethylhexyl) phthalates (DEHP) using MNP coated poly(phenyl-(4-(6-thiophen-3-yl-hexyloxy)-benzylidine)amine) (P3TArH),

c) The application of MNP coated P3TArH as a new sorbent for magnetic solid-phase extraction (MSPE) of phthalates in real sample analyses.

1.3 Scope of Study

In this study we utilized four different thiophene monomers functionalities as coating materials on the surface of magnetic nanoparticles (MNP). Figure 1.2 shows two commercially available monomers thiophene (Th) and 3-hexylthiophene (3Th), meanwhile N-phenyl-1-(2-thienyl)methanimine) (TCN) and phenyl(4-(6-thiophen-3-yl-hexyloxy)-benzylidine)amine (3TArH) were two successfully synthesized monomers. These functionalized materials had a potential within the molecular architecture that can extracts phthalates from aqueous solution. Among those nanocomposites, MNP coated P3TArH revealed superior determination capability of phthalates. Kinetic, isotherms and thermodynamic studies for adsorption of DEHP with MNP coated P3TArH was determined. Optimization parameters for magnetic solid-phase extraction (MSPE) were pH, extraction time, sample volume, elution solvent, elution solvent volume, desorption time, adsorbent dosage and effect of NaCl. Reusability studies were conducted for five cycles to determine the possibilities for reutilizing and regeneration.

Under the optimized conditions, analytical performance were carried out to determine linear dynamic range (LDR), limit of detection (LOD), limit of quantitation (LOQ), and repeatability. To evaluate reliability of proposed method for extraction and preconcentration of phthalates from real samples, two real water samples were tested. The real samples were water from commercial mineral water bottle and milk samples stored in PET bottle.

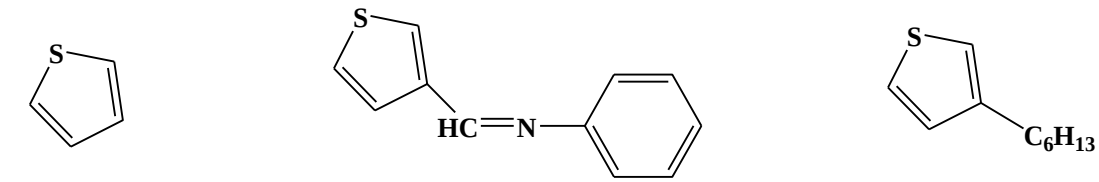

Thiophene (Th) **N-phenyl-1-(2-thienyl)methanimine) (TCN)** **3-hexylthiophene (3Th)**

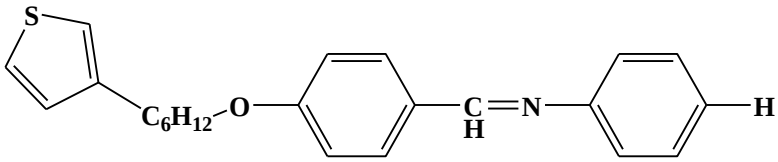

Phenyl(4-(6-thiophen-3-yl-hexyloxy)-benzylidine)amine (3TArH)

Figure 1.2: Functionalized thiophene monomers

1.4 Significance of Study

Functionalized thiophene monomers were polymerized on the surface of magnetic nanoparticles. The study of the molecular architecture of the functionalized thiophene monomers gave information on their capability for selectively extraction of phthalates from aqueous solution. This information is crucial in terms of developing a new, advanced and reusable material to extract contaminants from the environments.

1.5 Thesis Outline

The present thesis is organized into five chapters. Chapter 1 gives a brief introduction on background, research objectives of study, scope of study and significance of study. A review of related literature is presented in Chapter 2. Chapter 3 covered experimental methodologies on the preparation of functionalized polythiophene coated magnetic nanoparticle, screening studies, adsorption studies of DEHP with MNP coated P3TArH and application of MNP coated P3TArH as a sorbent for MSPE of phthalates. Chapter 4 presented the results and discussion which divided into three

parts. First part is the characterization of synthesized materials. Meanwhile, in second part, the results of adsorption studies of DEHP with MNP coated P3TArH were elaborated, whereas last part discussed on the application of MNP coated P3TArH as a sorbent for magnetic solid-phase extraction (MSPE) of phthalates and real sample analyses. Lastly, in Chapter 5, conclusions and recommendations were elaborated.

CHAPTER 2: LITERATURE REVIEW

2.1 Polymers

The term "polymer" originates from the ancient Greek word *polus*, meaning "many, much" and *meros*, "parts", and denotes to a molecule whose structure is composed of multiple repeating units, from which originates a characteristic of high relative molecular mass and attendant properties (Skotheim, 1997). The units composing polymers derive, actually or conceptually, from molecules of low relative molecular mass (Chen *et al.*, 2012).

Polymers are high molecular mass compounds formed by polymerization of monomers. The simple repeating structural units of a polymer are known as monomer. A polymer is chemically defined by its degree of polymerization, molecular weight distribution, tacticity, copolymer distribution, the degree of branching, end-groups, crosslinks, crystallinity and thermal properties such as its glass transition temperature and melting temperature. Polymers in solution have distinct characteristics with regard to solubility, viscosity and gelation. Many polymers are prepared by the mutual reaction of complementary monomers (Cornil *et al.*, 1998).

2.1.1 Conducting Polymers

Conducting polymers is a polymer having an extended n conjugated system, for example double and single bonds alternate along the polymer backbone known. Conjugated polymers have an ability to conduct electricity when partially oxidized and reduced. The development in the comprehensive study of greatly conducting polymers initiated in 1977 with the finding of the variation in the electrical conductivity of polyacetylene on doping with Br_2, I_2 and AsFs (Chiang *et al.*, 1978). Further conjugated

polymers which display fascinating electrical and electrochemical assets related with their extended n-bonding system are polyphenylene, polyaniline, polythiophene, polypyrrole and polyphenylene vinylene. The electrical conductivity of all these polymers can be augmented over suitable chemical or electrochemical oxidation (*p*-type doping) and reduction (*n*-type doping). Although, poly(acetylene) exhibits highly conducting on doping compares to other conjugated polymers, yet it is may susceptible to thermal and environmental perturbation, has insolubility issue and difficult to process (Schopf & Kossmehl, 1997).

Polymers containing conjugated heterocyclic units in the backbone such as polythiophene, has outstanding electrical conductivities and high stability in air/humid, thermal steadiness and mechanical robustness in doped and undoped states. The conjugated structure with alternating single and double bonds or conjugated segments coupled with atoms providing p-orbitals for a continuous orbital overlap (e.g. nitrogen, sulfur) seems to be necessary for polymers to become intrinsically conducting. This is because just as metals have high conductivity due to be free movement of electrons through their structure, in order for polymers to be electronically conductive they must possess not only charge carriers but also an orbital system that allows the charge carriers to move (Fichou, 2008).

2.1.2 Polythiophene

Polythiophene belongs to a class of heterocyclic compounds containing a five membered ring made up of one sulphur as heteroatom with the formula C_4H_4S. Thiophene and its derivatives isolated from petroleum or coal. Thiophene is taken from the word *theion*, the Greek word for sulfur, and another Greek word *phaino* which means shinning (Tourillon & Skotheim, 1986). Owing to their efficient light harvesting,

structural versatility and intrinsic charge transport behavior, thiophene-based π-conjugated systems have attracted much attention in developing high performance conducting cells. Figure 2.1 demonstrates structure of thiophene repeating units.

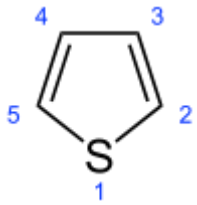

Figure 2.1: Repeating unit of polythiophene

Conjugated thiophene has been the focus of much research owing to its interesting properties that are well suited for organic electronic applications including field effect transducers (OFET), light emitting diodes (OLED), photovoltaics (OPD), and nonlinear optical devices (NLO) (Huo *et al.*, 2011; Mannerbro *et al.*, 2008; Yang & Jenekhe, 1991). This is in part due to its low oxidation potential relative to its homoaryl analogues. Subsequently, it can be chemically doped resulting in stable p-type materials with high conductivities and charge mobilities (Sinha *et al.*, 2009). Furthermore, property tuning to match a specific electronic application is possible by incorporating electronic groups along the conjugated framework in addition to copolymerizing with other heterocyclic monomers. Copolymerization and homopolymerization are typically done electrochemically. Alternatively, chemical polymerization is possible via oxidation using $FeCl_3$ Suzuki, Negishi, and Kumada coupling protocols (Xu *et al.*, 2008; Yokozawa *et al.*, 2008). It has been found that polythiophene exhibits inimitable properties and efficiency in terms of chemical stability, conjugation and flexibility to be functionalized (McCullough & Williams, 1993).

2.1.3 Functionalized Polythiophene

Poly(3-substituted thiophenes) with a diversity of substituents such as alkyl, alkoxy, alkyl heteroatom-functionalized side chains have been studied extensively. Overcoming insolubility problems by introducing alkylic chains in the 3-position of the thiophenic ring, thus providing soluble and processable materials. β-functionalized thiophene monomer is a thiophene monomer that has functional group in the β position of the carbon. Interestingly it exhibits advantages such as enhance more regioselective thiophene by electro polymerization, reduce the oxidation potential with electron-rich substituents and improving the mechanical property with introduction of alkyl chain functionalities.

Electron-releasing and electron-withdrawing group in β position of thiophene show different property. Electron-donor group reduces the oxidation potential of the thiophene monomer whereas electron-acceptor increases the oxidation potential (Waltman *et al.*, 1983). Physical property of the subjected polythiophene will enhance by introducing functionalized material as a dopant (McQuade *et al.*, 2000). Many approaches for functionalizing thiophene have been developed for examples the thiophene structure with addition of organic active species and introduction of inorganic metals to polythiophene compounds (inorganic-organic hybrid materials) (Aradilla *et al.*, 2012). Figure 2.2 exhibits examples of functionalized polythiophenes.

Recently, thiophene functionalized Schiff base has been extensively studied in the photovoltaic and environmental sensor application (Pedras *et al.*, 2007). Apart being a sensor, Issaadi et al. claimed that thiophene containing Schiff base is one of the best inhibitor that protects surface of a metal from corrosion in acidic media (Issaadi *et al.*,

2011). The functionalized Schiff base can enhance the stability of hybrid inorganic-organic polythiophene compounds from environmental perturbation (Ismail, 2007).

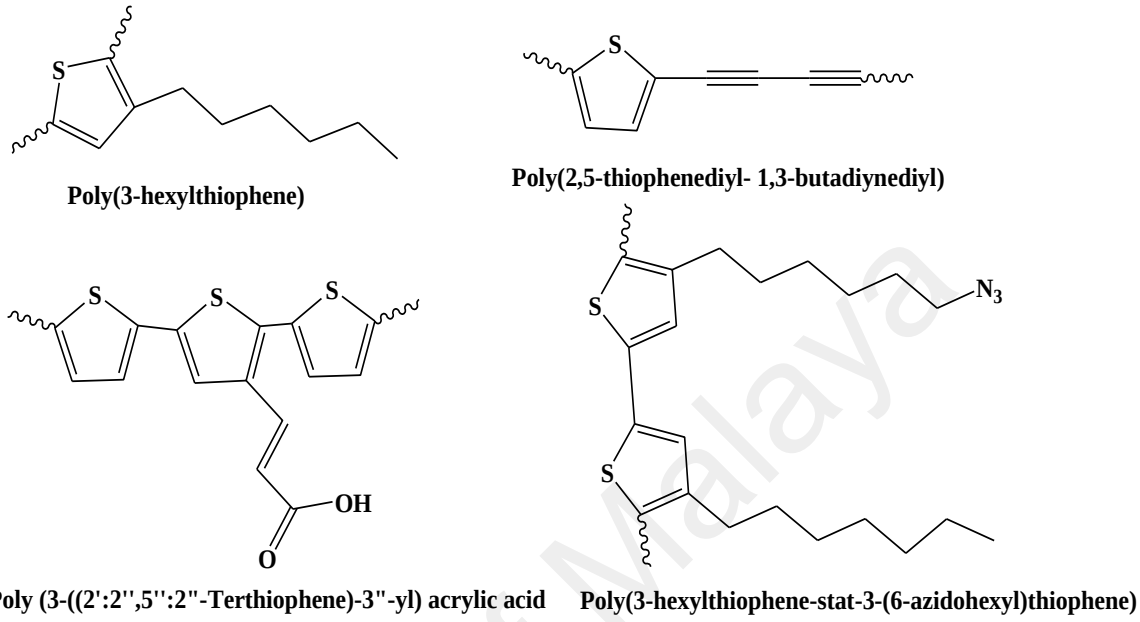

Figure 2.2: Functionalized polythiophenes (Cornil *et al.,* 1998)

Intensive studies of the development of organic-inorganic hybrid of polythiophene based materials have become one of the main focuses by many researchers. Owing to enhancement properties, these hybrid materials are being applied in various fields. Example of hybrid polythiophene based materials are magnetic nanoparticles coated polythiophene, titanium-dioxide functionalized polythiophene and polythiophene doped zinc chloride (Mrowetz *et al.*, 2003; Tahmasebi & Yamini, 2014).

2.1.4 Application of Polythiophene in Environmental Application

Due to its good environmental stability, ease of synthesis and good conducting properties, polythiophene, functionalized polythiophene and polythiophene metal composite have been widely applied in environmental fields, for examples, heavy metal

sensor, photocatalytic degradation and adsorption (Ansari *et al.*, 2015; Din *et al.*, 2014; Udhayakumari *et al.*, 2014).

Rapid environmental monitoring and management assisted in on-site and real time measurements of many different heavy metals. An approach to identify these heavy metals is based on deviation of electrical/fluorescence responses of the active species. Due to the high conductivity and stability many heavy metal sensors have been developed by polythiophene based compounds (Ng *et al.*, 1998). For instance, nanocomposite of regioregular poly(3-hexylthiophene) (P3HT) with metal oxide ZnO has been designed and applied as a sensor to detect zinc and lead (Saeteaw *et al.*, 2011). Moreover, rhodamine-thiophene conjugate has been proposed by Mandal *et al*. (2013) to sense mercury ion (Hg^{+}).

Band gap of polythiophene is in the range of 2.0 eV and may change rendering to the nature of doping. This band gap is adequately small compared to metal oxides, such as TiO_2, ZnO etc. Due to this sufficiently small band gap, it is possible to excite an electron from the valence band to the conduction band with UV and visible light, which is suited for photocatalysis application (Krüger *et al.*, 2011). High degradation of methyl orange was successfully obtained with poly hexylthiophene-titanium dioxide nanocomposite (P3Th/TiO_2). In addition, Chandra *et al.* (2015) described that a polythiophene-titanium dioxide-functionalized-copper composite (PTh/TiO_2–Cu) prepared by a sol–gel process has been photocatalytically degraded rhodamine-B dye.

Adsorption seems to be a competent tool for processing greater quantities of wastewater containing pollutant. Whole ranges of adsorbent from polythiophene based were developed. In the heavy metals removal, utilization of polythiophene based materials are due to the sulphur atom that can easily conjugate with heavy metals ion whereas, in removal of organic pollutants, interactions are mainly based on π-π

conjugation and hydrophobicity in the polythiophene (Julinová & Slavík, 2012; Shin & Jang, 2007). Recently, functionalization of polythiophene in the surface of nanoparticles has become research interest in environmental treatment management. These combinations of high surface area and great surface chemistry have enhanced the progress of water remediation for a wide range of pollutants (Khalili *et al.*, 2014).

2.2 Nanoparticles

2.2.1 Overview

Nanoparticles have been extensively used worldwide in many fields such as material sciences, physics, medicine, electronic and chemistry. Different kind of shapes and types of nanomaterials were prepared from organics and inorganics based including nanotubes, nanohorns and nanocages (de Dios & Díaz-García, 2010; Ozin *et al.,* 2009; Boal, 2004). Nanoscale often have different physical, chemical, and biological properties compares to macro, micro scale, due to the quantum size influence (Alivisatos, 2000). Nanoparticles considered exquisite materials since they have a high surface area-to-volume ratio and provides a surface functionalization which can be tailored according to applications.

2.2.2 Magnetic Nanoparticles

They are different kinds of magnetic nanoparticles, for examples iron oxides, ferrites of cobalt, manganese, nickel, magnesium and platinum. However, only iron oxides considered biological safe and, therefore, is the only nanoparticle material that have been permitted by the U.S. Food and Drug Administration. Besides, iron oxides is easy to synthesis and give high magnetic moment (Teja & Koh, 2009). Moreover, iron oxide nanoparticle showed an advanced property and widely used in many area such as

magnetic fluids, catalysis, magnetic resonance imaging, and environmental remediation (Chikazumi *et al.*, 1987; Farrukh *et al.*, 2013; Lin *et al.*, 2012). Due to increase in research interest for the iron oxide nanoparticles, intensive studies on nanoparticle structure, physical and chemical properties as well as toxicity has force to the evolution of magnetic nanoparticles for industrial and biomedical applications.

2.2.3 Properties of Iron Oxide Nanoparticles

Magnetite (Fe_3O_4), maghemite (γ-Fe_2O_3), and hematite (α-Fe_2O_3) is the most common of iron oxides present in nature (Cornell & Schwertmann, 2003). These types of iron oxides are widely used in the various applications. Table 2.1 summarized some of their physical properties. Recognized as black iron oxide, magnetite displays the sturdiest magnetism among transition metal oxide. Whereas, hematite typically known as ferric oxide or martite is the first iron oxide ever found and abundantly exists in rocks and soils. They are having blood-red color in bulk and grey in coarse crystal. Meanwhile, heating of iron oxides or effect of weathering could lead to formation of maghemite (Majewski & Thierry, 2007).

A reason for high magnetic moment in the iron atom is due to its four unpaired electrons in 3d orbitals. As demonstrates in Figure 2.3, different magnetic behaviours can occur upon crystallization for example paramagnetic, ferromagnetic, antiferromagnetic and ferrimagnetic. Zero magnetic moment was observed in paramagnetic state which each atomic magnetic moment are arbitrarily arranged. Meanwhile, ferromagnetism behaviour demonstrated the property when all the moments are aligned in the absence of external field. Whereas, ferrimagnetic crystals often have two diverse moments of strength and are organized in inverse orde

Table 2.1: Properties of iron oxides

Property	**Oxide**		
	Hematite	**Magnetite**	**Maghemite**
Molecular formula	α-Fe_2O_3	Fe_3O_4	γ-Fe_2O_3
Density (g cm^{-3})	5.26	5.18	4.87
Melting point (°C)	1350	1583-1597	-
Hardness	6.5	5.5	5
Type of magnetism	Weakly ferromagnetic or antiferromagnetic	Ferromagnetic	Ferrimagnetic
Curie temperature (K)	956	850	820-986
Magnetization saturation at 300 K (A-m^2 kg^{-1})	0.3	92-100	60-80
Standard free energy of formation $\Delta G_f°$ (kJ mol^{-1})	-742.7	-1012.6	-711.1
Crystallographic system	Rhombohedral, hexagonal	Cubic	Cubic or tetrahedral
Structural type	Corundum	Inverse spinel	Defect spinel
Space group	R3c (hexagonal)	Fd3m	$P4_332$ (cubic); $P4_12_12$ (tetragonal)
Lattice parameter (nm)	a = 0.5034, c = 1.375 (hexagonal) aRh = 0.5427, α = 55.3° (rhombohedral)	a = 0.8396	a = 0.83474 (cubic); a = 0.8347, c = 2.501 (tetragonal)

Source: (Cornell & Schwertmann, 2003)

The magnetic manners of hematite subject to its crystallinity, particle size and on the degree of cation substitution (Bodker & Morup, 2000; Raming *et al.*, 2002). Hematite displays paramagnetic at more than 956 K, but at 260 K, it demonstrates weakly ferromagnetic and go through a phase evolution to antiferromagnetic behaviour (Besser *et al.*, 1967; Morin, 1950; Zysler *et al.*, 2001). Superparamagnetic property which is a property when the material does not preserve magnetism after the elimination of an external field often observed in the iron oxide nanoparticles especially magnetite with size smaller than 20 nm, but, it is also depends on the approaches used in the preparation (Aydın *et al.*, 2011; Kado, 2008; Margulies *et al.*, 1996; Sena *et al.*, 1997; Xu *et al.*, 2012).

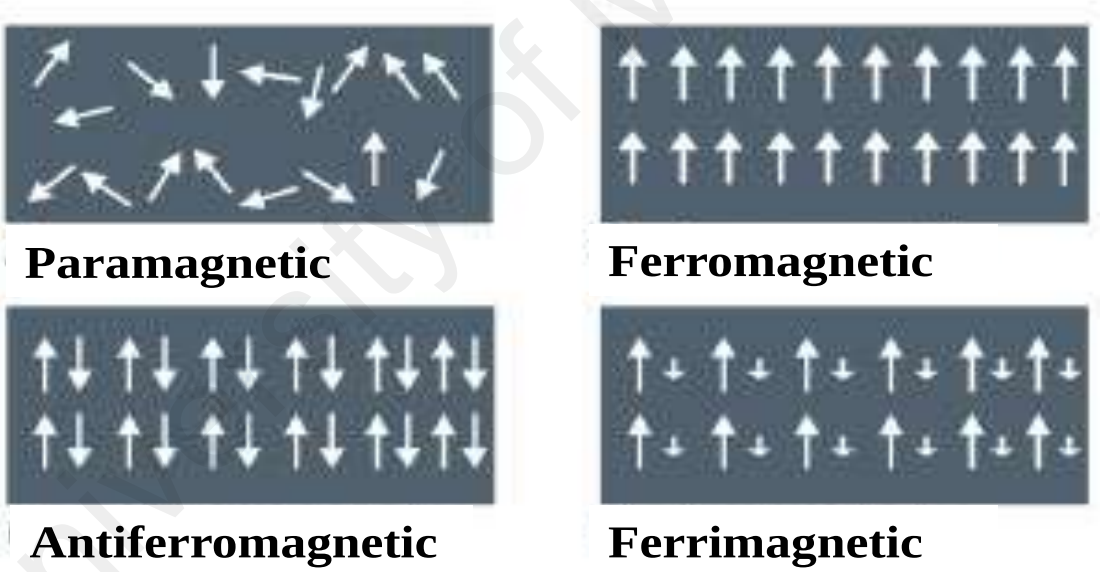

Figure 2.3: Alignment of atomic magnetic moments (Devine, 2013)

2.2.4 Method for Preparation of Magnetic Nanoparticles

Preparation method is important since it determines particle size distribution, shape and surface chemistry of the material. Recently, many synthesis pathways have

been established to manipulate particle size, polydispersity, shape, crystallinity and magnetic behaviours (Lian *et al.*, 2004; Takami *et al.*, 2007; Tartaj *et al.*, 2003). There several methods for the preparation of magnetite for example chemical vapour deposition, co-precipitation, two phase, sol-gel method and hydrothermal.

2.2.4.1 Chemical Vapour Deposition

Gas phase includes thermal decomposition, hydrolysis, and oxidation process to produce solid products via gas phase (Pierson, 1999). Example of gas phase method is chemical vapour deposition (CVD). In this process, a gas carrier delivers a precursor to a reaction compartment which is controlled at ~900 °C (Chang *et al.*, 1994; Tavakoli *et al.*, 2007). Figure 2.4 presents a schematic diagram of chemical vapour deposition reactor. Under extreme temperature condition, the products are joined to form nano powders. Particles growth and accumulation are alleviated by hasty extension of double phase gas stream in the reaction compartment. Compositional and structural alteration are made by continual heat treatment which include crystallization, purification as well as conversion to a anticipated size, arrangement and morphology (Tavakoli *et al.*, 2007).

In the preparation of iron oxide via chemical vapour deposition method, probability of accomplishment is highly influences by a low concentration of precursors and express enlargement and extinguishing of nanoparticles once they reached end of the process (Chang *et al.*, 1994). Park *et al.* (2006) synthesized magnetite thin films at 300 °C in oxygen using iron(II) dihydride complexes ($H_2Fe[P(CH_3)_3]_4$) as precursor. Another, magnetite successfully prepared via low pressure chemical vapour deposition by Dhara *et al*. (1994) utilizing metal-organic ferric dipivaloyl methanate. Chemical vapor deposition is capable to produce high purity products, but the yield is often low.

Besides, set up of the equipment is extremely expensive and tedious as it must be properly and precisely controlled (Casas *et al.*, 2001).

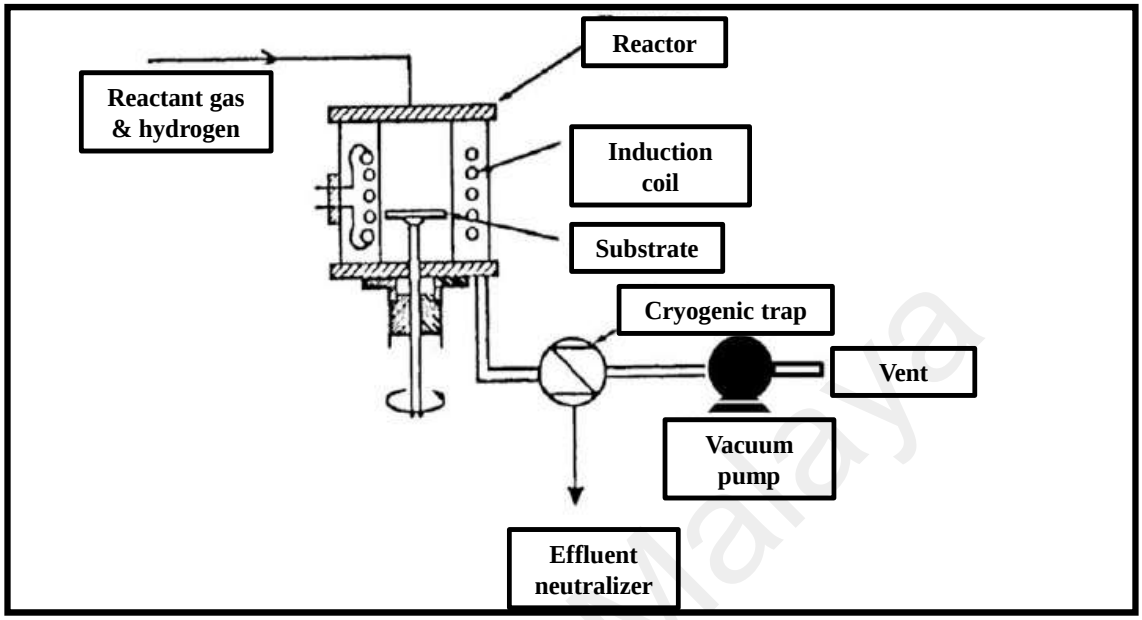

Figure 2.4: Schematic diagram of a CVD setup (Tavakoli *et al.*, 2007)

2.2.4.2 Two Phases Method

Magnetic nanoparticles can be prepared using water in oil micro emulsion. In this technique, a wetting agent (surfactant) is required to reduce the surface tension between oil and water. Various type of surfactant have been utilized in the preparation of magnetite nanoparticles for examples sodium dodecyl sulfate (SDS), cetyltrimethylammonium bromide (CTAB), polyvinylpyrrolid (PVP) and diethyl sulfosuccinate (DES) (Esquivel *et al.*, 2007; Hasany *et al.*, 2012; Nassar & Husein, 2006; Zhang *et al.*, 2008).

As demonstrates in Figure 2.5, there are three alternatives in micro emulsion techniques, these approaches are applicable according to application acquired. In the first approach, reactants A and B are liquefied in the solution, upon mixing, collision

and coalescence of between reactants molecules forming a precipitate AB. Meanwhile, in the second approach, nanoparticles are formed by reduction reaction of metal salts in the presence of reducing agent such as hydrazine or hydrogen. For the third approach, micro emulsion of soluble salts cations are bubbled with gas (O_2, NH_3, or CO_2) forming either oxide, hydroxide or carbonate precipitates (Pillai *et al.*, 1995). Limitations of micro emulsion technique are the challenging in producing high scale products and toxicity of remaining surfactants in the surface of particles (Teja & Koh, 2009).

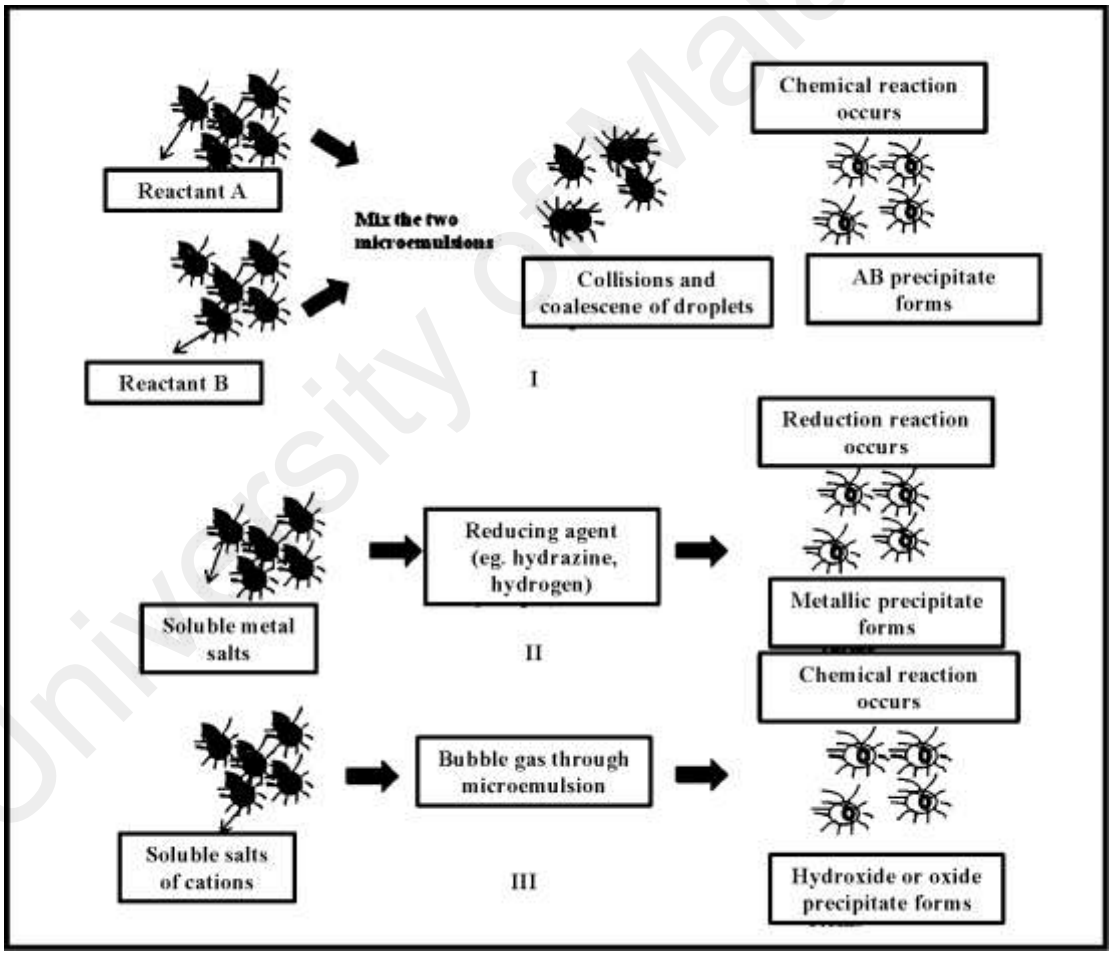

Figure 2.5: Diagram of nanoparticle synthesis in microemulsions (I) by mixing two microemulsions, (II) by adding a reducing agent and (III) by bubbling gas through the microemulsion (Teja & Koh, 2009)

2.2.4.3 Sol-gel Method

Sol-gel method involves in, hydrolysis and condensation of alkoxide precursors to form a solution of oxide particles, the solution ('sol') is removed ('gel') by solvent removal or chemical reaction. As describes in Figure 2.6, the sol-gel processes involve few synthesis routes. Solvent used in this method is normally water, but the precursor must be reagent that can be hydrolysed by acid or base. In the basic condition, a colloidal gel is produced, whereas in acidic condition a polymeric gel is formed (Lam *et al.*, 2008). Parameters in the sol-gel method that influenced the shape, size, morphology and surface chemistry of nanoparticles are rates of hydrolysis and condensation, solution composition, pH and temperature. For examples slower and controlled hydrolysis rate produced smaller nanoparticle size. (Tavakoli *et al.*, 2007). Iron oxide nanoparticles in the size range of 20 to 160 nm were synthesized by Casas *et al.* (2001), utilizing ethylene diaminetetraacetic acid (EDTA) as a precursor.

The sol-gel technique has successfully prepared magnetite and maghemite thin films, transparent iron-doped titanium oxide thin films, ferroelectromagnetic bismuth iron oxide films, mixed iron oxides and iron oxide-alumina nanocomposites (Chang *et al.*, 1997; Ismail, 2005; Lang, 2005; Liu *et al.*, 2006; Liu *et al.*, 2005). The major problem of sol-gel methods are occurrence of contamination from side products, extensive treatment of the products after reactions, difficulty to control reaction rates which eventually effect the material morphology and structure and different reactivity of metal oxides results in the lack of judgment over composition and homogeneity of the materials (Niederberger & Pinna, 2009).

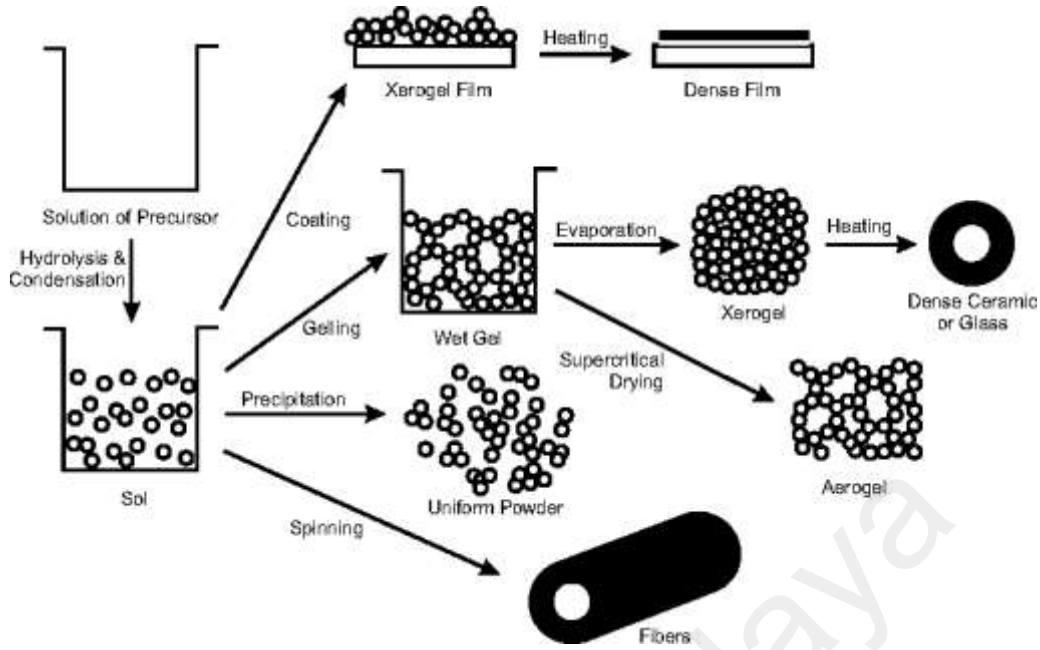

Figure 2.6: Steps in the sol-gel process (Niederberger & Pinna, 2009)

2.2.4.4 Hydrothermal Method

Hydrothermal method is environmental safe technique to synthesis nanoparticles since the method does not require any use of organic solvent and calcination (Sue *et al.*, 2004). Hydrothermal method is a method utilizing high temperature and high pressure for crystallizing substances. The hydrothermal setup shown in Figure 2.7 displays a hydrothermal, fine crystals which are obtained by this technique through formation of super saturation of metal salts at elevated pressure and temperature due to the low solubility of metal hydroxides and oxides (Eckert, 1996; Sue *et al.*, 2006). Variables that influence the crystal growth are pressure, temperature, reaction time and starting materials. For instance, mean particle size exhibits bigger size and different shape of the nanoparticles is observed when operation temperature is increased (Burda *et al.*, 2005).

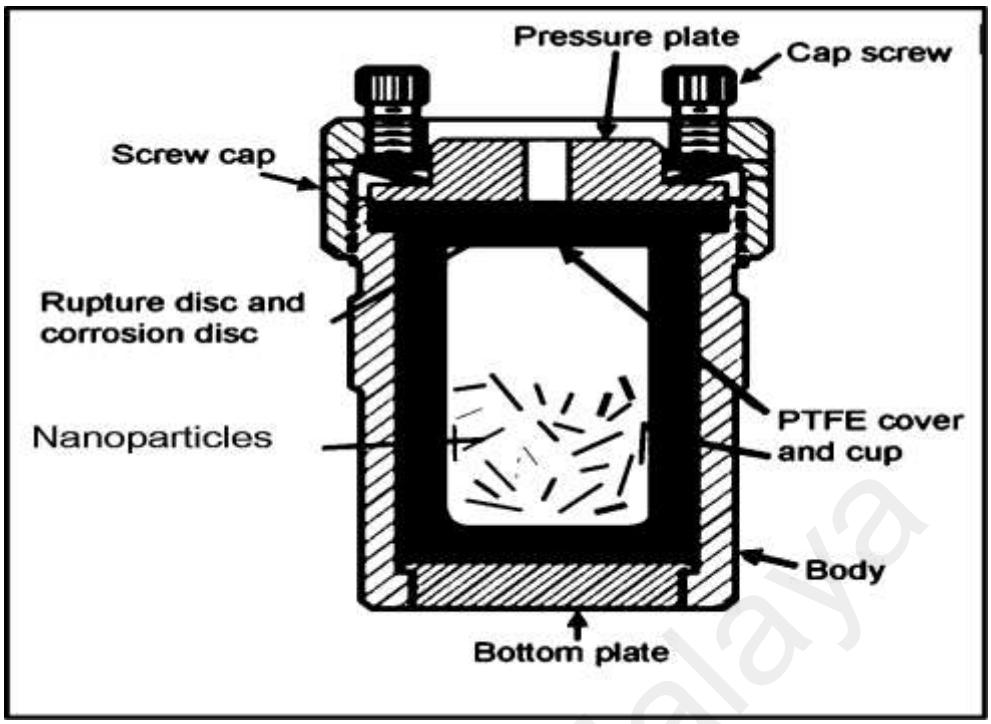

Figure 2.7: Diagram of hydrothermal setup (Grange *et al.*, 2011)

Hydrothermal 'continuous flow' reactor created by Matson *et al*. (1994) has been successfully prepared fine magnetite nanoparticles by rapid elevated temperature and supercritical water flows in the reactor for 5 to 30 seconds using ferrous sulphate and urea. Influence of precursor concentration, temperature and contact time on particle size and morphology were comprehensively studied, and as the precursor concentration increased the particle size also increases and monodisperse particles is obtained with short contact time (Xu *et al.*, 2008). Even though hydrothermal method offers advantages for controlling particle size and morphology, it required additional post-treatment steps and some of the surface functionalization cannot be achieved on the site.

2.2.4.5 Co-precipitation Method

Co-precipitation technique is one of the liquid phase techniques and widely used in preparation magnetite nanoparticles due to its simplicity, have economic value and good yields of product. This technique involves the reaction of stoichiometric mixtures of hydrated ferrous and ferric chloride with the presence of base in aqueous media (Sugimoto & Matijević, 1980). Spherical magnetite nanoparticles with mean diameters ranging from 30 to 100 nm were obtained from reaction of iron(II) salts, base and nitrate ions as oxidant (Tartaj *et al.*, 2003). Concentration of cations, counter ions involve and pH give influence to the phase and particle size distribution (Khaleel, 2004; Tamaura *et al.*, 1983; Tronc *et al.*, 1992).

Aggregation of nanoparticles may occur in the co-precipitation technique due to the large surface-area to volume ratio. Thus, addition of dispersing agent may stabilize the nanoparticles (Kim *et al*., 2003a). Examples of dispersing agents are protein, starches, non-ionic detergents, polyelectrolyte, oleic acid, saturated and unsaturated fatty acid as well as dodecanoic acid (Khalafalla & Reimers, 1980; Kim *et al*., 2003b; Mikhaylova *et al*., 2004; Wooding *et al*., 1991; Xu *et al*., 2006). Therefore, in this study we prepared magnetic nanoparticle by co-precipitation technique with water as medium of reaction because it is an effective technique to prepare magnetite with high yield of products, low cost and environmental safe.

2.2.5 Magnetic Nanoparticles in Environmental Application

In a determination to encounter water contamination, speedy and effective developments in wastewater handling have been made, including photocatalytic oxidation, adsorption, separation and biotreatment process. Nevertheless, their usages have been constrained by many aspects, for examples removal ability, technical routine,

energy supplies, and cost-effective value (Dastjerdi & Montazer, 2010). Recently, magnetic nanoparticles have been widely explored in the field of waste water treatment due to few advantages such as high surface area, simple preparation step, superparamagnetism, provide surface modification, low toxicity, inert, biocompatibility and low cost (Boyer *et al.*, 2010; Gupta & Gupta, 2005; Pan *et al.*, 2010).

A combination of adsorptive process with magnetic dissociation has therefore been used comprehensively in water and environmental purification especially as a solid sorbent in a magnetic solid-phase extraction (MSPE) (Ambashta & Sillanpaa, 2010; Mahdavian & Mirrahimi, 2010). Magnetic solid-phase extraction has been successfully preconcentrate many inorganics and organics pollutant in a very complex matrix. For example, Ballesteros-G´omez and Rubio (2009) performed a solid-phase extraction of carcinogenic polycyclic aromatic hydrocarbons from effluent water samples with high preconcentration factors and also low limit of detection in the range 0.2-0.5 ng L^{-1} . The capability of iron oxide nanoparticles to extract pollutants has been established at both laboratory and field scale tests (Girginova *et al.*, 2010; White *et al.*, 2009). Figure 2.8 depicts an illustration for the application of magnetic nanoparticles in magnetic solid-phase extraction (MSPE).

However, the smaller the particle the more it becomes unstable since it possess high surface energies and tend to accumulate to each other in the solution to reduce the surface energies (Lin *et al.*, 2005). This stability is affected by the electrostatic and Van der Waals interactions (Chen *et al.*, 2007). Besides, bare metallic nanoparticles are chemically active, and are readily oxidized, which eventually reduce its magnetism and ability to disperse (Xie *et al.*, 2014). Thus, the fact that surface of magnetite can be chemically functionalized, modification of magnetite nanoparticles can be one of the approaches to overcome the stability problem with appropriate functional group (Boyer

et al., 2010; Dias *et al.*, 2011). The strategies of modification are including grafting and coating the surface of magnetite. Besides, helping in stabilizing the magnetic core, functionalization or modification may also provide functional properties that can be tailored according to the application.

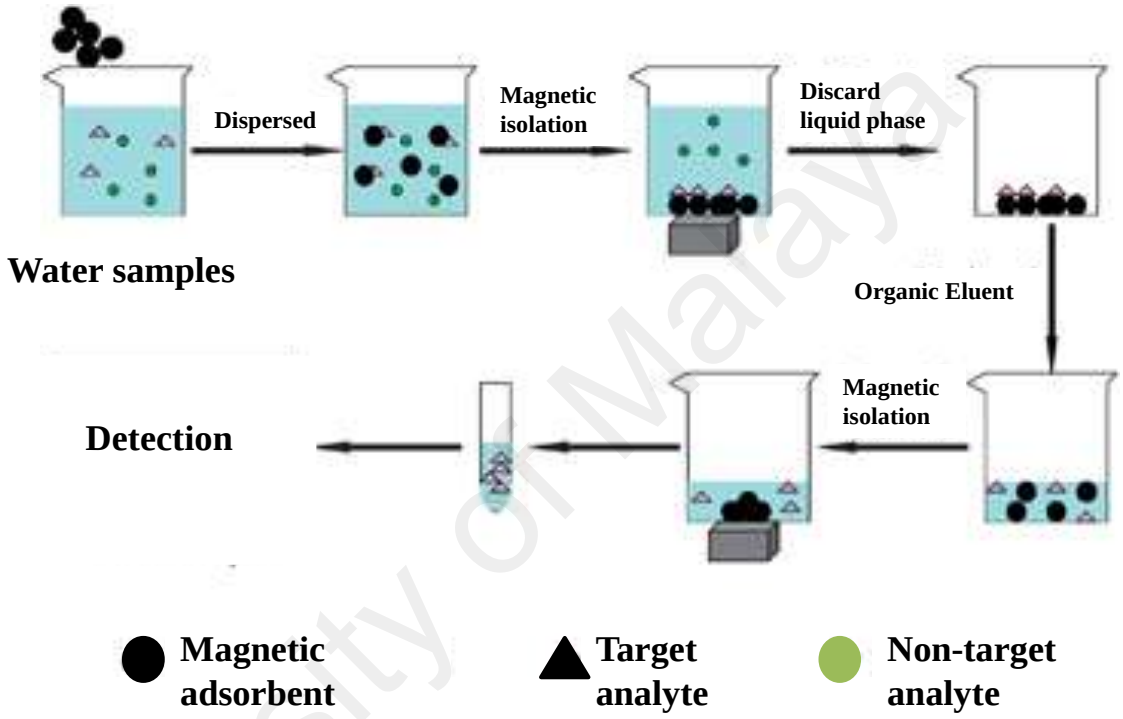

Figure 2.8: Illustration for the application of magnetic nanoparticles in magnetic solid-phase extraction (MSPE) (Zhang *et al.*, 2013)

2.2.6 Functionalized Magnetic Nanoparticle in Environmental Application

Due to the stability problem of bare magnetite nanoparticle, there has been an increase trend on the development of multifunctional magnetite nanoparticles. Functional agents that are used to modify the nanoparticles are from organic and inorganic based. Modification strategies and type of modifier greatly influence the particle size, morphology, magnetic behaviour and surface chemistry of the nanoparticles (Jeong *et al.*, 2007; Machala *et al.*, 2007).

2.2.6.1 Silica Coated Magnetic Nanoparticles

Silica is an outstanding material which is extensively used because of its low cost, chemically inert and thermodynamically stable. Furthermore, silica shell assists in shielding the magnetite core from unwanted interactions in the solution. The silanol group in the silica offers OH functionalities which can be modified with other molecules or biomolecules for examples titania, zirconia, proteins, nucleic acid and enzymes (Garcia-Calzon & Diaz-García, 2012). Figure 2.9 exhibits silane interaction on the surface of magnetic nanoparticles. O-H functionalities in magnetic nanoparticles reacted with -O-R bonds which results in formation of readily available sites for further substances impregnation (Arkles, 1977).

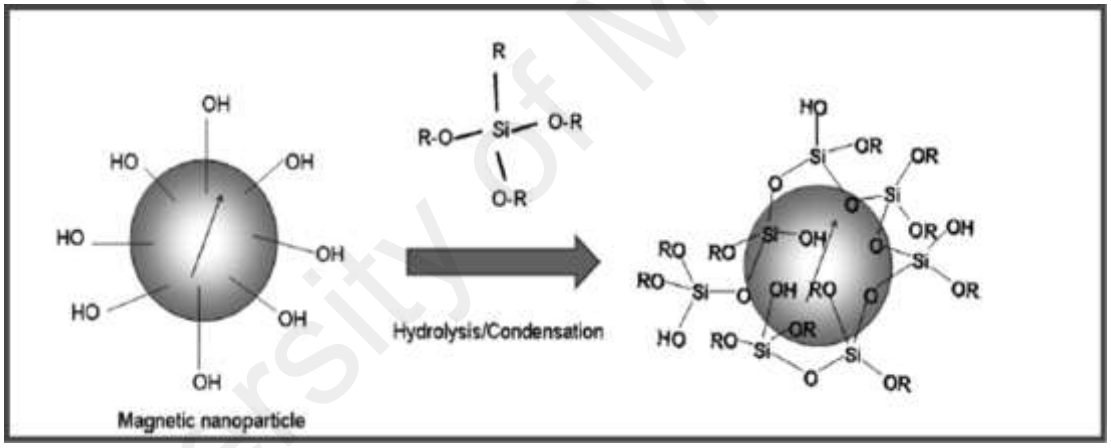

Figure 2.9: Silane coating on the surface of magnetic nanoparticles (Arkles, 1977)

Presence of non-magnetic coating agent reduces saturation magnetization (Ms) of the magnetic materials and provides low inter-particle diffusion. Thus, a proper optimization strategy is important to obtain useful materials. For instance, saturation magnetization of naked Fe_3O_4 nanoparticles reduced from 81.2 emu g^{-1} to 49.7 emu g^{-1} after coating with a 15 nm silica (Tian *et al.*, 2009).

Silica based materials such as 3-aminopropyltriethoxysilane (APTEOS), p-aminophenyltrimethoxysilane (APTS) and mercaptopropyltrimethoxysilane (γ-MPTES) are coating agents that provide amino and sulfhydryl functionalities. Tian *et al.* (2009) prepared γ-mercaptopropyltrimethoxysilane (γ-MPTMS)-modified silica coated magnetic nanoparticles as an adsorbent for extraction and enrichment of trace amounts of Cd, Cu, Hg, and Pb prior analysis via inductively coupled plasma mass spectrometry (ICP–MS) which have high adsorption capacity, high enrichment factor, high sensitivity and can be reused up to 10 times without significantly impact its extraction efficiencies . Furthermore, due to the presence of thiol functional group in (γ-MPTMS) modified silica coated magnetic nanoparticles, this nanocomposite also has been employed in separation of Tellurium (Te) in seawater (Huang & Hu, 2008). Despite the fact that, these agents enhance the selectivity of nanoparticles for target pollutant, there is some unavoidable problem associated with residual silanol group in the product leads to the incomplete dehydration reaction which eventually enhance chemical reactivity (de Dios & Díaz-García, 2010). Thus, further end capping with appropriate reagent must be employed to overcome this constraint. For instance, aminated-$CoFe_2O_4$–SiO_2 nanoparticles for scavenging cadmium from environmental samples successfully synthesized (Wang *et al.*, 2013a).

Recently, metal organic frame work (MOF) has been widely explored due to the high surface area, thermally stable, uniform pores, in-pore and surface modification readiness. Integration of metal organic frame work, MIL-101 with silica coated magnetic nanoparticles (Fe_3O_4–SiO_2–MIL-101) has been successfully removed polyaromatic hydrocarbon from aqueous solution under sonication. Existence of MIL-101 enhance adsorption capability as well sensitivity with only required small amount of adsorbent (Huo & Yan, 2012). Integration of silica coated magnetic nanoparticles

with organic frame work such as diphenyl group has been employed by Bianchi *et al.* (2012) in determining polyaromatic hydrocarbon in urine smokers and non-smokers.

Removal of metal from aqueous solution requires an efficient ligand to form a stable metal complex and at once treat the water. Silica coated magnetic nanoparticles functionalized Schiff base was utilized as solid-phase adsorbent for removal of Pb(II), Cd(II) and Cu(II) (Bagheri *et al.*, 2012). Example of Schiff base functionalizing agent is 3-(4-methoxybenylideneamino)-2-thioxothiazolidin-4-one. Figure 2.10 proposed a synthesis routes for Schiff base modified silica coated magnetic nanoparticles.

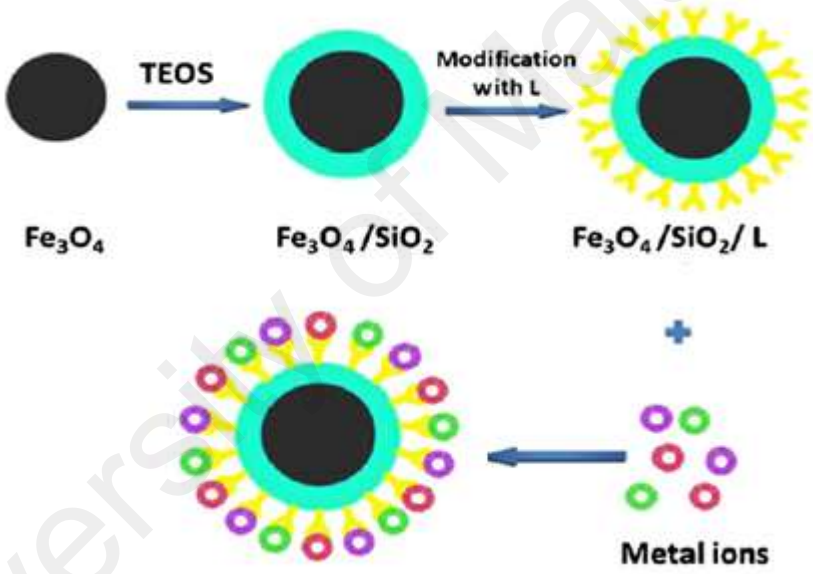

L = ligand TEOS = triethoxysilane

Figure 2.10: Synthesis routes for Schiff base silica coated magnetite nanoparticles (Bagheri *et al.*, 2012)

β-cyclodextrin silica coated magnetic nanoparticles (Fe_3O_4–SiO_2–β-CD) demonstrated great adsorption capacity in removing bisphenol A (BPA) and diethylstilbestrol (DES) from aqueous sample. This is because β-cyclodextrin has a unique structural properties which is truncated cone with both hydrophilic and hydrophobic hollow which can offers inclusion of many guest molecules (Ji *et al.*, 2009; Qin *et al.*, 2008). Moreover, carboxymethyl-β-cyclodextrin (CM-β-CD) has been

introduced in the surface of silica coated magnetic nanoparticles by Ghosh *et al*. (2011) via carbodiimide stimulation. This material has been employed in analysis of chiral aromatic enantiomers .

The C_{18}-functionalized silica coated magnetite microsphere (Fe_3O_4–SiO_2–C_{18}) was produced by of a sol–gel approach with the use of a surfactant. Abundant silanol groups on the outer surface and the functional C_{18} groups on the interior surface provide both hydrophilic and hydrophobic properties which gave good adsorption capacity for the extraction of phthalates from waste water sample (Deng *et al.*, 2008). Moreover, this adsorbents also assist in extraction of Sudan dye via ultra-fast liquid chromatography with limit of detection in the range 0.066 to 0.12 ng mL^{-1} (Jiang *et al.*, 2012).

2.2.6.2 Carbon Coated Magnetic Nanoparticles

Recently, magnetic nanoparticles carbon coated has fascinated researchers worldwide since it offers strong adsorption affinity to varieties of organics substances. The advantages of carbon based materials as compared to silica are higher chemical resistance, more thermal steadiness, and biological safer. Moreover, carbon based materials also provide surface functionalization as well as pores formation. Examples of carbon based materials are activated carbon, carbon nanotubes (CNTs), graphene and fullerene.

Activated carbon-magnetic nanocomposite designed by Bai *et al.* (2010) contained inner hydrophobic layer and outer hydrophilic surface. The hydrophobic property enhances extraction capacity for hydrophobic analytes, such as PAH, whereas hydrophilic property facilitates the dispersability of the sorbent in aqueous solution. Moreover, due to well distributed nanoparticles, there is no requirement for shaking and

stirring which offers on site sampling and extraction (Xie *et al.*, 2014). By utilizing hydrothermal technique, Zhang *et al*. (2010) managed to obtain Fe_3O_4–C sorbent which has high surface area and high adsorption affinity with the presence of carbon chain. 50 mg of the sorbent can efficiently remove 1 L PAH with recoveries in the range of 76-110 %. Another novel sorbent which is great in extraction of PAH is ceramic carbon coated Fe_3O_4 magnetic nanoparticle (Fe_3O_4–C–ceramic) which has been developed by Heidari *et al*. (2012) via sol-gel.

A carbon encapsulated metal nanoparticle (CEMNPs) has been extensively explored recently. The preparation of carbon-encapsulated metal nanoparticles (CEMNPs) is by cocarbonization in autogenous pressure at 420–510 °C using either heavy oil or phenolic resin as a carbon source and ferrocene as metal source (Huo *et al.*, 2007). Surface properties of carbon encapsulated metal nanoparticles (CEMNPs) can be tailored by modifying the graphitization degree and monitor the oxygen-containing substances at different heat phases. In carbon-encapsulated metal nanoparticles (CEMNPs) the adsorption of organic contaminants involves in the interaction of π–π stacking, hydrophobic and hydrogen bonding. Although, in carbon encapsulated metal nanoparticles (CEMNPs), the method of preparation is simple and have good potential in scavenging organic pollutant, yet it involves in the usage of toxic materials (Niu *et al.*, 2011).

Ever since carbon nanotubes (CNTs) first discovered by Iijima in 1991, this material has been widely studied in many different fields due to their outstanding mechanical, electrical and thermal characteristic. Utilizing wet chemical method, Qu *et al.* (2008) managed to diffuse magnetic nanoparticles into multiwall carbon nanotube which further used as an adsorbent to remove dyes as methylene blue and neutral red. Magnetic nanoparticles coated multi-wall carbon nanotube was applied as a sorbent in

the adsorption of bisphenol A (BPA), bisphenol F (BPF), and their diglycidyl ethers as well as phthalates in drinking water samples (Jiao *et al.*, 2012a; Jiao *et al*., 2012b). Recently, Ding *et al.* (2012) prepared magnetic carbon nanotube by wrapping the magnetic nanoparticles inside the carbon nanotubes bundles during aggregation process. This material has been successfully employed as a sorbent to extract phthalic acid from beverages, environmental water and perfume. Limit of the detection found was in the range of 4.9 to 38 ng L^{-1}. Magnetic silica particles coated with hydroxyl terminated multi-walled carbon nanotubes prepared by sol–gel technology was synthesized to overcome the solubility limitation of conventional magnetic nanoparticle coated multi wall carbon nanotube. This functionalized MWCNTs-OH was effective in extraction of diethylstilbestrol, estrone and estriol from water (Guan *et al.*, 2010).

Another type of carbon based material is graphene. Graphene is an inimitable material which has two dimensional planar structure, high surface area and good electrical, thermal and mechanical properties (Yang *et al.*, 2009). Since graphene has a large delocalized π-electron system, it can readily produce a steady π- π interaction with organic substances especially benzenoic compounds (Chen *et al.*, 2010). Outstanding adsorption performance was observed in magnetic nanoparticles coated graphene (Fe_3O_4-G). For instance, a variety of pollutants in environmental sample were extracted using magnetic nanoparticles coated graphene (Fe_3O_4-G) as a sorbent which were neonicotinoid insecticides, imide fungicides, carbamate pesticides, fuchsine, triazine herbicides and chloroacetanilide herbicides (Li *et al*., 2013a; Li *et al.*, 2013b; Wang *et al.*, 2011; Wang *et al*., 2012; Wu *et al*., 2011). Magnetic nanoparticles functionalized graphene oxide (Fe_3O_4–GO) also proved to be competitive sorbent for extraction several kinds of contaminants.

2.2.6.3 Surfactants Coated Magnetic Nanoparticles

Ionic surfactants such as sodium dodecylesulfate (SDS), cetyltrimethylammonium bromide (CTAB), cetylpyridinium chloride (CPC) or dioctadecyldimethylammonium chloride (DODMAC) functionalized magnetic nanoparticles offer to an establishment of hemimicelles sorbents. Hemimicelles contains ionic head group and hydrocarbon in the tail group. Li *et al.* (2008) developed cetyltrimethylammonium bromide coated Fe_3O_4 nano-magnets (Fe_3O_4–CTAB) as a sorbent to remove chlorophenols in water samples. Moreover, this sorbent also managed to extract phenolic compounds in contaminated aqueous samples (Zhao *et al*., 2008).

Meanwhile, sulfonamides from environmental water samples was preconcentrated using magnetic functionalized octadecyl octadecyltrimethylammonium bromide (Fe_3O_4-OTAB) nanocomposite by Sun *et al*. (2009). Cheng *et al*. (2012) reported a preparation of magnetic functionalized hexadecyl-3-methylimidazolium bromide nanocomposites (Fe_3O_4-C16mimBr) and further employed in the extraction of chlorophenols with satisfactory extraction recoveries. Magnetic nanoparticles have also been functionalized with sodium dodecylesulfate (SDS) and applied as sorbent to remove mercury(II), malachite green, and leuco-malachite green from water samples (Afkhami *et al.*, 2010; Faraji *et al.*, 2010).

Thus, a suitable surfactant which can form a covalent bonding with magnetic nanoparticles is crucial. For instance, several alkyl carboxylates or n-octadecylphosphonic acid were chemically adsorbed on magnetic nanoparticles and further employed for the extraction of organic substances (Roman *et al.*, 2011).

2.2.6.4 Polymer Coated Magnetic Nanoparticles

Hybrid polymer magnetic nanoparticles are a potent material which can be applied in various fields. The polymers linked to the magnetic nanoparticles can be attached either by covalent or electrostatic interaction. For instance, covalent bond formed when polypyrrole or molecurlarly imprinted polymer (MIP) reacts with magnetic nanoparticles, whereas electrostatic interaction occurred when use biopolymers as chitosan and alginates (Geng *et al.*, 2012). The sorbent having mean particle size distribution in the range of 300-700 nm and the coating thickness was measured approximately 10 nm.

Magnetic nanoparticles coated polydopamine (Fe_3O_4–PDA) was prepared by Wang *et al.* (2013b) without using any organic solvents. 20 mg of the sorbent was adequate to remove 500 mL PAH in natural water. Furthermore, another fascinating sorbent proposed by Reyes-Gallardo *et al.* (2013) using an intergration of cobalt magnetic nanoparticles coated Oasis MCX. Oasis MCX was a commercial polymeric microparticles which is a cation-exchanger and water-wettable polymer. This nanocomposite were effectively applied in the determination of nitroaromatic hydrocarbon in water. Some of nanocomposites of polymer coated magnetic nanoparticles may not be able to withstand in an acidic condition, thus an appropriate coating layer must first introduce to the magnetic nanoparticles prior polymerization. For instance, polymethyl methacrylate coated magnetic silica (Fe_3O_4–SiO_2–PMMA) as an adsorbent to confiscate sulphonamides for aqueous samples has recently been reported (Gao *et al.*, 2010).

Synthesis of chitosan functionalized octadecyl coated magnetic nanoparticles was reported by Zhang *et al*. (2010) involves in the introduction of magnetic nanoparticles to the octadecyl group by silylation, then the functionalized Fe_3O_4–C_{18} was

encapsulated with chitosan tripolyphosphate via ionotropic gelation. The synthesized material has inner side of hydrophobic C_{18} and outer side of hydrophilic chitosan which was successfully extracted phthalates and perfluorinated compounds .

Recently, an application molecular imprinting polymer (MIP) in environmental treatment has increased significantly. Their approaches to targeted pollutant are similar to the recognition process in antigens and antibodies. MIP contains template and monomer in the existence of cross-linking agent. Integration of magnetic nanoparticles with molecularly imprinted polymer microspheres enhances the selectivity and magnetic separation. For example, a newly designed magnetic and hydrophilic molecularly imprinted polymers (Fe_3O_4-MIPs) were prepared by converse emulsion–suspension polymerization to eliminate acid dyes from polluted water with 1-(α-methyl acrylate)-3-methylimidazolium bromide (1-MA-3MI-Br) being exploited as a monomer (Luo *et al.*, 2011). The superparamagnetic Fe_3O_4@MIP for bisphenol A (BPA) were obtained coated with a polychloromethylstyrene (PCMS) sheet by mini-emulsion polymerization (Liu *et al.*, 2011).

Magnetic nanoparticles functionalized conducting polymers offers interesting diverse properties with prominence stability and simplicity of synthesis. Examples of conducting polymers that were comprehensively studied are polypyrrole (PPy), polyaniline (PANI) and polythiophene (PTh). Phthalates from water samples were effectively removed by polypyrrole coated Fe_3O_4 with the involvement of π–π and hydrophobic interaction between polypyrrole and phthalates (Meng *et al.*, 2011). Besides, this material also being employed as sorbent to remove pesticides residues in tea, juices and natural water samples (Zhao *et al.*, 2013). Application of polyaniline coated Fe_3O_4 as extractor of methyl mercury was designed with diameters in the range of 50 to 100 nm (Mehdinia *et al.*, 2011). Sulfate functionalized polyaniline coated

magnetic nanoparticles was obtained by Tahmasebi *et al.* (2013) for the removal of ionizable parabens. Both electrostatic, π–π and hydrophobic interaction enhanced the adsorption affinity of the sorbent to the targeted analytes. Moreover, polyaniline coated carbon magnetic nanoparticles (Fe_3O_4–C–PANI) prepared via hydrothermal technique was effectively remove phenolic compounds with low limit of detection and high recoveries (Meng *et al.*, 2011).

Among conducting polymers, polythiophene exhibited remarkable stability in air and humid environment. Recently, the polythiophene coated magnetic nanoparticles (Fe_3O_4–PTh) was properly designed and employed as a sorbent to extract some of phthalates in environmental water samples prior analysis by gas chromatography with flame ionization detector (GC-FID) (Tahmasebi *et al.*, 2013). For this work, we have modified the thiophene monomers with certain functionalities to tailor with the required applications (Baharin *et al.*, 2016).

2.4 Phthalates

2.4.1 Overview

Non-halogenated ester of phthalic acid (1, 2-benzene dicarboxilic acid), generally known as phthalates, have wide-ranging use in industrial applications. Normally, high molecular mass of phthalates become a useful plasticizers which improves the flexibility of vinyl resins. Addition of plasticizers is able to reduce intramolecular forces by decreasing the glass transition temperature of the respective molecules which lead to desirable properties of high polymeric chain such lowered brittleness, enhanced elasticity, decreased hardness and improved adhesion when needed (Staples, 2003). Supreme plasticizer must be unscented, colourless, unaffected against water, light,

neutral, not toxic and it should offer low inflammability and low volatility (Stales *et al.*, 1997). Table 2.2 demonstrates uses of phthalates.

Table 2.2: Some uses of phthalates

Phthalates	Uses
DEP	Personal care products, cosmetics
BBP	Vinyl tiles; food conveyor belts, artificial leather, automotive trim, traffic cones
DBP	PVC plastics, latex adhesives, cosmetics, personal care products, cellulose plastics, solvent for dyes
DEHP	Building products (wallpaper, wire and cable insulation), car products (vinyl upholstery, car seats), clothing (footwear, raincoats), food packaging, children's products (toys, grip bumpers), medical devices
DnHP	Dip-molded products, such as tool handles, dish-washer baskets; flooring, vinyl gloves, flea collars, conveyer belts used in food processing
DNOP	In mixtures C6–C10 phthalates: garden hoses, pool liners, flooring tiles, tarps Seam cements, bottle cap liners, conveyor belts (indirect food additive)
DINP	Garden hoses, pool liners, flooring tiles, tarps, toys
DIDP	PVC plastics, covering on wires and cables, artificial leather, toys, carpet backing, pool liners

Source: (Heudorf *et al*., 2007; Fromme *et al.*, 2002)

Low molecular weight of phthalates are normally utilized as plasticizers in few of non-vinyl resins for examples acrylics, urethanes and cellulosics. Phthalates with alkyl

chain 1 to 4 carbon atoms are not commonly used as plasticizers due to the volatility distresses however they are widely used in the production of consumer products including pharmaceuticals. For example DMP, is utilized as stabilizing eluent for transportation of organic peroxides. Meanwhile, DEP acts as compounder in cellulosic films and as preservatives in fragrances. DBP is mainly used as a plasticizer in PVC. Overall, factors for the selection of phthalates in industrial applications are its functionality, adaptability, durability, competence and process ability and economical value (Heudorf *et al.*, 2007).

By 21st century, there are arisen fears over the application of phthalates in production of children's toys and other regularly used household items since they are not chemically bound in plastics and could easily being released onto the environment; readily leaching out from products (Serodio & Nogueira, 2006). Due to the fact that phthalates are hazardous to human, a regulatory oversight of the manufacture, transport, use and disposal of phthalates have been implemented and with that huge data regarding the properties, environmental fate, exposure, and toxicity of phthalates were collected. These critical data enhance the safety practice for the production, effluent discharge limits, and human exposure limits for a better environment.

2.4.2 Occurrence of Phthalates in Environment

During industrial process, only a small amount phthalates is leached out to the environment and air. Basically phthalates are discharged in wastewater during manufacture and processing. Poorly functioning furnaces may also contribute to the existence of phthalates into air. However, foremost contribution of phthalates especially DMP, DEP, DBP, BBP, DINP, DIDP and DEHP that are found in environment are from the plastics and other phthalates containing products since it not chemically linked and

can be diffused out slowly (Schettler, 2006; Wormuth *et al.*, 2006). Thus, usage of phthalates containing product during lifetime may lead to a sustainable phthalates concentration in the earth.

Polymer toys, bottles and pacifier contained phthalates were alleged as a possible cause of phthalate exposure in infant and children. DINP was estimated of contacts ranged from 5 to 44 mg kg^{-1} bodyweight per day (Kavlock *et al.*, 2002). Meanwhile, Agency for Toxic Substance and Disease Registry (2002a) recorded the DEHP exposure from the imbibing or chewing of the pacifier or toys for everyday use projected up to 85 mg kg^{-1} bodyweight per day. Overall, the exposure of phthalates to children surpasses adults. Significant concentration of DMP and DEP were found in indoor air due to the usage of consumer products for example skin care, shampoo and body wash adults (Wormuth *et al.*, 2006).

Medical tools comprising DEHP for example PVC/DEHP tubing is one of major source of phthalates exposure specifically for patient that undertaking severe attention, blood transfusion, haemodialysis and extracorporeal membrane oxygenation (ECMO) (infants) (Karle *et al.*, 1997). In addition, usage of specific coatings for dosage medication containing DEP and DBP also contributes to the exposure of phthalates to the patient (Hauser *et al.*, 2004). However, due to low concentration of these substances, it were permitted as inert ingredient by U.S. Food and Drug Administration (2003).

Several phthalates also found in food or drink packaging or processing. In 1999, the utilization of disposable PVC gloves throughout meals preparation is one of the main source of DEHP contamination, the concentration found was in the range of 10 to 4400 ng g^{-1} (Tsumura *et al.*, 2001, 2003). In 2009 and 2013 a studies conducted by Pinto *et al*. (2009), Plotan *et al*. (2013) and Wagner *et al.* (2009) have found an

endocrine disruptor activity in most of the examined PET bottled water samples. Even though, concentration found was not grasped to the serious levels, but the effects on glucocorticoid activity is unidentified. Keresztes *et al.* (2013) claimed that, the migration of phthalates from PET bottle to water samples are influenced by PET bottle material (virgin vs. polymer comprising reused PET), pH (carbonated vs. non-carbonated samples), packaging volume and temperature. From their study, DEHP, DIBP and DBP were found in recycled PET bottle, low pH (carbonated samples) showed no activity of phthalates compared to non-carbonated, low volume of packaging contributed to high surface/volume ratio and at 60 °C, majority of phthalates studied was observed. In 2011, Hong Kong was shocked by the existence of DEHP in the flavour wrapper of ramen noodle (Huang, 2011).

Furthermore, the contamination of Canadian dairy samples with phthalates also being tested, among other phthalates, DBP and DEHP found were 11.9 mg kg^{-1} and 47.8 mg kg^{-1} (Wagner & Oehlmann, 2009). The exposure to phthalates to dairy products may arise from the containers also from the tubing during milk processing. Other published works emphasized on the existence of DEP, DBP, BBP, DEHP, DNOP and DINP in all kinds of food packaging including; paper, cardboard, plastic, glass jar metal cap and cans (Balafas *et al.*, 1999; Bononi & Tateo, 2009; Fankhauser-Noti *et al.*, 2006; Jarošová, 2006; Lopez-Espinosa *et al.*, 2007; Nerin *et al.*, 1993).

2.4.3 Adverse Effects

Toxicology evaluations on phthalates have been performed by different expert panels in Europe and America, for examples European Chemicals Bureau (2008), European Food Safety Authority (2005), European Scientific Committee on Toxicity, Ecotoxicity and the Environment (2004), U.S. Agency for Toxic Substances and

Disease Registry (2002a, 2002b) and U.S Department of Health and Human Service (2006).

Normally, toxicology tests were executed with rats, mice and other rodents since these organisms are seem to be more delicate to toxic effects of phthalates than humans. Organs studied were liver, kidney and testis. The most extensively applied phthalate is DEHP, which not only is supervised under the strictest regulation but is also viewed as the trickiest from the perspective of adverse effects on health. Other frequently used phthalates are DBP, DEP, DINP, BBP, DIDP and DNOP. DEHP and DBP were categorized as reprotoxic (toxic toward reproductives organs) substances by European Union in the guideline 67/548/EHS. All phthalates have been verified negative for mutagenicity and/ or genotoxicity (Heudorf *et al.*, 2007).

BBP and DINP were found to be harmful to reproductive organs (Regulation, 2001). However, the most serious case occurred with DINP where it attacks liver function and regarded as nephrotoxicity (Keresztes *et al.*, 2013). Moreover, a significant concentration of DEHP in household dust is one of the caused for the incidence of asthma, whereas high level of BBP amounts resulted in rhinitis and eczema in children (Bornehag *et al.*, 2004).

Recent study investigated DEP possibility on the retardation of sperm development in men since it is widely used as additives in fragrances (Duty *et al.*, 2003). Overall, DEHP demonstrated utmost toxicity, resulting in the definition of specific risk groups such as children below 1 year, critically sick children and pregnant women undertaking treatments using medical devices with DEHP (U.S. Department of Health and Services, 2006). As for DNOP, animal studies concluded no toxicity effects up to 7500 mg kg^{-1} day^{-1}, but in exposure in the range of 5000–10,000 kg^{-1} day^{-1} toxic effects were observed in all groups (U.S. Department of Health and Services, 2003a).

Tumor stimulating activity was found with DBP and exposure of DEHP promoting hepatocellular carcinoma, proliferation of peroxysomes and mitochondria which escalates in Cyp4A1 and PCoA activities, liver tissue propagation, destruction of apoptosis in mice (U.S. Department of Health and Services, 2003b). Exposure to phthalates also contributes to increases in stillbirth, growth and birth weight retardation, incomplete formation of skeletal and visceral (Heudorf *et al.*, 2007).

Due to high production volume and limitless toxic effects, phthalates are subjected to strict regulations covering manufacturing process, shipping and transportation, utilization and discarding. In United State, phthalates are monitored under Clean Water Act Section 307, according to this act all effluent must be treated and follow pre-treatment standard before being discharge. (U.S. Environmental Protection Agency, 1999) legalizes maximum pollution restrictions for DEHP and DEHA 6 mg L^{-1} and 400 mg L^{-1}. In addition to the standard, the screening of phthalates in drinking water must be done at the concentration above 0.6 µg L^{-1}. Whereas, DEHP tolerable daily intake is 20 µg kg^{-1} body weight per day.

European Union (EU) has listed DBP, BBP and DEHP as endocrine disruptor subtances. Thus, these types of substances are strictly monitored. European Union and World Health Organization (WHO) has set a limit for DEHP in fresh and drinking water 8 mg L^{-1} (Serodio & Nogueira, 2006). European Union Scientific Committee on Toxicity, Ecotoxicity and the Environment 13 (CSTEE) has recognized an acceptable daily consumption value for DEHP of 37 µg kg^{-1} body weight per day (Koch *et al.*, 2003).

2.4.4 Analysis of Phthalates

The determination of phthalates in environmental samples is challenging due to their trace amounts and the intervention of an intricate matrix (Sha *et al.*, 2011). Therefore, a sample preparation step for the extraction and preconcentration of the analytes is required (Lopez-Espinosa *et al.*, 2007). Sample preparation technique depends on the nature of the samples. For water samples two classes of methods will be described which are solid-phase extraction and liquid-liquid extraction. These techniques are briefly discussed below.

Liquid-liquid extraction involves in a high volume of water samples (1-2 L) and low solubility solvent. Common solvents which offer high extraction efficiency are for water samples are dichloromethane, cyclohexane or hexane (Braaten *et al.*, 1996). Important parameter that needs to be monitor is the ratio of the water sample volume to the volume of the organic solvent. The optimum ratio should be less than 20. Higher ratio results in the high recovery for high molecular weight phthalates as DEHP whereas low recovery was obtained for low molecular weight phthalates as DMP. This is because, low molecular weight of phthalates is more prone to the water (Cousins & Mackay, 2000). Post-extraction organic phase is dried over anhydrous magnesium sulphate and enriched. For samples with complex matrices, several compounds are co-extracted and can be further refined by column chromatography with packed column for examples alumina or silica.

Disadvantages in liquid-liquid extraction are existence of contamination from the trace levels of phthalates in some commercially available solvents gives error to the preconcentration factor. For instance, Vikelsoe *et al.*, (1998) reported a questionable result on the contamination of 1 ng L^{-1} of DEHP leads to 50 ng L^{-1} background value . Besides, a huge amount of solvent are used in this techniques results in more waste

issues. Recent, development over traditional liquid-liquid extraction, micro liquid-liquid extraction have been designed and applied (Cinelli *et al.*, 2013). In this method, solvent usage is low and extraction can be accomplished in a small volume (10-15 mL). Micro liquid-liquid extraction for BBP, DBP, DCP and DEHP were employed in water samples (Sha *et al.*, 2011). Typically, liquid-liquid extraction technique is preferable to heavily contaminated waste water. For determination of phthalates in less complex matrices such as drinking water, beverages, river water, surface water, sea water solid phase extraction is favoured (Staples, 2003).

In solid phase extraction (SPE), solvent consumption is low and a solid sorbent is used as an analyte extractor from the samples. Most commonly applied sorbent for determination of phthalates is octadecyl silicagel (ODS, C18). In solid phase extraction strategies, samples are passed through the adsorbent, adsorbent will attract targeted analyte to the specific active sites in the adsorbent. Then, the water phase is removed and the sorbent is eluted with different type of solvents for examples dichloromethane, ethyl acetate, methanol or acetonitrile. Targeted analyte in the elution solvent is dried via nitrogen gas prior instrument detection. Recently, many sorbents were synthesized and utilized in the solid phase extraction for analysis of phthalates. Jiao *et al.* (2012b) designed and applied multi-walled carbon nanotube as a sorbent in SPE to preconcentrate DEHP, DPP, DIBP and DCP in river and sea water samples. Another examples of sorbents are bamboo charcoal, Nylon6 nanofibers mat, graphene, 1-dodecyl-3-methylimidazolium bromide ([C_{12}mim]Br)-coated silica and etc. (Li *et al*., 2008; Wu *et al.*, 2013; Xu *et al*., 2010; Zhao *et al*., 2008).

Furthermore, the application of nanoparticles as a sorbent in determination of phthalates also widely studied. This is due to nanoparticles offers high surface area, tuneable functionalization, chemically and thermally stable, facile synthesis routes,

sustainable and cost-effective (Han *et al.*, 2012). For example, TiO_2 nanoparticles deposited into stainless steel fibres was applied to enriched DEHP prior gas chromatography flame ionization detector analysis (Banitaba *et al.*, 2013). Recently, a quite numbers of publications have been applied magnetic nanoparticles as a sorbent for magnetic solid-phase extraction (MSPE) (Reyes-Gallardo *et al.*, 2013; Roman *et al.*, 2011). This is because magnetic nanoparticles can give a prompt response to the external magnetic field which helps in magnetic isolation. Magnetic isolation offer facile and rapid sample preparation steps without the need of any centrifugation or filtration (Xie *et al.*, 2014).

Solid-phase extraction offers advantage over liquid-liquid extraction in terms of high enrichment factor, cost effectives, rapidness, simplicity, environmental benign and low trace level contamination from the organic solvent. Besides, chosen of high selective sorbent for extraction provide good sensitivity and high extraction efficiency (Liška, 2000).

CHAPTER 3: RESEARCH METHODOLOGY

3.1 Reagent and Materials

Analytical grade ferric chloride ($FeCl_3 \cdot 6H_2O$), ferrous chloride ($FeCl_2 \cdot 4H_2O$), ammonia solution (25 wt. %), benzene, thiophene, tetrahydrofuran, potassium iodide, potassium carbonate, acetonitrile, methanol, hydrochloric acid, acetone, ethyl acetate, polyvinyl alcohol, 3-bromothiophene, acetic acid, sodium hydrogen bicarbonate and 4-hydroxybenzaldehyde were purchased from Merck (Darmstadt, Belgium). 3-thiophene carboxaldehyde, 1, 6-dibromohexane, 3-hexylthiophene, *n*-butylithium, DMP, DEP, DPP, DBP, BBP, DCP, DEHP, DNOP were obtained from Sigma Aldrich (Milwaukee,WI USA). Acetone and aniline bought from Fisher Scientific (UK). Magnesium sulphate anhydrous, ethanol denatured and hexane purchased from Friedemann Schmidt (Parkwood, Australia). 18-crown 6, chloroform ($CDCl_3$) and CaH_2 attained from Acros Organics (UK). The ultrapure water was prepared by a model Aqua Max-Ultra ultra-pure water purification system (United State). Stock solutions of 1000 mg L^{-1} of standards were prepared by dissolving appropriate amount of compounds in methanol, which remain stable for three months if stored in a fridge at 4 °C. Working standard solutions were prepared daily by diluting the stock standard solution with methanol to the required concentrations.

3.2 Instrumentation

The Fourier transform infrared (FT-IR) spectra were recorded on a Perkin–Elmer FT-IR between 4000 and 400 cm^{-1} (Perkin Elmer, Massachusetts, USA). Structural elucidation was determined using ^1H NMR, JEOL 400 MHz (JEOL, Tokyo Japan). X-ray powder diffraction (XRD) analysis was conducted with Panalytical model Empyrean at 40 kV and 35 mA using Cu Kα radiation (λ= 1.54059 Å) (Panalytical,

Almelo, Netherlands). Morphological analysis of the synthesized products were performed using JEOL JSM-7600F field emission scanning electron microscope operated at 3 kV (JEOL, Tokyo Japan) and transmission electron microscopy (TEM) analysis using an FEI Tecnai G2 spectra microscope (FEI, Hillsboro, USA). The magnetic property was tested using a vibration sample magnetometer (VSM) Model 9600 (Quantum Design Inc., San Diego, USA). Magnetization measurements were carried out in an external field of up to 15 kOe at room temperature. The thermal stability was investigated by thermo gravimetric analysis (TGA); model TGA-STA 1500, with heating rate of 10 °C min^{-1} between 25–900 °C under nitrogen atmosphere (Perkin Elmer, Massachusetts, USA). Brunauer-Emmett-Teller (BET) analysis was carried out using Micromeritics ASAP2020 surface area analyser for determining the pore diameter and the specific surface area of nanosorbents (Micromeritics, Georgia, USA). Adsorption studies were investigated using Shimadzu Ultraviolet-Visible spectroscopy (UV–Vis), equipped with 1 cm quartz cells (Shimadzu, Kyoto, Japan).

3.3 Chromatographic Condition

Separation and detection of target analytes were performed by a Shimadzu 2010 gas chromatograph (Shimadzu, Kyoto, Japan) equipped with a split/splitless injector and a flame ionization detector (FID). A DB-5 Agilent fused-silica capillary column (Agilent, California, USA) (30 m × 0.32 mm i.d. × 0.25 µm film thickness) was applied for separation of analytes. Helium (with 99.999% purity) was used as the carrier gas at a constant flow rate of 4 mL min^{-1}. Chromatographic conditions were controlled as described; the temperatures of the injector and detector were set at 260 °C and 280 °C, respectively. The injection port was operated at splitless mode. Oven temperature was held at 150 °C for 1 min and increased to 280 °C at 8 °C min^{-1} for 3 min.

3.4 Preparation of MNP Coated Functionalized Polythiophene Nanocomposites

3.4.1 Synthesis of Functionalized Thiophene Monomers

Figure 3.1 shows thiophene and its derivatives used in this study. Two were commercially available monomers; thiophene (Th) and 3-hexylthiophene (3Th) were distilled prior used. Other two monomers were synthesized as shown in Scheme 3.1 and Scheme 3.2.

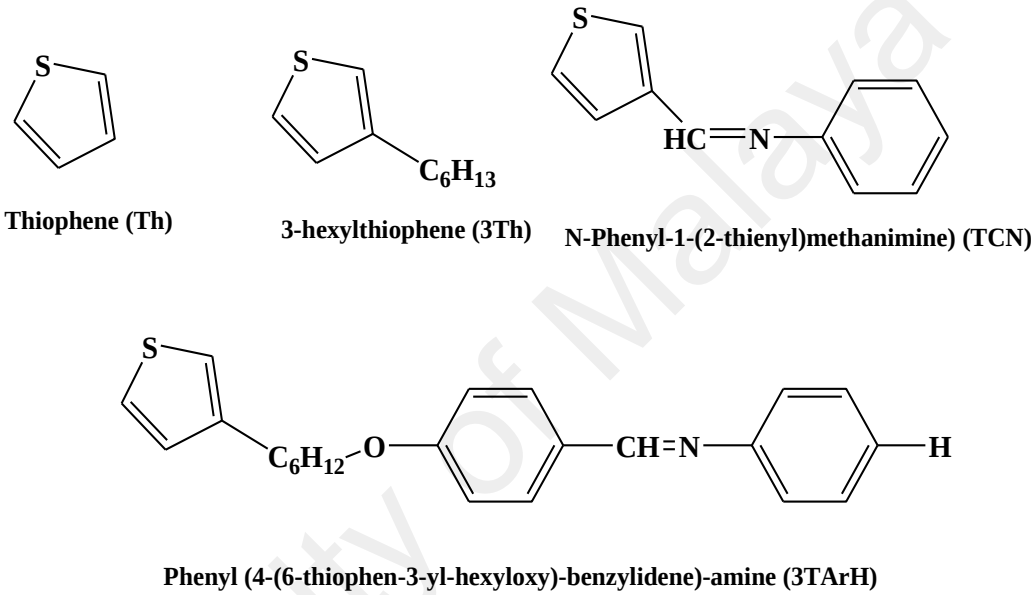

Figure 3.1: Thiophene monomers used in this study

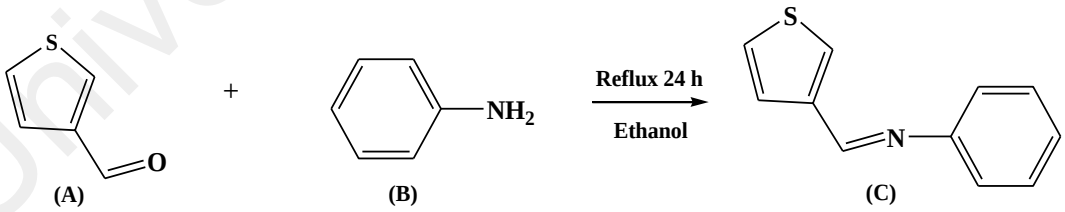

Scheme 3.1: Reaction pathway of N-phenyl-1-(2-thienyl)methanimine) (TCN)

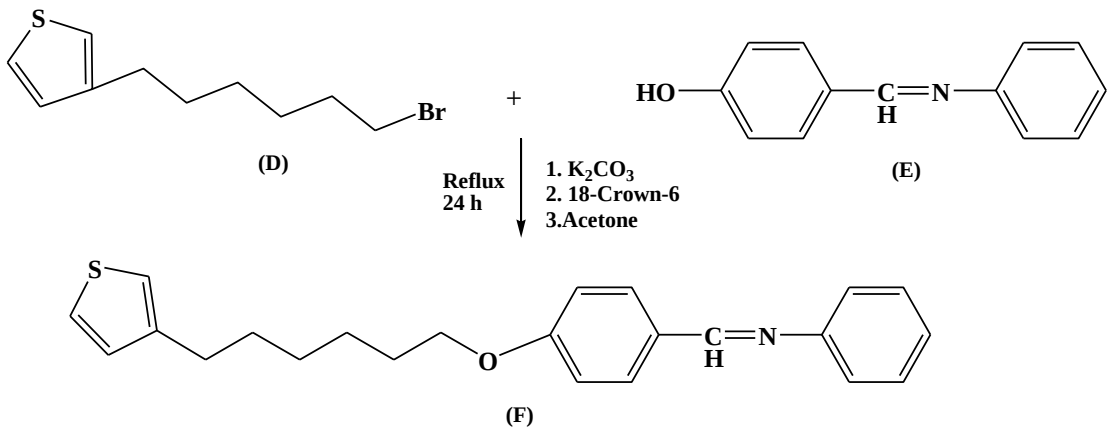

Scheme 3.2: Reaction pathway of phenyl (4-(6-thiophen-3-yl-hexyloxy)-benzylidene)amine (3TArH)

3.4.1.1 Synthesis of N-phenyl-1-(2-thienyl)methanimine) (TCN)

- N-phenyl-1-(2-thienyl)methanimine), TCN prepared from method established by Borque (2010) with some modifications. 3-thiophene carboxaldehyde (A) (10 mmol, 1.12 g) was added to 30 mL of absolute ethanol. Subsequently, (10 mmol, 0.93 g) of aniline (B) was poured into the solution. The mixture was refluxed at 70 °C for 4 h and stirred at room temperature for 15 h. Solvent removal by vacuum distillation (0.8 Torr) gave viscous orange oil. Yield: 78 %. ^{1}H NMR (400 MHz, $CDCl_3$) δ (ppm): 7.18 (m, 1H, C*H*=$C_{thiophene}$), 7.36 (m, 2H, C*H*-S-C*H*), 7.59-7.63 (m, 5H, Ar*H*), 8.55 (s, 1H, C*H*=N), refer Appendix B. FT-IR (cm^{-1}): 3062 (C-$H_{aromatic}$), 1623.05 (C=N), 1589.22, 1423.89 (C=C), 709.86 (C-S).

3.3.1.2 Synthesis of Phenyl(4-(6-thiophen-3-yl-hexyloxy)-benzylidene)amine (3TArH)

Synthesis of phenyl(4-(6-thiophen-3-yl-hexyloxy)-benzylidene)amine, 3TArH consists of two steps. The first step is to prepare the intermediates which were 3-

bromohexylthiophene, 3BHT and 4-((phenylimino)methyl)phenol, 4PIMP. Second step was combining the two intermediates by Williamson etherification method.

- 3-bromohexylthiophene, 3BHT: 3-bromothiophene (2 mL, 21.3 mmol) was added to the dry, degassed hexane (50 mL). The reaction started by cooling the flask at -78 ^{o}C. *n*-butylithium in hexane (2.0 M, 10.16 mL) was poured into the reaction flask and stirred for 10 min. THF (5 mL) was injected drop wise for 15 minutes and continuously stirred for 1 h which produced white precipitate and clear supernatant liquid. The supernatant liquid was removed and changed with hexane/THF (10:1 v/v, 55 mL). 1, 6-dibromohexanes (32.7 mL, 213 mmol) was added and stirred for 2 h. The reaction was stopped with addition of saturated $NaHCO_3$ (50 mL), diluted diethyl (100 mL). The organic layer was washed with water (100 mL), brine (100 mL), dried with magnesium sulfate anhydrous, treated with decolorizing charcoal, filtered and concentrated in vacuum to give orange oil. Removed excess 1, 6-dibromohexane via vacuum distillation (0.04 torr, 55 ^{o}C) and purified silica gel column chromatography (ethyl acetate/hexane, 1/99 to 5/95 v/v) to obtain oily product. Yield: 52 %. ^{1}H NMR (400 MHz, $CDCl_3$) δ (ppm): 1.25-1.50 (m, 4H, (CH_2)$_2$(CH$_2$)$_2$Br), 1.57 (m, 2H, CH_2CH$_2$C=CH$_{thiophene}$), 1.78 (m, 2H, CH_2CH$_2$Br), 2.45-2.60 (m, 2H, CH_2 C=CH$_{thiophene}$), 3.51 (m, 2H, CH_2Br), 6.98 (m, 2H, *H*C=CC*H*$_{thiophene}$), 7.42 (m, 1H, SC*H*=CH$_{thiophene}$), refer Appendix C. FT-IR (cm^{-1}): 3005.47 (C-H$_{aromatic}$), 2933.71 (C-H$_{aliphatic}$), 1551.4, 1459.60 (C=C$_{aromatic}$), 773.32 (C-S$_{thiophene}$), 643.4 (C-Br), refer Appendix A (b).
- 4-((phenylimino)methyl)phenol, 4PIMP: 4-hydroxybenzaldehyde (122 mg, 10 mmol) was added to (112 mg, 10 mmol) 2-aminobenzenethiol in 50 mL ethanol. The mixture was refluxed for 3 h. Yellow crystal was obtained after recrystallized with ethanol. Yield: 95 %.^{1}H NMR (400 MHz, $CDCl_3$) δ (ppm):

6.91 (m, 2H, Ar*H*OH), 7.10-7.41 (m, 5H, Ar*H*), 7.77 (m, 2H, Ar*H*OH), 8.46 (s, 1H, HC=N), 10.13 (s, 1H, ArHO*H*), refer Appendix D. FT-IR (cm^{-1}): 3411 (C-OH), 3098 (C-$H_{aromatic}$), 1609 (C=N), 1588, 1504 (C=$C_{aromatic}$), refer Appendix A (a).

- Phenyl(4-(6-thiophen-3-yl-hexyloxy)-benzylidene)amine, 3TArH**:** A mixture of 4PIMP (1.97 g, 10 mmol), anhydrous potassium carbonate (4.14 g, 30 mmol) and 18-Crown-6 (16.6 mg, 0.1 mmol) was stirred in dried acetone (50 mL) at room temperature. Then compound 3BHT (0.81 g, 2 mmol) was added. The reaction mixture was refluxed under nitrogen with stirring for 24 h. After cooling to room temperature, the reaction mixture was poured into the saturated solution of potassium carbonate. The organic phase was collected and washed by water (3 × 100 ml), dried by anhydrous sodium sulphate. The solvent was removed by reduced pressure, and the residue was dried by vacuum to give the crude product. Purification was accomplished by column chromatography on silica with 25 % hexane in chloroform to afford the monomer (Chen *et al.*, 2012). Yield: 67.6 %. ^{1}H NMR (400 MHz, DMSO-D_6) δ (ppm)**:** ^{1}H NMR (400 MHz, $CDCl_3$) δ (ppm): 0.88 (m, 2H, C*H*$_2$$(CH_2)_2$O), 1.35-1.55 (m, 2H, C*H*$_2$$(CH_2)_2$C=$CH_{thiophene}$), 1.65 (m, 2H, C*H*$_2$$CH_2$C=$CH_{thiophene}$), 1.85 (m, 2H, C*H*$_2$$CH_2$O), 2.75 (m, 2H, C*H*$_2$C=$CH_{thiophene}$), 4.02 (t, 2H, C*H*$_2$O), 6.67 (m, 1H, C*H*-$C_{thiophene}$), 6.75 (m, 1H, SC*H*=$C_{thiophene}$), 6.88 (m, 1H, SC*H*=$CH_{thiophene}$), 6.97 (m, 2H, Ar*H*CH=N), 7.10 (m, 2H, Ar*H*), 7.20 (m, 2H, OAr*H*), 7.35 (m, 1H, Ar*H*), 7.85 (m, 2H, Ar*H*N=CH), 8.48 (s, 1H, *H*C=N), refer Appendix E. FT-IR (cm^{-1})**:** 2980 (C-$H_{aromatic}$), 2934 (C-$H_{aliphatic}$), 1617 (C=N), 1599.9, 1426.71 (C=$C_{aromatic}$), 1239.71, 1018.26 (C-O), 709.24 (C-S), refer Appendix A (c).

3.4.2 Synthesis of Fe_3O_4 Nanoparticles (MNP)

Briefly, Fe_3O_4 has been prepared by co-precipitation method refer to previous study (Shen *et al.*, 1999). $FeCl_3 \cdot 6H_2O$ (8.48 g) and $FeCl_2 \cdot 4H_2O$ (2.25 g) were dissolved in 400 mL deionized water under nitrogen atmosphere with vigorous stirring (1000 rpm) at 80 °C. Then, 20 mL ammonia solution (25% wt.) was added to the solution. The colour of bulk solution immediately changed from orange into black. After stirring the mixture for 5 min, the Fe_3O_4 NPs precipitate obtained was separated by magnetic decantation and washed several times with deionized water. Finally, the Fe_3O_4 NPs obtained were dried in a vacuum oven at 70 °C for 12 h.

3.4.3 Synthesis of MNP Coated Functionalized Polythiophene Nanocomposites

The surface of Fe_3O_4 nanoparticles were modified by coating with newly designed modified thiophene monomers via oxidation polymerization with generation of ferric cations on the MNP surface (Shin & Jang, 2007). The preparation of MNP coated functionalized polythiophene is illustrated in Figure 3.2 by giving example of schematic diagram for the preparation of MNP coated poly(phenyl(4-(6-thiophen-3-yl-hexyloxy)-benzylidene)amine) (P3TArH). MNP (1 mmol, 0.235 g) were discreted in polyvinyl alcohol aqueous solution (0.001 M). Later, monomer (10 mmol) was added into the mixed solution with vigorous stirring. Subsequently, 30 mL of HCl (0.5 M) solution was introduced into the mixture. Then the obtained product was dried in a vacuum oven at 70 °C for 12 h. The experiment was repeated for other different monomers (thiophene, 3-hexylthiophene and N-phenyl-1-(2-thienyl)methanimine)).

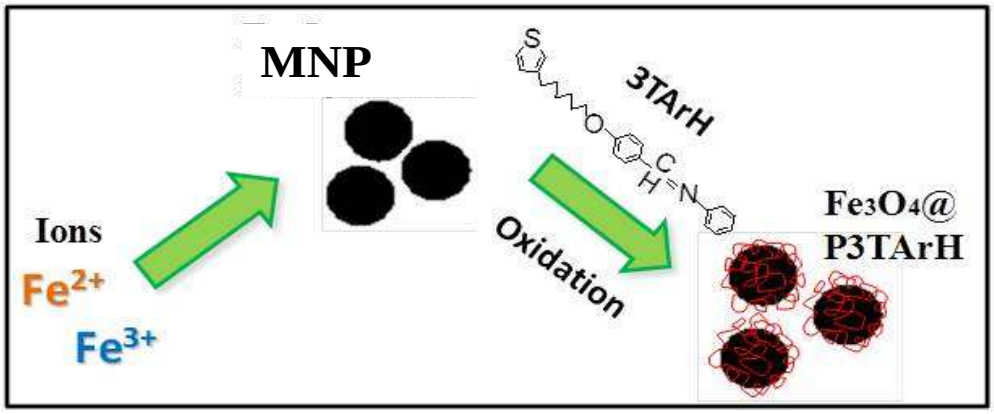

Figure 3.2: Schematic diagram for preparation of Fe_3O_4 coated poly(phenyl(4-(6-thiophen-3-yl-hexyloxy)-benzylidene)-amine) (P3TArH) (Baharin *et al.*, 2016)

3.5 Screening Study

All the synthesized nanocomposites were screened to determine optimum sorbent for the extraction of phthalates. Screening procedures were conducted with 10 mg of each synthesized nanocomposites (MNP@PTh, MNP@P3Th, MNP@PTCN and MNP@P3TArH) to the 20 mL of phthalate solution at pH 7. Samples were shaken via orbital shaker for 30 min. Then, the sorbent were separated from the liquid via magnetic decantation. After that, sorbents were added with 500 µL ethyl acetate with and shaken for 10 min. The supernatant liquid were collected and dried with purified nitrogen prior analysis using GC-FID.

3.6 Adsorption Studies of DEHP on MNP Coated Poly(phenyl(4-(6-thiophen-3-yl-hexyloxy)-benzylidene)amine) (P3TArH).

Experimental parameters were optimized using batch experiments for effect of pH, kinetics and thermodynamic studies, effect of initial concentration, equilibrium studies and reusability studies. Sorption experiments were determined by the following

batch method: in each experiment, 5 mg of adsorbent was mixed with 5 mL of an aqueous solution of DEHP at a known concentration in a tightly sealed vial. The solution was shaken for 1 h on a shaker at room temperature. After the adsorption process, the adsorbent was separated by magnetic decantation, and the residual concentration was determined using Shimadzu Ultraviolet-Visible spectroscopy (UV–Vis), equipped with 1 cm quartz cells (Shimadzu, Kyoto, Japan). All the samples were performed in triplicate. The removal efficiency, R (%) was calculated using the following equation:

$$R\ (\%) = \frac{(C_o - C_e)}{C_o} \times 100 \quad \textbf{(3.1)}$$

The amount of DEHP adsorbed per unit mass of the adsorbent (q_e) was calculated as:

$$q_e = \frac{(C_o - C_e)}{W} V \quad \textbf{(3.2)}$$

C_o and C_e are the initial and equilibrium concentrations of the solutions (mg L^{-1}), respectively. V (L) is the volume of the solution, and W (g) is the mass of the dry adsorbent being used.

3.7 Application of MNP Coated Poly(phenyl-(4-(6-thiophen-3-yl-hexyloxy)-benzylidine)amine) as a New Sorbent for Magnetic Solid-Phase Extraction (MSPE) of Phthalates

3.7.1 Optimization Parameters

Factors affecting the extraction efficiency of the proposed method such as pH, extraction time, sample volume, elution solvent, elution solvent volume, desorption time, adsorbent dosage and effect of NaCl were studied. Reusability studies were

conducted for five cycles to determine the possibilities for reutilizing and regeneration were investigated and optimized. The study and optimization of the above-mentioned variables were performed using the one variable at a time method. The chromatographic peak area was used to evaluate influence of the factors on the extraction efficiency of MSPE of the target analytes. All the experiments were performed in triplicate, and the means of the results were used in plotting of the optimization curves.

10 mg of MNP coated poly(phenyl-(4-(6-thiophen-3-yl-hexyloxy)-benzylidine)amine) was dispersed to the 20 mL of phthalates solution at pH 7 containing 15 g L^{-1} concentration of NaCl. Samples were shaken via orbital shaker for 30 min. Then, the sorbent were separated from the liquid via magnetic decantation. After that, sorbents were added with 500 µL ethyl acetate with and shaken for 10 min. The supernantant liquid were collected and dried with purified nitrogen prior analysis using GC-FID.

3.7.2 Method Validation

In order to evaluate the figures of merit of the proposed technique, linearity, limit of detection (LOD) and repeatability were investigated under optimized conditions. The linearity was analysed through the standard curves ranging from 0.08 to 1 µgL^{-1} by diluting appropriate amounts of phthalates stock solution (1000 mgL^{-1}) with methanol and prepared in triplicate. The calibration curves were prepared using 10 spiking levels of analytes concentration. For each level, three replicate experiments were performed. Method chosen for this study is linear regression that can be exposed to model as;

$$y = mx + c \quad \textbf{(3.3)}$$

This model is used to determine the sensitivity in the LOD and LOQ. Therefore, the LOD and LOQ can be stated as;

$$\mathrm{LOD} = \frac{3\ s.d}{\mathrm{m}} \quad \textbf{(3.4)}$$

$$\mathrm{LOQ} = \frac{10\ s.d}{\mathrm{m}} \quad \textbf{(3.5)}$$

where *s.d* is the standard deviation of the response and m is the slope of the calibration curve. The standard deviation of the response can be estimated by the standard deviation of *y*-intercepts (Shrivastava & Gupta, 2011). Preconcentration factor (P.F) can be calculated as following equation;

$$\mathrm{P.F} = \frac{\text{Sample Volume}}{\text{Eluent volume}} \quad \textbf{(3.6)}$$

Precision of the method was investigated by repeatability (intra-day) and intermediate precision (inter-day) of both standard and sample solutions. Precision was determined in seven replicates of phthalates on the same day (intra-day precision) and daily for 3 days (inter-day precision). Results were presented as RSD (%) (Bhadra *et al.*, 2011).

$$\mathrm{RSD}(\%) = \frac{\mathrm{s.d}}{\mathrm{mean}} \times 100 \quad \textbf{(3.7)}$$

3.7.2.1 Real Sample Analyses

To evaluate reliability of the proposed method for extraction and preconcentration of the plasticizers from real samples, two real water samples were selected, spiked (50 µg L^{-1}) and subjected to the MSPE–GC–FID analysis with the optimized condition of

10 mg of MNP coated poly(phenyl-(4-(6-thiophen-3-yl-hexyloxy)-benzylidine)amine) was dispersed to the 20 mL of samples volume solution at pH 7 containing 15 g L^{-1} concentration of NaCl. Samples were shaken via orbital shaker for 30 min. Then, the sorbent were separated from the liquid via magnetic decantation. After that, sorbents were added with 500 µL ethyl acetate with and shaken for 10 min. The supernantant liquid were collected and dried with purified nitrogen prior analysis using GC-FID.

Two real samples were a commercial bottled mineral water and a bottled of fresh milk. Recovery was calculated using following equation;

$$\text{Recovery (\%)} = \frac{\text{Spiked concentration} - \text{unspiked concentration}}{\text{spiked concentration}} \; x \; 100 \quad \textbf{(3.8)}$$

CHAPTER 4: RESULTS AND DISCUSSION

4.1 Characterization of Samples

Characterization of naked magnetic nanoparticles (MNP) and synthesized nanocomposites (MNP@PTh, MNP@P3Th, MNP@PTCN and MNP@P3TArH) were performed and elaborated at below section.

4.1.1 Fourier Transform Infra-Red Spectroscopy (FT-IR)

Figure 4.1 shows several additional peaks in the spectrum of nanocomposites, proportional to the iron oxide spectrum, which might be due to the surface functionalization. The strong absorption peaks in the range of ~3400 cm^{-1} for naked MNP and all nanocomposites indicated the presence of OH vibration, while the peak at 530–632 cm^{-1} corresponds to Fe–O stretching modes (Aydın *et al.*, 2011).

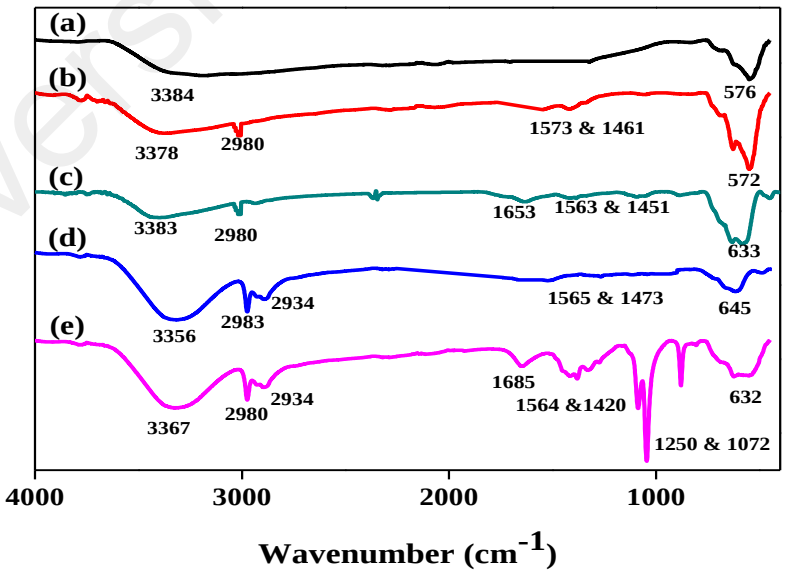

Figure 4.1: FT-IR spectrum of (a) naked magnetic nanoparticles, (b) MNP@PTh, (c) MNP@PTCN, (d) MNP@P3Th and (e) MNP@P3TArH nanocomposites

The C–H aromatic stretching peak was observed for all nanocomposites, which falls at ~2980 cm^{-1}. C–H sp^3 stretching (hexyl aliphatic side) occurred at 2934 cm^{-1} for MNP@P3Th and MNP@P3TArH. Schiff base peaks C=N was observed at 1653 cm^{-1} MNP@PTCN and 1685 cm^{-1} for MNP@P3TArH (Vasanthi & Ravikumar, 2013). C=C aromatic symmetric and asymmetric absorption bands demonstrated in the range of 1573–1461 cm^{-1} for MNP@PTh, 1563-1451 cm^{-1} for MNP@PTCN, 1565-1473 cm^{-1} for MNP@P3Th and 1564-1420 cm^{-1} for MNP@P3TArH. Two absorption band peaks at 1250 and 1072 cm^{-1} indicated the presence of C–O in MNP@P3TArH. Hence, FT-IR study clearly revealed that all nanocomposites prepared has been successfully coated.

4.1.2 X-Ray Difractometer (XRD)

Figure 4.2 displays the characteristic peaks observed for naked MNP and all nanocomposites prepared (MNP@PTh, MNP@P3Th, MNP@PTCN and MNP@P3TArH). The peak of the nanocomposites was slightly wider than MNP. This is might be because of the presence of amorphous and polymeric materials (Cótica *et al.*, 2010). The characteristic peaks of were observed at 2Θ = 30°, 35.7°, 43°, 53.4°, 57.0°, and 62.6°, which are marked by their respective indices [(220), (311), (400), (422), (511) and (440)] (Giri *et al.*, 2005). This showed that the surface functionalization does not change crystalline phase of MNP.

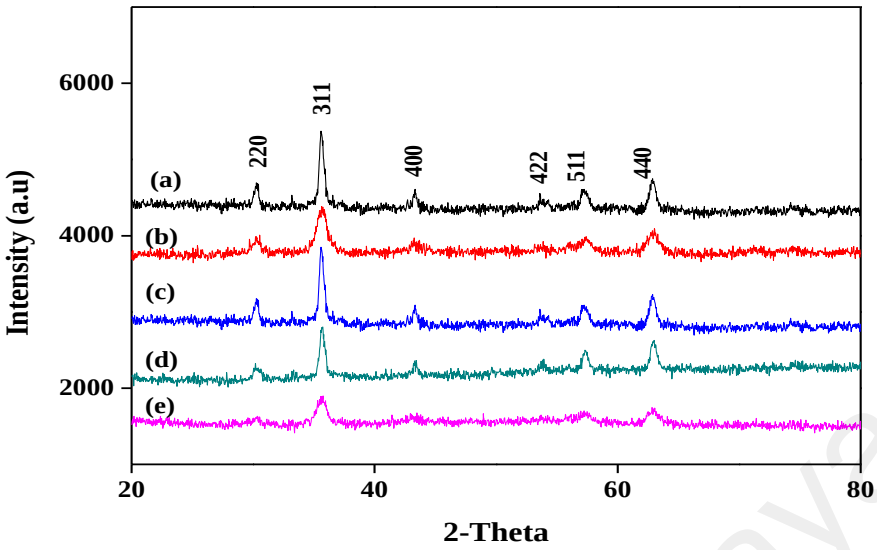

Figure 4.2: Diffractograms of (a) naked magnetic nanoparticles, (b) MNP@PTh, (c) MNP@PTCN, (d) MNP@P3Th and (e) MNP@P3TArH nanocomposites

4.1.3 Brunauer–Emmett–Teller (BET)

The BET surface area is measured using the multipoint BET method, within the relative pressure (P/P_0) range of 0.05 to 1. As described in Appendix F, the MNP and all nanocomposites display a H3 type hysteresis loop based on the Brunauer-Deming-Deming-Teller (BDDT) classification, demonstrating the existence of mesopores with pore diameters between 2-50 nm (Sing, 1985). The pore size and BET surface area of MNPs and nanocomposites are tabulated in Table 4.1. The decrease in pore size of nanocomposites is due to the addition of polymer coating on the surface. Increase in the surface area maybe attributed by the aggregation of particles that resulted in the enhancement of the spaces between them (Darab *et al.*, 1994; Wang *et al.*, 2008).

Table 4.1: BET pore size and surface area

Sample	Pore size (nm)	Surface Area (m^2 g^{-1})
MNP	20.2	37.37
MNP@PTh	18.3	95.6
MNP@PThC=N	13.3	97.3
MNP@P3HexTh	12.6	96.5
MNP@P3TARH	12.09	103.80

.

4.1.4 Thermo Gravimetric Analysis (TGA)

Figure 4.3 shows TG analysis for MNP and nanocomposites. Small weight loss was detected under 200 °C in MNP and nanocomposite, speculated to be due to desorption of adsorbed water on the surface of the nanoparticles. Since Fe-O is thermodynamically steady within a temperature range of 280 °C to 850 °C, thus no weight loss is observed for Fe_3O_4 after 200 °C (Mahdavi *et al.*, 2013). The thermograms of nanocomposite indicated that it is stable up to 210 °C. However, above this temperature all nanocomposites exhibited rapid weight loss in the temperature ranging from 240 °C and 450 °C. This might be due to the decomposition of polymer coating. Herein, thermal analysis study showed that the surface of MNP has been successfully coated with functionalized polythiophenes.

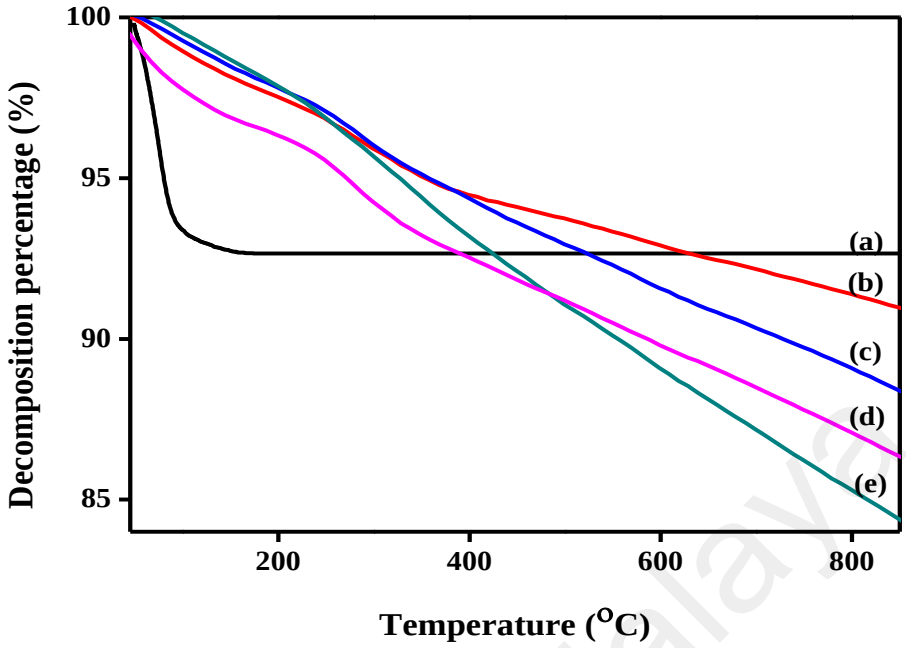

Figure 4.3: Thermogram of (a) naked magnetic nanoparticles, (b) MNP@PTh, (c) MNP@PTCN, (d) MNP@P3TArH and (e) MNP@P3Th nanocomposites

4.1.5 Vibrating Sample Magnetometer (VSM)

Magnetic properties of the samples were recorded at room temperature with an external field of ±15 kOe. M-H hysteris curves of MNP, MNP@PTh, MNP@PThC=N, MNP@P3HexTh and MNP@P3TArH are presents in Figure 4.4. Important magnetic parameter, which is saturation magnetization (M_S), was assessed. As clear from the hysteresis loops, magnetization did not occur until maximum applied field and exhibited superparamagnetic behavior (Jayabharathi *et al.*, 2015). Maximum saturation (M_S) of MNP and nanocomposites appeared at 92 (bulk magnetization) and ~63.2 emu g^{-1}, respectively. MNP@PTCN and MNP@P3TArH demonstrated high magnetization saturation compares to other nanocomposites. This can be due to the Schiff base groups have been designed for shielding the magnetic core of MNP from oxidation that may reduce its magnetization (Issaadi *et al.*, 2011).

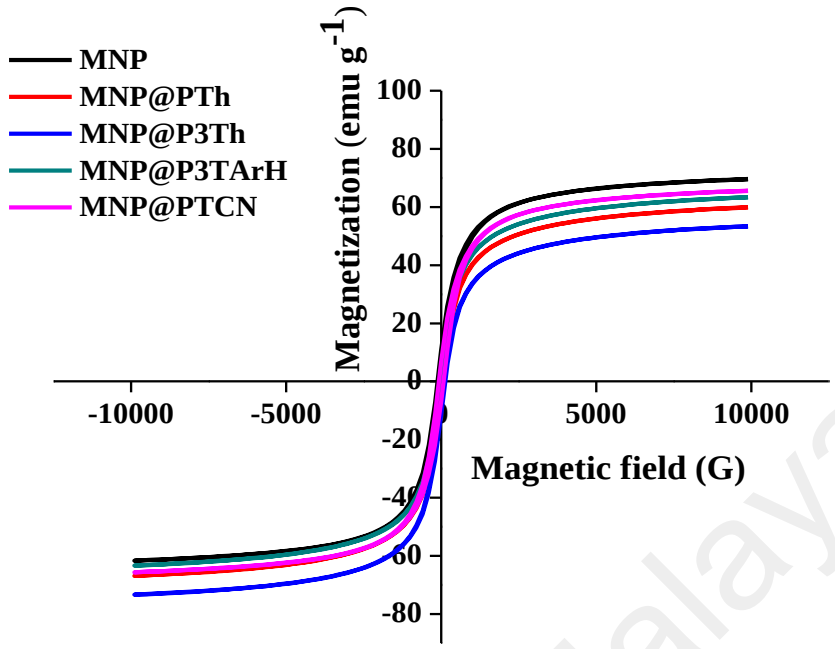

Figure 4.4: Magnetization analysis of MNP and nanocomposites

Reduced magnetization signify the presence of a dead magnetic layer on the surface of the nanocomposites (Aydın *et al.*, 2011). Although magnetization is reduced in nanocomposite, but still the value of magnetization falls within the acceptable range, which suggest that they can be separated conveniently from a solution with an external magnetic field (Ma *et al.*, 2005).

4.1.6 Morphological Analysis

Significance improvement in surface area of MNP@P3TArH as shown by BET results, we decided to further study its morphological properties. Figure 4.5 demonstrates morphological analyses of the MNP and MNP@P3TArH using field emission scanning electron microscopy (FESEM) and transmission electron microscopy (TEM) techniques. FESEM and TEM images of all materials exhibited a sphere-shaped geometry. As evident from the TEM analysis, the distribution of the modified

nanoparticles (MNP@P3TArH) is very uniform and nanoparticles are segregated. This may be due to the presence of polymeric material coating, reduces the aggregation and stabilizes the magnetic nanoparticles (Shin & Jang, 2007).

Analysis of TEM images using the IMAGEJ software determined the average of particle diameter distribution by computing the values corresponding to at least 300 nanoparticles. Based on the histogram plotted in Figure 4.5 (e) and (f), D_{TEM}, an average diameter, and σ, a standard deviation values were calculated. TEM average particle size for MNP@P3TArH was found to be 13.070 ± 2.916 nm. The average particle size MNP was larger than the average particle size of MNP@P3TArH determined from the TEM which might be due to many nanoparticles are accumulated and overlaid on top of one another, and cannot be measured accordingly (Cótica *et al.*, 2010).

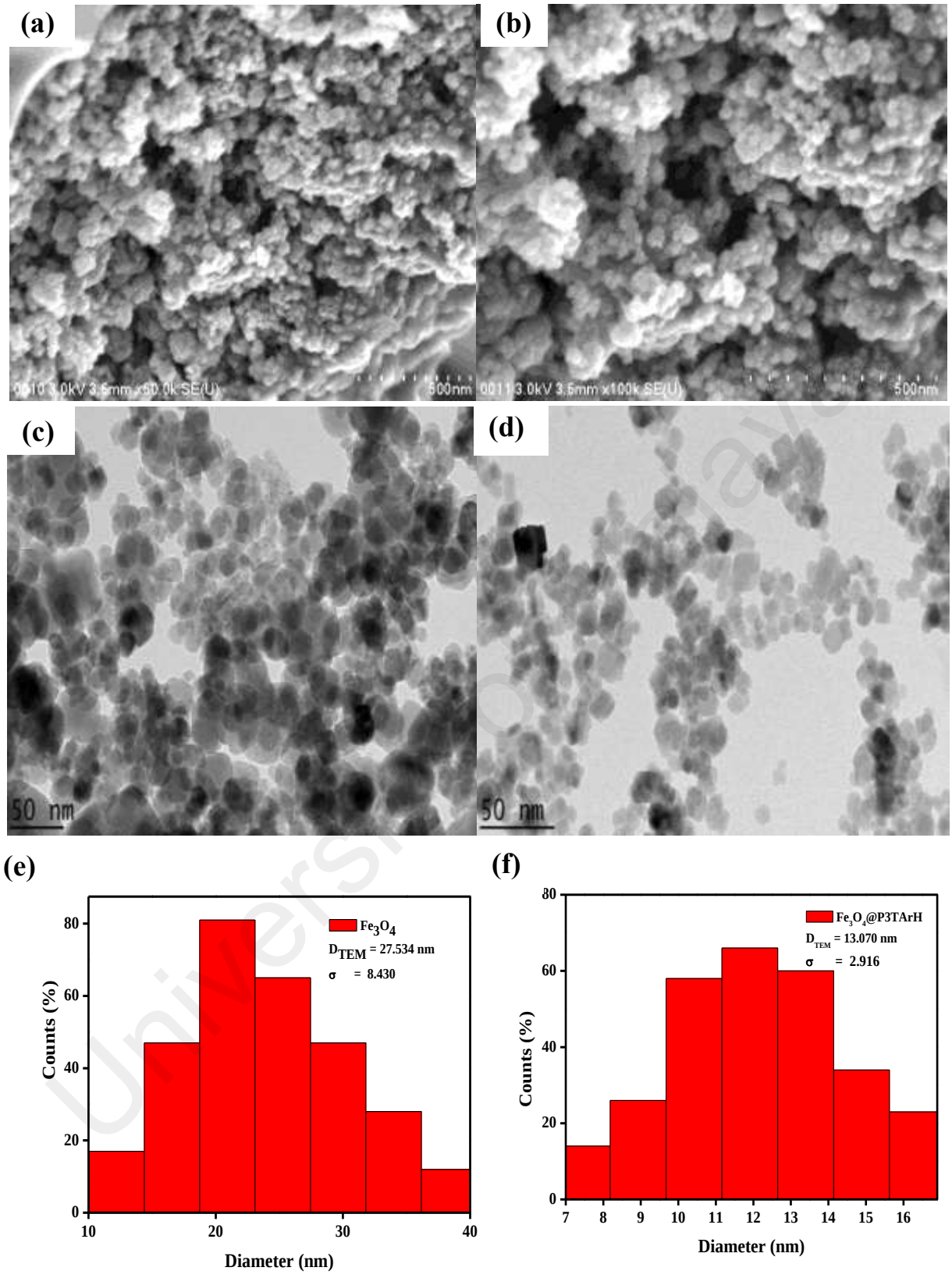

Figure 4.5: FESEM images of a) MNP, b) MNP@P3TArH; TEM images of c) MNP, d) MNP@P3TArH; and diameter distribution of e) MNP, f) MNP@P3TArH

4.2 Screening Studies

Hypothetically, the adsorption of phthalates is based on the hydrophobicity and π–π dispersion (Moreno-Castilla, 2004). To prove that the structure architecture can influence the adsorption of phthalates, five different types of sorbent, which are naked magnetic nanoparticles (MNP), MNP@PTh, MNP@PTCN, MNP@P3Th, and MNP@P3TArH were tested. As shows in Figure 4.6, MNP resulted in an insignificant peak area for all of the analytes studied. After the introduction of polythiophene derivatives on the surface of MNP, the peak area of phthalates increased

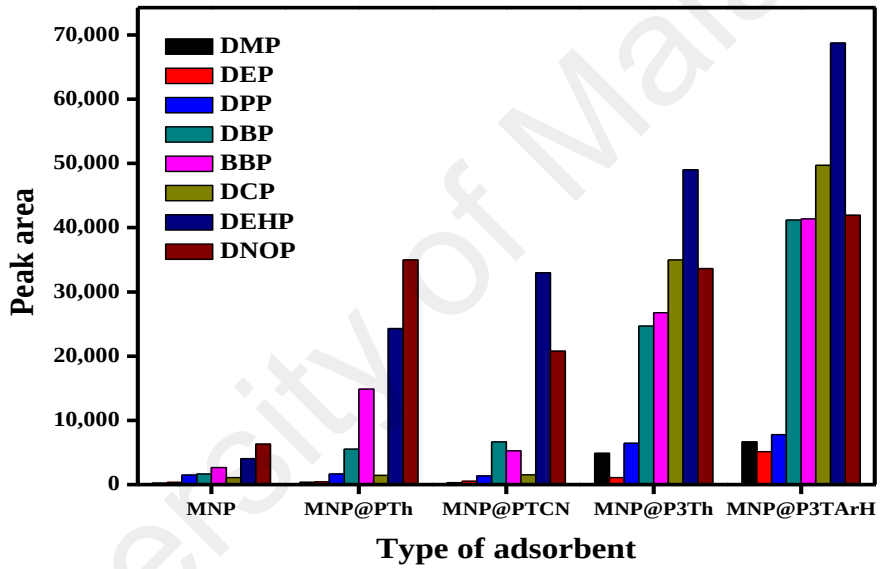

Figure 4.6: Effect of adsorbent for the extraction of the targeted phthalates

The presence of aliphatic and aromatic groups in the MNP@P3TArH enhances the dispersion of phthalates, which enhances the π–π dispersion and hydrophobic interactions. As evidenced, butyl benzyl phthalate (BBP) is more prone to the adsorbent with more aromatic sides, as in the MNP@PT3ArH, compared to the other adsorbents. Besides, the high surface area of MNP@P3TArH also contributes to the increase of extraction performance. Since the MNP@P3TArH has demonstrated the high peak area for all analytes studied, it was selected for further adsorption and MSPE optimization.

4.3 Adsorption of Studies of DEHP on P3TArH Coated Magnetic Nanoparticles

4.3.1 Effect of Magnetic Nanoparticle Loading

Optimum amount Fe_3O_4 loading on P3TArH for the adsorption of DEHP was investigated. As described in Figure 4.7, when the loading of Fe_3O_4 reached to 10 % the adsorption efficiency increased and decreased later after 10 %. This can be due to the, less amount of loading, contributes to low surface area and reduced the actives site for adsorption, while the increase of loading beyond the optimum can caused particles agglomeration (Akpan & Hameed, 2009; Munusamy *et al.*, 2013). Therefore, 10 % of Fe_3O_4 from the total moles of monomer was chosen as the optimized loading and used for further experiments.

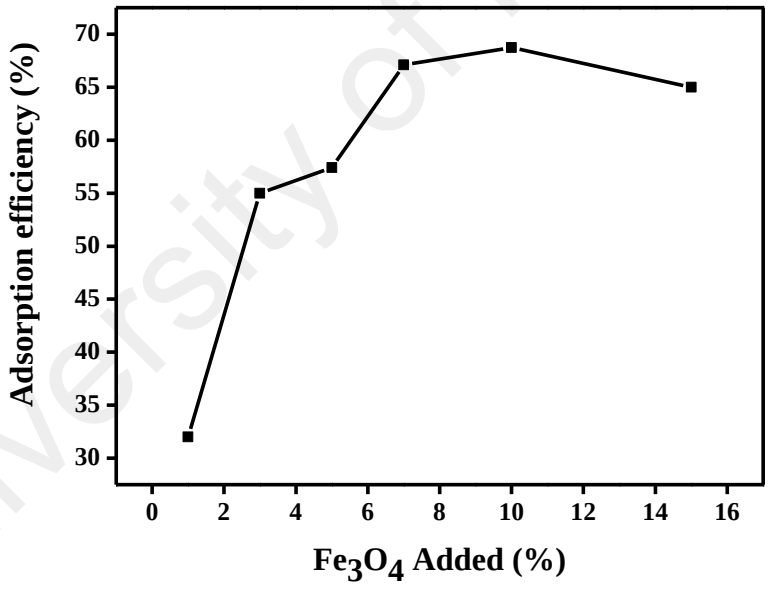

Figure 4.7: Percentage of Fe_3O_4 nanoparticles added to the total mole of monomer for adsorption of DEHP

4.3.2 Effect of pH

Adsorption was performed under different pH conditions, ranging from pH 3 - 10. As evidenced by Figure 4.8(a), adsorption efficiency increases when the pH increases

from 5 to 7, but decreases later from 7 to 10. Whereas, Figure 4.8(b) demonstrated zeta potential analysis of MNP@P3TArH with effect of pH range 3 to 9 which represents the surface charge of MNP@P3TArH. At low pH, C=N groups in MNP@P3TArH were protonated, making the adsorbent surface positively charge. As described in Scheme 4.1 (a)**,** at pH<7, DEHP hydrolyzes to phthalic acid, since the carbonyl group in the phthalic acid is nucleophilic in nature, it can easily react with hydrogen ions in the solution to form positively charged species. Due to both absorbate and adsorbent acquiring positive charges, the electrostatic repulsion occurred and retarded the adsorption performance (Mohan *et al.*, 2002).

Moreover, based on zeta potential result at higher pH, surface of the adsorbent became negatively charge due to deprotonation of C=N in MNP@P3TArH, whereas adsorbate hydrolyzes to phthalate anions as shown in Scheme 4.1(b) resulting in the repulsion and thereby, reduces the adsorption efficiency (Fang & Huang, 2009). Strong adsorptive performance in neutral pH can be explained by strong interactions between the hydrophobic and π-π interactions in MNP@P3TArH with DEHP. Since the optimum performance of adsorption of DEHP was demonstrated at pH 7, this pH was selected for the entire experiments.

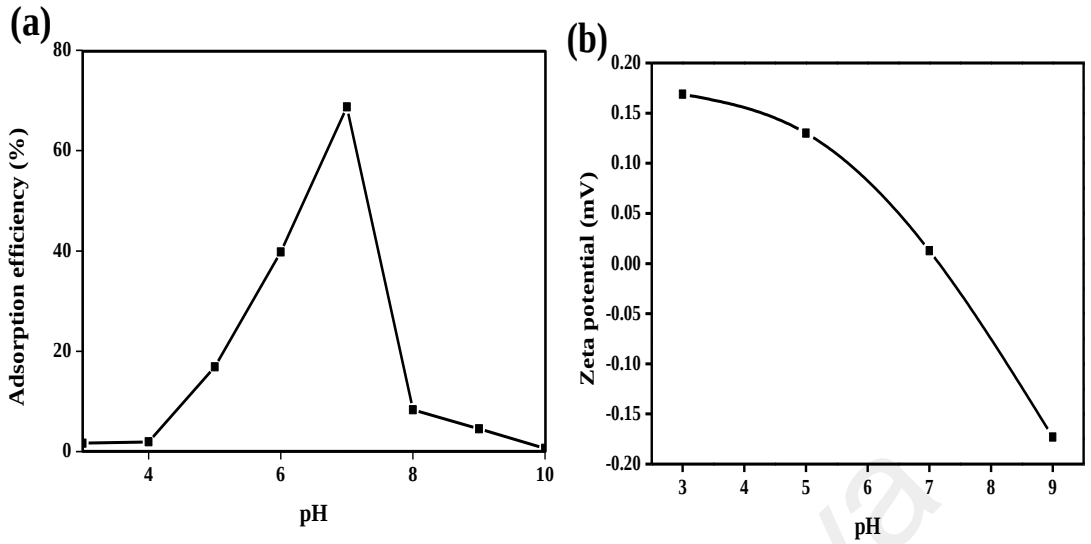

Figure 4.8: (a) Effect of solution pH (b) The zeta potential of MNP@P3TArH at various pHs

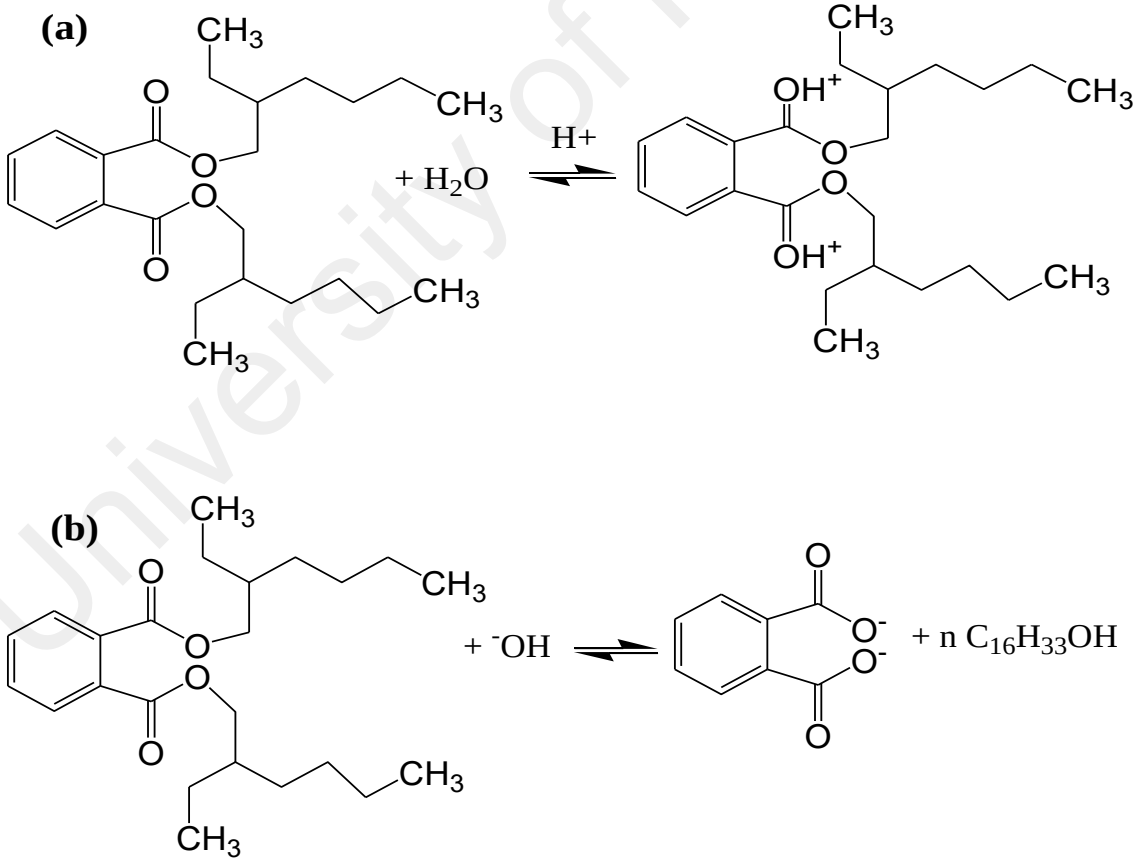

Scheme 4.1: (a) DEHP at pH<7 and (b) DEHP at pH>7

4.3.3 Kinetic and Thermodynamic Studies

The effect of contact time for the removal of DEHP by MNP@P3TArH was investigated in the time range of 0–180 min at four different temperatures of 298.15 K, 318.15 K, 323.15 K and 333.15 K. Figure 4.9 demonstrates that the adsorption capacity was rapid for the first 15 min; which might be due to the many available active sites for adsorption. From 120 min to 180 min, the removal capacity was observed to be constant; therefore, 120 min could be regarded as the equilibrium time.

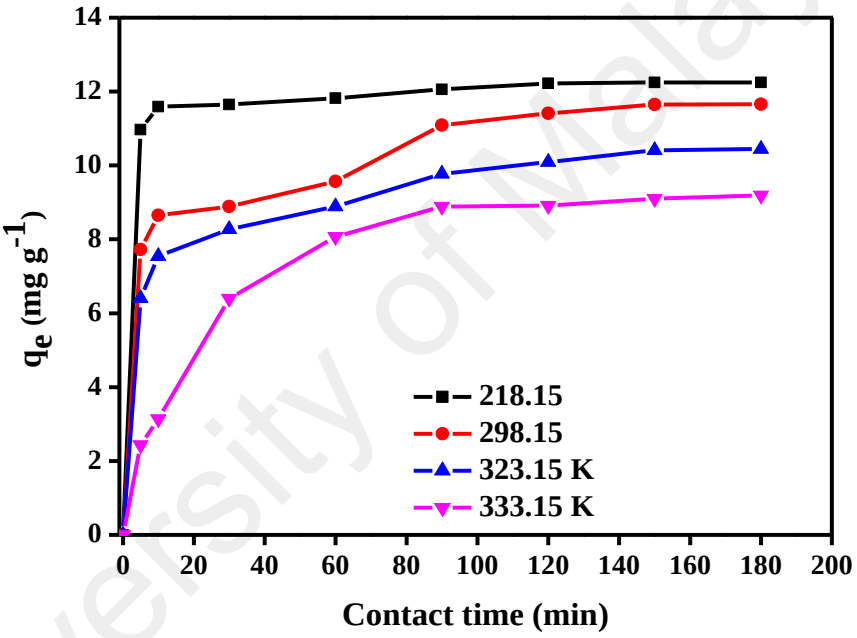

Figure 4.9: Effect of contact time and temperature for the adsorption of DEHP onto MNP@P3TArH

To further determine the adsorption mechanism and kinetics parameters, the data gained were fitted into three types of kinetics models, pseudo first-order, pseudo second-order, and intraparticle diffusion (Febrianto *et al.*, 2009; Ho & McKay, 2000; Memon *et al.*, 2011; Pan *et al.*, 2008; Weber & Rumer, 1965). The pseudo first-order kinetic model is extensively used to study the adsorption of an adsorbate from an aqueous solution. The equation can be expressed as;

$$log(q_e - q_t) = log\ qe - (\frac{k_1}{2.30})t \quad \textbf{(4.1)}$$

where q_e and q_t are the amount of DEHP adsorbed (mg g^{-1}) at equilibrium and time, t is the contact time (min), and k_1 is the rate constant of this equation (min^{-1}). k_1 and q_e were determined from the plot of $log(q_e - q_t)$ versus t. Meanwhile, pseudo-second order kinetic model is based on the assumption that the adsorption mechanism depends on the both adsorbate and adsorbent (Pavan *et al.*, 2008). The linear equations pertaining to this area follows;

$$\frac{t}{q_t} = \frac{1}{k_2 {q_e}^2} + \frac{1}{q_e} t \text{ , where } h = k_2 {q_e}^2 \text{ and } t_{\frac{1}{2}} = k_2 {q_e}^{-1} \quad \textbf{(4.2)}$$

where h is the initial adsorption rate (mg g^{-1}) min, $t_{1/2}$ is half equilibrium time (min), and k_2 is the pseudo second-order rate constant (g mg^{-1} min). A linear plot of t/q_t vs. t could be used to determine the value of q_e, k_2, h and $t_{1/2}$ respectively. The kinetics parameters and correlation coefficient are listed in Table 4.2. It can be seen that the experimental data is fitted with pseudo second-order kinetic model with R^2 near to unity and can be further confirmed by the nearness of the calculated and experimental q_e value. Similar adsorption behavior was also found for the removal of diethyl phthalate by activated carbon (Venkata Mohan *et al.*, 2007). Next, the parameters for intraparticle diffusion models were calculated according to the linear equation as follows;

$$q_t = Kt^{0.5} + c \quad \textbf{(4.3)}$$

where c is thickness of boundary layer (mg g^{-1}) and K is the rate constant (mg g^{-1} min^{-1}).

Table 4.2: Kinetic parameters for the adsorption of DEHP onto MNP@P3TArH

Kinetic Models	**MNP@P3TArH**			
	298.15 K	**318.15 K**	**323.15 K**	**333.15 K**
Pseudo-first order				
q_e, *exp*(mg g^{-1})	12.22	11.413	10.09	8.914
q_e, *cal*(mg g^{-1})	10.6	7.45	6.06	11.57
k_1(min^{-1})	0.0363	0.0317	0.0221	0.0603
R^2	0.7296	0.8754	0.8193	0.9216
Pseudo-second order				
q_e, *cal*(mg g^{-1})	12.30	11.89	10.60	9.85
k_2(min^{-1})	0.083	0.015	0.014	0.008
R^2	0.9999	0.9957	0.9936	0.9926
Intraparticle Diffusion				
K (mg g^{-1} min^{-1})	0.831	0.744	0.695	0.692
c (mg g^{-1})	3.278	3.251	3.214	1.321
R^2	0.705	0.842	0.957	0.9057

Figure 4.10 reveals that the plots are not linear throughout the contact time, however, a similar trend for four temperatures were observed, and the plots were divided into two parts; at the start of the experiment, a steeper line was detected, which might be due to a massive transfer of DEHP from the boundary layer to the surface of the MNP@P3TArH. After 8 min, the line continued to be linear, due to diffusion of DEHP through the mesopores of MNP@P3TArH (Jalil *et al.*, 2010).

From the intraparticle diffusion model parameters, the adsorption of DEHP onto MNP@P3TArH can be assumed as an exothermic reaction, since the value of boundary layer thickness decreases with the increases of temperature (Tewari *et al.*, 1972). Higher temperature resulting the increment of solubility of DEHP to aqueous solution and increased the collision between adsorbents molecules which led to lower intraparticle diffusion rate (Yadava *et al.*, 1989).

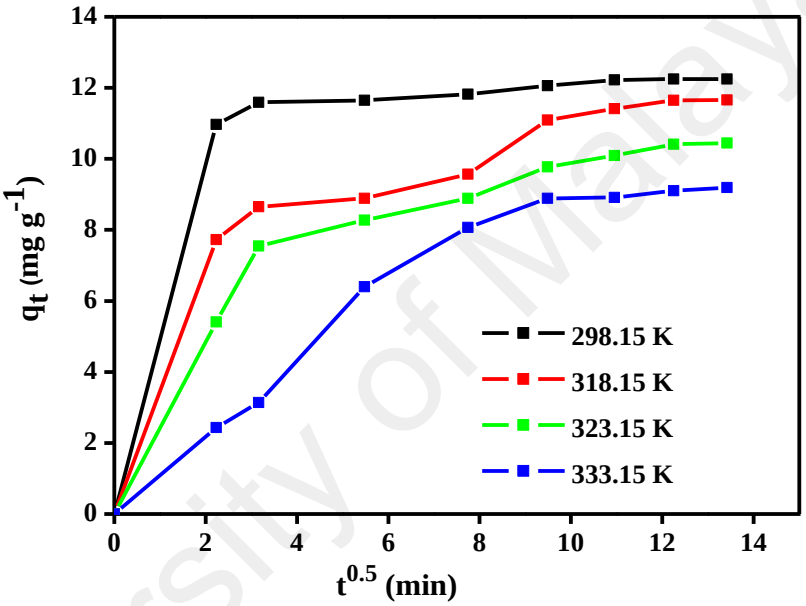

Figure 4.10: Intraparticle diffusion plots

The thermodynamic parameters were determined to investigate the mechanism of the adsorption process. The values of adsorption enthalpy (ΔH°), entropy (ΔS) and Gibbs free energy (ΔG°), are revealed in Table 4.3, which were calculated using the following equations;

$$\ln K_c = \frac{\Delta S}{R} - \frac{\Delta H}{RT} \quad \textbf{(4.4)}$$

$$K_c = \frac{C_{e\,(adsorbent)}}{C_{e\,(solution)}} \quad \textbf{(4.5)}$$

$$\Delta G° = -RT \ln K_c \quad \textbf{(4.6)}$$

From the plot of ln K_c against 1/T, the (ΔH°) value was found to be negative, which confirms that the adsorption process is exothermic in nature. The increase in temperature enhanced the surface activity of DEHP, increasing its affinity to water (Minling *et al.*, 2015). The (ΔS) value was negative, demonstrating that the system reached an ordered state due to the decrease in the randomness of adsorbate/aqueous phase (Aydın & Aksoy, 2009). Decreased ΔG° values with elevating temperature indicated that the process favours low temperature (Salleh *et al.*, 2015). Moreover, negative values of ΔG° was in the range between -20 and 0 kJ mol^{-1}, indicating that the adsorption process is thermodynamically feasible, physically controlled, and spontaneous (Kilic *et al.*, 2011; Zarrouk *et al.*, 2011). The activation energy of the adsorption process can be calculated from the plot of k_2 (pseudo second order rate constant) against 1/T using the Arrhenius equation;

$$lnk_2 = \ln A - \frac{E_a}{R}\left(\frac{1}{T}\right) \quad \textbf{(4.7)}$$

The value of activation energy for the adsorption of DEHP onto MNP@P3TArH was found to be -40.6 kJ mol^{-1} K^{-1}. Negative value of sorption activation energy demonstrating the process favors at low temperature (Saha & Chowdhury, 2011). Moreover, the value of activation energy could be used to determine the adsorption behavior; if the value is less than <40 kJ mol^{-1}, the process is physisorption, and if its >40 kJ mol^{-1}, it is predominantly a chemical adsorption process.

Table 4.3: Thermodynamic parameters for DEHP adsorption onto MNP@P3TArH

T (K)	q_e, (mg g^{-1})	ΔG° (kJ mol^{-1})	ΔH° (kJ mol^{-1})	ΔS (kJ mol^{-1} K^{-1})
298.15	12.22	-2.883		
318.15	11.41	-1.650	-19.77	-0.057
323.15	10.09	-1.151		
333.15	9.10	-0.881		

4.3.4 Effect of Initial DEHP Concentration and Isotherms Equilibrium Studies

Figure 4.11 demonstrates the effect of initial concentration of DEHP in the range of 5-90 mg L^{-1} at 298 K. The adsorptive capacity increases with the increasing of initial concentration of DEHP from 5 mg L^{-1} and reaches equilibrium at 15 mg L^{-1} with 11.8 mg g^{-1}. This indicates that a maximum concentration for 5 mg of MNP@P3TArH in 5 mL aqueous solution is 15 mg L^{-1} DEHP to give significant adsorption efficiency. At low concentration, the removal is significant due to the readiness of many active sites for adsorption whereas at high concentration, the removal is persistent due to all available active sites in adsorbent are fully occupied by DEHP.

To study the adsorption isotherm, four models, Langmuir, Freundlich, Temkin, and Dubinin-Radushkevich (D-R) were utilized to explain the adsorption behaviour of DEHP onto MNP@P3TArH. The Langmuir isotherms model is based on the expectations that the monolayer adsorption homogenously occurred on all active sites, with no additional adsorption after the sites are fully occupied by the solute at uniform energy (Srivastava *et al.*, 2006).The Langmuir equation is,

$$\frac{1}{q_e} = \frac{1}{bq_m} + \frac{C_e}{q_m} \quad \textbf{(4.8)}$$

where C_e (mg L^{-1}) is the equilibrium concentration of the adsorbate, C_o (mg L^{-1}) is the initial adsorbate concentration, q_e (mg g^{-1}) is the adsorption capacity at equilibrium,

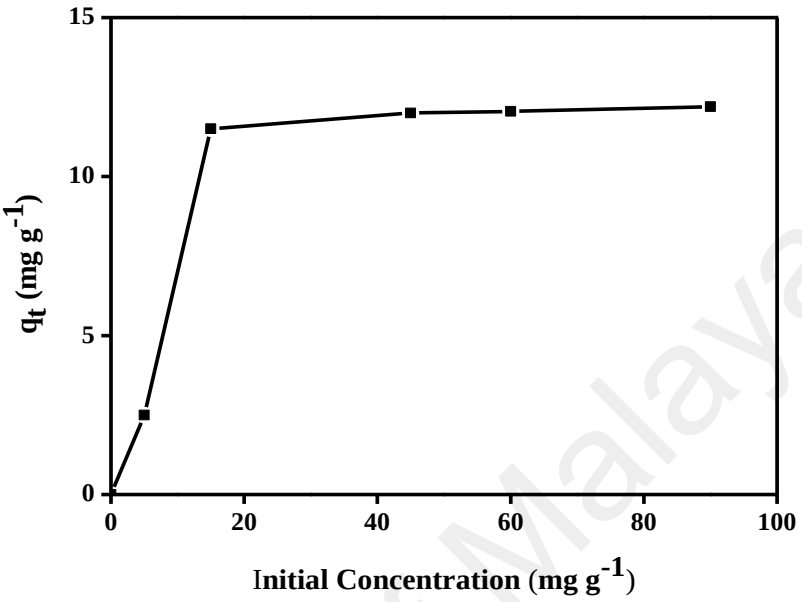

Figure 4.11: Effect of DEHP initial concentration

q_m (mg g^{-1}) and b (L mg^{-1}) are Langmuir constant related to the adsorption capacity and rate of adsorption, respectively. To determine whether the process is either favourable or unfavourable, the dimensionless separation factor (R_L) can be calculated from;

$$R_L = \frac{1}{1+bC_o} \quad \textbf{(4.9)}$$

From the plot of C_e/q_e versus C_e, the values of Langmuir parameters were determined. In contrast to the Langmuir isotherm model, the Freundlich isotherm model assumed that adsorption heterogeneously occurred on the adsorbent's surfaces, with different energies of active sites (Mckay *et al.*, 1982). The following equations determined the values of Freundlich constant;

$$\log q_e = \log K_F + \frac{1}{n}\log C_e \quad \textbf{(4.10)}$$

where K_F ((mg g^{-1}) (L mg^{-1})$^{1/n}$) is the adsorption capacity, while 1/*n* represents Freundlich constants, respectively. The Dubinin-Radushkevich isotherm model takes into account the porosity of the adsorbent. The experimental data was fitted with a plot of ln q_e against ϵ^2 as a linear equation in the following form;

$$\ln q_e = \ln q_m - \beta\epsilon^2 \quad \textbf{(4.11)}$$

where β (mol^2 kJ^{-2}) denotes the adsorption energy constant and the Polanyi potential (ε) is mean free energy respectively. E (kJmol^{-1}) can be obtained using the following equations;

$$\epsilon = RT \ln(1 + \frac{1}{C_e}), \quad \textbf{(4.12)}$$

$$E\ (kJ\ mol^{-1}) = \left(2\beta^{-0.5}\right) \quad \textbf{(4.13)}$$

where *R* is the universal gas constant in kJ mol^{-1} K^{-1}, and T is the temperature. The Temkin model was established on the basis that the heat of adsorption would reduce linearly as the layer is covered, resulting in an uneven relationship of adsorbent–adsorbate interfaces on heterogeneous surfaces in adsorption systems (Temkin & Pyzhev, 1940). The Temkin model linear equation is as follows:

$$q_e = \beta \ln K_T + \beta \ln C_e\ , \quad \text{where } b_T = \frac{RT}{\beta} \quad \textbf{(4.14)}$$

A plot of q_e versus ln C_e from the linear equation could be used to determine the Temkin constant, where K_T (L mg^{-1}) is the Temkin constant related to the equilibrium binding energy, and b_T (J mol^{-1}) is Temkin constant related to the heat of adsorption.

Amid the four isotherms studied, from Table 4.4, the result showed that the adsorption of DEHP onto MNP@P3TArH was better described by Freundlich isotherm

models (R^2 = 0.9833), suggesting that adsorption occurred heterogeneously on adsorption sites. Comparable studies were also found for the adsorption of diethyl phthalate (DEP) using multiwall carbon nanotubes (Wang *et al.*, 2010). Additionally, the Freundlich constant, adsorption capacity K_F, and adsorption intensity 1/*n* value were determined to be 0.6945 mg g^{-1} and 1.168, respectively. High K_F value represented great adsorption affinity towards adsorbate (Xu *et al.*, 2007). Whereas $1/n \geq 1$ indicated favourable adsorption process (Pelit *et al.*, 2011).

Table 4.4: Isotherms parameters for DEHP adsorption of onto MNP@P3TArH

Isotherms model	**Fe_3O_4@P3TArH**
Langmuir	
q_m *(mg* g^{-1}*)*	52.63
b (L mg^{-1}*)*	0.010
R^2	0.8259
R_L	0.8695
Freundlich	
K_F *((mg* g^{-1}*) (L* mg^{-1}*)1/n)*	0.6945
1/n	1.168
R^2	0.9833
Temkin	
K_T *(L* mg^{-1}*)*	0.217
b_T *(kJ/mol)*	276.88
R^2	0.9682
Dubinin-Radushkevich	
q_m *(mg* g^{-1}*)*	20.00
β	10.575
E	0.615
R^2	0. 8502

Figure 4.12 demonstrates an illustration of proposed interaction for multilayer adsorption according to the Freundlich isotherms. When DEHP and MNP@P3TArH come into contact, sorbent active sites which are mesopores (which are confirmed by BET), hydrophobicity (aliphatic) and π-π interaction (aromatic) enhance the attraction of DEHP. At the same time, DEHP-DEHP also attracts to each other which create multilayer adsorption that often observed as physical adsorption process (Lyubchik *et al.*, 2011; Venkata Mohan *et al.*, 2007).

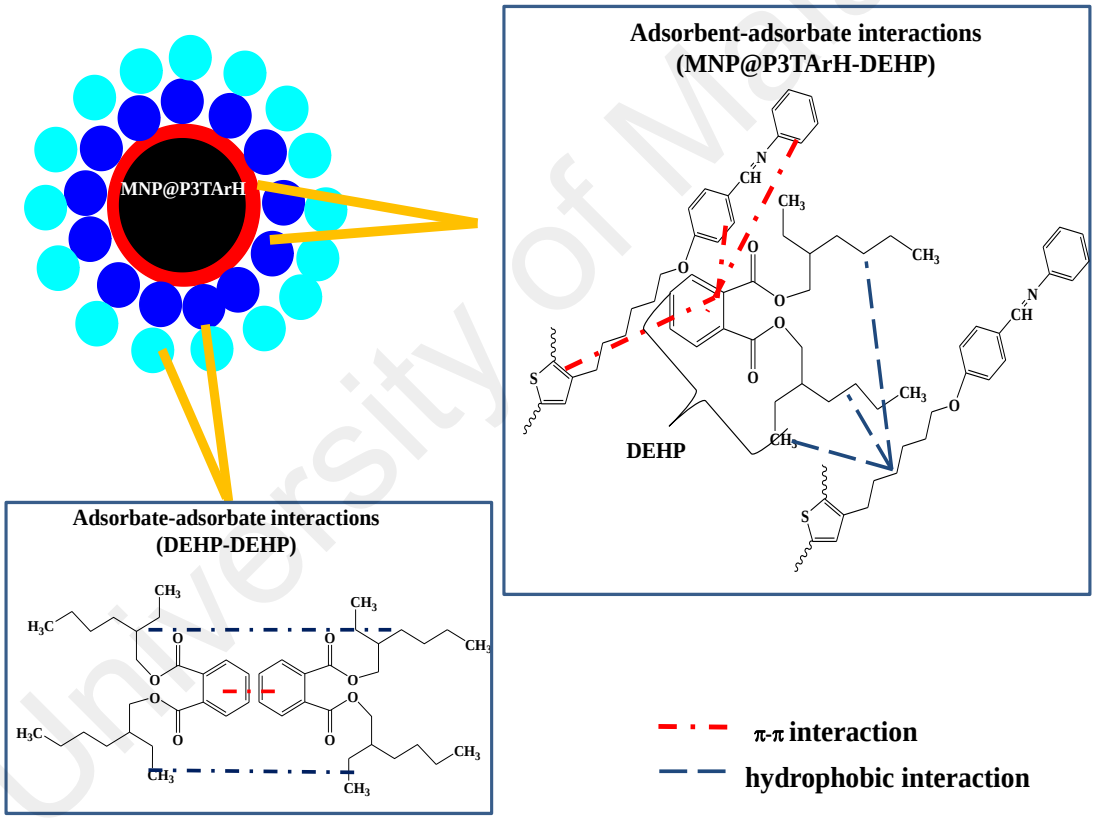

Figure 4.12: Propose interactions for multilayer adsorption (Freundlich)

4.3.5 Reusability Studies

To determine reusability of MNP@P3TArH for adsorption of DEHP, the adsorbent was recycled after being washed with methanol and water, and was dried in vacuum at 70 °C for 12 hours. From Figure 4.13, it could be summarized that after five repeated experiments, the adsorption performance was reduced from 84 % to 64 %. To further confirm the modifications on the sorbent properties, BET surface area analysis and FT-IR of the sorbent were performed after the fifth cycles.

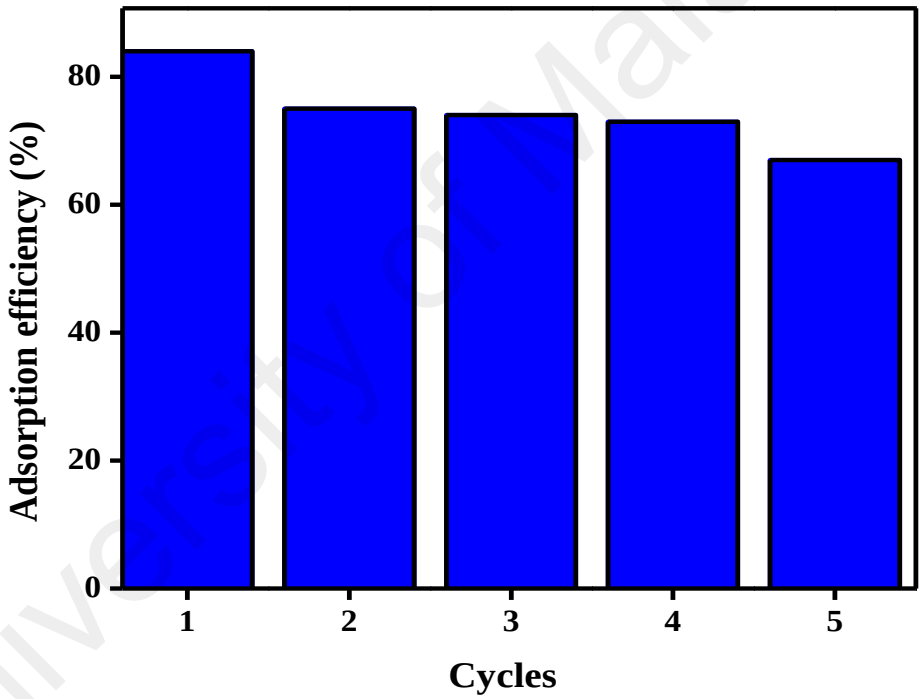

Figure 4.13: Reusability graph for five cycles

From the surface area analysis in Table 4.5, it was found that surface area of the recycled sorbent was significantly reduced. This can be due to the surface modification of the sorbent material which occur up until fifth cycle as confirmed by FT-IR analysis of the recycled sorbent (Cherian *et al.*, 2002). The IR spectrum of recycled sorbent is presented in Figure 4.14, which clearly reveals that the intensity of the polymer coating

reduced significantly after the fifth cycle. As a result, active sites (mesopores) and other physical interactions which have played significant role in adsorption (hydrophobicity, π-π interaction) of DEHP were decreased from the recycled MNP@P3TArH which eventually hampered theirs adsorptive performance with every cycle.

Table 4.5: BET surface area analysis of MNP@P3TArH and recycled MNP@P3TArH

Sample	BET Surface Area (m^2 g^{-1})
MNP@P3TArH	103.8
Recycled MNP@P3TArH	49.566

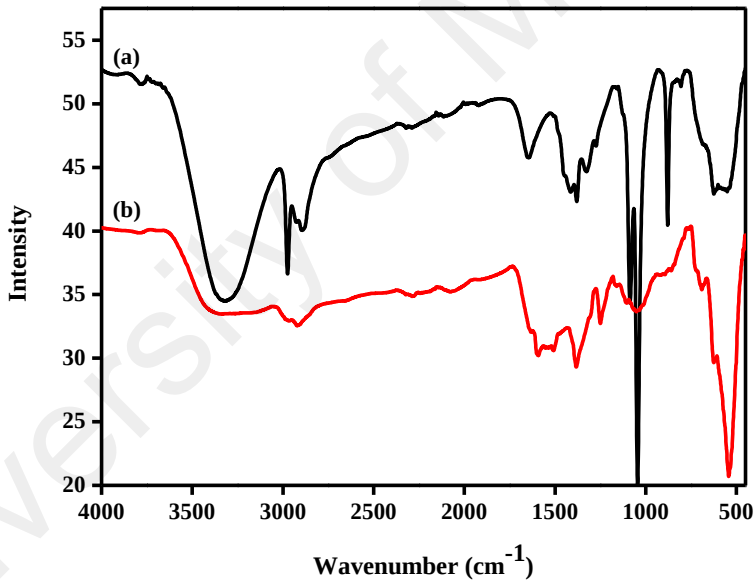

Figure 4.14: FT-IR spectrum of (a) MNP@P3TArH; (b) recycled MNP@P3TArH

4.3.6 Comparative studies

Table 4.6 reveals the comparison of the maximum adsorption capacities of various adsorbents. Chan. H *et al.* (2004) confirmed that breached seaweed resulted in higher adsorption capacity (5.68 mg g^{-1}) as compared to *S.siliquastrum* (6.54 mg g^{-1}) for an adsorbent mass of 0.025 g at 3 hours reaction time. Cheng and Chung (2006) utilized

chitosan bead as an adsorbent to remove DEHP from a plastic manufacturing plant. The value of q_{max} in this study was found to be 11.8 mg g^{-1}, which suggests the MNP@P3TArH used could readily adsorb DEHP.

Table 4.6: Comparison on adsorption capacities

Adsorbent	**Analyte**	**Reaction time (Hours)**	**Maximum adsorption Capacities (mg g^{-1})**	**References**
S. siliquastrum	DEHP	3	5.68	(Chan *et al.*, 2004)
Beached seaweed	DEHP	3	6.54	
Chitosan bead	DEHP	6	0.49	(Chen & Chung, 2006)
Chitosan bead/α - cyclodextrine	DEHP	6	3.09	(C.-Y. Chen *et al.*, 2007)
Bioslurry	DEHP	264	0.972	(Shailaja *et al.*, 2008)
Biofilms	DEHP	-	0.161	(Cao *et al.*, 2014)
MNP@P3TArH	DEHP	2	52.63	This study

4.4 Magnetic Solid-Phase Extraction (MSPE) of Phthalates by Functionalized Polythiophene Coated Magnetic Nanoparticles.

4.4.1. Solid-Phase Extraction Optimization

4.4.1.2 Effect of Sample pH

To study the influence of the surface charge of adsorbent/adsorbate in the extraction process, experiments were performed under different pH conditions, ranging from pH 2–9. Zeta potential analysis for MNP@P3TArH surface charges at different pH were described in previous discussion (Figure 4.8(b)). As described from Figure 4.15, the peak areas for phthalates increase when the pH rise from 2–7, but decline later from 8–9. At low pH, C=N, alkoxy in P3TArH was protonated, making the adsorbent surface positively charged.

At pH<7, phthalates hydrolyze to phthalic acid, thus making the carbonyl group nucleophilic, reacting with hydrogen ions in the aqueous solution, producing positive charges (see Scheme 4.1(a)). Due to both the absorbate and adsorbent acquiring positive charges, the electrostatic repulsion occurred and retarded the adsorption performance (Mohan *et al.*, 2002). At basic conditions, the surface adsorbent became negatively charged, while the adsorbate hydrolyzed to phthalate anions (see Scheme 4.1(b)), reducing the extraction efficiency (Fang & Huang, 2009). Thus, in neutral pH, the extraction increased due to the absence of electrostatic repulsion that disturbed the extraction capability. As the optimum performance was demonstrated at pH 7, this pH was selected for all of the experiments.

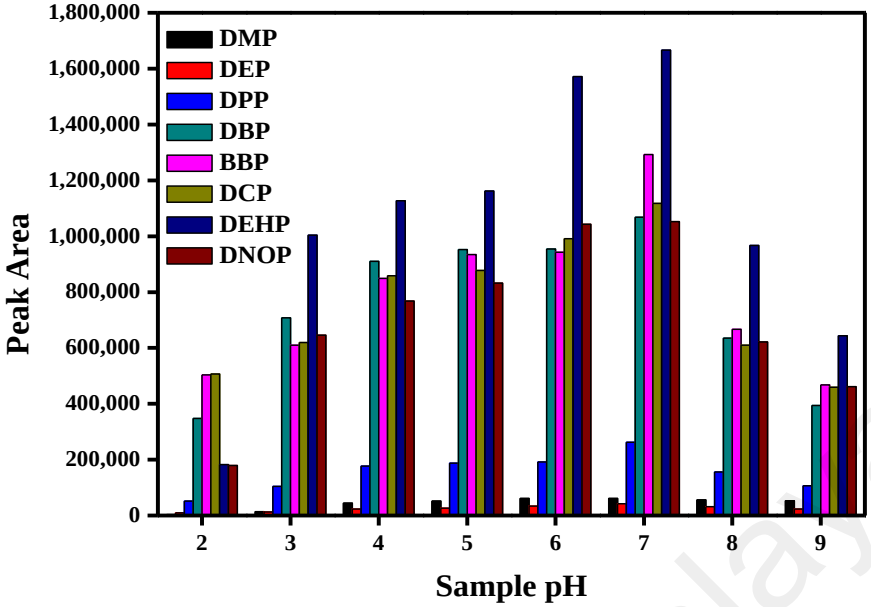

Figure 4.15: Effect of sample pH for the extraction of the targeted phthalates

4.4.1.3 Extraction Time

It has been understood that prolonged extraction time might increase the recovery of analytes. Thus, the influence of extraction time on the recoveries of the analyte has been investigated. As demonstrated in Figure 4.16, the peak area increased rapidly for the first 20 min, since more adsorption sites were available and phthalates could easily interact with these sites. After 30 min, the peak area was almost persistent; therefore, 30 min was sufficient to extract the maximum of the target analytes. In order to ensure that the extraction time was satisfactory, further experiments were carried out until 90 min, and they were found to be constant.

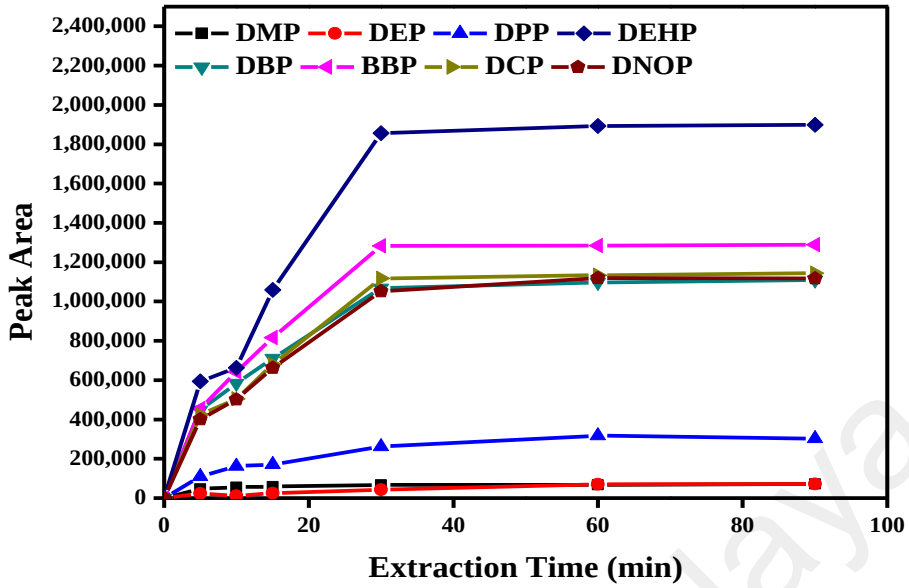

Figure 4.16: Effect of extraction time for the extraction of the targeted phthalates

4.4.1.4 Desorption Studies

The elution solvent is one of the crucial parameters to be considered. In order to determine the best elution solvent, the solvent must be able to elute all of the analytes that were retained from the adsorbent in a small volume (Miskam *et al.*, 2014). Six eluting solvents with dissimilar polarities, namely hexane, toluene, diethyl ether, acetonitrile, methanol and ethyl acetate were studied. As evidenced by Figure 4.17, polar solvents (acetonitrile, methanol and ethyl acetate) were the best solvents, with high peak areas compared to non-polar solvents (hexane, toluene and diethyl ether), since phthalates contain a polar carbonyl group (Wade, 2016). Among the polar solvents, ethyl acetate showed high solvent strength; since it gave the maximum peak area for the phthalates studied and was thus selected to be the eluent.

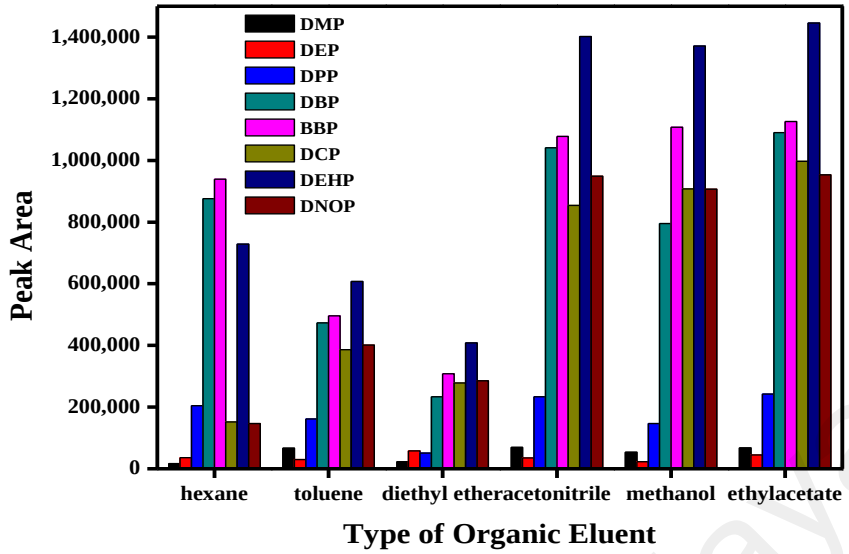

Figure 4.17: Type of organic eluent for the extraction of targeted phthalates

The volume of ethyl acetate was tested from 0.1 mL–2.5 mL. As observed in Figure 4.18, the peak area increased from 0.1 mL and remained constant after 0.5 mL. This shows that 0.5 mL may accommodate the maximum phthalates extracted from the sorbent.

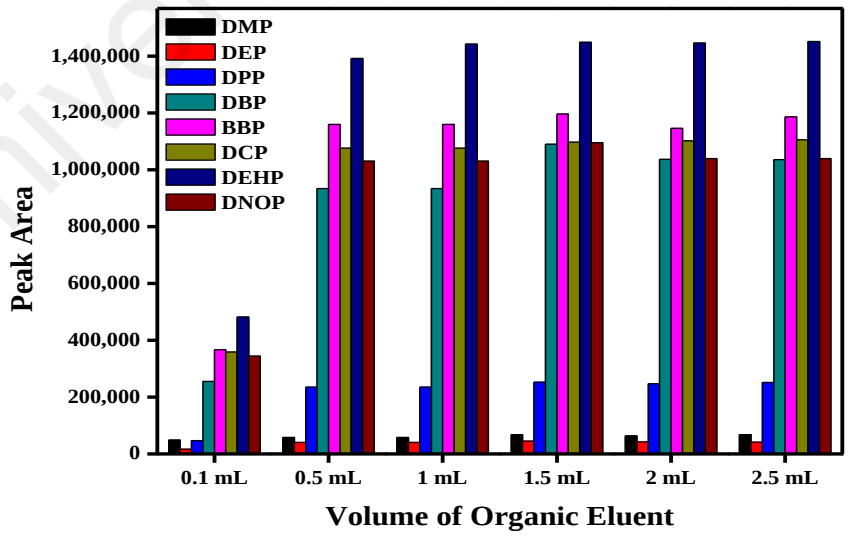

Figure 4.18: Volume of organic eluent for the extraction of targeted phthalates

Further, desorption time was optimized to investigate the best time taken for the analytes to desorb from the sorbent ranging from 0–12 min. As reveals in Figure 4.19, analytes were desorbed rapidly in the first 4 min and started to become linear after 10 min. This indicated that 10 min of time are sufficient to desorb back all of the analytes from the adsorbent. As for the case of BBP, desorption was found to be slower than other phthalates. This could be due to the presence of an additional aromatic ring in BBP, which makes it less polar to the eluent (ethyl acetate). After 6 min of desorption, most of the phthalates had reached near to equilibrium, whereas BBP was desorbed steeply after 6 min until it reached equilibrium at 10 min.

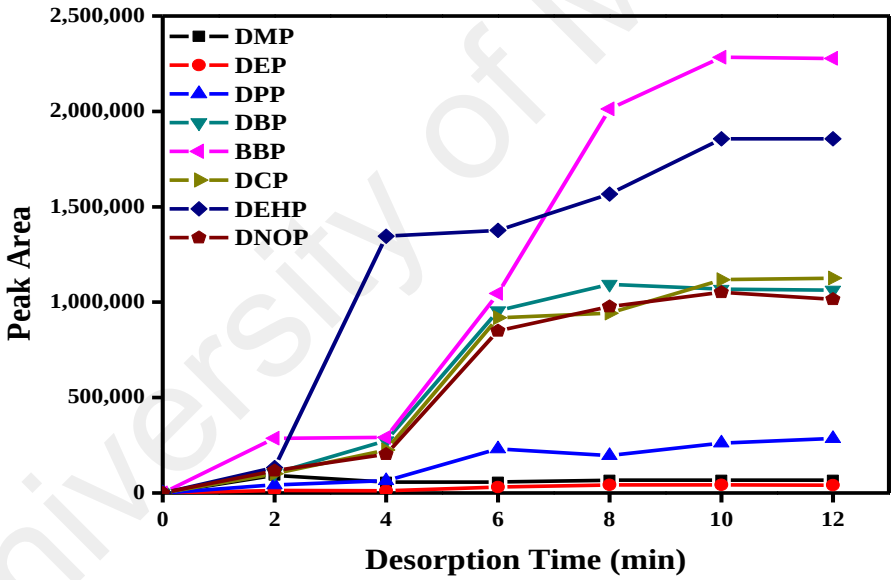

Figure 4.19: Desorption time for the extraction of targeted phthalates

4.4.1.5 Mass of Adsorbent

Investigation of the adsorbent amount was executed in the range of 1–25 mg. As exposes in Figure 4.20, the extraction peak area increased up to 10 mg, but decreased later with a further increase of the adsorbent. Increasing the adsorbent amount provides

more active sites for the adsorption of target analytes. However, a high amount of adsorbent at a specific volume has weakened elution efficiency (Tahmasebi & Yamini, 2014). It is shown that this adsorbent only required a small amount of adsorbent to remove phthalates efficiently, which added the advantage of economic value. Therefore, for further experiments, the adsorbent amount of 10 mg was applied.

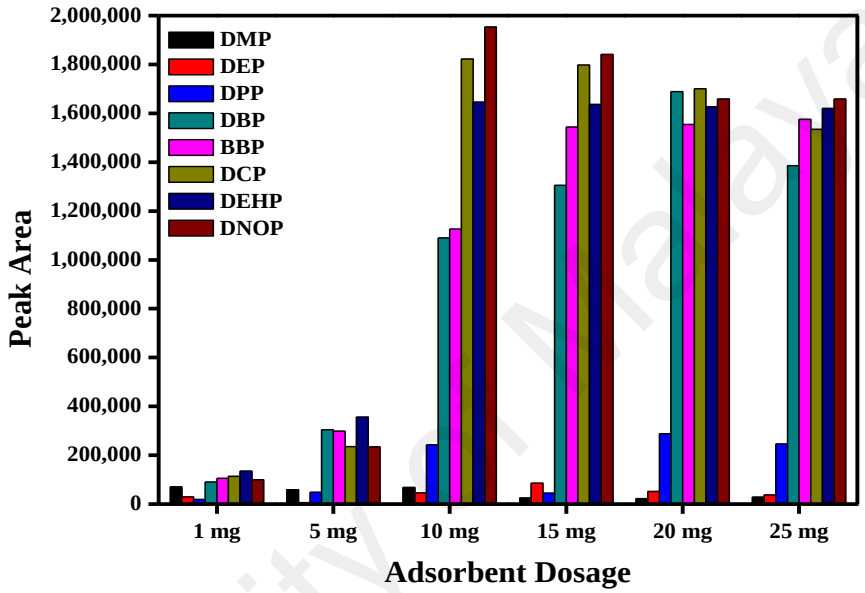

Figure 4.20: Adsorbent dosage for the extraction of targeted phthalates

4.4.1.6 Sample Loading Volume

The effect of sample volume was investigated by the extraction of the phthalates ranging from 5–100 mL and reveals in Figure 4.21. Each sample was spiked with 10 mg L^{-1} analytes and 10 mg adsorbent. As can be seen, peak area increased until 20 mL and further decreased till 100 mL. A 20 mL volume of sample demonstrated the most efficient extraction. An increase in sample volume could lead to a high distribution of adsorbent to the aqueous phase, which lowered the amount of adsorbent in the volume unit sample solution, and the extraction became less effective (Tahmasebi *et al.*, 2013). Thus, a 20 mL sample volume was chosen as the optimized sample volume.

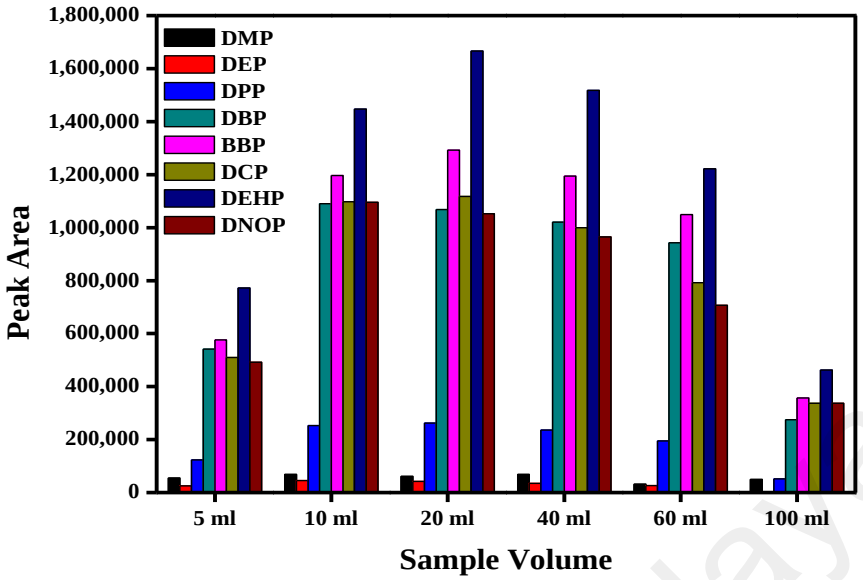

Figure 4.21: Adsorbent dosage for the extraction of targeted phthalates

4.4.1.7 Effect of NaCl

Indeed, the addition of salt in the sample matrices affects the extraction efficiency. Thus, studies on the concentration of NaCl ranging from 0–25 g L^{-1} were conducted. Figure 4.22 demonstrates peak areas of the studied analytes increased from 0–15 g L^{-1}, but decreased later from 20–25 g L^{-1}. This can be due to the addition of salt, which increases the ionic strength and eventually decreases the solubility of the analytes in the media. However, as the concentration of salt increases, the diffusion rate of the analytes may reduce, since the solvation cage of the analytes is disturbed (Tahmasebi *et al.*, 2012). Since a 15 g L^{-1} NaCl concentration gave a high peak area for all analytes studied, it was chosen for subsequent experiments.

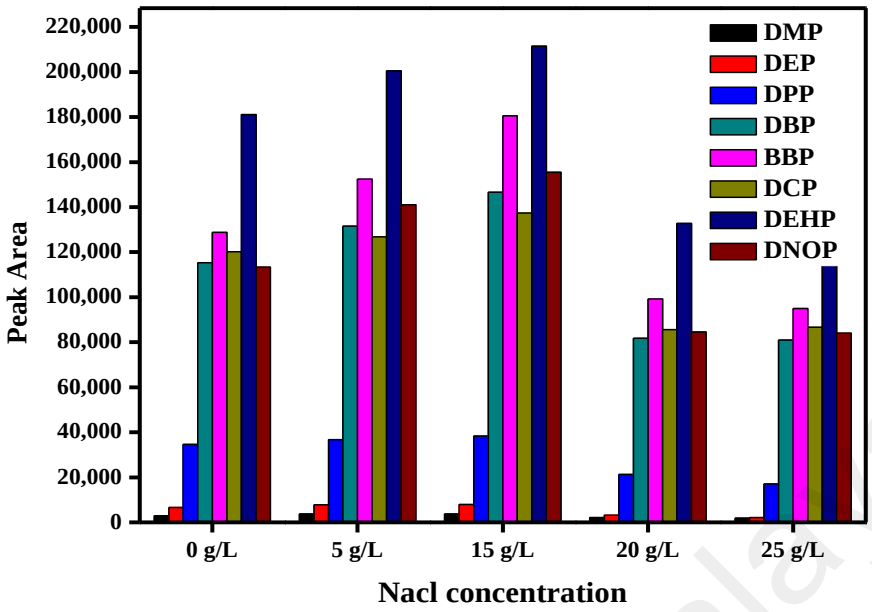

Figure 4.22: Effect of NaCl concentration for the extraction of targeted phthalates

4.4.2 Reusability Studies

To investigate the probability of reusing and regenerating the sorbent, a reusability test was designed and implemented for MNP@P3TArH, which was recycled after being washed with methanol and water and was dried in a vacuum at 70 °C for 12 h. From Figure 4.23, it could be surmised that after five repeated experiments extraction efficiency was reduced. This might cause by the adsorbent surface properties was modified which decreases the surface area as confirmed by BET surface area (see Table 4.5) and FT-IR analysis (see Figure 4.14) of the sorbent after five cycles.

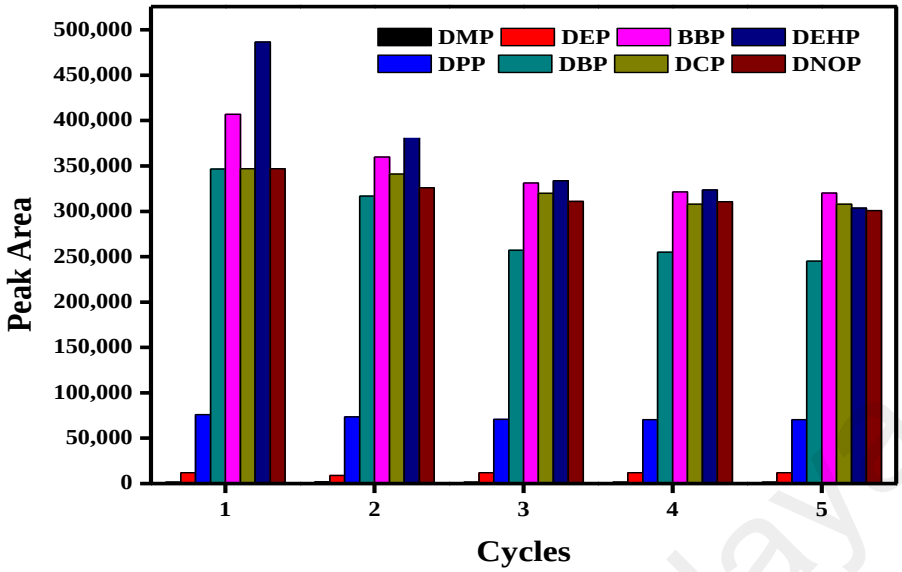

Figure 4.23: Reusability cycles

4.4.3 Analytical Performances

The optimized method obtained for the extraction of phthalates using MNP@P3TArH involved the sample at pH 7, 30 min extraction time, ethyl acetate as the elution solvent, 500 µL elution solvent volumes, 10 min desorption time, 10 mg adsorbent dosage, 20 mL sample loading volume and a 15 g L^{-1} concentration of NaCl. In order to assess the validation of the proposed method, linearity, the limit of detection, the limit of quantitation and repeatability were performed under optimum conditions. Analytical performance figures of merits are tabulated in Table 4.7.

Calibration curves obtained for the studied phthalates were linear over the range of 0.1–50 µg L^{-1} with R^2 more than 0.99. As per the U.S. EPA standard, the screening of phthalates in drinking water must be done at a concentration above 0.6 µg L^{-1} (Serôdio & Nogueira, 2006). However, the LOD of our method lies within the range of 0.054–0.468, indicating the suitability of this method as an efficient phthalate extractor.

Table 4.7: Method validation data for magnetic-solid phase extraction (MSPE) of phthalates with MNP@P3TArH

Analytes	R^2	Linear range (µg L^{-1})	LOD (µg L^{-1})	LOQ (µg L^{-1})	RSD (%) Inter-day, n = 3	RSD (%) Intra-day, n = 7
DMP	0.992	0.5–50	0.462	1.539	3.4	4.8
DEP	0.992	0.5–50	0.468	1.562	5.0	4.3
DPP	0.997	0.5–50	0.286	0.954	4.6	3.7
DBP	0.998	0.1–50	0.063	0.213	4.5	4.5
BBP	0.996	0.1–50	0.080	0.268	4.8	4.3
DCP	0.993	0.5–50	0.332	1.106	4.7	4.0
DEHP	0.997	0.1–50	0.054	0.182	3.0	4.0
DNOP	0.997	0.1–50	0.073	0.244	3.6	4.9

Repeatability studies were conducted for inter-day (three consecutives replicates for three days) and intra-day (seven consecutives replicates on the same day). The results were expressed as relative standard deviations RSD (%). This method demonstrated good precision, since the RSD (%) values were in the range of 3%–5% (Le Zhang *et al.*, 2010). Comparative studies on the analytical performance between the proposed methods with other developed methods are shown in Table 4.8. Obviously, the extraction of phthalates using MNP@P3TArH provides sensitivity and repeatability.

Table 4.8: Comparatives study of the proposed method with other MSPE adsorbents for the extraction of phthalates

Analyte	Method	LOD (μg L^{-1})	LDR (μg L^{-1})	RSD (%)	Ref.
-DBP, DEHP, DOA	MNP@PTh-GC-FID	0.2–0.4	0.4–100	4–12	(Tahmasebi *et al.*, 2013)
-DPP, DBP, DCP, DNOP	MNP@Chitosan-C18-HPLC-UV	0.012–0.037	0.001–0.01	2–6	(Le Zhang *et al.*, 2010)
-DBP, DEHP	MNP@Zeolite-GC-FID	2.8–3.2	10–1200	10–13	(Mollahosseini *et al.*, 2015)
-DMP, DEP, DBP, BBP, DNOP	MNP@ZIF-8-HPLC	0.08–0.24	1–100	<5	(Liu *et al.*, 2015)
-DMP, DPP, DEP, DBP, BBP, DCP, DEHP, DNOP	MNP@P3TArH- GC-FID	0.05–0.09	0.1–50	3–5	This study

4.4.3.1 Real Sample Analyses

To endorse the reliability of the method using MNP@P3TArH, it was applied to determine phthalates in the water from the mineral bottle store in room temperature, and from the commercial fresh milk. Figure 4.24 shows the chromatogram of all samples unspiked and spiked with phthalates. None of the targeted phthalates were found in the samples under the optimized condition described. To evaluate the matrix effect, all

samples were spiked with 50 µg L^{-1} of the studied phthalates. Recoveries and RSD % for the real samples were determined and are tabulated in Table 4.9.

From the optimization procedures until the real sample analyses, DMP, DEP and DPP demonstrated lower recoveries; this could be due to the lower molecular weights of phthalates being more prone to aqueous solution than to the adsorbent (Staples, 2003). The recoveries obtained for water in the mineral bottle in both storage conditions demonstrated higher values compared to the recovery for the milk sample. This may be caused by the matrix effect that holds the analyte in the milk sample to be higher compared to the water sample. RSD (%) values were found to be in the range of 1.3 %–5.8 %, which indicated a precise method.

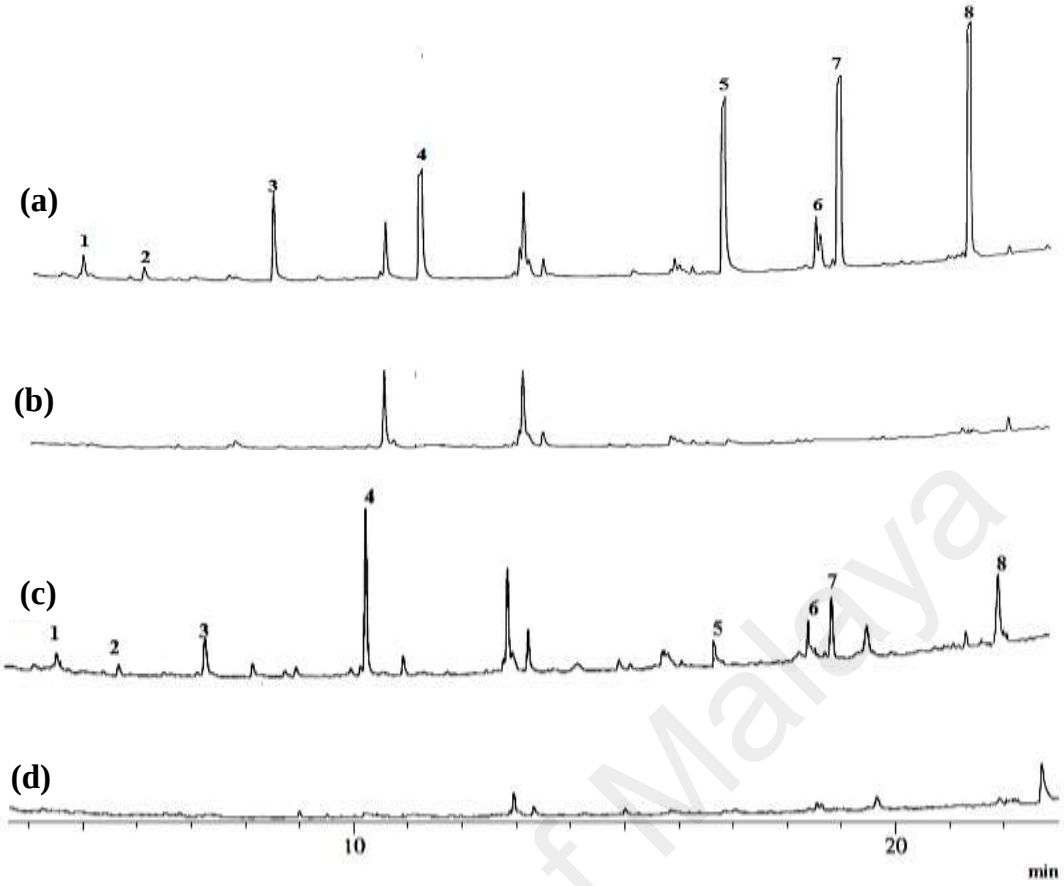

Figure 4.24: GC-FID chromatogram of mineral water stored at room temperature: a) spiked (50 µg L^{-1}), b) unspiked phthalates; and commercial fresh milk: c) spiked (50 µg L^{-1}), d) unspiked phthalates; and peaks: 1) DMP, 2) DEP, 3) DPP, 4) DBP, 5) BBP, 6) DCP; 7) DEHP, 8) DNOP

Table 4.9: Recovery values obtained from the spiked sample in different matrices

	Recoveries of MNP@P3TArH MSPE (%) (± RSD (%), n=3)	
Analyte	**Mineral water**	**Commercial fresh milk**
DMP	85(5.8)	68(5.0)
DEP	85 (4.9)	67(3.0)
DPP	88(1.3)	72(7.7)
DBP	95(2.4)	85(3.3)
BBP	93(3.0)	82(3.8)
DCP	90(4.7)	77(5.8)
DEHP	99(1.3)	89(4.5)
DNOP	101(4.2)	91(3.3)

CHAPTER 5: CONCLUSIONS AND RECOMMENDATIONS

5.1 Conclusion

Unmodified polythiophene and three functionalized polythiophene were successfully coated on the surface of Fe_3O_4 magnetic nanoparticles. The synthesized nanocomposites were characterized by Fourier transform infra-red (FTIR), X-ray diffractometry (XRD), Brunauer–Emmett–Teller (BET) surface area analysis and vibrating sample magnetometer (VSM). From the FT-IR results, the presence of functional groups of the modified polythiophenes were found in the spectra indicated that the coating has taken place. X-ray diffraction exhibits no change in magnetic nanoparticles crystalline phase after coating. Magnetization saturation analyses by VSM showed MNP@PTCN and MNP@P3TArH have high magnetization saturation compared to other nanocomposites. Among nanocomposites, MNP@P3TArH displayed high BET surface area and its morphology was further confirmed with field emission scanning electron microscope (FESEM). In addition, the transmission electron microscopy (TEM) result has verified the high dispersity of MNP@P3TArH with average particle size at 13.070 ± 2.916 nm after coating was performed.

The adsorption processes of DEHP onto MNP@P3TArH were shown to be pH dependent, with the optimum removal being observed at pH 7. Kinetics analysis indicated that the kinetic data is well fitted in the pseudo second-order equation model. Thermodynamic studies revealed that the adsorption process was exothermic, spontaneous, and in an ordered state. The equilibrium isotherm data fitted well into the Freundlich isotherm with *1/n* indicating a favorable process. The adsorption suggests a multilayer adsorption behavior by considering π-π interaction and hydrophobic interaction of the MNP@P3TArH with DEHP. The reusability studies suggested that

after five cycles, surface modification of MNP@P3TArH occurred; thus, retarded the adsorption efficiency.

Overall performances for the extraction of selected phthalates were in the order of MNP@P3TArH>MNP@P3Th>MNP@PTCN>MNP@PTh>MNP. The presence of new interfaces (π-π and hydrophobic interactions) among the sorbent and target analytes increased the adsorption capability. The optimized conditions of MNP@P3TArH for MSPE were carefully selected as follows: sample at pH 7, 30 min extraction time, ethyl acetate as the elution solvent, 500 µL elution solvent volume, 10 min desorption time, 10 mg adsorbent dosage, 20 mL sample loading volume and 15 g L^{-1} concentration of NaCl. The steadiness and reusability studies suggested that the MNP@P3TArH could be used up to five cycles without significantly impacting its extraction capacity. The adsorbent covers a wide range of phthalates with a dynamic linear range of 0.1–50 µg L^{-1} and a limit of detection at 0.054–0.468 µg L^{-1}. The application of MNP@P3TArH as the MSPE sorbent was successfully executed by the analysis of phthalates in the mineral water and commercial fresh milk.

5.2 Recommendations

The weaknesses and limitations techniques developed in the research study have indicated the following areas as recommendations for future work.

a) Synthesis and application for extraction of different functionalized conducting polymers.
b) Study adsorption and extraction efficiencies for various kinds of magnetic nanoparticles beside iron oxide.
c) Magnetic solid-phase extraction of phthalates via different kind of polymer coating.

d) Extend the scope of study with extraction of other possible pollutants such as heavy metals and organic compounds with simultaneous detection.

REFERENCES

Afkhami, A., Moosavi, R., & Madrakian, T. (2010). Preconcentration and spectrophotometric determination of low concentrations of malachite green and leuco-malachite green in water samples by high performance solid phase extraction using maghemite nanoparticles. *Talanta, 82*(2): 785-789.

Aguilar-Arteaga, K., Rodriguez, J., Miranda, J., Medina, J., & Barrado, E. (2010). Determination of non-steroidal anti-inflammatory drugs in wastewaters by magnetic matrix solid phase dispersion–HPLC. *Talanta, 80*(3): 1152-1157.

Akpan, U. G., & Hameed, B. H. (2009). Parameters affecting the photocatalytic degradation of dyes using TiO2-based photocatalysts: a review. *Journal of Hazardous Materials, 170*(2–3): 520-529.

Alivisatos, P. (2000). Colloidal quantum dots. From scaling laws to biological applications. *Pure and Applied Chemistry, 72*(1-2): 3-9.

Ambashta, R. D., & Sillanpaa, M. (2010). Water purification using magnetic assistance: a review. *Journal of Hazardous Materials, 180*(1): 38-49.

Amiridou, D., & Voutsa, D. (2011). Alkylphenols and phthalates in bottled waters. *Journal of Hazardous Materials, 185*(1): 281-286.

Ansari, M. O., Khan, M. M., Ansari, S. A., & Cho, M. H. (2015). Polythiophene nanocomposites for photodegradation applications: past, present and future. *Journal of Saudi Chemical Society, 19*(5): 494-504.

Aradilla, D., Azambuja, D., Estrany, F., Casas, M. T., Ferreira, C. A., & Aleman, C. (2012). Hybrid polythiophene-clay exfoliated nanocomposites for ultracapacitor devices. *Journal of Materials Chemistry, 22*(26): 13110-13122.

Arkles, B. (1977). Tailoring surfaces with silanes. *Chemtech, 7*(12): 766-778.

Aydın, M., Durmus, Z., Kavas, H., Esat, B., Sözeri, H., Baykal, A., ... Toprak, M. S. (2011). Synthesis and characterization of poly (3-thiophene acetic acid)/Fe_3O_4 nanocomposite. *Polyhedron, 30*(6): 1120-1126.

Aydın, Y. A., & Aksoy, N. D. (2009). Adsorption of chromium on chitosan: optimization, kinetics and thermodynamics. *Chemical Engineering Journal, 151*(1): 188-194.

Bach, C., Dauchy, X., Chagnon, M.C., & Etienne, S. (2012). Chemical compounds and toxicological assessments of drinking water stored in polyethylene terephthalate (PET) bottles: a source of controversy reviewed. *Water Research, 46*(3): 571-583.

Bagheri, H., Afkhami, A., Saber-Tehrani, M., & Khoshsafar, H. (2012). Preparation and characterization of magnetic nanocomposite of Schiff base/silica/magnetite as a preconcentration phase for the trace determination of heavy metal ions in water,

food and biological samples using atomic absorption spectrometry. *Talanta, 97*: 87-95.

Baharin, S. N. A., Sarih, N. M., Mohamad, S., Shahabuddin, S., Sulaiman, K., & Ma'amor, A. (2016). Removal of endocrine disruptor di-(2-ethylhexyl) phthalate by modified polythiophene-coated magnetic nanoparticles: characterization, adsorption isotherm, kinetic study, thermodynamics. *RSC Advances, 6*(50): 44655-44667.

Bai, L., Mei, B., Guo, Q. Z., Shi, Z. G., & Feng, Y. Q. (2010). Magnetic solid-phase extraction of hydrophobic analytes in environmental samples by a surface hydrophilic carbon-ferromagnetic nanocomposite. *Journal of Chromatography A, 1217*(47): 7331-7336.

Balafas, D., Shaw, K., & Whitfield, F. (1999). Phthalate and adipate esters in Australian packaging materials. *Food Chemistry, 65*(3): 279-287.

Ballesteros-Gomez, A., & Rubio, S. (2009). Hemimicelles of alkyl carboxylates chemisorbed onto magnetic nanoparticles: study and application to the extraction of carcinogenic polycyclic aromatic hydrocarbons in environmental water samples. *Analytical Chemistry, 81*(21): 9012-9020.

Banitaba, M. H., Davarani, S. S. H., & Pourahadi, A. (2013). Solid-phase microextraction of phthalate esters from aqueous media by electrophoretically deposited TiO_2 nanoparticles on a stainless steel fiber. *Journal of Chromatography A, 1283*: 1-8.

Besser, P., Morrish, A., & Searle, C. (1967). Magnetocrystalline anisotropy of pure and doped hematite. *Physical Review, 153*(2): 632.

Bhadra, S., Das, S. C., Roy, S., Arefeen, S., & Rouf, A. S. S. (2011). Development and validation of RP-HPLC method for quantitative estimation of vinpocetine in pure and pharmaceutical dosage forms. *Chromatography Research International, 2011*: 7.

Bianchi, F., Chiesi, V., Casoli, F., Luches, P., Nasi, L., Careri, M., & Mangia, A. (2012). Magnetic solid-phase extraction based on diphenyl functionalization of Fe_3O_4 magnetic nanoparticles for the determination of polycyclic aromatic hydrocarbons in urine samples. *Journal of Chromatography A, 1231*: 8-15.

Boal, A. K. (2004). Synthesis and application of magnetic nanoparticles. In Rotello, V. M. (Eds.), *Nanoparticles: building blocks for nanotechnology* (pp. 1-19). New York, NY: Springer Science & Business Media.

Bodker, F., & Morup, S. (2000). Size dependence of the properties of hematite nanoparticles. *Europhysics Letters, 52*(2): 217.

Bononi, M., & Tateo, F. (2009). Identification of diisobutyl phthalate (DIBP) suspected as possible contaminant in recycled cellulose for take-away pizza boxes. *Packaging Technology and Science, 22*(1): 53-58.

Bornehag, C.-G., Sundell, J., Weschler, C. J., Sigsgaard, T., Lundgren, B., Hasselgren, M., & Hagerhed-Engman, L. (2004). The association between asthma and allergic symptoms in children and phthalates in house dust: a nested case-control study. *Environmental Health Perspectives*: 1393-1397.

Bourque, A. N. (2010). *Photophysical investigations of thiophene azomethine derivatives* (pp. 2-5) (Doctoral Dissertation, Universite de Montreal). Retrieved from http://hdl.handle.net/1866/3565.

Boyer, C., Whittaker, M. R., Bulmus, V., Liu, J., & Davis, T. P. (2010). The design and utility of polymer-stabilized iron-oxide nanoparticles for nanomedicine applications. *NPG Asia Materials, 2*(1): 23-30.

Burda, C., Chen, X., Narayanan, R., & El-Sayed, M. A. (2005). Chemistry and properties of nanocrystals of different shapes. *Chemical Reviews, 105*(4): 1025-1102.

Cao, X., Li, X., & Meng, X. (2014). Adsorption kinetics and equilibrium studies of an endocrine disruptor, di-(2-ethylhexyl) phthalate, from wastewater by biofilms. *Environmental Engineering Science, 31*(2): 55-60.

Casas, L., Roig, A., Rodrıguez, E., Molins, E., Tejada, J., & Sort, J. (2001). Silica aerogel–iron oxide nanocomposites: structural and magnetic properties. *Journal of Non-Crystalline Solids, 285*(1): 37-43.

Chan, H., Lau, T., Ang, P., Wu, M., & Wong, P. (2004). Biosorption of di-(2-ethylhexyl) phthalate by seaweed biomass. *Journal of Applied Phycology, 16*(4): 263-274.

Chandra, M. R., Rao, T. S., Pammi, S., & Sreedhar, B. (2015). An enhanced visible light active rutile titania–copper/polythiophene nanohybrid material for the degradation of rhodamine B dye. *Materials Science in Semiconductor Processing, 30*: 672-681.

Chang, H., Chiou, C. C., Chen, Y. W., & Sheen, S. (1997). Synthesis, characterization, and magnetic properties of Fe_3O_4 thin films prepared via a sol–gel method. *Journal of Solid State Chemistry, 128*(1): 87-92.

Chang, W., Skandan, G., Danforth, S. C., Kear, B., & Hahn, H. (1994). Chemical vapor processing and applications for nanostructured ceramic powders and whiskers. *Nanostructured Materials, 4*(5): 507-520.

Chen, Mylon, S. E., & Elimelech, M. (2007). Enhanced aggregation of alginate-coated iron oxide (hematite) nanoparticles in the presence of calcium, strontium, and barium cations. *Langmuir, 23*(11): 5920-5928.

Chen, C.Y., Chen, C.C., & Chung, Y.C. (2007). Removal of phthalate esters by α-cyclodextrin-linked chitosan bead. *Bioresource Technology, 98*(13): 2578-2583.

Chen, C.-Y., & Chung, Y. C. (2006). Removal of phthalate esters from aqueous solutions by chitosan bead. *Journal of Environmental Science and Health, Part A, 41*(2): 235-248.

Chen, J., Zou, J., Zeng, J., Song, X., Ji, J., Wang, Y., ... Chen, X. (2010). Preparation and evaluation of graphene-coated solid-phase microextraction fiber. *Analytica Chimica Acta, 678*(1): 44-49.

Chen, W., Chen, Y., Li, F., Chen, L., Yuan, K., Yao, K., & Wang, P. (2012). Ordered microstructure induced by orientation behavior of liquid-crystal polythiophene for performance improvement of hybrid solar cells. *Solar Energy Materials and Solar Cells, 96*: 266-275.

Cheng, Q., Qu, F., Li, N. B., & Luo, H. Q. (2012). Mixed hemimicelles solid-phase extraction of chlorophenols in environmental water samples with 1-hexadecyl-3-methylimidazolium bromide-coated Fe_3O_4 magnetic nanoparticles with high-performance liquid chromatographic analysis. *Analytica Chimica Acta, 715*: 113-119.

Cherian, M., Rao, M. S., Yang, W. T., Jehng, J. M., Hirt, A. M., & Deo, G. (2002). Oxidative dehydrogenation of propane over Cr_2O_3/Al_2O_3 and Cr_2O_3 catalysts: effects of loading, precursor and surface area. *Applied Catalysis A: General, 233*(1): 21-33.

Chiang, C., Gau, S., Fincher Jr, C., Park, Y., MacDiarmid, A., & Heeger, A. (1978). Polyacetylene,(CH)x: n-type and p-type doping and compensation. *Applied Physics Letters, 33*(1): 18-20.

Chikazumi, S., Taketomi, S., Ukita, M., Mizukami, M., Miyajima, H., Setogawa, M., & Kurihara, Y. (1987). Physics of magnetic fluids. *Journal of Magnetism and Magnetic Materials, 65*(2-3): 245-251.

Cinelli, G., Avino, P., Notardonato, I., Centola, A., & Russo, M. V. (2013). Rapid analysis of six phthalate esters in wine by ultrasound-vortex-assisted dispersive liquid–liquid micro-extraction coupled with gas chromatography-flame ionization detector or gas chromatography–ion trap mass spectrometry. *Analytica Chimica Acta, 769*: 72-78.

Cornell, R. M., & Schwertmann, U. (2003). *The iron oxides: structure, properties, reactions, occurrences and uses* (pp. 15-28). Germany: John Wiley & Sons.

Cornil, J., Beljonne, D., Bredas, J., Mullen, K., & Wegner, G. (1998). *Electronic materials: the oligomers approach* (pp.432-447). New York, NY: Wiley-VCH

Cotica, L. F., Santos, I. A., Girotto, E. M., Ferri, E. V., & Coelho, A. A. (2010). Surface spin disorder effects in magnetite and poly (thiophene)-coated magnetite nanoparticles. *Journal of Applied Physics, 108*(6): 064325.

Cousins, I., & Mackay, D. (2000). Correlating the physical–chemical properties of phthalate esters using the three solubility approach. *Chemosphere, 41*(9): 1389-1399.

Darab, J. G., Linehan, J. C., & Matson, D. W. (1994). Effect of agglomerate size on the catalytic activity of an iron oxyhydroxide nanocrystalline powder toward carbon-carbon bond scission in naphthylbibenzylmethane. *Energy & Fuels, 8*(4): 1004-1005.

Dastjerdi, R., & Montazer, M. (2010). A review on the application of inorganic nano-structured materials in the modification of textiles: focus on anti-microbial properties. *Colloids and Surfaces B: Biointerfaces, 79*(1): 5-18.

De Dios, A. S., & Diaz-Garcia, M. E. (2010). Multifunctional nanoparticles: analytical prospects. *Analytica Chimica Acta, 666*(1): 1-22.

Deng, Y., Qi, D., Deng, C., Zhang, X., & Zhao, D. (2008). Superparamagnetic high-magnetization microspheres with an Fe_3O_4@SiO_2 core and perpendicularly aligned mesoporous SiO_2 shell for removal of microcystins. *Journal of the American Chemical Society, 130*(1): 28-29.

Devine, M., & Schilling, M. (2013, June 27). The attraction of medical magnets :understanding biomagnetic separation. *Today's Medical Development*. Retrieved from http://www.onlinetmd.com/article/tmd0713-medical-magnets-attraction/.

Dhara, S., Awasthy, B., Rastogi, A., Das, B., Gelfond, N., Fedotova, N., ... Igumenov, I. (1994). Parametric investigation for direct chemical vapour deposition of magnetite films. *Journal of Magnetism and Magnetic Materials, 134*(1): 29-33.

Dias, A., Hussain, A., Marcos, A., & Roque, A. (2011). A biotechnological perspective on the application of iron oxide magnetic colloids modified with polysaccharides. *Biotechnology Advances, 29*(1): 142-155.

Din, M. I., Ata, S., Mohsin, I. U., Rasool, A., & Aziz, A. A. (2014). Evaluation of conductive polymers as an adsorbent for eradication of As(III) from aqueous solution using inductively coupled plasma optical emission spectroscopy (ICP-OES). *International Journal of Science and Engineering, 6*(2): 154-162.

Ding, J., Gao, Q., Li, X. S., Huang, W., Shi, Z. G., & Feng, Y. Q. (2011). Magnetic solid-phase extraction based on magnetic carbon nanotube for the determination of estrogens in milk. *Journal of Separation Science, 34*(18): 2498-2504.

Duty, S. M., Singh, N. P., Silva, M. J., Barr, D. B., Brock, J. W., Ryan, L., ... Hauser, R. (2003). The relationship between environmental exposures to phthalates and DNA damage in human sperm using the neutral comet assay. *Environmental Health Perspectives, 111*(9): 1164.

Eckert, C. A. (1996). Supercritical fluids as solvents for chemical and materials processing. *Nature, 383*: 313-318.

Esquivel, J., Facundo, I. A., Treviño, M. E., & López, R. G. (2007). A novel method to prepare magnetic nanoparticles: precipitation in bicontinuous microemulsions. *Journal of Materials Science, 42*(21): 9015-9020.

European Chemical Bureau (2008). *Risk assessment report for bis(2-ethylhexyl) phthalate* (Report No. PL-2 80). Sundbyberg, Sweden.

European Food Safety Authority. (2005). Statement on the scientific panel on food additives, flavourings, processing aids and materials in contact with food (AFC) on the reclassification of some phthalates for consistency with the new SCF guidelines for food contact materials. *EFSA Journal, 244*: 1-18.

European Commision. (2001). *Communication on the implementation of the community strategy for endocrine disruptors - a range of substances suspected of interfering with the hormone systems of humans and wildlife* (No. 262/2001/CE). Brussels, Belgium: Environment Directorate.

Fang, Z., & Huang, H. (2009). Adsorption of di-*n*-butyl phthalate onto nutshell-based activated carbon. Equilibrium, kinetics and thermodynamics. *Adsorption Science & Technology, 27*(7): 685-700.

Fankhauser-Noti, A., Biedermann-Brem, S., & Grob, K. (2006). PVC plasticizers/additives migrating from the gaskets of metal closures into oily food: Swiss market survey June 2005. *European Food Research and Technology, 223*(4): 447-453.

Farahani, H., Ganjali, M. R., Dinarvand, R., & Norouzi, P. (2008). Screening method for phthalate esters in water using liquid-phase microextraction based on the solidification of a floating organic microdrop combined with gas chromatography–mass spectrometry. *Talanta, 76*(4): 718-723.

Faraji, M., Yamini, Y., & Rezaee, M. (2010). Extraction of trace amounts of mercury with sodium dodecyle sulphate-coated magnetite nanoparticles and its determination by flow injection inductively coupled plasma-optical emission spectrometry. *Talanta, 81*(3): 831-836.

Farrukh, A., Akram, A., Ghaffar, A., Hanif, S., Hamid, A., Duran, H., & Yameen, B. (2013). Design of polymer-brush-grafted magnetic nanoparticles for highly efficient water remediation. *ACS Applied Materials & Interfaces, 5*(9): 3784-3793.

Fayazi, M., Taher, M. A., Afzali, D., & Mostafavi, A. (2016). Fe_3O_4 and MnO_2 assembled on halloysite nanotubes: a highly efficient solid-phase extractant for electrochemical detection of mercury(II) ions. *Sensors and Actuators B: Chemical, 228*: 1-9.

Febrianto, J., Kosasih, A. N., Sunarso, J., Ju, Y.-H., Indraswati, N., & Ismadji, S. (2009). Equilibrium and kinetic studies in adsorption of heavy metals using biosorbent: a summary of recent studies. *Journal of Hazardous Materials, 162*(2): 616-645.

Fichou, D. (2008). *Handbook of oligo and polythiophenes* (pp. 13-23). Weinheim,Germany: John Wiley & Sons.

Foster, P. (2006). Disruption of reproductive development in male rat offspring following in utero exposure to phthalate esters. *International Journal of Andrology, 29*(1): 140-147.

Franck, H. G., & Stadelhofer, J. (1988). *Production and uses of xylene derivatives. Industrial aromatic chemistry* (pp. 265-290). New York,NY: Springer-Verlag.

Fromme, H., Küchler, T., Otto, T., Pilz, K., Müller, J., & Wenzel, A. (2002). Occurrence of phthalates and bisphenol A and F in the environment. *Water Research, 36*(6): 1429-1438.

Gao, Q., Luo, D., Bai, M., Chen, Z. W., & Feng, Y. Q. (2011). Rapid determination of estrogens in milk samples based on magnetite nanoparticles/polypyrrole magnetic solid-phase extraction coupled with liquid chromatography–tandem mass spectrometry. *Journal of Agricultural and Food Chemistry, 59*(16): 8543-8549.

Gao, Q., Luo, D., Ding, J., & Feng, Y. Q. (2010). Rapid magnetic solid-phase extraction based on magnetite/silica/poly(methacrylic acid–co–ethylene glycol dimethacrylate) composite microspheres for the determination of sulfonamide in milk samples. *Journal of Chromatography A, 1217*(35): 5602-5609.

Garcia-Calzon, J., & Diaz-Garcia, M. E. (2012). Synthesis and analytical potential of silica nanotubes. *TrAC Trends in Analytical Chemistry, 35*: 27-38.

Geng, Y., Ding, M., Chen, H., Li, H.-F., & Lin, J.-M. (2012). Preparation of hydrophilic carbon-functionalized magnetic microspheres coated with chitosan and application in solid-phase extraction of bisphenol A in aqueous samples. *Talanta, 89*: 189-194.

Ghosh, S., Badruddoza, A., Uddin, M., & Hidajat, K. (2011). Adsorption of chiral aromatic amino acids onto carboxymethyl-β-cyclodextrin bonded Fe_3O_4/SiO_2 core–shell nanoparticles. *Journal of Colloid and Interface Science, 354*(2): 483-492.

Girginova, P. I., Daniel-da-Silva, A. L., Lopes, C. B., Figueira, P., Otero, M., Amaral, V. S., Pereira, E., & Trindade, T. (2010). Silica coated magnetite particles for magnetic removal of Hg^{2+} from water. *Journal of Colloid and Interface Science, 345*(2): 234-240.

Giri, S., Trewyn, B. G., Stellmaker, M. P., & Lin, V. S. Y. (2005). Stimuli-responsive controlled-release delivery system based on mesoporous silica nanorods capped with magnetic nanoparticles. *Angewandte Chemie International Edition, 44*(32): 5038-5044.

Gomez-Hens, A., & Aguilar-Caballos, M. (2003). Social and economic interest in the control of phthalic acid esters. *TrAC Trends in Analytical Chemistry, 22*(11): 847-857.

Grange, R., Dutto, F., & Radenovic, A. (2011). Niobates nanowires: synthesis, characterization and applications. In Hashim, A. (Eds), *Nanowires-implementations and applications* (pp. 509-524). Rijeka, Croatia: Intech.

Guan, Y., Jiang, C., Hu, C., & Jia, L. (2010). Preparation of multi-walled carbon nanotubes functionalized magnetic particles by sol–gel technology and its application in extraction of estrogens. *Talanta, 83*(2): 337-343.

Gupta, A. K., & Gupta, M. (2005). Synthesis and surface engineering of iron oxide nanoparticles for biomedical applications. *Biomaterials, 26*(18): 3995-4021.

Han, Q., Wang, Z., Xia, J., Chen, S., Zhang, X., & Ding, M. (2012). Facile and tunable fabrication of Fe_3O_4/graphene oxide nanocomposites and their application in the magnetic solid-phase extraction of polycyclic aromatic hydrocarbons from environmental water samples. *Talanta, 101*: 388-395.

Hasany, S., Ahmed, I., Rajan, J., & Rehman, A. (2012). Systematic review of the preparation techniques of iron oxide magnetic nanoparticles. *Nanoscience and Nanotechnology, 2*(6): 148-158.

Hauser, R., Duty, S., Godfrey-Bailey, L., & Calafat, A. M. (2004). Medications as a source of human exposure to phthalates. *Environmental Health Perspectives, 112*(6): 751.

Heidari, H., Razmi, H., & Jouyban, A. (2012). Preparation and characterization of ceramic/carbon coated Fe_3O_4 magnetic nanoparticle nanocomposite as a solid-phase microextraction adsorbent. *Journal of Chromatography A, 1245*: 1-7.

Heudorf, U., Mersch-Sundermann, V., & Angerer, J. (2007). Phthalates: toxicology and exposure. *International Journal of Hygiene and Environmental Health, 210*(5): 623-634.

Ho, Y. S., & McKay, G. (2000). The kinetics of sorption of divalent metal ions onto sphagnum moss peat. *Water Research, 34*(3): 735-742.

Holadova, K., & Hajslova, J. (1995). A comparison of different ways of sample preparation for the determination of phthalic acid esters in water and plant matrices. *International Journal of Environmental Analytical Chemistry, 59*(1): 43-57.

Huang, C., & Hu, B. (2008). Speciation of inorganic tellurium from seawater by ICP-MS following magnetic SPE separation and preconcentration. *Journal of Separation Science, 31*(4): 760-767.

Huang, S. (2011, June 15). DOH opens probe after KH food scare. *Taipei Times*, p. 2.

Huo, J., Song, H., Chen, X., Zhao, S., & Xu, C. (2007). Structural transformation of carbon-encapsulated iron nanoparticles during heat treatment at 1000 °C. *Materials Chemistry and Physics, 101*(1): 221-227.

Huo, L., Guo, X., Zhang, S., Li, Y., & Hou, J. (2011). PBDTTTZ: a broad band gap conjugated polymer with high photovoltaic performance in polymer solar cells. *Macromolecules, 44*(11): 4035-4037.

Huo, S. H., & Yan, X. P. (2012). Facile magnetization of metal–organic framework MIL-101 for magnetic solid-phase extraction of polycyclic aromatic hydrocarbons in environmental water samples. *Analyst, 137*(15): 3445-3451.

Ibarra, I. S., Miranda, J. M., Rodriguez, J. A., Nebot, C., & Cepeda, A. (2014). Magnetic solid phase extraction followed by high-performance liquid chromatography for the determination of sulphonamides in milk samples. *Food Chemistry, 157*: 511-517.

International Agency for Research on Cancer. (2000). *Some industrial chemicals. IARC Monographs 77*: 41-148.

Ismail. (2007). Evaluation of cysteine as environmentally friendly corrosion inhibitor for copper in neutral and acidic chloride solutions. *Electrochimica Acta, 52*(28): 7811-7819.

Ismail, A. A. (2005). Synthesis and characterization of $Y_2O_3/Fe_2O_3/TiO_2$ nanoparticles by sol–gel method. *Applied Catalysis B: Environmental, 58*(1): 115-121.

Issaadi, S., Douadi, T., Zouaoui, A., Chafaa, S., Khan, M., & Bouet, G. (2011). Novel thiophene symmetrical Schiff base compounds as corrosion inhibitor for mild steel in acidic media. *Corrosion Science, 53*(4): 1484-1488.

Jalil, A. A., Triwahyono, S., Adam, S. H., Rahim, N. D., Aziz, M. A. A., Hairom, N. H. H., ... Mohamadiah, M. K. A. (2010). Adsorption of methyl orange from aqueous solution onto calcined Lapindo volcanic mud. *Journal of Hazardous Materials, 181*(1): 755-762.

Jarosova, A. (2006). Phthalic acid esters (PAEs) in the food chain. *Czech J. Food Sci, 24*: 223-231.

Jayabharathi, J., Ramanathan, P., Thanikachalam, V., & Karunakaran, C. (2015). Optical and theoretical studies on Fe_3O_4–imidazole nanocomposite and clusters. *New Journal of Chemistry, 39*(5): 3801-3812.

Jeong, U., Teng, X., Wang, Y., Yang, H., & Xia, Y. (2007). Superparamagnetic colloids: controlled synthesis and niche applications. *Advanced Materials, 19*(1): 33-60.

Ji, Y., Liu, X., Guan, M., Zhao, C., Huang, H., Zhang, H., & Wang, C. (2009). Preparation of functionalized magnetic nanoparticulate sorbents for rapid extraction of biphenolic pollutants from environmental samples. *Journal of Separation Science, 32*(12): 2139-2145.

Jiang, C., Sun, Y., Yu, X., Zhang, L., Sun, X., Gao, Y., Zhang, H., & Song, D. (2012). Removal of sudan dyes from water with C18-functional ultrafine magnetic silica nanoparticles. *Talanta, 89*: 38-46.

Jiao, Y., Ding, L., Fu, S., Zhu, S., Li, H., & Wang, L. (2012a). Determination of bisphenol A, bisphenol F and their diglycidyl ethers in environmental water by solid phase extraction using magnetic multiwalled carbon nanotubes followed by GC-MS/MS. *Analytical Methods, 4*(1): 291-298.

Jiao, Y., Fu, S., Ding, L., Gong, Q., Zhu, S., Wang, L., & Li, H. (2012b). Determination of trace leaching phthalate esters in water by magnetic solid phase extraction based on magnetic multi-walled carbon nanotubes followed by GC-MS/MS. *Analytical Methods, 4*(9): 2729-2734.

Jones-Lepp, T., Gerlach, C. L., & Cooter, E. J. (2000). The power of analytical methods for measuring suspected endocrine disrupting compounds: a pilot field study. *TrAC Trends in Analytical Chemistry, 19*(5): 286-291.

Julinova, M., & Slavík, R. (2012). Removal of phthalates from aqueous solution by different adsorbents: a short review. *Journal of Environmental Management, 94*(1): 13-24.

Kado, T. (2008). Structural and magnetic properties of magnetite-containing epitaxial iron oxide films grown on MgO substrates. *Journal of Applied Physics, 103*(4): 3902.

Karle, V. A., Short, B. L., Martin, G. R., Bulas, D. I., Getson, P. R., Luban, N. L., ... Rubin, R. J. (1997). Extracorporeal membrane oxygenation exposes infants to the plasticizer, di-(2-ethylhexyl) phthalate. *Critical Care Medicine, 25*(4): 696-703.

Kavlock, R., Boekelheide, K., Chapin, R., Cunningham, M., Faustman, E., Foster, P., ... Little, R. (2002). Evaluation of risks to human reproduction: phthalates expert panel report on the reproductive and developmental toxicity of di-*n*-butyl phthalate. *Reproductive Toxicology, 16*(5): 489-527.

Keresztes, S., Tatar, E., Czegeny, Z., Zaray, G., & Mihucz, V. G. (2013). Study on the leaching of phthalates from polyethylene terephthalate bottles into mineral water. *Science of the Total Environment, 458*: 451-458.

Keriene, I., Maruska, A., & Sitonyte, J. (2011). Solid phase extraction and gas chromatographic-mass spectrometric analysis of phthalates in surface water: method development and validation. *Chemija, 22*(4): 204-209.

Khalafalla, S. E., & Reimers, G. W. (1980). Preparation of dilution-stable aqueous magnetic fluids. *Magnetics, IEEE Transactions On, 16*(2): 178-183.

Khaleel, A. A. (2004). Nanostructured Pure γ-Fe_2O_3 via Forced Precipitation in an Organic Solvent. *Chemistry–A European Journal, 10*(4): 925-932.

Khalili, R., Shabanpour, F., & Eisazadeh, H. (2014). Synthesis of polythiophene/Sb_2O_3 nanocomposite using sodium dodecylbenzenesulfonate for the removal of Pb(II). *Advances in Polymer Technology, 33*(2): 1098-2329.

Khan, N. A., Jung, B. K., Hasan, Z., & Jhung, S. H. (2015). Adsorption and removal of phthalic acid and diethyl phthalate from water with zeolitic imidazolate and metal–organic frameworks. *Journal of Hazardous Materials, 282*: 194-200.

Kilic, M., Apaydin-Varol, E., & Putun, A. E. (2011). Adsorptive removal of phenol from aqueous solutions on activated carbon prepared from tobacco residues: equilibrium, kinetics and thermodynamics. *Journal of Hazardous Materials, 189*(1): 397-403.

Kim, D. K., Mikhaylova, M., Wang, F. H., Kehr, J., Bjelke, B., Zhang, Y., ... Muhammed, M. (2003a). Starch-coated superparamagnetic nanoparticles as MR contrast agents. *Chemistry of Materials, 15*(23): 4343-4351.

Kim, D. K., Mikhaylova, M., Zhang, Y., & Muhammed, M. (2003b). Protective coating of superparamagnetic iron oxide nanoparticles. *Chemistry of Materials, 15*(8): 1617-1627.

Koch, H., Gonzalez-Reche, L., & Angerer, J. (2003). On-line cleanup by multidimensional LC-ESI-MS/MS for high throughput quantification of primary and secondary phthalate metabolites in human urine. *Journal of Chromatography B, 784*: 169-182.

Kruger, R. A., Gordon, T. J., Sutherland, T. C., & Baumgartner, T. (2011). Band-gap engineering of polythiophenes via dithienophosphole doping. *Journal of Polymer Science Part A: Polymer Chemistry, 49*(5): 1201-1209.

Kvistad, A., Lundanes, E., & Greibrokk, T. (1998). Determination of alkylphenols in water samples by solid-phase extraction on to poly(styrene-divinylbenzene) and quantification by liquid chromatography with UV-detection. *Chromatographia, 48*(9-10): 707-713.

Lam, U. T., Mammucari, R., Suzuki, K., & Foster, N. R. (2008). Processing of iron oxide nanoparticles by supercritical fluids. *Industrial & Engineering Chemistry Research, 47*(3): 599-614.

Lang, S. B. (2005). Guide to the literature of piezoelectricity and pyroelectricity. *Ferroelectrics, 321*(1): 91-204.

Latini, G., Verrotti, A., & De Felice, C. (2004). Di-2-ethylhexyl phthalate and endocrine disruption: a review. *Current Drug Targets-Immune, Endocrine & Metabolic Disorders, 4*(1): 37-40.

Laws of Malaysia. (1985). *Food Act 1985, Food Regulations 1985* (P.U.(A) 437 of 1985 C.F.R. 34). W. P. Putrajaya: Attorney General's Chambers.

Le Zhang, X., Niu, H. Y., Zhang, S. X., & Cai, Y. Q. (2010). Preparation of a chitosan-coated C18-functionalized magnetite nanoparticle sorbent for extraction of phthalate ester compounds from environmental water samples. *Analytical and Bioanalytical Chemistry, 397*(2): 791-798.

Leivadara, S. V., Nikolaou, A. D., & Lekkas, T. D. (2008). Determination of organic compounds in bottled waters. *Food Chemistry, 108*(1): 277-286.

Li, J., Cai, Y., Shi, Y., Mou, S., & Jiang, G. (2008). Analysis of phthalates via HPLC-UV in environmental water samples after concentration by solid-phase extraction using ionic liquid mixed hemimicelles. *Talanta, 74*(4): 498-504.

Li, J., Zhao, X., Shi, Y., Cai, Y., Mou, S., & Jiang, G. (2008). Mixed hemimicelles solid-phase extraction based on cetyltrimethylammonium bromide-coated nano-magnets Fe_3O_4 for the determination of chlorophenols in environmental water samples coupled with liquid chromatography/spectrophotometry detection. *Journal of Chromatography A, 1180*(1): 24-31.

Li, Q., Lam, M. H., Wu, R. S., & Jiang, B. (2010). Rapid magnetic-mediated solid-phase extraction and pre-concentration of selected endocrine disrupting chemicals in natural waters by poly (divinylbenzene-co-methacrylic acid) coated Fe_3O_4 core-shell magnetite microspheres for their liquid chromatography–tandem mass spectrometry determination. *Journal of Chromatography A, 1217*(8): 1219-1226.

Li, Z., Bai, S., Hou, M., Wang, C., & Wang, Z. (2013a). magnetic graphene nanoparticles for the preconcentration of chloroacetanilide herbicides from water samples prior to determination by GC-ECD. *Analytical Letters, 46*(6): 1012-1024.

Li, Z., Hou, M., Bai, S., Wang, C., & Wang, Z. (2013b). Extraction of imide fungicides in water and juice samples using magnetic graphene nanoparticles as adsorbent followed by their determination with gas chromatography and electron capture detection. *Analytical Sciences, 29*(3): 325-331.

Li, Z., Wei, L., Gao, M., & Lei, H. (2005). One-Pot Reaction to Synthesize Biocompatible Magnetite Nanoparticles. *Advanced Materials, 17*(8): 1001-1005.

Lian, S., Wang, E., Kang, Z., Bai, Y., Gao, L., Jiang, M., ... Xu, L. (2004). Synthesis of magnetite nanorods and porous hematite nanorods. *Solid State Communications, 129*(8): 485-490.

Lin, C. L., Lee, C. F., & Chiu, W. Y. (2005). Preparation and properties of poly (acrylic acid) oligomer stabilized superparamagnetic ferrofluid. *Journal of Colloid and Interface Science, 291*(2): 411-420.

Lin, P. C., Yu, C. C., Wu, H. T., Lu, Y. W., Han, C. L., Su, A. K., ... Lin, C. C. (2012). A chemically functionalized magnetic nanoplatform for rapid and specific biomolecular recognition and separation. *Biomacromolecules, 14*(1): 160-168.

Ling, W., Jiang, G. B., Cai, Y. Q., Bin, H., Wang, Y. W., & Shen, D. Z. (2007). Cloud point extraction coupled with HPLC-UV for the determination of phthalate esters in environmental water samples. *Journal of Environmental Sciences, 19*(7): 874-878.

Liska, I. (2000). Fifty years of solid-phase extraction in water analysis historical development and overview. *Journal of Chromatography A, 885*(1–2): 3-16.

Liu, H. C., Den, W., Chan, S. F., & Kin, K. T. (2008). Analysis of trace contamination of phthalate esters in ultrapure water using a modified solid-phase extraction procedure and automated thermal desorption–gas chromatography/mass spectrometry. *Journal of Chromatography A, 1188*(2): 286-294.

Liu, H., Liu, Z., Li, X., Li, X., & Yao, K. (2006). $Bi_{1-x}La_xFeO_3$ films on $LaNiO_3$ bottom electrode by the sol–gel process. *Journal of Physics D: Applied Physics, 40*(1): 242.

Liu, J., Wang, W., Xie, Y., Huang, Y., Liu, Y., Liu, X., ... Chen, Y. (2011). A novel polychloromethylstyrene coated superparamagnetic surface molecularly imprinted core–shell nanoparticle for bisphenol A. *Journal of Materials Chemistry, 21*(25): 9232-9238.

Liu, M., Li, H., Xiao, L., Yu, W., Lu, Y., & Zhao, Z. (2005). XRD and Mossbauer spectroscopy investigation of Fe_2O_3–Al_2O_3 nano-composite. *Journal of Magnetism and Magnetic Materials, 294*(3): 294-297.

Liu, X., Sun, Z., Chen, G., Zhang, W., Cai, Y., Kong, R., ... You, J. (2015). Determination of phthalate esters in environmental water by magnetic zeolitic imidazolate framework-8 solid-phase extraction coupled with high-performance liquid chromatography. *Journal of Chromatography A, 1409*: 46-52.

Lopez-Espinosa, M. J., Granada, A., Araque, P., Molina-Molina, J. M., Puertollano, M. C., Rivas, A., . . . Lopez, C. (2007). Oestrogenicity of paper and cardboard extracts used as food containers. *Food Additives and Contaminants, 24*(1): 95-102.

Lopez-Jimenez, F. J., Rubio, S., & Perez-Bendito, D. (2005). Determination of phthalate esters in sewage by hemimicelles-based solid-phase extraction and liquid chromatography–mass spectrometry. *Analytica Chimica Acta, 551*(1): 142-149.

Luo, X., Zhan, Y., Huang, Y., Yang, L., Tu, X., & Luo, S. (2011). Removal of water-soluble acid dyes from water environment using a novel magnetic molecularly imprinted polymer. *Journal of Hazardous Materials, 187*(1): 274-282.

Lyubchik, S., Lyubchik, A., Fonseca, I., Lygina, O., & Lyubchik, S. (2011). Comparison of the thermodynamic parameters estimation for the adsorption process of the metals from liquid phase on activated carbons. In Moreno-pirajan J. C. (Eds), *Thermodynamics- interaction studies- solids, liquids and gases* (pp. 95-122). Rijeka, Croatia: Intech.

Ma, Z., Guan, Y., & Liu, H. (2005). Synthesis and characterization of micron-sized monodisperse superparamagnetic polymer particles with amino groups. *Journal of Polymer Science Part A: Polymer Chemistry, 43*(15): 3433-3439.

Machala, L., Zboril, R., & Gedanken, A. (2007). Amorphous iron(III) oxide a review. *The Journal of Physical Chemistry B, 111*(16): 4003-4018.

Mahdavi, M., Ahmad, M. B., Haron, M. J., Namvar, F., Nadi, B., Rahman, M. Z. A., & Amin, J. (2013). Synthesis, surface modification and characterisation of biocompatible magnetic iron oxide nanoparticles for biomedical applications. *Molecules, 18*(7): 7533-7548.

Mahdavian, A. R., & Mirrahimi, M. A. S. (2010). Efficient separation of heavy metal cations by anchoring polyacrylic acid on superparamagnetic magnetite nanoparticles through surface modification. *Chemical Engineering Journal, 159*(1): 264-271.

Majewski, P., & Thierry, B. (2007). Functionalized magnetite nanoparticles—synthesis, properties, and bio-applications. *Critical Reviews in Solid State and Materials Sciences, 32*(3-4): 203-215.

Mandal, S., Banerjee, A., Lohar, S., Chattopadhyay, A., Sarkar, B., Mukhopadhyay, S. K., ... Das, D. (2013). Selective sensing of Hg^{2+} using rhodamine–thiophene conjugate: red light emission and visual detection of intracellular Hg^{2+} at nanomolar level. *Journal of Hazardous Materials, 261*: 198-205.

Mannerbro, R., Ranlof, M., Robinson, N., & Forchheimer, R. (2008). Inkjet printed electrochemical organic electronics. *Synthetic Metals, 158*(13): 556-560.

Margulies, D., Parker, F., Spada, F., Goldman, R., Li, J., Sinclair, R., & Berkowitz, A. (1996). Anomalous moment and anisotropy behavior in Fe_3O_4 films. *Physical Review B, 53*(14): 9175.

Matson, D., Linehan, J., Darab, J., & Buehler, M. (1994). Nanophase iron-based liquefaction catalysts: synthesis, characterization, and model compound reactivity. *Energy & Fuels, 8*(1): 10-18.

McCullough, R. D., & Williams, S. P. (1993). Toward tuning electrical and optical properties in conjugated polymers using side-chains: highly conductive head-to-tail, heteroatom functionalized polythiophenes. *Journal of the American Chemical Society, 115*(24): 11608-11609.

Mckay, G., Blair, H., & Gardner, J. (1982). Adsorption of dyes on *chitin. I.* Equilibrium studies. *Journal of Applied Polymer Science, 27*(8): 3043-3057.

McQuade, D. T., Pullen, A. E., & Swager, T. M. (2000). Conjugated polymer-based chemical sensors. *Chemical Reviews, 100*(7): 2537-2574.

Mehdinia, A., Roohi, F., & Jabbari, A. (2011). Rapid magnetic solid phase extraction with in situ derivatization of methylmercury in seawater by Fe_3O_4/polyaniline nanoparticle. *Journal of Chromatography A, 1218*(28): 4269-4274.

Mehdinia, A., Rouhani, S., & Mozaffari, S. (2016). Microwave-assisted synthesis of reduced graphene oxide decorated with magnetite and gold nanoparticles, and its application to solid-phase extraction of organochlorine pesticides. *Microchimica Acta*: 1-9.

Memon, S., Memon, N., Memon, S., & Latif, Y. (2011). An efficient calix[4]arene based silica sorbent for the removal of endosulfan from water. *Journal of Hazardous Materials, 186*(2): 1696-1703.

Meng, J., Bu, J., Deng, C., & Zhang, X. (2011). Preparation of polypyrrole-coated magnetic particles for micro solid-phase extraction of phthalates in water by gas chromatography–mass spectrometry analysis. *Journal of Chromatography A, 1218*(12): 1585-1591.

Meng, J., Shi, C., Wei, B., Yu, W., Deng, C., & Zhang, X. (2011). Preparation of Fe_3O_4@C@PANI magnetic microspheres for the extraction and analysis of phenolic compounds in water samples by gas chromatography–mass spectrometry. *Journal of Chromatography A, 1218*(20): 2841-2847.

Mikhaylova, M., Kim, D. K., Bobrysheva, N., Osmolowsky, M., Semenov, V., Tsakalakos, T., & Muhammed, M. (2004). Superparamagnetism of magnetite nanoparticles: dependence on surface modification. *Langmuir, 20*(6): 2472-2477.

Minling, G., Xiaojun, M., Wenhua, S., Yun, Q., & Lin, W. (2015). Adsorption mechanism of di-n-butyl phthalate ester on brown soil and red soil. *International Journal of Environment Research, 9*(2): 605-612.

Miskam, M., Bakar, N. K. A., & Mohamad, S. (2014). Determination of polar aromatic amines using newly synthesized sol–gel titanium(IV) butoxide cyanopropyltriethoxysilane as solid phase extraction sorbent. *Talanta, 120*: 450-455.

Mohan, S. V., Rao, N. C., Prasad, K. K., & Karthikeyan, J. (2002). Treatment of simulated reactive yellow 22 (azo) dye effluents using *Spirogyra* species. *Waste Management, 22*(6): 575-582.

Mollahosseini, A., Toghroli, M., & Kamankesh, M. (2015). Zeolite/Fe_3O_4 as a new sorbent in magnetic solid-phase extraction followed by gas chromatography for determining phthalates in aqueous samples. *Journal of Separation Science, 38*(21): 3750-3757.

Moreno-Castilla, C. (2004). Adsorption of organic molecules from aqueous solutions on carbon materials. *Carbon, 42*(1): 83-94.

Morin, F. (1950). Magnetic susceptibility of αFe_2O_3 and αFe_2O_3 with added titanium. *Physical Review, 78*(6): 819.

Mrowetz, M., Pirola, C., & Selli, E. (2003). Degradation of organic water pollutants through sonophotocatalysis in the presence of TiO_2. *Ultrasonics Sonochemistry, 10*(4): 247-254.

Munusamy, S., Aparna, R., & Prasad, R. (2013). Photocatalytic effect of TiO_2 and the effect of dopants on degradation of brilliant green. *Sustainable Chemical Processes, 1*(4).

National Environment Research Institute. (1998). *Sources of phthalates and nonylphenoles in municipal waste water* (NERI technical report 225). Roskilde, Denmark: Vikelsoe, J., Thomsen, M., & Johansen, E.

Nassar, N., & Husein, M. (2006). Preparation of iron oxide nanoparticles from $FeCl_3$ solid powder using microemulsions. *Physica Status Solidi A, 203*(6): 1324-1328.

Nerin, C., Cacho, J., & Gancedo, P. (1993). Plasticizers from printing inks in a selection of food packagings and their migration to food. *Food Additives & Contaminants, 10*(4): 453-460.

Ng, S., Zhou, X., Chen, Z., Miao, P., Chan, H., Li, S., & Fu, P. (1998). Quartz crystal microbalance sensor deposited with Langmuir-Blodgett films of functionalized polythiophenes and application to heavy metal ions analysis. *Langmuir, 14*(7): 1748-1752.

Niederberger, M., & Pinna, N. (2009). Aqueous and non aqueous sol-gel chemistry: *metal oxide nanoparticles in organic solvents: synthesis, formation, assembly and application*, (pp. 7-18). London: Springer-Verlag.

Niu, H., Wang, Y., Zhang, X., Meng, Z., & Cai, Y. (2011). Easy synthesis of surface-tunable carbon-encapsulated magnetic nanoparticles: adsorbents for selective isolation and preconcentration of organic pollutants. *ACS Applied Materials & Interfaces, 4*(1): 286-295.

Norweign Institute for Water Research (1996). *Occurrence of phthalates and organotins in sediments and water in Norway* (Report No.3552). Oslo,Norway: Braaten, B., Berge, J., Berglind, L., & Baekken, T.

Ohtani, H., Miura, I., & Ichikawa, Y. (2000). Effects of dibutyl phthalate as an environmental endocrine disruptor on gonadal sex differentiation of genetic males of the frog Rana rugosa. *Environmental Health Perspectives, 108*(12): 1189-1193.

Ozin, G. A., Arsenault, A. C., & Cademartiri, L. (2009). *Nanochemistry: a chemical approach to nanomaterials* (pp. 75-78). Cambridge, UK: Royal Society of Chemistry.

Pitter, P. (1999). *Hydrochemie* (pp. 45-56) Prague: Vydavatelstvi VSCHT.

Pan, B., Pan, B., Zhang, W., Zhang, Q., Zhang, Q., & Zheng, S. (2008). Adsorptive removal of phenol from aqueous phase by using a porous acrylic ester polymer. *Journal of Hazardous Materials, 157*(2): 293-299.

Pan, B., Qiu, H., Pan, B., Nie, G., Xiao, L., Lv, L., ... Zheng, S. (2010). Highly efficient removal of heavy metals by polymer-supported nanosized hydrated Fe(III) oxides: behavior and XPS study. *Water Research, 44*(3): 815-824.

Park, S., Lim, S., & Choi, H. (2006). Chemical vapor deposition of iron and iron oxide thin films from Fe(II) dihydride complexes. *Chemistry of Materials, 18*(22): 5150-5152.

Pavan, F. A., Dias, S. L., Lima, E. C., & Benvenutti, E. V. (2008). Removal of congo red from aqueous solution by anilinepropylsilica xerogel. *Dyes and Pigments, 76*(1): 64-69.

Pedras, B., Santos, H. M., Fernandes, L., Covelo, B., Tamayo, A., Bertolo, E., ... Lodeiro, C. (2007). Sensing metal ions with two new azomethine–thiophene pincer ligands (NSN): fluorescence and MALDI-TOF-MS applications. *Inorganic Chemistry Communications, 10*(8): 925-929.

Pelit, L., Ertaş, F., Eroğlu, A., Shahwan, T., & Tural, H. (2011). Biosorption of Cu(II) and Pb(II) ions from aqueous solution by natural spider silk. *Bioresource Technology, 102*(19): 8807-8813.

Pierson, H. O. (1999). *Handbook of chemical vapor deposition: principles, technology and applications* (pp. 36-67). Norwich, NY: William Andrew Inc.

Pillai, V., Kumar, P., Hou, M., Ayyub, P., & Shah, D. (1995). Preparation of nanoparticles of silver halides, superconductors and magnetic materials using water-in-oil microemulsions as nano-reactors. *Advances in Colloid and Interface Science, 55*: 241-269.

Pinto, B., & Reali, D. (2009). Screening of estrogen-like activity of mineral water stored in PET bottles. *International Journal of Hygiene and Environmental Health, 212*(2): 228-232.

Plotan, M., Frizzell, C., Robinson, V., Elliott, C. T., & Connolly, L. (2013). Endocrine disruptor activity in bottled mineral and flavoured water. *Food Chemistry, 136*(3): 1590-1596.

Qin, L., He, X. W., Li, W. Y., & Zhang, Y. K. (2008). Molecularly imprinted polymer prepared with bonded β-cyclodextrin and acrylamide on functionalized silica gel for selective recognition of tryptophan in aqueous media. *Journal of Chromatography A, 1187*(1): 94-102.

Qu, S., Huang, F., Yu, S., Chen, G., & Kong, J. (2008). Magnetic removal of dyes from aqueous solution using multi-walled carbon nanotubes filled with Fe_2O_3 particles. *Journal of Hazardous Materials, 160*(2): 643-647.

Raming, T., Winnubst, A., Van Kats, C., & Philipse, A. (2002). The synthesis and magnetic properties of nanosized hematite (αFe_2O_3) particles. *Journal of Colloid and Interface Science, 249*(2): 346-350.

Raoov, M., Mohamad, S., Abas, M. R., & Surikumaran, H. (2014). New macroporous β-cyclodextrin functionalized ionic liquid polymer as an adsorbent for solid phase extraction with phenols. *Talanta, 130*: 155-163.

Reyes-Gallardo, E. M., Lasarte-Aragones, G., Lucena, R., Cardenas, S., & Valcarcel, M. (2013). Hybridization of commercial polymeric microparticles and magnetic nanoparticles for the dispersive micro-solid phase extraction of nitroaromatic hydrocarbons from water. *Journal of Chromatography A, 1271*(1): 50-55.

Roman, I. P., Chisvert, A., & Canals, A. (2011). Dispersive solid-phase extraction based on oleic acid-coated magnetic nanoparticles followed by gas chromatography–mass spectrometry for UV-filter determination in water samples. *Journal of Chromatography A, 1218*(18): 2467-2475.

Saeteaw, K., Tumcharern, G., Piyakulawat, P., Asawapirom, U., Porntheeraphat, S., Duangkaew, P., ... Pratontep, S. (2011). *Heavy metal detection by electrochemical electronic tongue with poly (thiophene)-metal oxide nanoparticle composite electrodes.* Paper presented at the Nanotechnology Materials and Devices Conference (NMDC).

Saha, P., & Chowdhury, S. (2011). Insight into adsorption thermodynamics. In Tadashi, M. (Eds.), *Thermodynamics* (pp. 350-367). Rijeka, Croatia: Intech.

Salleh, N., Jalil, A., Triwahyono, S., Efendi, J., Mukti, R., & Hameed, B. (2015). New insight into electrochemical-induced synthesis of $NiAl_2O/Al_2O_3$: Synergistic effect of surface hydroxyl groups and magnetism for enhanced adsorptivity of Pd(II). *Applied Surface Science, 349*: 485-495.

Sathyanarayana, S., Karr, C. J., Lozano, P., Brown, E., Calafat, A. M., Liu, F., & Swan, S. H. (2008). Baby care products: possible sources of infant phthalate exposure. *Pediatrics, 121*(2): 260-268.

Schettler, T. (2006). Human exposure to phthalates via consumer products. *International Journal of Andrology, 29*(1): 134-139.

Schmid, P., Kohler, M., Meierhofer, R., Luzi, S., & Wegelin, M. (2008). Does the reuse of PET bottles during solar water disinfection pose a health risk due to the migration of plasticisers and other chemicals into the water? *Water Research, 42*(20): 5054-5060.

Schopf, G., & Kossmehl, G. (1997). *Polythiophenes-electrically conductive polymers* (pp. 3-36). New York, NY: Springer-Verlag

Sena, S., Lindley, R., Blythe, H., Sauer, C., Al-Kafarji, M., & Gehring, G. (1997). Investigation of magnetite thin films produced by pulsed laser deposition. *Journal of Magnetism and Magnetic Materials, 176*(2): 111-126.

Serodio, P., & Nogueira, J. (2006). Considerations on ultra-trace analysis of phthalates in drinking water. *Water Research, 40*(13): 2572-2582.

Sha, C., Yi-Sheng, Z., Shui-Yuan, C., Tian, Q., & Hao, S. (2011). Development of an ionic liquid-based dispersive liquid–liquid micro-extraction method for the determination of phthalate esters in water samples. *Journal of Separation Science, 34*(13): 1503-1507.

Shahabuddin, S., Muhamad Sarih, N., Mohamad, S., & Joon Ching, J. (2016). $SrTiO_3$ nanocube-doped polyaniline nanocomposites with enhanced photocatalytic degradation of methylene blue under visible light. *Polymers, 8*(2): 27.

Shailaja, S., Venkata Mohan, S., Rama Krishna, M., & Sarma, P. N. (2008). Degradation of di-ethylhexyl phthalate (DEHP) in bioslurry phase reactor and identification of metabolites by HPLC and MS. *International Biodeterioration & Biodegradation, 62*(2): 143-152.

Shen, L., Laibinis, P. E., & Hatton, T. A. (1999). Bilayer surfactant stabilized magnetic fluids: synthesis and interactions at interfaces. *Langmuir, 15*(2): 447-453.

Shin, S., & Jang, J. (2007). Thiol containing polymer encapsulated magnetic nanoparticles as reusable and efficiently separable adsorbent for heavy metal ions. *Chemical Communications 41*: 4230-4232.

Shrivastava, A., & Gupta, V. (2011). Methods for the determination of limit of detection and limit of quantitation of the analytical methods. *Chronicles of Young Scientists, 2*(1): 21-25.

Sing, K. S. W. (1985). Reporting physisorption data for gas/solid systems with special reference to the determination of surface area and porosity. *Pure and Applied Chemistry 57*: 603-605.

Sinha, J., Sahoo, R., & Kumar, A. (2009). Processable, regioregular, and "Click" able monomer and polymers based on 3,4-Propylenedioxythiophene with tunable solubility. *Macromolecules, 42*(6): 2015-2022.

Skotheim, T. A. (1997). *Handbook of conducting polymers, processing and application* (pp. 8-49). Raton, FL: CRC press Taylor and Francis Group.

Srivastava, V. C., Swamy, M. M., Mall, I. D., Prasad, B., & Mishra, I. M. (2006). Adsorptive removal of phenol by bagasse fly ash and activated carbon: equilibrium, kinetics and thermodynamics. *Colloids and Surfaces A: Physicochemical and Engineering Aspects, 272*(1): 89-104.

Stales, C. A., Peterson, D. R., Parkerton, T. F., & Adams, W. J. (1997). The environmental fate of phthalate esters: a literature review. *Chemosphere, 35*(4): 667-749.

Standard Malaysia. (2014). *Plastic materials and articles intended to come into contact with food* (MS 2234:2014). Cyberjaya, Selangor.

Staples, C. (2003). *Phthalate esters* (pp. 1-7). Germany: Springer-Verlag.

Sue, K., Kimura, K., & Arai, K. (2004). Hydrothermal synthesis of ZnO nanocrystals using microreactor. *Materials Letters, 58*(25): 3229-3231.

Sue, K., Suzuki, M., Arai, K., Ohashi, T., Ura, H., Matsui, K., ... Hiaki, T. (2006). Size-controlled synthesis of metal oxide nanoparticles with a flow-through supercritical water method. *Green Chemistry, 8*(7): 634-638.

Sugimoto, T., & Matijevic, E. (1980). Formation of uniform spherical magnetite particles by crystallization from ferrous hydroxide gels. *Journal Of Colloid And Interface Science, 74*(1): 227-243.

Sun, L., Chen, L., Sun, X., Du, X., Yue, Y., He, D., ... Ding, L. (2009). Analysis of sulfonamides in environmental water samples based on magnetic mixed hemimicelles solid-phase extraction coupled with HPLC–UV detection. *Chemosphere, 77*(10): 1306-1312.

Sun, L., Sun, X., Du, X., Yue, Y., Chen, L., Xu, H., ... Ding, L. (2010). Determination of sulfonamides in soil samples based on alumina-coated magnetite nanoparticles as adsorbents. *Analytica Chimica Acta, 665*(2): 185-192.

Swan, S. H., Main, K. M., Liu, F., Stewart, S. L., Kruse, R. L., Calafat, A. M., ... Sullivan, S. (2005). Decrease in anogenital distance among male infants with prenatal phthalate exposure. *Environmental Health Perspectives*: 1056-1061.

Tahmasebi, E., & Yamini, Y. (2014). Polythiophene-coated Fe_3O_4 nanoparticles as a selective adsorbent for magnetic solid-phase extraction of silver(I), gold(III), copper(II) and palladium(II). *Microchimica Acta, 181*(5-6): 543-551.

Tahmasebi, E., Yamini, Y., Mehdinia, A., & Rouhi, F. (2012). Polyaniline-coated Fe_3O_4 nanoparticles: An anion exchange magnetic sorbent for solid-phase extraction. *Journal of Separation Science, 35*(17): 2256-2265.

Tahmasebi, E., Yamini, Y., Moradi, M., & Esrafili, A. (2013). Polythiophene-coated Fe_3O_4 superparamagnetic nanocomposite: synthesis and application as a new sorbent for solid-phase extraction. *Analytica Chimica acta, 770*: 68-74.

Takami, S., Sato, T., Mousavand, T., Ohara, S., Umetsu, M., & Adschiri, T. (2007). Hydrothermal synthesis of surface-modified iron oxide nanoparticles. *Materials Letters, 61*(26): 4769-4772.

Tamaura, Y., Ito, K., & Katsura, T. (1983). Transformation of γFeO(OH) to Fe_3O_4 by adsorption of iron(II) ion on γFeO(OH). *Journal of the Chemical Society, Dalton Transactions* (2): 189-194.

Tartaj, P., Del Puerto Morales, M., Veintemillas-Verdaguer, S., Gonzalez-Carreno, T., & Serna, C. J. (2003). The preparation of magnetic nanoparticles for applications in biomedicine. *Journal of Physics D: Applied Physics, 36*(13): 182-190.

Tavakoli, A., Sohrabi, M., & Kargari, A. (2007). A review of methods for synthesis of nanostructured metals with emphasis on iron compounds. *Chemical Papers, 61*(3): 151-170.

Teja, A. S., & Koh, P. Y. (2009). Synthesis, properties, and applications of magnetic iron oxide nanoparticles. *Progress in Crystal Growth and Characterization of Materials, 55*(1): 22-45.

Temkin, M., & Pyzhev, V. (1940). Recent modifications to langmuir isotherms. *Acta Physiochim URSS, 12*: 217-222.

Tewari, P., Campbell, A., & Lee, W. (1972). Adsorption of Co^{2+} by oxides from aqueous solution. *Canadian Journal of Chemistry, 50*(11): 1642-1648.

Tian, H., Li, J., Shen, Q., Wang, H., Hao, Z., Zou, L., & Hu, Q. (2009). Using shell-tunable mesoporous Fe_3O_4@HMS and magnetic separation to remove DDT from aqueous media. *Journal of Hazardous Materials, 171*(1): 459-464.

Tourillon, G., & Skotheim, T. (1986). *Handbook of conducting polymers* (pp. 293-294). New York: Marcel Dekker.

Tronc, E., Belleville, P., Jolivet, J. P., & Livage, J. (1992). Transformation of ferric hydroxide into spinel by iron(II) adsorption. *Langmuir, 8*(1): 313-319.

Tsumura, Y., Ishimitsu, S., Saito, I., Sakai, H., Kobayashi, Y., & Tonogai, Y. (2001). Eleven phthalate esters and di-(2-ethylhexyl) adipate in one week duplicate diet samples obtained from hospitals and their estimated daily intake. *Food Additives & Contaminants, 18*(5): 449-460.

Tsumura, Y., Ishimitsu, S., Saito, I., Sakai, H., Kobayashi, Y., & Tonogai, Y. (2003). Estimated daily intake of plasticizers in 1-week duplicate diet samples following regulation of DEHP-containing PVC gloves in Japan. *Food Additives & Contaminants, 20*(4): 317-324.

Udhayakumari, D., Suganya, S., Velmathi, S., & MubarakAli, D. (2014). Naked eye sensing of toxic metal ions in aqueous medium using thiophene-based ligands and its application in living cells. *Journal of Molecular Recognition, 27*(3): 151-159.

U.S Agency for Toxic Substance and Disease Registry. (2002a). *Toxicological profile for di(2-ethylhexyl) phthalate.* Atlanta, GA.

U.S Agency for Toxic Substance and Disease Registry.(2002b). *Toxicological profile for di(2-ethylhexyl) phthalate.* Atlanta, GA.

U.S. Department Health and Human Service. (2006). *NTP-CERHR monograph on the potential human reproductive and developmental effects of di-(2-ethylhexyl) phthalate (DEHP)* (NIH Publ No. 06-4476). Washington, DC.

U.S. Department Health and Human Service. (2003a). *NTP-CERHR monograph on the potential human reproductive and developmental effects of di-n-octyl phthalate (DnOP)* (NIH Publ No. 03-4488). Washington, DC.

U.S. Department Health and Human Service. (2003b). *NTP-CERHR monograph on the potential humanreproductive and developmental effects of di-n-butyl phthalate (DBP)* (NIH Publ No. 03-4486). Washington, DC.

U.S. Environmental Protection Agency. (1999). *Water quality standards* (CFR title 21 Part 131.6). Washington, *DC.*

U.S. Food and Drug Administration. (2003). *Inactive ingredient search for approved drug products* (CFR title 21 Part 210.3(b)(8)). Rockville, MD.

U.S. Food and Drug Administration. (2000). *Indirect food additives: adhesives and components of coatings adhesives* (CFR code 21 Part 175). Silver Spring, MD.

Vasanthi, B. J., & Ravikumar, L. (2013). Synthesis and characterization of poly (azomethine ester)s with a pendent dimethoxy benzylidene group. *Open Journal of Polymer Chemistry, 3*(3): 70-77.

Venkata Mohan, S., Shailaja, S., Rama Krishna, M., & Sarma, P. N. (2007). Adsorptive removal of phthalate ester di-ethyl phthalate from aqueous phase by activated carbon: a kinetic study. *Journal of Hazardous Materials, 146*(1–2): 278-282.

Wade, L. G. (2016). Electronegativity and bond polarity. *Organic chemistry* (pp. 91-96). London, England: Pearson College Division.

Wagner, M., & Oehlmann, J. (2009). Endocrine disruptors in bottled mineral water: total estrogenic burden and migration from plastic bottles. *Environmental Science and Pollution Research, 16*(3): 278-286.

Waltman, R. J., Bargon, J., & Diaz, A. (1983). Electrochemical studies of some conducting polythiophene films. *The Journal of Physical Chemistry, 87*(8): 1459-1463.

Wang, C., Feng, C., Gao, Y., Ma, X., Wu, Q., & Wang, Z. (2011). Preparation of a graphene-based magnetic nanocomposite for the removal of an organic dye from aqueous solution. *Chemical Engineering Journal, 173*(1): 92-97.

Wang, F., Yao, J., Sun, K., & Xing, B. (2010). Adsorption of dialkyl phthalate esters on carbon nanotubes. *Environmental Science & Technology, 44*(18): 6985-6991.

Wang, Q., Chen, Y. F., Yang, M., Wu, X. F., & Tian, Y. J. (2008). Synthesis of low agglomerating spherical αFe_2O_3 nanopowders. *Key Engineering Materials 368-372*: 1568-1569.

Wang, W., Li, Y., Wu, Q., Wang, C., Zang, X., & Wang, Z. (2012). Extraction of neonicotinoid insecticides from environmental water samples with magnetic

graphene nanoparticles as adsorbent followed by determination with HPLC. *Analytical Methods, 4*(3): 766-772.

Wang, Y., Tian, T., Wang, L., & Hu, X. (2013a). Solid-phase preconcentration of cadmium(II) using amino-functionalized magnetic-core silica-shell nanoparticles, and its determination by hydride generation atomic fluorescence spectrometry. *Microchimica Acta, 180*(3-4): 235-242.

Wang, Y., Wang, S., Niu, H., Ma, Y., Zeng, T., Cai, Y., & Meng, Z (2013b). Preparation of polydopamine coated Fe_3O_4 nanoparticles and their application for enrichment of polycyclic aromatic hydrocarbons from environmental water samples. *Journal of Chromatography A, 1283*: 20-26.

Weber, W. J., & Rumer, R. R. (1965). Intraparticle transport of sulfonated alkylbenzenes in a porous solid: diffusion with nonlinear adsorption. *Water Resources Research, 1*(3): 361-373.

White, B. R., Stackhouse, B. T., & Holcombe, J. A. (2009). Magnetic γFe_2O_3 nanoparticles coated with poly-l-cysteine for chelation of As(III), Cu(II), Cd(II), Ni(II), Pb(II) and Zn(II). *Journal of Hazardous Materials, 161*(2): 848-853.

Wooding, A., Kilner, M., & Lambrick, D. B. (1991). Studies of the double surfactant layer stabilization of water-based magnetic fluids. *Journal of Colloid and Interface Science, 144*(1): 236-242.

Wormuth, M., Scheringer, M., Vollenweider, M., & Hungerbuhler, K. (2006). What are the sources of exposure to eight frequently used phthalic acid esters in Europeans? *Risk Analysis, 26*(3): 803-824.

Wu, M. T., Wu, C. F., Wu, J. R., Chen, B. H., Chen, E. K., Chao, M. C., ... Ho, C. K. (2012). The public health threat of phthalate-tainted food stuffs in Taiwan: the policies the government implemented and the lessons we learned. *Environment International, 44*: 75-79.

Wu, Q., Zhao, G., Feng, C., Wang, C., & Wang, Z. (2011). Preparation of a graphene-based magnetic nanocomposite for the extraction of carbamate pesticides from environmental water samples. *Journal of Chromatography A, 1218*(44): 7936-7942.

Wu, X., Hong, H., Liu, X., Guan, W., Meng, L., Ye, Y., & Ma, Y. (2013). Graphene-dispersive solid-phase extraction of phthalate acid esters from environmental water. *Science of the Total Environment, 444*: 224-230.

Wypych, G. (2004). Effect of plasticizers on properties of plasticized materials. *Handbook of plasticizers* (pp. 193-272). Ontario: ChemTec Publishing.

Xie, L., Jiang, R., Zhu, F., Liu, H., & Ouyang, G. (2014). Application of functionalized magnetic nanoparticles in sample preparation. *Analytical and Bioanalytical Chemistry, 406*(2): 377-399.

Xu, C., Lee, J., & Teja, A. S. (2008). Continuous hydrothermal synthesis of lithium iron phosphate particles in subcritical and supercritical water. *The Journal of Supercritical Fluids, 44*(1): 92-97.

Xu, H., Yang, L., Wang, P., Liu, Y., & Peng, M. (2007). Removal mechanism of aqueous lead by a novel eco-material: carbonate hydroxyapatite. *Journal of Materials Science and Technology Shenyang, 23*(3): 417.

Xu, P., Zeng, G. M., Huang, D. L., Feng, C. L., Hu, S., Zhao, M. H., ... Xie, G. X. (2012). Use of iron oxide nanomaterials in wastewater treatment: a review. *Science of the Total Environment, 424*: 1-10.

Xu, Q., An, L., Yu, M., & Wang, S. (2008). Design and synthesis of a new conjugated polyelectrolyte as a reversible pH sensor. *Macromolecular Rapid Communications, 29*(5): 390-395.

Xu, Q., Yin, X., Wu, S., Wang, M., Wen, Z., & Gu, Z. (2010). Determination of phthalate esters in water samples using Nylon6 nanofibers mat-based solid-phase extraction coupled to liquid chromatography. *Microchimica Acta, 168*(3-4): 267-275.

Xu, Z. P., Zeng, Q. H., Lu, G. Q., & Yu, A. B. (2006). Inorganic nanoparticles as carriers for efficient cellular delivery. *Chemical Engineering Science, 61*(3): 1027-1040.

Yadava, K., Tyagi, B., & Singh, V. (1989). Fly-Ash for the treatment of water enriched in lead(II). *Journal of Environmental Science & Health Part A, 24*(7): 783-808.

Yang, C. J., & Jenekhe, S. A. (1991). Conjugated aromatic poly (azomethines): characterization of structure, electronic spectra, and processing of thin films from soluble complexes. *Chemistry of Materials, 3*(5): 878-887.

Yang, H., Li, F., Shan, C., Han, D., Zhang, Q., Niu, L., & Ivaska, A. (2009). Covalent functionalization of chemically converted graphene sheets via silane and its reinforcement. *Journal of Materials Chemistry, 19*(26): 4632-4638.

Yokozawa, T., Ajioka, N., & Yokoyama, A. (2008). Reaction control in condensation polymerization. *New frontiers in polymer synthesis* (pp. 1-77). Germany: Springer-Verlag.

Yuan, B. L., Li, X. Z., & Graham, N. (2008). Aqueous oxidation of dimethyl phthalate in a Fe(VI)-TiO_2-UV reaction system. *Water Research, 42*(6): 1413-1420.

Yuan, S., Liu, C., Liao, C., & Chang, B. (2002). Occurrence and microbial degradation of phthalate esters in Taiwan river sediments. *Chemosphere, 49*(10): 1295-1299.

Zarrouk, A., Hammouti, B., Zarrok, H., Al-Deyab, S., & Messali, M. (2011). Temperature effect, activation energies and thermodynamic adsorption studies of l-cysteine methyl ester hydrochloride as copper corrosion inhibitor in nitric acid 2M. *International Journal of Electrochemical Science, 6*: 6261-6274.

Zhai, Y., He, Q., Yang, X., & Han, Q. (2010). Solid phase extraction and preconcentration of trace mercury(II) from aqueous solution using magnetic nanoparticles doped with 1, 5-diphenylcarbazide. *Microchimica Acta, 169*(3-4): 353-360.

Zhang, Niu, H., Hu, Z., Cai, Y., & Shi, Y. (2010). Preparation of carbon coated Fe_3O_4 nanoparticles and their application for solid-phase extraction of polycyclic aromatic hydrocarbons from environmental water samples. *Journal of Chromatography A, 1217*(29): 4757-4764.

Zhang, J., Shao, J., Guo, P., & Huang, Y. (2013). A simple and fast Fe_3O_4 magnetic nanoparticles-based dispersion solid phase extraction of Sudan dyes from food and water samples coupled with high-performance liquid chromatography. *Analytical Methods, 5*(10): 2503-2510.

Zhang, M., Cushing, B. L., & O'Connor, C. J. (2008). Synthesis and characterization of monodisperse ultra-thin silica-coated magnetic nanoparticles. *Nanotechnology, 19*(8): 085601.

Zhao, Q., Lu, Q., & Feng, Y. Q. (2013). Dispersive microextraction based on magnetic polypyrrole nanowires for the fast determination of pesticide residues in beverage and environmental water samples. *Analytical and Bioanalytical Chemistry, 405*(14): 4765-4776.

Zhao, R. S., Wang, X., Yuan, J. P., & Lin, J. M. (2008). Investigation of feasibility of bamboo charcoal as solid-phase extraction adsorbent for the enrichment and determination of four phthalate esters in environmental water samples. *Journal of Chromatography A, 1183*(1): 15-20.

Zhao, X., Shi, Y., Cai, Y., & Mou, S. (2008). Cetyltrimethylammonium bromide-coated magnetic nanoparticles for the preconcentration of phenolic compounds from environmental water samples. *Environmental Science & Technology, 42*(4): 1201-1206.

Zysler, R., Fiorani, D., & Testa, A. (2001). Investigation of magnetic properties of interacting Fe_2O_3 nanoparticles. *Journal of Magnetism and Magnetic Materials, 224*(1): 5-11.

LIST OF PUBLICATIONS AND PAPERS PRESENTED

1. Baharin, S. N. A., Sarih, N. M., & Mohamad, S. (2016). Novel Functionalized Polythiophene-Coated Fe_3O_4 Nanoparticles for Magnetic Solid-Phase Extraction of Phthalates. *Polymers*, *8*(5): 117.

2. Baharin, S. N. A, Sarih, N. M., Mohamad, S., Shahabuddin, S., Sulaiman, K., & Ma'amor, A. (2016). Removal of endocrine disruptor di-(2-ethylhexyl) phthalate by modified polythiophene-coated magnetic nanoparticles: characterization, adsorption isotherm, kinetic study, thermodynamics. *RSC Advances*, *6*(50): 44655-44667.

APPENDIX

Appendix A: FT-IR for Compounds (a) 4-((phenylimino)methyl)phenol (4PIMP) (b) 3-(6-bromohexyl) thiophene (3BHT) and (c) Phenyl-(4-(6-thiophen-3-yl-hexyloxy)-benzylidine)-amine (3TArH).

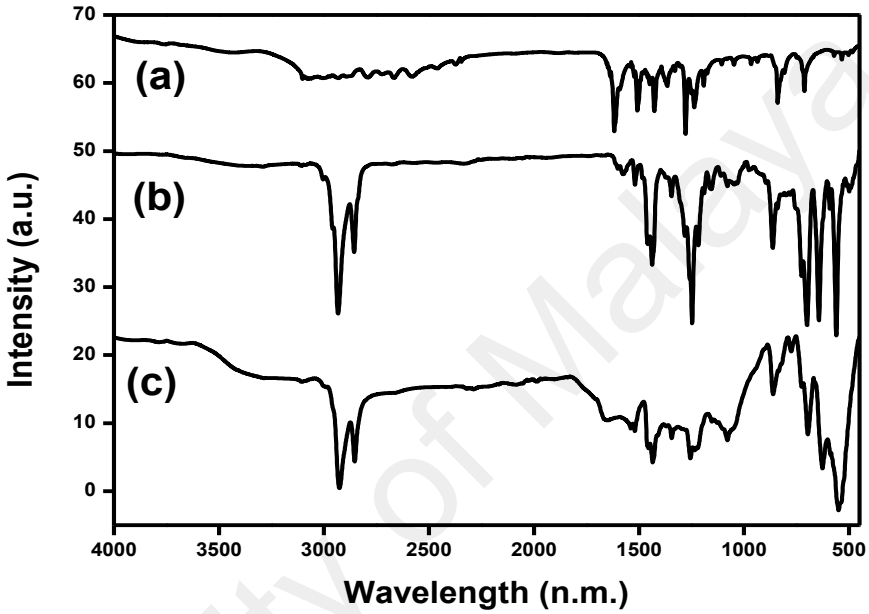

Appendix B: ^{1}H NMR of N-phenyl-1-(2-thienyl)methanimine) (TCN)

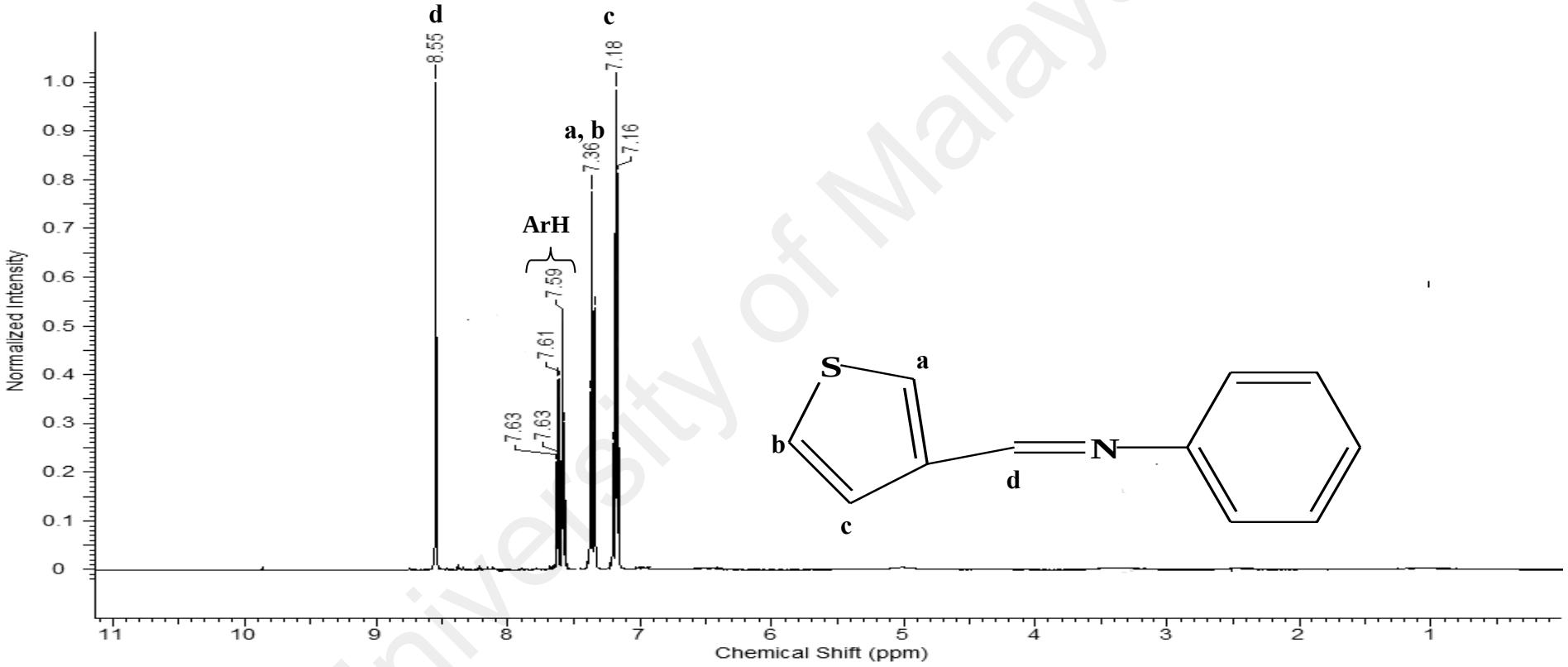

Appendix C: ^{1}H NMR for 3-bromohexylthiophene (3BHT)

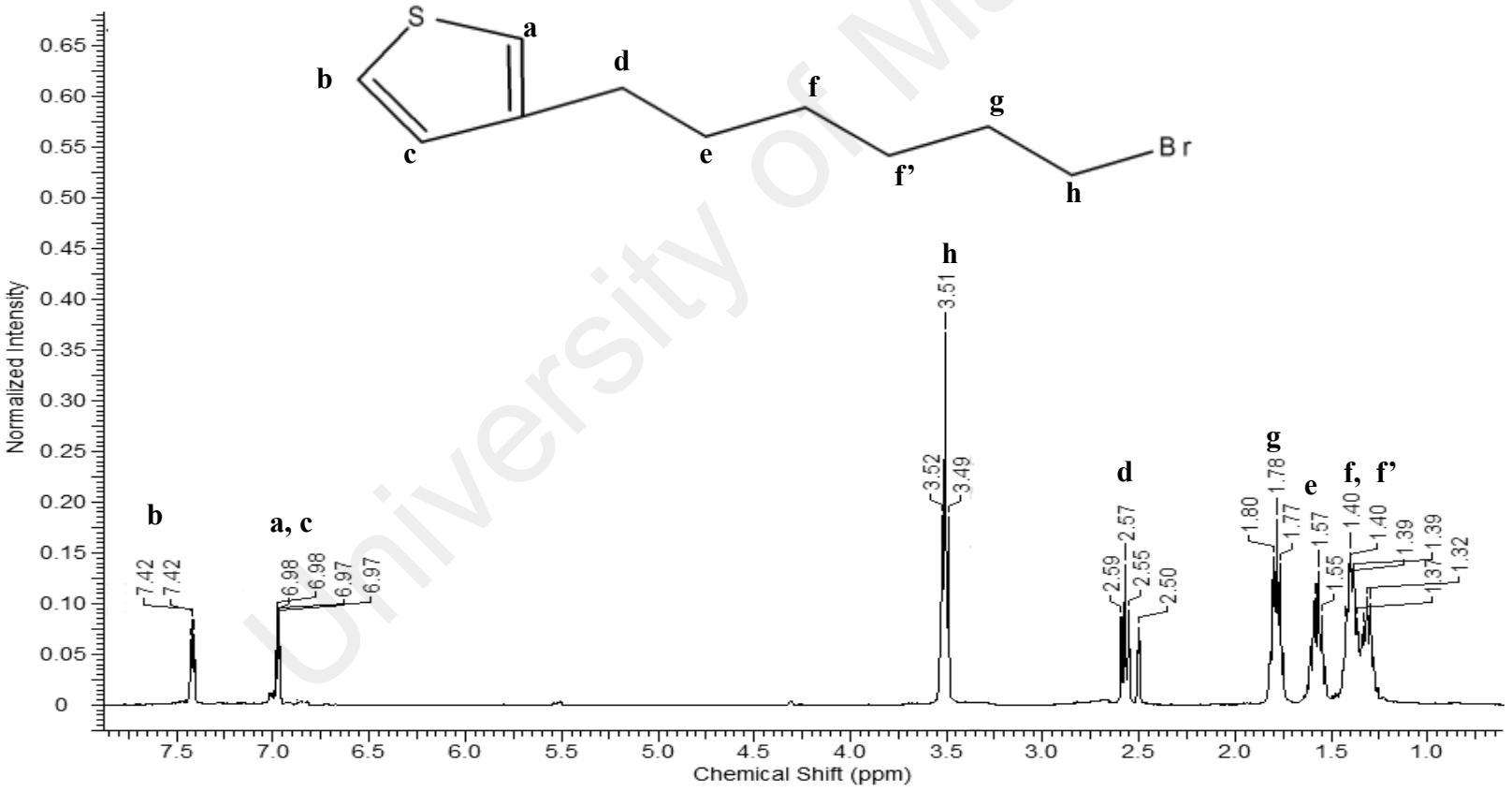

Appendix D: ^{1}H NMR for 4-((phenylimino)methyl)phenol (4PIMP)

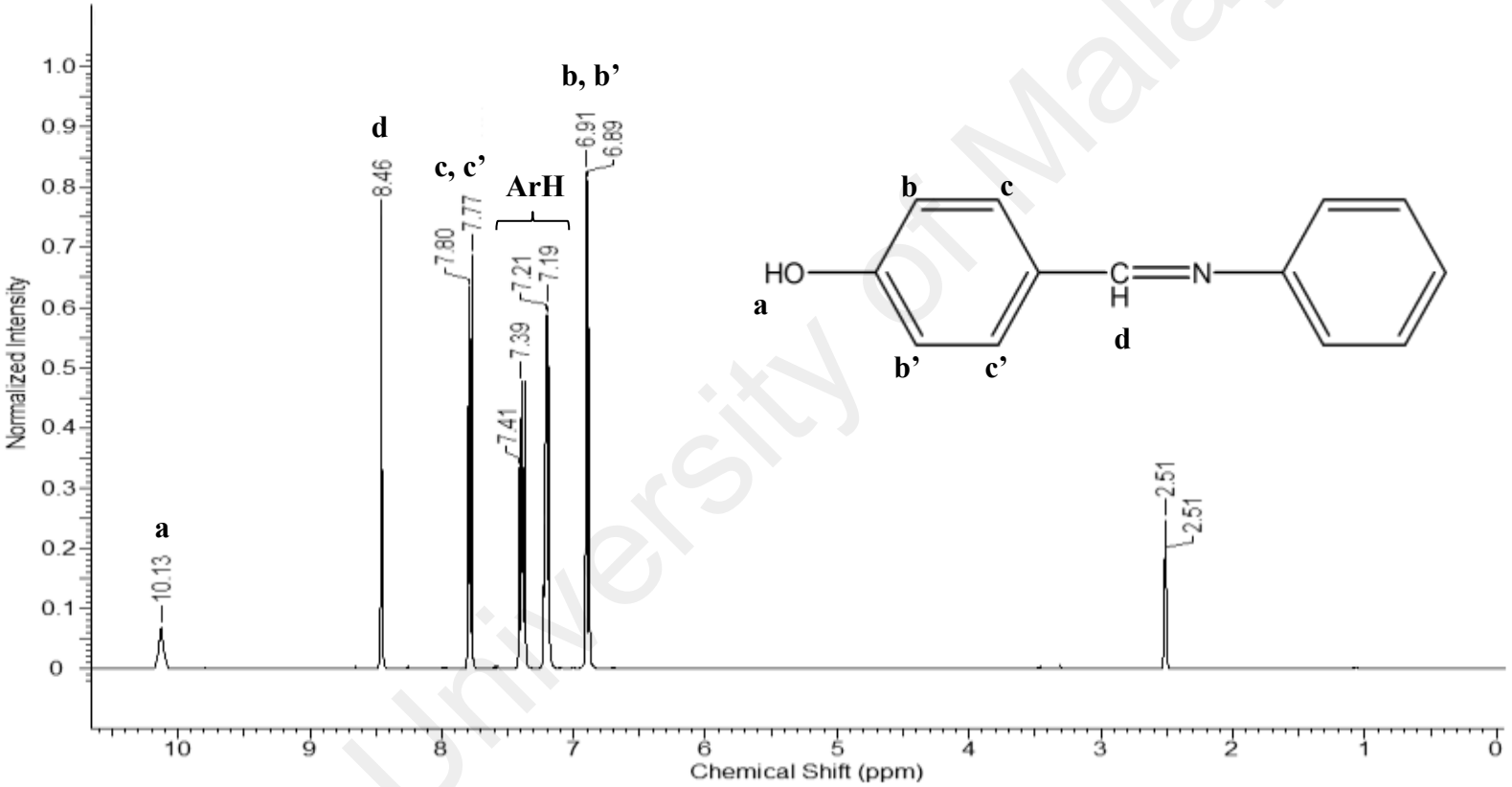

Appendix E: ^{1}H NMR for Phenyl(4-(6-thiophen-3-yl-hexyloxy)-benzylidene)amine (3TArH)

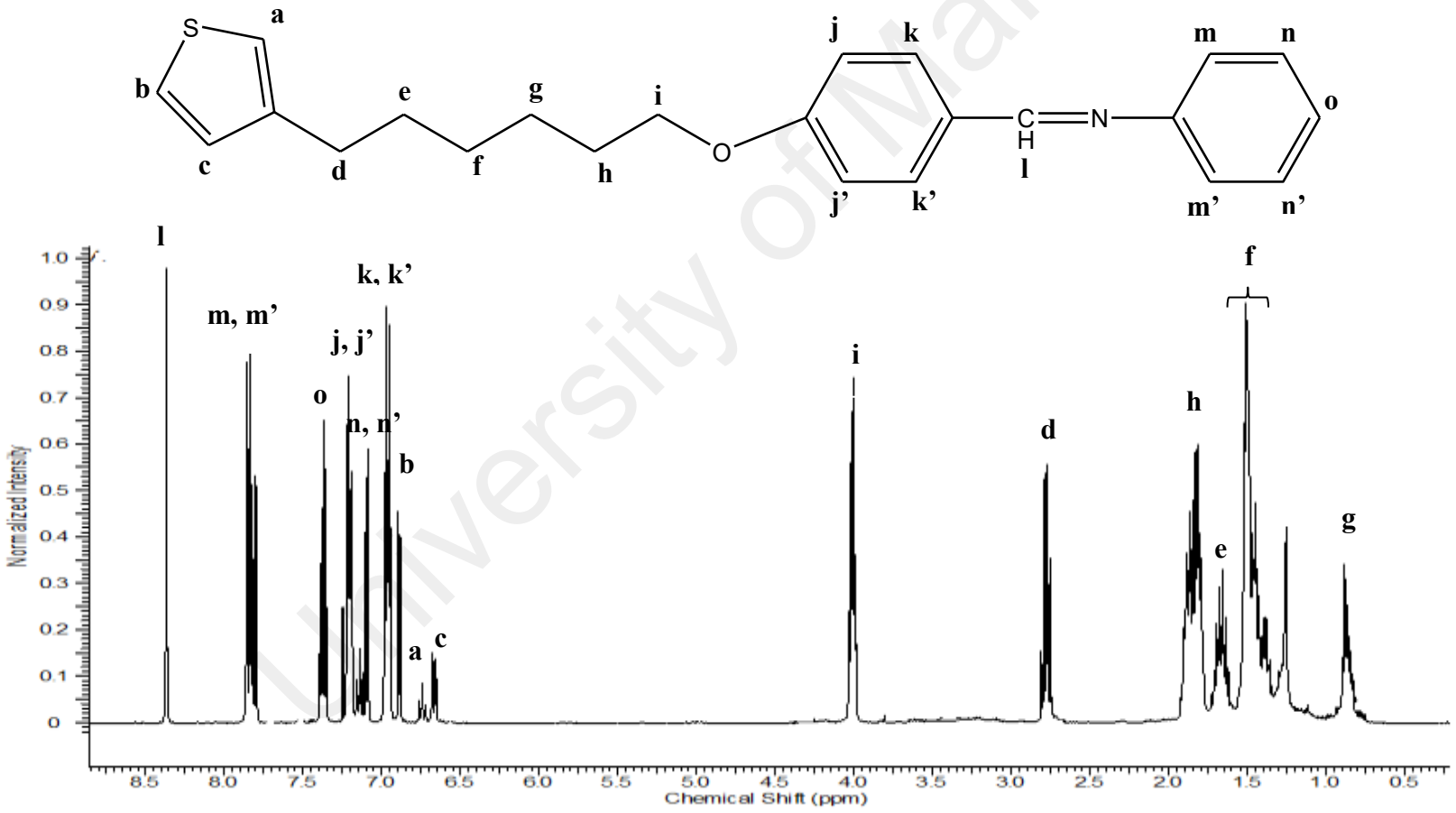

Appendix F: BET Profile a) MNP and b) MNP@P3TArH

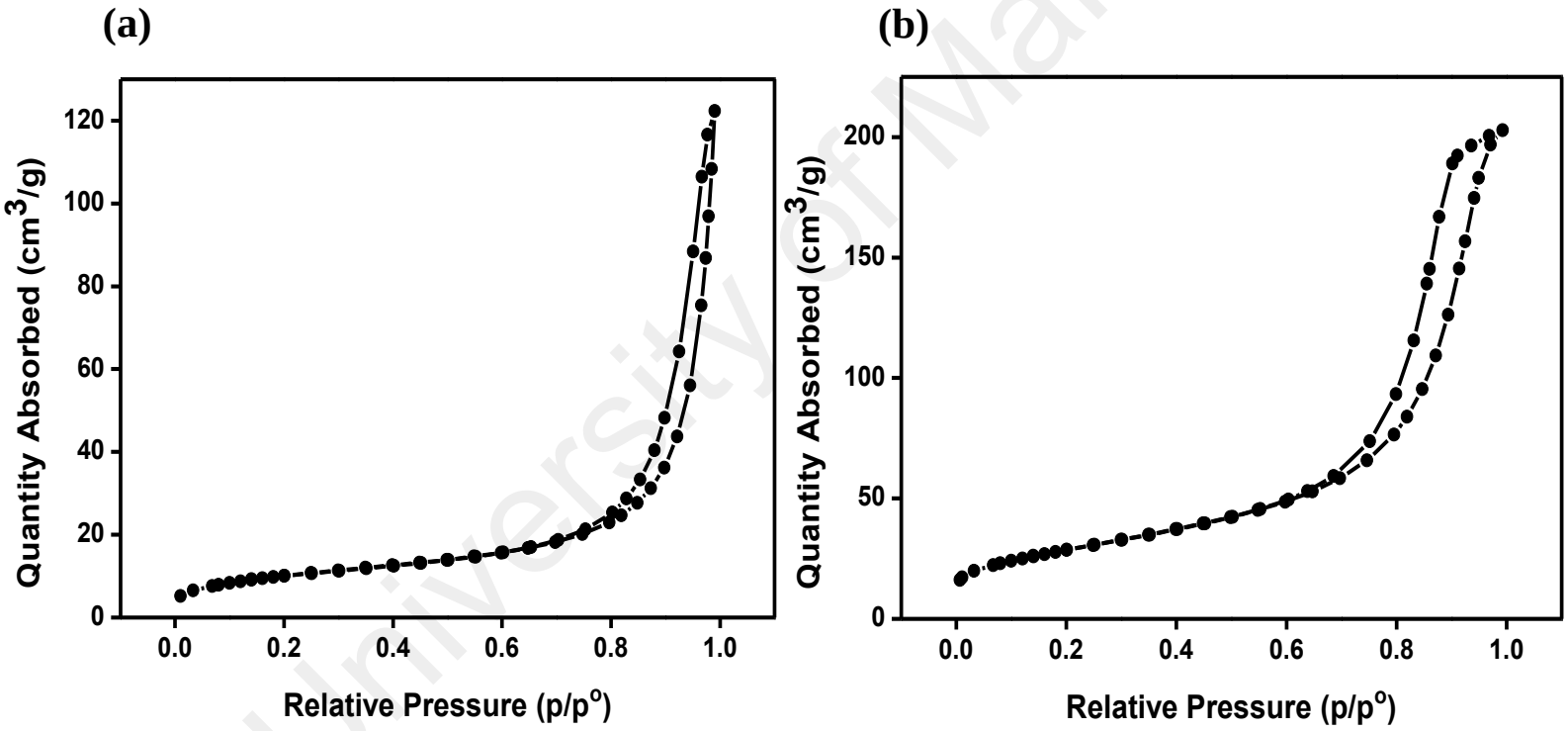

Appendix G: a) Pseudo Second-Order Kinetics Model and b) Van't Hoff Function

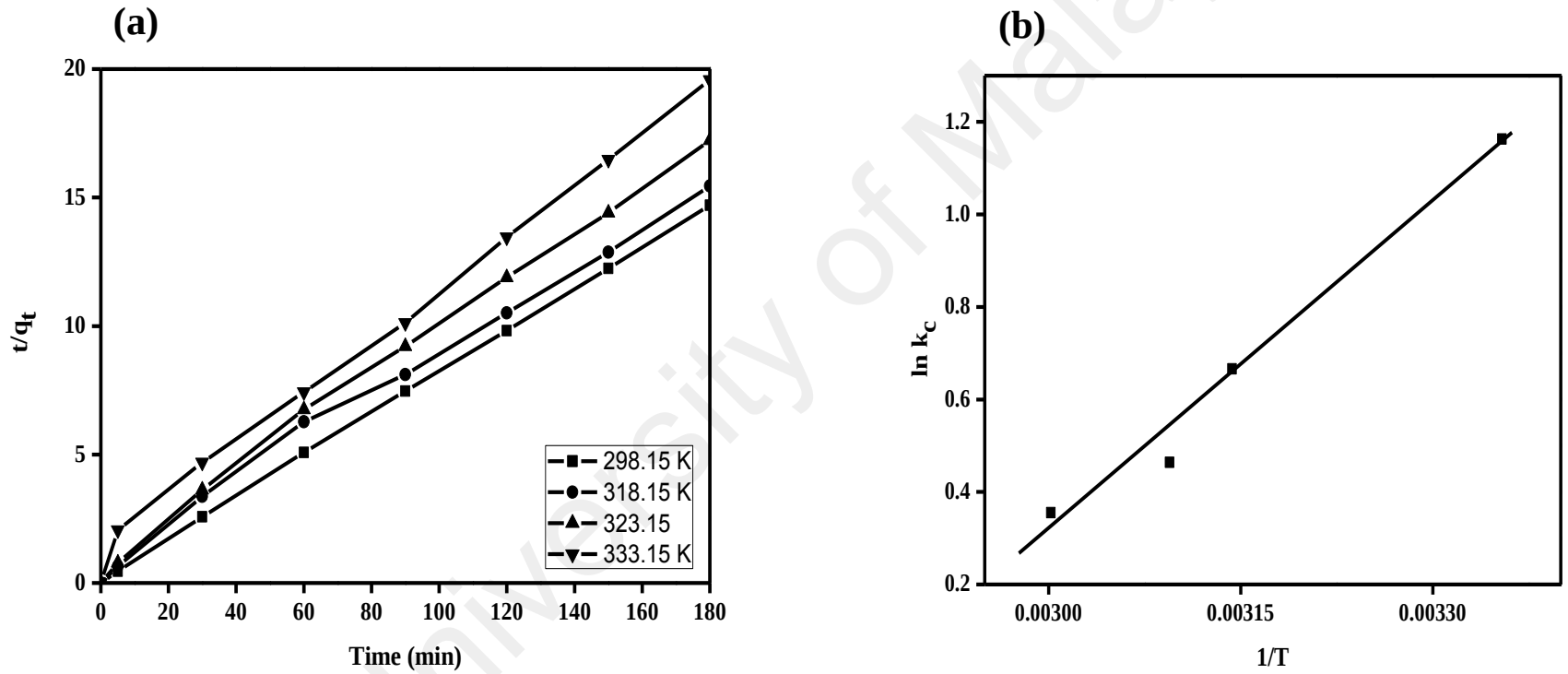

Appendix H: a) Adsorption Efficiency over Time and b) Arrhenius Function

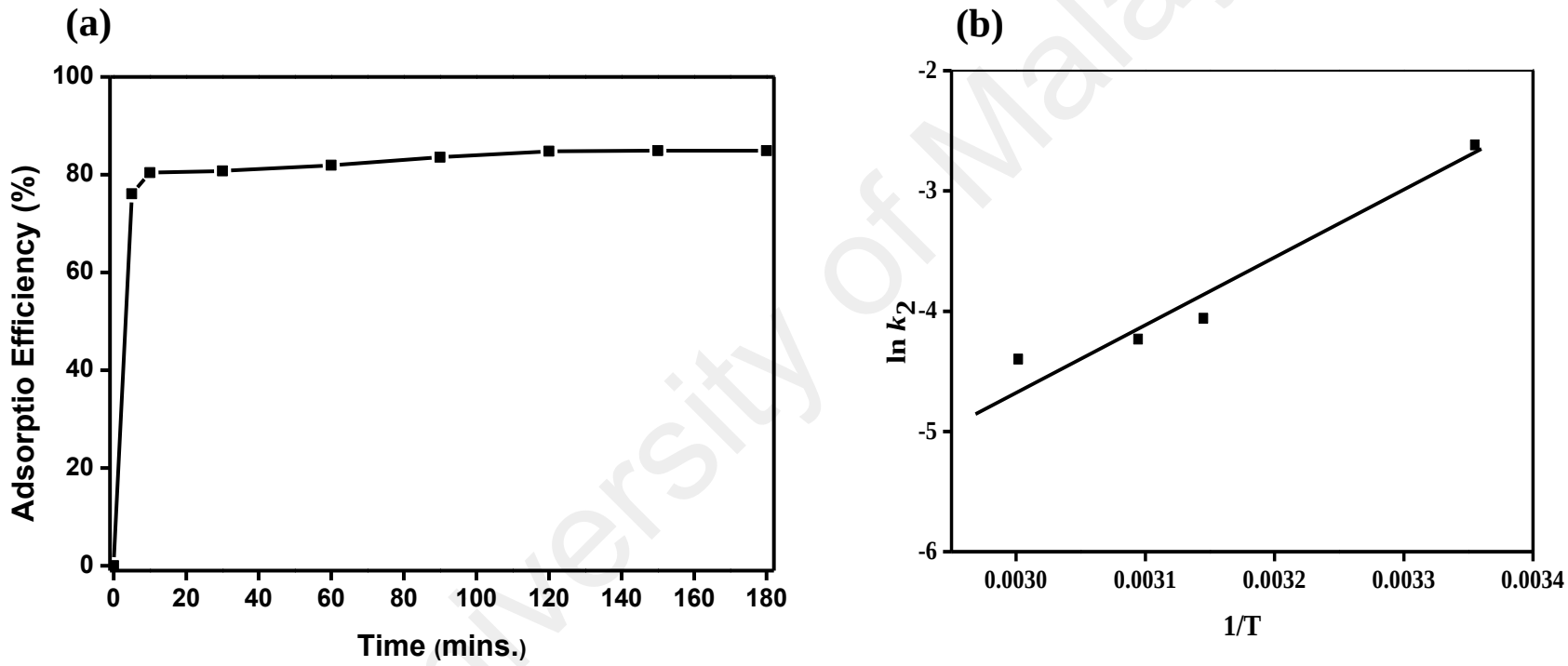

Appendix I: a) Langmuir Isotherm Model and b) Temkin Isotherm Model

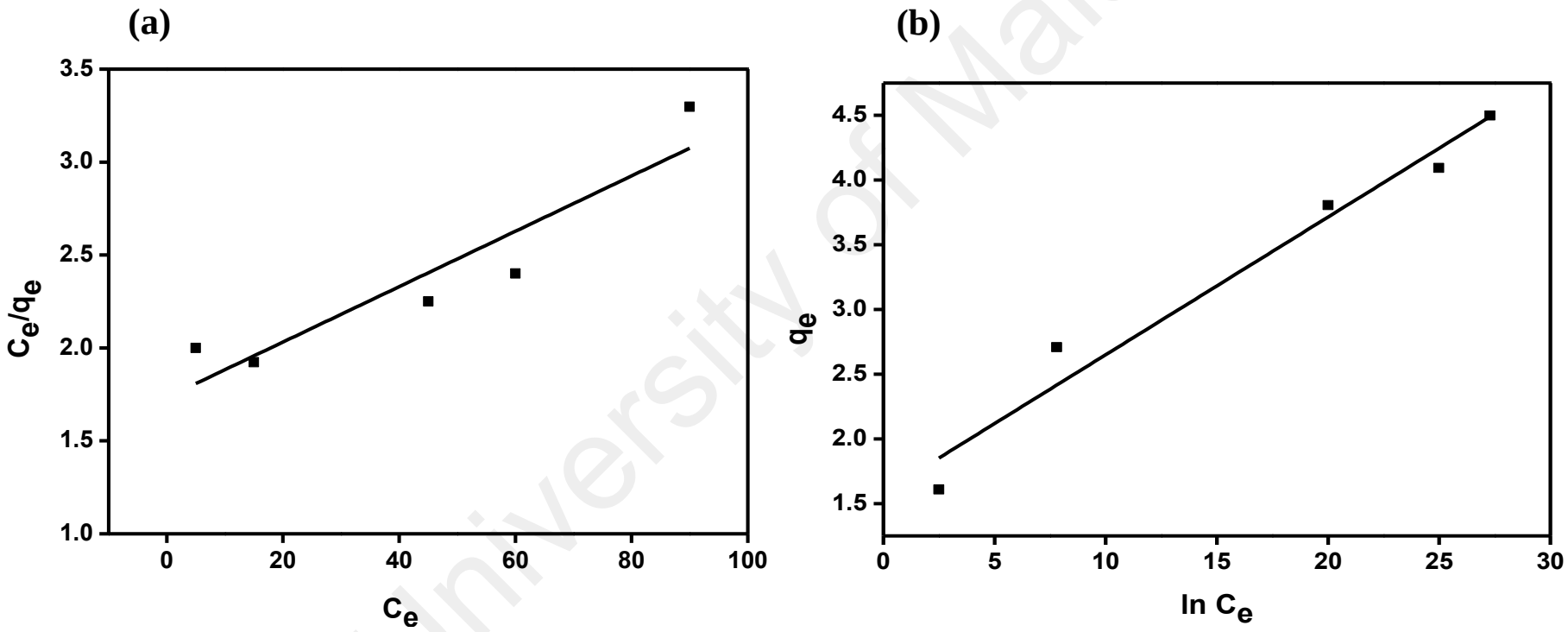

RSC Advances

PAPER

View Article Online
View Journal | View Issue

Cite this: *RSC Adv.*, 2016, **6**, 44655

Removal of endocrine disruptor di-(2-ethylhexyl) phthalate by modified polythiophene-coated magnetic nanoparticles: characterization, adsorption isotherm, kinetic study, thermodynamics†

Siti Nor Atika Baharin,[ad] Norazilawati Muhamad Sarih,*[a] Sharifah Mohamad,[ab] Syed Shahabuddin,[a] Khaulah Sulaiman[c] and Azman Ma'amor[a]

Core–shell magnetic nanoparticles have received significant attention and are actively explored due to their prospective applications. In the current study, superparamagnetic nanosorbent poly(phenyl(4-(6-thiophen-3-yl-hexyloxy)-benzylidene)-amine)/Fe_3O_4 nanoparticles (Fe_3O_4@P3TArH) was successfully synthesized *via* a simplistic method for the enhanced extraction of a potent endocrine disruptor, di-(2-ethylhexyl)phthalate (DEHP). The synthesized materials were characterized by Fourier transform infra-red (FTIR), X-ray diffractometry (XRD), Brunauer–Emmett–Teller (BET) surface area analysis, field emission scanning electron microscope (FESEM), transmission electron microscopy (TEM), and vibrating sample magnetometer (VSM). The extraction efficiencies of the synthesized sorbent materials were evaluated by monitoring the extraction of DEHP from aqueous solution. Removal of DEHP using Fe_3O_4@P3TArh was found to be pH and temperature dependent with a maximum adsorption capacity found to be at 298.15 K at pH 7 and the adsorption kinetics followed a pseudo second-order kinetics model. Thermodynamic studies revealed that adsorption occurred heterogeneously on the adsorption sites, and adsorption of di-(2-ethylhexyl)phthalate onto Fe_3O_4@P3TArh was found to be spontaneous, feasible, ordered, and exothermic. The activation energy was determined to be −40.6 kJ mol^{-1}, which indicated the adsorption process was physisorption.

Received 16th February 2016
Accepted 15th April 2016

DOI: 10.1039/c6ra04172h

www.rsc.org/advances

1. Introduction

Contamination caused by phthalates in the form of plasticizers for polyvinyl chloride resins, adhesives, and cellulose film coatings has recently increased due to widespread use.[1] They are favored as plasticizing agents due to their capabilities of enhancing the placidity and the flexibility of plastics.[2,3] To date, 93% of plasticizers are phthalates, while the rest are esters and polyesters of adipate, phosphoric acid, and sebacic acid.[4] Due to massive consumption of phthalates by many industries, these toxic materials eventually penetrate into the environment. Di-(2-ethylhexyl)phthalate (DEHP) is an important molecule in the phthalates family which is extensively used in medical devices, children's toys, water containers, textiles, and all kinds of packaging.[5–8] It is harmful to humans, especially children, due to the fact that there is no chemical linkage between DEHP molecules and the plastic-based compound, making them easily released to the environment where they can come into contact with consumers.[9] DEHP is also classified as an endocrine disruptor in the context of reproductive health.[10–12] Moreover, DEHP is listed as a significant pollutant in many countries due to its carcinogenic nature.[13]

Due to its toxic and carcinogenic nature, removal of DEHP from waste waters recently has gained immense scientific interest with many crucial methods being reported by several researchers for its removal from an aqueous environment. Biodegradation of phthalates using bacteria culture is one of the potential techniques and has been reported by many researchers.[14,15] However, this method is time consuming, and does not result in complete degradation of phthalates. The coagulation step, during the water treatment process, is useful for removing organic pollutants. Nevertheless, degrading phthalates *via* coagulation using ferric chloride seemed ineffective.[16,17] Another method, called the advanced oxidation

[a]*Department of Chemistry, Faculty of Science, University of Malaya, Malaysia. E-mail: nmsarih@um.edu.my*

[b]*University of Malaya Centre for Ionic Liquids (UMCiL), University of Malaya, 50603 Kuala Lumpur, Malaysia*

[c]*Department of Physics, Faculty of Science, University of Malaya, Malaysia*

[d]*Faculty of Applied Science, Universiti Teknologi MARA, Malaysia*

† Electronic supplementary information (ESI) available. See DOI: 10.1039/c6ra04172h

process (AOP), is based on addition of a highly active oxidizing agent which proficiently oxidizes very stable molecules, such as the degradation of DEHP *via* UV/H_2O_2.[18] Despite the fact that the AOP technique could result in significant degradation, this method requires expensive and toxic reagents, which themselves are considered as pollutants, and are difficult to handle. The adsorption method has been proved to be an effective technique with higher efficacy and capability to remove pollutants on a large scale besides having other advantages including recovery and recycling of adsorbents. Thus, adsorption would be a competent technique for the efficient removal of larger quantities of phthalates from polluted wastewater.[19]

Fe_3O_4 magnetic nanoparticles are one of the most important nanomaterials and technologically important objects for physical and chemical research, with many promising applications. Magnetic nanoparticles (MNPs) were demonstrated to be an efficient adsorbent for adsorption of trace amounts of organic and inorganic analytes from complex media, since they do not require any centrifugations or filtrations.[20] Use of MNPs coated with polymeric material gained much interest, as it enhances surface functionalization and protects the magnetic core from environmental agitation. Moreover, the presence of polymeric surface coated magnetic nanoparticles prevented aggregation and homogenized the nanoparticles core shell distribution within the suspension media.[21] Elevating research interest on using conducting polymer as a polymeric coating material is due to its multifunctional and diverse properties, which includes its cheaper costs, environmental stability, and mechanical robustness.[22–24]

Herein, we report a facile synthesis route to develop a newly designed magnetic nanoparticle of Fe_3O_4 coated with polythiophenes containing Schiff-base, biphenyl pendant, and aliphatic linkage, with its adsorptive performance linked to the removal of DEHP from aqueous solutions. The presence of aliphatic and aromatic side groups in the material significantly enhanced the adsorptive performance for the removal of DEHP from aqueous solution in terms of hydrophobic and π–π interactions. Oxidation/corrosion may reduce magnetic moment of Fe_3O_4 which is responsible for diminishing its magnetization and therefore became a limiting factor in efficient utilization of Fe_3O_4 in various applications. To the best of our knowledge, some Schiff bases containing thiophene substituents have been previously reported as effective erosion inhibitors.[25–27] In the present investigation, Schiff base groups were designed for shielding the magnetic core of Fe_3O_4 from corrosion besides augmenting the adsorption of phthalates due to physical interactions. Simplistic synthesis, cost-effectiveness, and enhanced adsorption behaviour towards DEHP make these nanosorbents a potential adsorbent material for phthalates waste water treatment.

2. Materials and methods

2.1 Reagent and chemicals

Analytical grade ferric chloride, ferrous chloride, ammonia solution (25 wt%), thiophene, 4-hydroxybenzaldehyde, acetonitrile, potassium permanganate, 4-aminophenol, 3-bromothiophene, 1,6-dibromohexane, *N*-bromosuccinimide, acetic acid, sodium hydrogen bicarbonate, potassium iodide, potassium carbonate, tetrahydrofuran, methanol, hydrochloric acid, acetone, and ethyl acetate were purchased from Merck (Darmstadt, Germany). Acetone was procured from Fisher Scientific (Loughborough, UK). Thiophene carboxaldehyde, polyvinyl alcohol, and *n*-butyllithium (2.0 M in cyclohexane) were obtained from Sigma-Aldrich (Milwaukee, WI, USA). Magnesium sulfate anhydrous, ethanol denatured, and hexane were received from J. Kollins (Parkwood, Australia), while dimethyl sulfoxide-d6 (DMSO-d6) and di-(2-ethylhexyl)phthalate (DEHP) were purchased from Acros Organics (Geel, Belgium). Ultrapure water was prepared with a model Aqua Max-Ultra ultra-pure water purification system (Zef Scientific Inc., San Diego, CA, USA). Stock solutions of 1000 mg L^{-1} of standards were prepared by dissolving appropriate amounts of compounds in methanol, which remains stable for three months if stored in a refrigerator at 4 °C. Working standard solutions were prepared daily by diluting the stock standard solution to the required concentrations.

2.2 Synthesis method

2.2.1 Preparation of (phenyl-(4-(6-thiophen-3-yl-hexyloxy)-benzylidine)-amine) (3TArH). A mixture of 4-((phenylimino) methyl)phenol (1.97 g, 10 mmol) (S1) anhydrous potassium carbonate (4.14 g, 30 mmol) (S2), and 18-crown-6 ether (16.6 mg, 0.1 mmol) was stirred in dry and degassed acetone (50 mL) at room temperature followed by the addition of 3-(6-bromohexylthiophene) (0.81 g, 2 mmol) (Scheme 1). The reaction mixture was refluxed under nitrogen with stirring for 24 h. Later, the reaction mixture was cooled to room temperature and poured into the saturated solution of potassium carbonate. The organic phase was collected and washed with water (100 mL), dried with anhydrous sodium sulfate, and subsequently filtered. The solvent was removed *via* reduced pressure, and the residue was dried under vacuum to produce a crude product.[28] Purification was accomplished by column chromatography using silica, with 25% hexane in chloroform to afford the monomer.

2.2.2 Preparation of modified polythiophene-coated magnetic nanoparticles (Fe_3O_4@P3TArH NP) and polythiophene coated magnetic nanoparticles (Fe_3O_4@PTh). Fe_3O_4@P3TArH NPs were synthesized in two steps. Briefly, Fe_3O_4 was prepared by a co-precipitation method.[29] $FeCl_3 \cdot 6H_2O$ (8.48 g) and $FeCl_2 \cdot 4H_2O$ (2.25 g) were dissolved in 400 mL deionized water under nitrogen atmosphere *via* vigorous

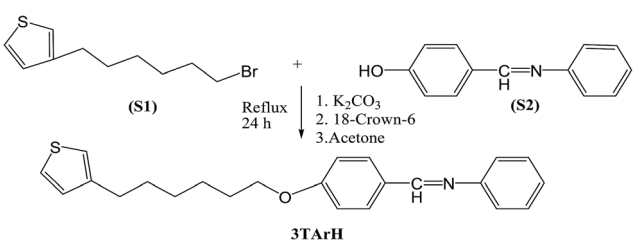

Scheme 1 Synthesis of 3TArH.

stirring (1000 rpm) at 80 °C. Then, a 20 mL ammonia solution (25% wt) was added to the solution. The color of the bulk solution immediately changed from orange to black. After stirring the mixture for 5 min, the Fe_3O_4 NPs precipitates were obtained *via* magnetic decantation, and washed several times with deionized water. Finally, the Fe_3O_4 NPs were dried in a vacuum oven at 70 °C for 12 h. Next, the surface of the Fe_3O_4 NPs was modified by coating with newly designed modified thiophene monomers containing biphenyl pendant (3TArH) *via* oxidation polymerization with the generation of ferric cations on Fe_3O_4 NPs surface.[21] Fe_3O_4 NPs (1 mmol, 0.236 g) was discretized in a PVA aqueous solution (0.5 M). Later, 3TArH (10 mmol, 3.640 g) was added into the mixed solution *via* vigorous stirring. Subsequently, 30 mL of HCl (0.5 M) solution was introduced into the mixture. Then, the product was dried under vacuum at 70 °C for 12 h.

Additionally, the above experiments were repeated using freshly distilled thiophene monomer (10 mmol, 0.84 g) to obtain polythiophene coated magnetic nanoparticles (Fe_3O_4@PTh) which acted as a control adsorbent for comparative study of the adsorption efficiency of different adsorbents.

2.3 Characterization of the samples

Fourier transform infrared (FT-IR) spectra were recorded on a PerkinElmer FT-IR between 4000 and 400 cm^{-1} (PerkinElmer, Massachusetts, USA). Structural elucidation was determined using ^1H NMR, JEOL 400 MHz (JEOL, Tokyo Japan). X-ray powder diffraction (XRD) analysis was conducted with Panalytical model Empyrean at 40 kV and 35 mA using Cu Kα radiation (λ = 1.54059 Å) (Panalytical, Almelo, Netherlands). Morphological analysis of the synthesized products were performed using a JEOL JSM-7600F field emission scanning electron microscope operated at 3 kV (JEOL, Tokyo Japan) and transmission electron microscopy (TEM) analysis using an FEI Tecnai G2 spectra microscope (FEI, Hillsboro, USA). The magnetic property was tested using a vibration sample magnetometer (VSM) Model 9600 (Quantum Design Inc., San Diego, USA). Magnetization measurements were carried out in an external field of up to 15 kOe at room temperature. The thermal stability of Fe_3O_4@P3TArH was investigated by thermogravimetric analysis (TGA); model TGA-STA 1500, with a heating rate of 10 °C min^{-1} between 25 and 900 °C under nitrogen atmosphere (PerkinElmer, Massachusetts, USA). Brunauer–Emmett–Teller (BET) analysis was carried out using a Micromeritics ASAP2020 surface area analyser for determining the pore diameter and the specific surface area of nanosorbents (Micromeritics, Georgia, USA).

2.4 Batch experiments

Experimental parameters were optimized using batch experiments for type of adsorbent, effect of pH, kinetics and thermodynamic studies, effect of initial concentration, equilibrium studies, and reusability studies. Sorption experiments were determined by the following batch method: in each experiment, 5 mg of adsorbent was mixed with 5 mL of an aqueous solution of (DEHP) at a known concentration in a tightly sealed vial. The solution was shaken for 1 h on a shaker at room temperature. After the adsorption process, the adsorbent was separated by magnetic decantation, and the residual concentration was determined using a Shimadzu Ultraviolet-Visible spectrophotometer (UV-Vis), equipped with 1 cm quartz cells (Shimadzu, Kyoto, Japan). All the samples were performed in triplicate. The removal efficiency, R (%) was calculated using the following equation:

$$R\% = \frac{(C_o - C_e)}{C_o} \times 100 \quad (1)$$

The amount of DEHP adsorbed per unit mass of the adsorbent (q_e) was calculated as:

$$q_e = \frac{(C_o - C_e)}{W} V \quad (2)$$

C_o and C_e are the initial and equilibrium concentrations of the solutions (mg L^{-1}), respectively. V (L) is the volume of the

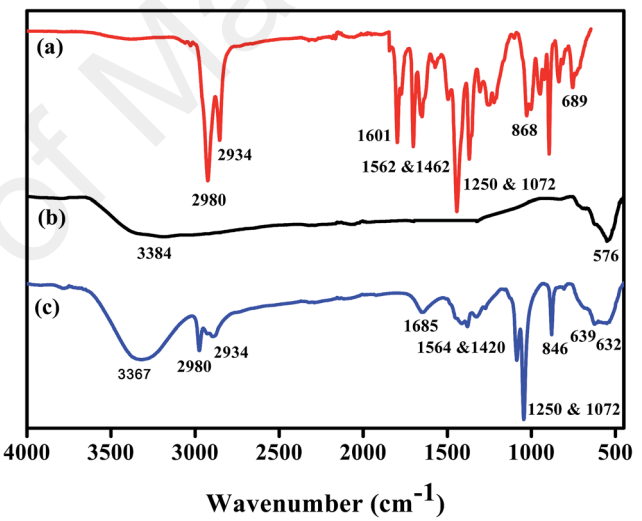

Fig. 1 FT-IR of (a) P3TArH, (b) Fe_3O_4, (c) Fe_3O_4@P3TArH.

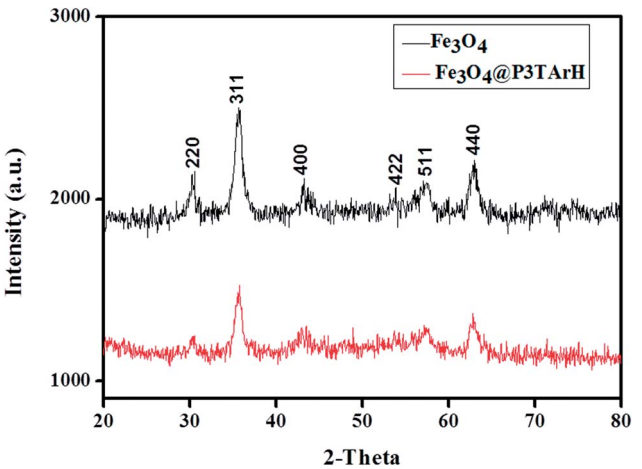

Fig. 2 XRD of Fe_3O_4 and Fe_3O_4@P3TArH.

solution, and W (g) is the mass of the dry adsorbent being used.

3. Result and discussion

3.1 Characterization of the nanocomposites

3.1.1 FT-IR analysis. Fig. 1 show several additional peaks in the spectrum of Fe_3O_4@P3TArH, proportional to the Fe_3O_4 NPs spectrum, which belong to the coating. The intense peaks in the range of ~3400 cm^{-1} for Fe_3O_4 and Fe_3O_4@P3TArH indicated the presence of OH vibration. For both P3TArH and Fe_3O_4@-P3TArH, the C–H aromatic stretching peaks were observed at 2980 cm^{-1}, whereas C–H sp^3 stretching (hexyl aliphatic side) occurred at 2934 cm^{-1}. Meanwhile, Schiff base (C=N) was observed at 1601 cm^{-1} for P3TArH, and 1685 cm^{-1} for the Fe_3O_4@P3TArH.[30] C=C aromatic stretching peaks exhibited at

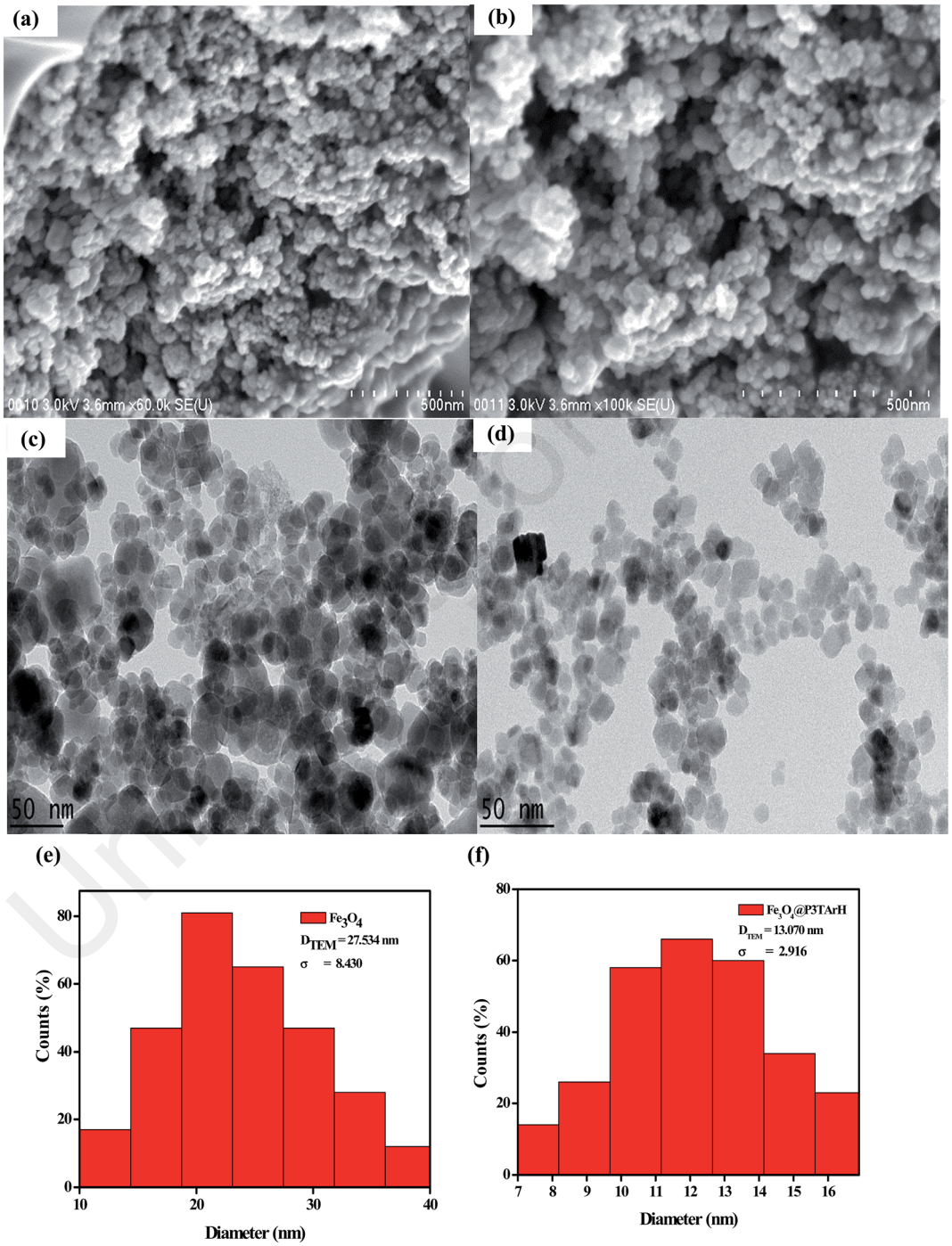

Fig. 3 FESEM images of (a) Fe_3O_4; (b) Fe_3O_4@P3TArH, TEM images of (c) Fe_3O_4; (d) Fe_3O_4@P3TArH and diameter distribution of (e) Fe_3O_4; (f) Fe_3O_4@P3TArH.

1562 cm^{-1} and 1462 cm^{-1} for P3TArH, whereas 1564 cm^{-1} and 1462 cm^{-1} for Fe_3O_4@P3TArH. Two absorption band peaks at 1250 and 1072 cm^{-1} indicated the presence of C–O observed in the P3TArH as well as Fe_3O_4@P3TArH. The strong absorption peaks at 868 cm^{-1} for P3TArH and 846 cm^{-1} for the nanocomposite indicated the presence of C=C symmetric stretching from the thiophene ring. The C–S bending mode occurred at 689 cm^{-1} for P3TArH and 639 cm^{-1} for nanocomposites. Meanwhile, Fe–O stretching modes occurred at 530–632 cm^{-1}.[31] Hence, the FT-IR study clearly revealed the functionalization of Fe_3O_4 NPs with P3TArH.

3.1.2 XRD analysis. Fig. 2 shows the XRD pattern which revealed presence of the characteristic peaks of Fe_3O_4 in the synthesized materials. The peak of the nanocomposites was slightly broader than the ones corresponding to Fe_3O_4. This could be due to the presence of amorphous and polymeric materials.[32] The distinctive peaks of Fe_3O_4 and nanocomposites were observed at $2\theta = 30°$, 35.7°, 43°, 53.4°, 57.0°, and 62.6°, which are marked by their respective indices [(220), (311), (400), (422), (511), and (440)].[33] This indicated that the coating process with P3TArH does not change the crystalline phase of Fe_3O_4.

3.1.3 Morphological analysis. Fig. 3 demonstrates morphological analysis of the synthesized products using FESEM and TEM techniques. FESEM and TEM images of all materials exhibited a sphere-shaped geometry. As evident from the TEM analysis, the distribution of the modified nanoparticles (Fe_3O_4@P3TArH) is very uniform and nanoparticles are segregated. This may be due to the presence of polymeric material coating, which reduces the aggregation and stabilizes the magnetic nanoparticles.[21] Analysis of TEM images using the IMAGEJ software determined the average of particle diameter distribution by computing the values corresponding to at least 300 nanoparticles. Based on the histogram plotted in Fig. 3(e) and (f), D_{TEM}, an average diameter, and σ (standard deviation values) were calculated. TEM average particle size for Fe_3O_4@P3TArH was found to be 13.070 nm ± 2.916. The average particle size Fe_3O_4 was larger than the average particle size of Fe_3O_4@P3TArH as determined from the TEM; this may be due to the fact that many nanoparticles are accumulated and overlaid on top of one another, and thus cannot be measured accordingly.[32]

3.1.4 VSM analysis. Magnetic properties of the samples were recorded at room temperature with an external field of ±15 kOe. *M–H* hysteresis curves of Fe_3O_4 and Fe_3O_4@P3TArH are presented in Fig. 4. An important magnetic parameter, which is saturation magnetization (M_S), was assessed. As is clear from the hysteresis loops, magnetization did not occur until the maximum applied field and exhibited superparamagnetic behavior.[34] Maximum saturation (M_S) of Fe_3O_4 and Fe_3O_4@P3TArH appeared at 92 (bulk magnetization) and 63.2 emu g^{-1}, respectively. Reduced magnetization signifies the presence of a dead magnetic layer on the surface of the nanocomposites.[31] Magnetization is reduced in nanocomposite, but still the value of magnetization falls within the acceptable range, which suggested that the nanocomposites still can be separated conveniently from a solution with an external magnetic field.[35]

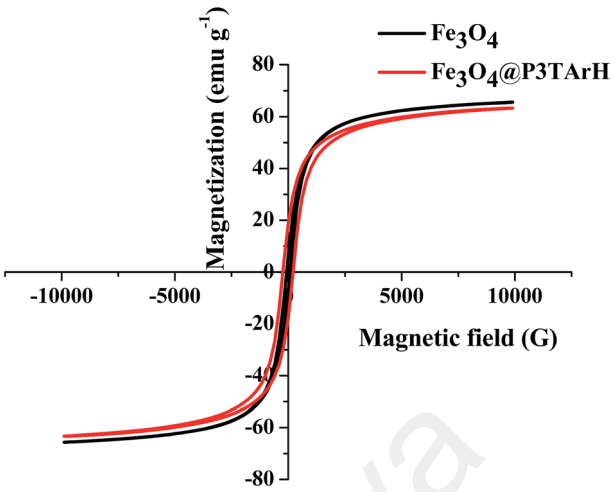

Fig. 4 VSM spectra of Fe_3O_4 and Fe_3O_4@P3TArH.

3.1.5 Thermal analysis. Fig. 5 shows TG and DTG analyses for Fe_3O_4 and Fe_3O_4@P3TArH. A small weight loss was detected under 200 °C in Fe_3O_4 and was speculated to be due to desorption of adsorbed water on the surface of the nanoparticles. Since Fe–O is thermodynamically steady within a temperature range of 280 °C to 850 °C, no weight loss was observed for Fe_3O_4 after 200 °C.[36] The TGA thermogram of the nanocomposite indicated that it is stable up to 210 °C. However, above this temperature Fe_3O_4@P3TArH exhibited rapid weight loss in the temperature range from 240 °C and 450 °C. This might be due to the decomposition of P3TArH. Herein, thermal analysis study showed that the surface of Fe_3O_4 was successfully coated with P3TArH.

3.1.6 N_2 physisorption analysis. The BET surface area was measured using the multipoint BET method within the relative pressure (P/P_0) range of 0.05 to 1. As described in Fig. S5 (ESI†), the Fe_3O_4 and Fe_3O_4@P3TArH displays a H3 type hysteresis loop, based on the Brunauer–Deming–Deming–Teller (BDDT)

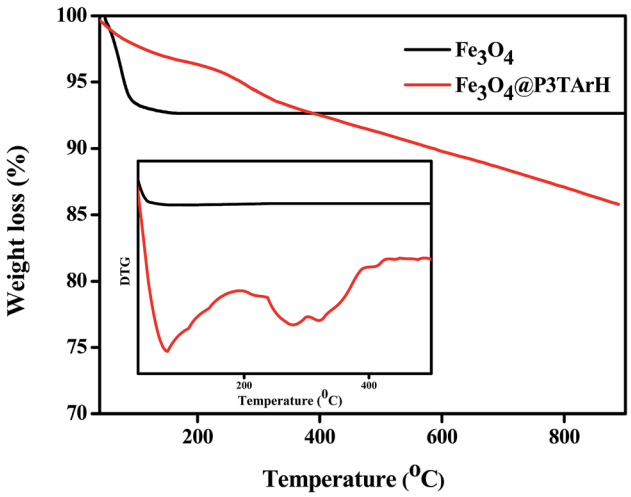

Fig. 5 TGA and DTG (inset) thermograms of Fe_3O_4, and Fe_3O_4@P3TArH.

Table 1 BET pore size and surface area

Sample	Pore size (nm)	Surface area (m^2 g^{-1})
Fe_3O_4	20.2	37.37
Fe_3O_4@P3TArH	12.09	103.80

classification, indicating the presence of mesopores with pore diameters between 2 and 50 nm.[37] The pore size and BET surface area of both Fe_3O_4 and nanocomposites are tabulated in Table 1. The decrease in pore size of nanocomposites is due to the addition of polymer coating on the surface. Increase in the surface area may be attributed to the aggregation of particles that resulted in the enhancement of the spaces between them.[38,39]

3.2 Adsorptive performance

3.2.1 Type of adsorbent. The adsorption efficiency of DEHP for three different types of sorbent namely, Fe_3O_4, polythiophene coated Fe_3O_4 (Fe_3O_4@PTh), and Fe_3O_4@P3TArH is shown in Fig. 6. As evident from the figure, Fe_3O_4 showed adsorption efficiency of 32.52%, while with Fe_3O_4@PTh the value increased to 46.93%. After coating the surface of Fe_3O_4 with P3TArH, the adsorption efficiency increased to 68.73%. This might be due to the presence of more active sites in the Fe_3O_4@P3TArH as well as various physical interactions between adsorbent and adsorbate (hydrophobicity and π–π interaction) as compared to other sorbents, which enhanced the adsorption of DEHP.[40]

3.2.2 Effect of pH. Adsorption was performed under different pH conditions, ranging from pH 3–10. As evidenced from Fig. 7(a), adsorption efficiency increased when the pH increased from 5 to 7, but decreased later from 7 to 10. Fig. 7(b) demonstrated zeta potential analysis of Fe_3O_4@P3TArH with effects of pH range 3 to 9 which represented the surface charge

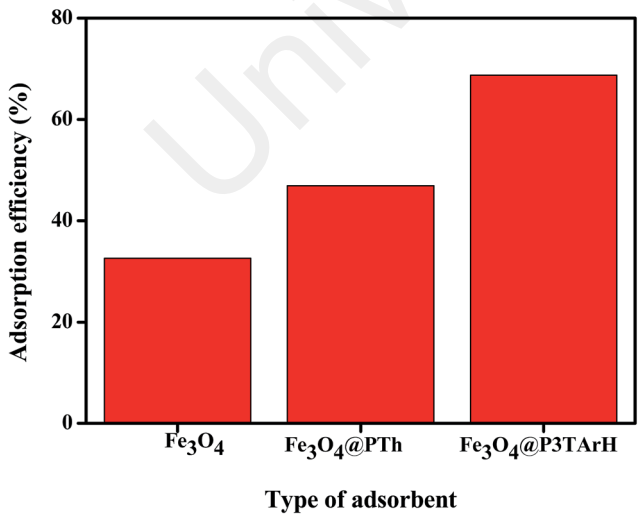

Fig. 6 Type of adsorbent (DEHP concentration, 15 mg L^{-1}; adsorbent, 1 mg L^{-1}; contact time, 60 min; pH 7).

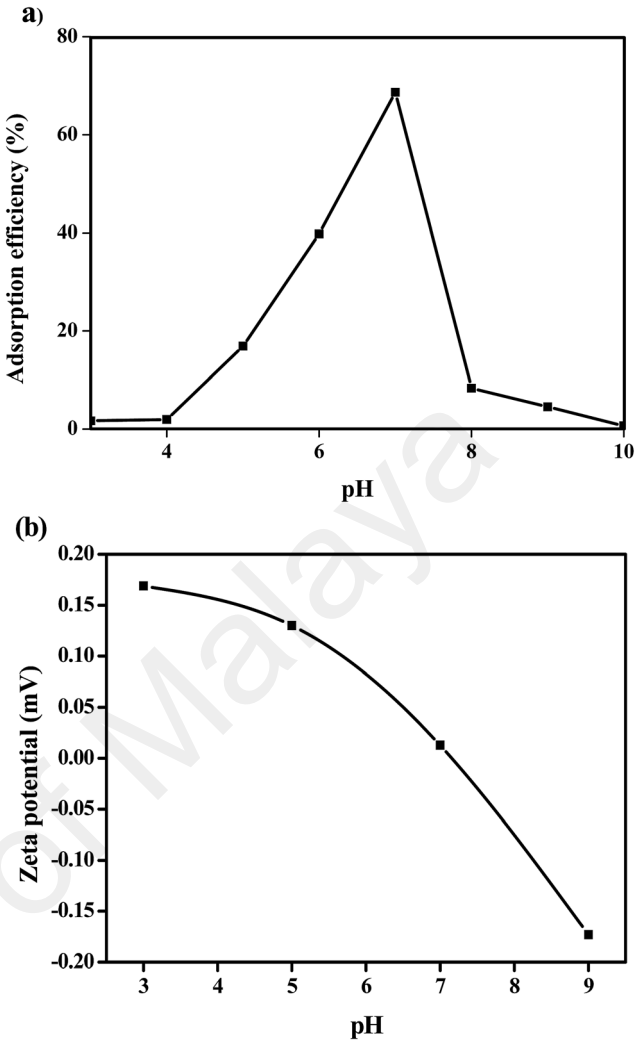

Fig. 7 (a) Effect of solution pH (DEHP concentration, 15 mg L^{-1}; adsorbent, 1 mg L^{-1}; contact time, 60 min); (b) the zeta potential of Fe_3O_4@P3TArH at various pHs.

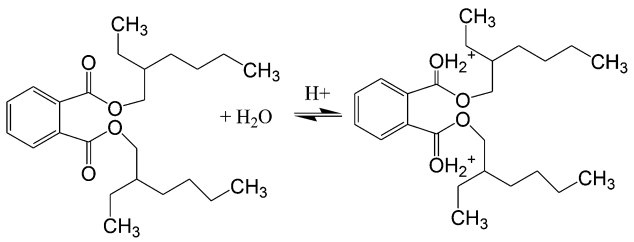

Scheme 2 DEHP at pH < 7.

of Fe_3O_4@P3TArH. At low pH, C=N groups in Fe_3O_4@P3TArH were protonated, making the adsorbent surface positively charged. As described in Scheme 2, at pH < 7, DEHP hydrolyzes to phthalic acid; since the carbonyl group in the phthalic acid is nucleophilic in nature, it can easily react with hydrogen ions in the solution to form positively charged species. Due to both adsorbate and adsorbent acquiring positive charges, electrostatic repulsion occurred and retarded the adsorption

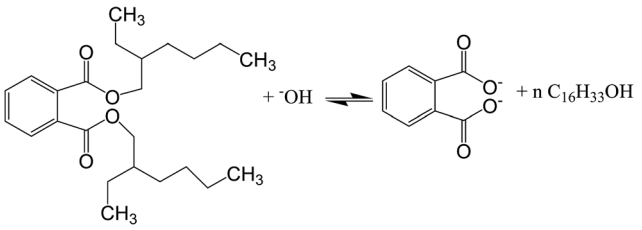

Scheme 3 DEHP at pH > 7.

performance.[41] Moreover, based on zeta potential results at higher pH, the surface of the adsorbent became negatively charged due to deprotonation of C=N in Fe_3O_4@P3TArH, whereas the adsorbate hydrolyzed to phthalate anions as shown in Scheme 3, resulting in repulsion and, thereby, reduced the adsorption efficiency.[42] Strong adsorptive performance in neutral pH can be explained by strong interactions between the hydrophobic and π–π interactions in Fe_3O_4@P3TArH with DEHP. Since the optimum performance of adsorption of DEHP is demonstrated at pH 7, this pH was selected for all of the experiments.

3.2.3 Kinetic and thermodynamic studies. The effect of contact time for the removal of DEHP by Fe_3O_4@P3TArH was investigated in the time range of 0–180 min at four different temperatures of 298.15 K, 318.15 K, 323.15 K, and 333.15 K. Fig. 8 demonstrated that the adsorption capacity was rapid for the first 15 min; which might be due to the many available active sites for adsorption. From 120 min to 180 min the removal capacity was observed to be constant; therefore, 120 min could be regarded as the equilibrium time. To further determine the adsorption mechanism and kinetics parameters, the data gained were fitted into three types of kinetic models: pseudo first-order, pseudo second-order, and intraparticle diffusion.[43–47] The pseudo first-order kinetic model was extensively used to study the adsorption of an adsorbate from an aqueous solution. The equation can be expressed as;

Table 2 Kinetics parameters of DEHP adsorption onto Fe_3O_4@P3TArH

	Fe_3O_4@P3TArH			
Kinetic models	298.15 K	318.15 K	323.15 K	333.15 K
Pseudo-first order				
$q_{e,exp}$ (mg g^{-1})	12.22	11.413	10.09	8.914
$q_{e,cal}$ (mg g^{-1})	10.6	7.45	6.06	11.57
k_1 (min^{-1})	0.0363	0.0317	0.0221	0.0603
R^2	0.7296	0.8754	0.8193	0.9216
Pseudo-second order				
$q_{e,cal}$ (mg g^{-1})	12.30	11.89	10.60	9.85
k_2 (min^{-1})	0.083	0.015	0.014	0.008
R^2	0.9999	0.9957	0.9936	0.9926
Intraparticle diffusion				
K (mg g^{-1} min^{-1})	0.831	0.744	0.695	0.692
c (mg g^{-1})	3.278	3.251	3.214	1.321
R^2	0.705	0.842	0.957	0.9057

$$\log(q_e - q_t) = \log\ q_e - \left(\frac{k_1}{2.30}\right)t \quad (3)$$

where q_e and q_t are the amount of DEHP adsorbed (mg g^{-1}) at equilibrium and time, t is the contact time (min), and k_1 is the rate constant of this equation (min^{-1}). k_1 and q_e were determined from the plot of $\log(q_e - q_t)$ *versus* t. Meanwhile, a pseudo-second order kinetic model is based on the assumption that the adsorption mechanism depends on both adsorbate and adsorbent.[48] The linear equations pertaining to this area follows;

$$\frac{t}{q_t} = \frac{1}{k_2 q_e^2} + \frac{1}{q_e}t, \quad \text{where } h = k_2 q_e^2 \text{ and } t_{\frac{1}{2}} = k_2 q_e^{-1} \quad (4)$$

where h is the initial adsorption rate (mg g^{-1}) min, $t_{1/2}$ is half equilibrium time (min), and k_2 is the pseudo second-order rate constant (g mg^{-1} min). A linear plot of t/q_t *vs.* t could be used to

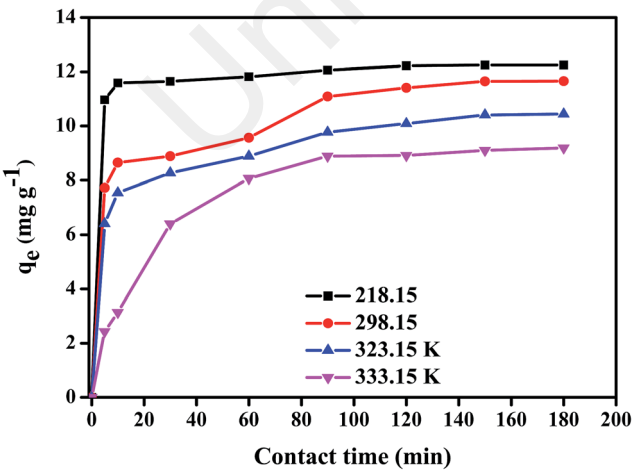

Fig. 8 Effect of contact time and temperature (DEHP concentration, 15 mg L^{-1}; adsorbent, 1 mg L^{-1}; pH 7).

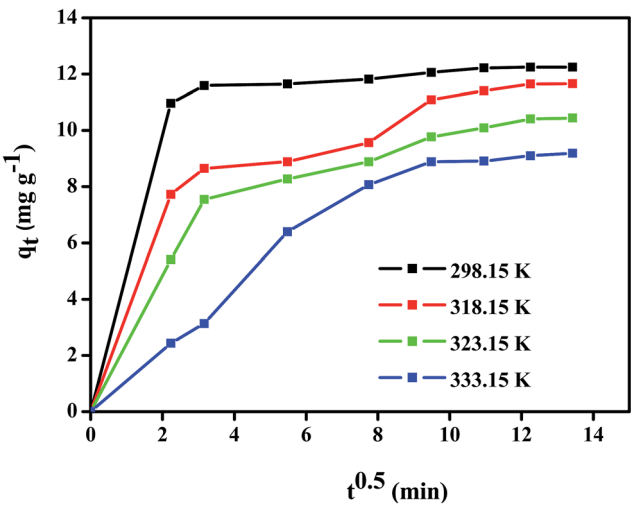

Fig. 9 Intraparticle diffusion plots.

determine the value of q_e, k_2, h, and $t_{1/2}$ respectively. The kinetics parameters and correlation coefficients are listed in Table 2. It can be seen that the experimental data is fitted with the pseudo second-order kinetic model with R^2 near to unity and can be further confirmed by the nearness of the calculated and experimental q_e value. Similar adsorption behavior is also found for the removal of diethyl phthalate by activated carbon.[49] Next, the parameters for intraparticle diffusion models were calculated according to the linear equation as follows;

$$q_t = Kt^{0.5} + c \quad (5)$$

where c is thickness of boundary layer (mg g^{-1}) and K is the rate constant (mg g^{-1} min^{-1}). Fig. 9 reveals that the plots are not linear throughout the contact time. However, a similar trend for four temperatures were observed, and the plots were divided into two parts: at the start of the experiment, a steeper line is detected, which might be due to a massive transfer of DEHP from the boundary layer to the surface of the Fe_3O_4@P3TArH. After 8 min the line continued to be linear, due to diffusion of DEHP through the mesopores of Fe_3O_4@P3TArH.[50]

From the intraparticle diffusion model parameters, the adsorption of DEHP onto Fe_3O_4@P3TArH may be assumed as an exothermic reaction, since the value of boundary layer thickness decreases with increasing temperature.[51] Higher temperature resulted in the solubility of DEHP in aqueous solution increasing and that increased the collision between adsorbent molecules which led to a lower intraparticle diffusion rate.[52]

The thermodynamic parameters were determined to investigate the mechanism of the adsorption process. The values of adsorption enthalpy (ΔH°), entropy (ΔS), and Gibbs free energy (ΔG°), as shown in Table 3, were calculated using the following equations;

$$\ln K_c = \frac{\Delta S}{R} - \frac{\Delta H}{RT} \quad (6)$$

$$K_c = \frac{C_{e(adsorbent)}}{C_{e(solution)}} \quad (7)$$

$$\Delta G^\circ = -RT \ln K_c \quad (8)$$

From the plot of $\ln K_c$ against $1/T$, the (ΔH°) value was found to be negative, which confirms that the adsorption process is exothermic in nature. The increase in temperature enhanced the surface activity of DEHP, increasing its affinity to water.[53] The (ΔS) value was negative, demonstrating that the system reached an ordered state due to the decrease in the randomness of adsorbate/aqueous phase.[54] Decreased ΔG° values with elevating temperature indicated that the process favors low temperature.[55] Moreover, negative values of ΔG° were in a range between −20 and 0 kJ mol^{-1}, indicating that the adsorption process is thermodynamically feasible, physically controlled, and spontaneous.[56,57] The activation energy of the adsorption process can be calculated from the plot of k_2 (pseudo second order rate constant) against $1/T$ using the Arrhenius equation;

$$\ln k_2 = \ln A - \frac{E_a}{R}\left(\frac{1}{T}\right) \quad (9)$$

The value of activation energy for the adsorption of DEHP onto Fe_3O_4@P3TArH was found to be −40.6 kJ mol^{-1} K^{-1}. The negative value of sorption activation energy demonstrated that the process favors low temperature.[58] Moreover, the value of activation energy could be used to determine the adsorption behavior; if the values are less than <40 kJ mol^{-1}, then the process is physisorption, and if it's >40 kJ mol^{-1}, then it is predominantly a chemical adsorption process.

3.2.4 Effect of initial DEHP concentration and isotherm equilibrium studies. Fig. 10 demonstrates the effect of initial concentrations of DEHP in the range of 5–90 mg L^{-1} at 298 K. The adsorptive efficiency increased with increasing initial concentration of DEHP from 5 mg L^{-1} and equilibrium was reached at 15 mg L^{-1} with 83.4%. This indicated that a maximum concentration for 5 mg of Fe_3O_4@P3TArH in 5 mL aqueous solution is 15 mg L^{-1} DEHP, giving significant adsorption efficiency. At low concentration the removal is significant due to the readiness of many active sites for adsorption, whereas at high concentration the removal is persistent due to all the available active sites in adsorbent being fully occupied by DEHP.

To study the adsorption isotherm, four models (Langmuir, Freundlich, Temkin, and Dubinin–Radushkevich (D–R)) were utilized to explain the adsorption behaviour of DEHP onto Fe_3O_4@P3TArH. The Langmuir isotherms model is based on

Table 3 Thermodynamic parameters for DEHP adsorption onto Fe_3O_4@P3TArH

T (K)	$q_{e,exp}$ (mg g^{-1})	ΔG° (kJ mol^{-1})	ΔH° (kJ mol^{-1})	ΔS (kJ mol^{-1} K^{-1})	E_a (kJ mol^{-1} K^{-1})
298.15	12.22	−2.883	−19.77	−0.057	−40.6
318.15	11.41	−1.650			
323.15	10.09	−1.151			
333.15	9.10	−0.881			

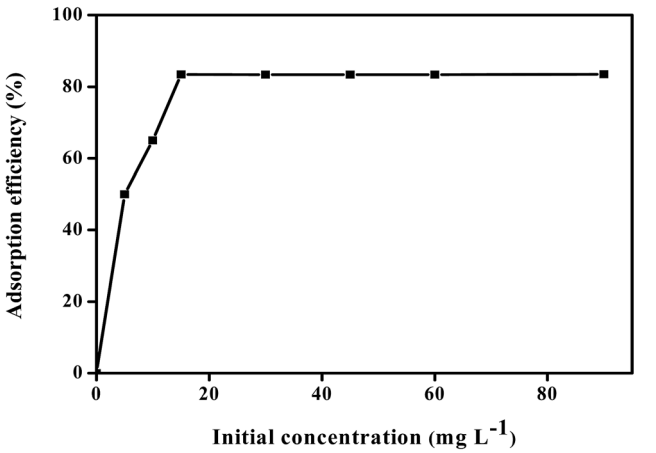

Fig. 10 Effect of DEHP initial concentration (contact time 60 min; adsorbent, 1 mg L^{-1}; pH 7, 298.15 K).

Table 4 Isotherms parameters for DEHP adsorption of onto Fe_3O_4@P3TArH

Isotherms model	Fe_3O_4@P3TArH
Langmuir	
q_m (mg g^{-1})	52.63
b (L mg^{-1})	0.010
R^2	0.8259
R_L	0.8695
Freundlich	
K_F ((mg g^{-1}) (L $mg^{-1})^{1/n}$)	0.6945
$1/n$	1.168
R^2	0.9833
Temkin	
K_T (L mg^{-1})	0.217
b_T (kJ mol^{-1})	276.88
R^2	0.9682
Dubinin–Radushkevich	
q_m (mg g^{-1})	20.00
β	10.575
E	0.615
R^2	0.8502

the expectations that the monolayer adsorption homogenously occurred on all active sites, with no additional adsorption after the sites are fully occupied by the solute at uniform energy.[59] The Langmuir equation is,

$$\frac{1}{q_e} = \frac{1}{bq_m} + \frac{C_e}{q_m} \quad (10)$$

where C_e (mg L^{-1}) is the equilibrium concentration of the adsorbate, C_o (mg L^{-1}) is the initial adsorbate concentration, q_e (mg g^{-1}) is the adsorption capacity at equilibrium, q_m (mg g^{-1}) and b (L mg^{-1}) is the Langmuir constant related to the adsorption capacity and rate of adsorption, respectively. To determine whether the process is either favourable or unfavourable, the dimensionless separation factor (R_L) can be calculated from;

$$R_L = \frac{1}{1 + bC_o} \quad (11)$$

From the plot of C_e/q_e *versus* C_e, the values of Langmuir parameters were determined and listed in Table 4. In contrast to the Langmuir isotherm model, the Freundlich isotherm model assumed that adsorption heterogeneously occurred on the adsorbent's surfaces, with different energies of active sites.[60]

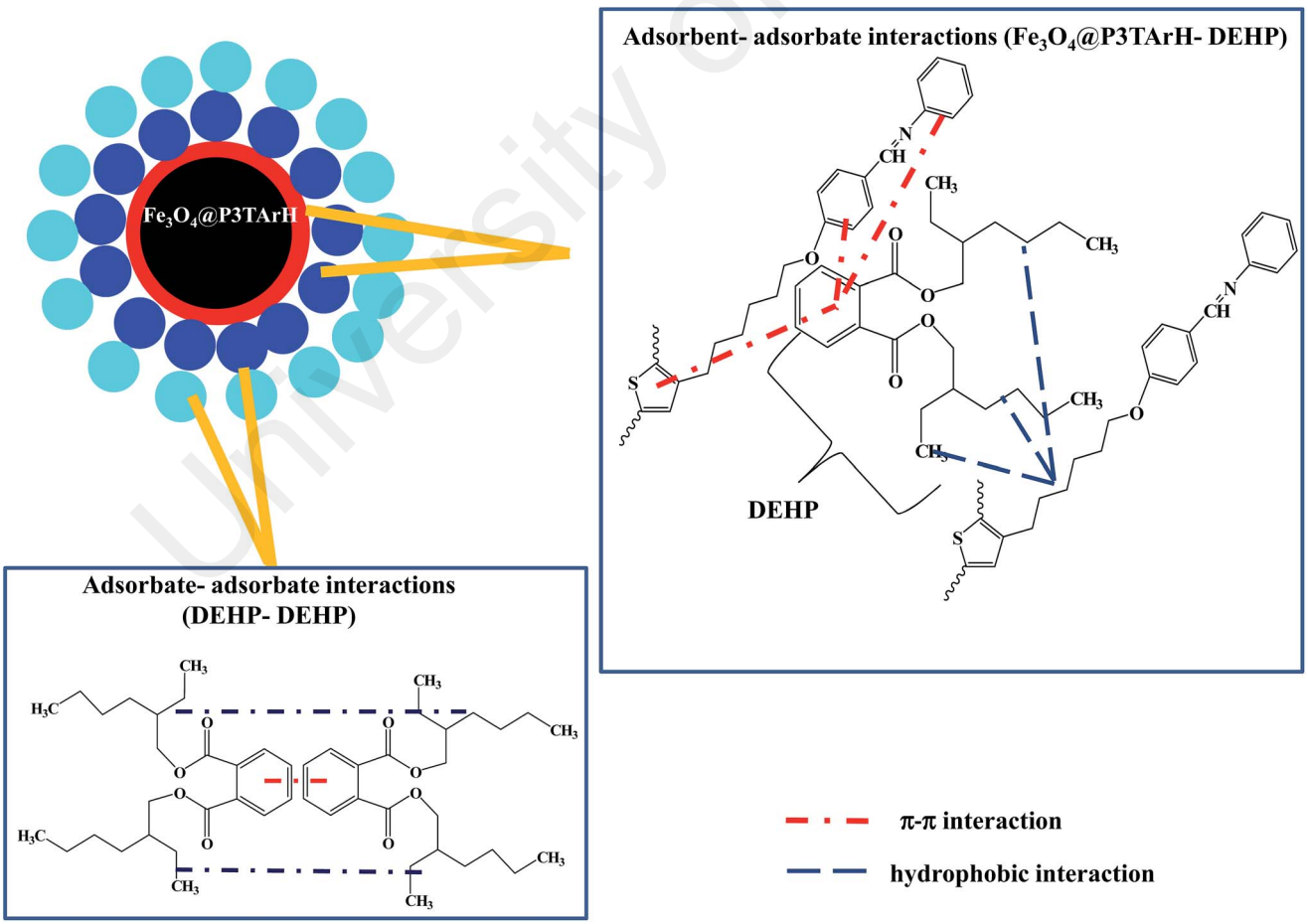

Fig. 11 Proposed interactions for multi-layer adsorption (Freundlich).

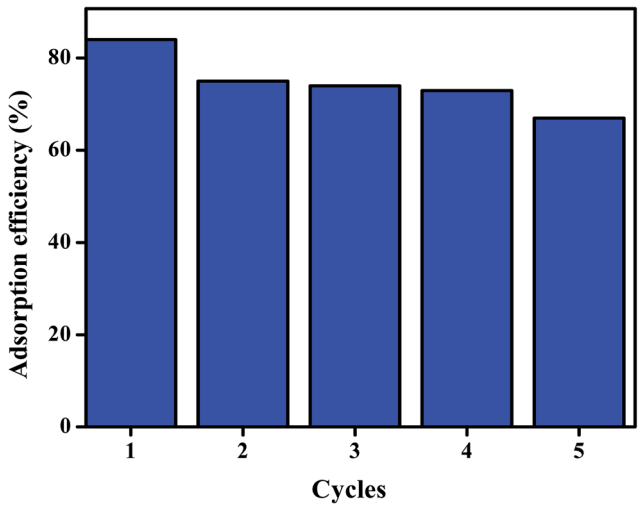

Fig. 12 Reusability graph for five cycles.

The following equations determined the values of Freundlich constant;

$$\log q_e = \log K_F + \frac{1}{n} \log C_e \quad (12)$$

where K_F ((mg g^{-1}) (L mg^{-1})$^{1/n}$) is the adsorption capacity, while $1/n$ represents Freundlich constants, respectively. The Dubinin–Radushkevich isotherm model takes into account the porosity of the adsorbent. The experimental data was fitted with a plot of ln q_e against ε^2 as a linear equation in the following form;

$$\ln q_e = \ln q_m - \beta\varepsilon^2 \quad (13)$$

where β (mol^2 kJ^{-2}) denotes the adsorption energy constant and the Polanyi potential (ε) is mean free energy respectively. E (kJ mol^{-1}) can be obtained using the following equations;

$$\varepsilon = RT \ln\left(1 + \frac{1}{C_e}\right), \quad (14)$$

$$E \text{ (kJ mol}^{-1}) = (2\beta^{-0.5}) \quad (15)$$

where R is the universal gas constant in kJ mol^{-1} K^{-1}, and T is the temperature. The Temkin model was established on the basis that the heat of adsorption would reduce linearly as the layer is covered, resulting in an uneven relationship of adsorbent–adsorbate interfaces on heterogeneous surfaces in adsorption systems.[61] The Temkin model linear equation is as follows:

$$q_e = \beta \ln K_T + \beta \ln C_e, \quad \text{where } b_T = \frac{RT}{\beta} \quad (16)$$

A plot of q_e *versus* ln C_e from the linear equation could be used to determine the Temkin constant, where K_T (L mg^{-1}) is the Temkin constant related to the equilibrium binding energy, and b_T (J mol^{-1}) is Temkin constant related to the heat of adsorption.

Amid the four isotherms studied, the result showed that the adsorption of DEHP onto Fe_3O_4@P3TArH was better described by Freundlich isotherm models ($R^2 = 0.9833$), suggesting that adsorption occurred heterogeneously on adsorption sites. Comparable studies were also found for the adsorption of diethyl phthalate (DEP) using multiwall carbon nanotubes.[62] Additionally, from the linear plot illustrated from Table 4 values, the Freundlich constant, adsorption capacity K_F, and adsorption intensity $1/n$ value were determined to be 0.6945 mg g^{-1} and 1.168, respectively. A high K_F value represented great adsorption affinity towards adsorbate,[63] whereas $1/n \geq 1$ indicated favourable adsorption process.[64] Fig. 11 demonstrated an illustration of proposed interaction for multilayer adsorption according to the Freundlich isotherms. When DEHP and Fe_3O_4@P3TArH come into contact, sorbent active sites which are mesopores (confirmed by BET), hydrophobicity (aliphatic) and π–π interaction (aromatic) enhance the attraction of DEHP. At the same time, DEHP–DEHP also attract each other causing multilayer adsorption which is often observed as a physical adsorption process.[49,65]

3.3 Reusability studies

To determine reusability of Fe_3O_4@P3TArH for adsorption of DEHP, the adsorbent was recycled after being washed with methanol and water, and was dried in vacuum at 70 °C for 12 hours. From Fig. 12, it could be summarized that after five repeated experiments, the adsorption performance was reduced from 84% to 64%. To further confirm the modifications on the sorbent properties, BET surface area analysis and FT-IR of the sorbent was performed after the fifth cycles. From the surface

Table 5 BET surface area analysis of Fe_3O_4@P3TArH and recycled Fe_3O_4@P3TArH

Sample	BET surface area (m^2 g^{-1})
Fe_3O_4@P3TArH	103.8
Recycled Fe_3O_4@P3TArH	49.566

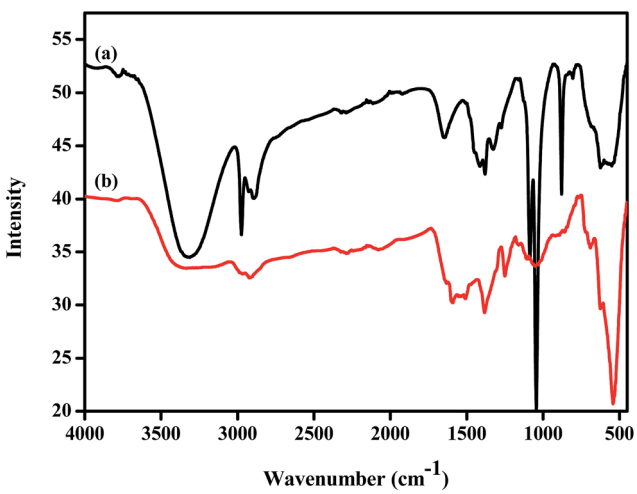

Fig. 13 FT-IR spectrum of (a) Fe_3O_4@P3TArH; (b) recycled Fe_3O_4@P3TArH.

Table 6 Comparison on adsorption capacities

Adsorbent	Analyte	Adsorbent mass (g)	Reaction time (hours)	Maximum adsorption capacities (mg g^{-1})	References
S. siliquastrum	DEHP	0.025	3	5.68	64
Beached seaweed	DEHP	0.025	3	6.54	
Chitosan bead	DEHP	1.5	6	0.49	65
Chitosan bead/α-cyclodextrin	DEHP	1.5	6	3.09	66
Bioslurry	DEHP	15	264	0.972	67
Biofilms	DEHP	1	—	0.161	68
Fe_3O_4@P3TArH	DEHP	0.01	2	52.63	This study

area analysis in Table 5, it was found that surface area of the recycled sorbent was significantly reduced. This may be due to the surface modification of the sorbent material which occurred until fifth cycle as confirmed by FT-IR analysis of the recycled sorbent.[66] The IR spectrum of the recycled sorbent is presented in Fig. 13, and clearly reveals that the intensity of the polymer coating was reduced significantly after the fifth cycle. As a result, active sites (mesopores) and other physical interactions, which played a significant role in adsorption (hydrophobicity, π–π interaction) of DEHP, were decreased from the recycled Fe_3O_4@P3TArH which eventually hampered its adsorptive performance with every cycle.

3.4 Comparative studies

Table 6 reveals a comparison of the maximum adsorption capacities of various adsorbents. Chan H. *et al.* confirmed that breached seaweed resulted in higher adsorption capacity (5.68 mg g^{-1}) compared to *S. siliquastrum*, (6.54 mg g^{-1}) for an adsorbent mass of 0.025 g and 3 hours reaction time,[67] Chen and Chung utilized chitosan bead as an adsorbent to remove DEHP from a plastic manufacturing plant. The maximum adsorption capacity gained from 1.5 g adsorbent dosage and a reaction time of 6 hours was 0.494 mg g^{-1}.[68] The adsorption capacity of DEHP (3.09 mg g^{-1}) was enhanced by modifying chitosan *via* the introduction of α-cyclodextrin by the same author.[69] Shailaja *et al.*, who determined the maximum adsorption capacity was 0.97 mg g^{-1}, removed DEHP through a soil slurry.[70] A study conducted by Cao *et al.* using biofilms obtained 0.161 mg g^{-1} adsorption capacity with 1 g adsorbent.[71] The value of q_{max} in this study was found to be 52.64 mg g^{-1}, which suggests the Fe_3O_4@P3TArH used could readily adsorb DEHP.

4. Conclusion

Magnetic nanoparticles of Fe_3O_4 coated with modified polythiophenes (Fe_3O_4@P3TArH) were successfully synthesized and characterized. FTIR confirmed the presence of P3TArH on the surface of nanoparticles after surface modification. The adsorption processes were shown to be pH dependent, with the optimum removal being observed at a pH of 7. Kinetics analysis indicated that the kinetic data is well fitted in a pseudo second-order equation model. Thermodynamic studies revealed that the adsorption process was exothermic, spontaneous, and in an ordered state. The equilibrium isotherm data fit well into the Freundlich isotherm with $1/n$ indicating a favorable process. The adsorption suggests a multilayer adsorption behavior by considering π–π interaction and hydrophobic interaction of the Fe_3O_4@P3TArH with DEHP. Reusability studies suggested that after five cycles, surface modification of Fe_3O_4@P3TArH occurred; thus, retarding adsorption efficiency.

Acknowledgements

We acknowledge the financial support of the Institute of Research Management and Monitoring (PG044-2012B) University of Malaya and the Ministry of Higher Education for High Impact Research grant (HIR/MOHE/SC/F0031). We also acknowledge the financial support of the Universiti Teknologi MARA and Ministry of Higher Education Malaysia for funding PhD studies to one of the authors-cum-researchers, Siti Nor Atika Baharin.

References

1 X. Li, X. Wang, L. Li, H. Duan and C. Luo, *Talanta*, 2015, **131**, 354–360.
2 P. Serôdio and J. Nogueira, *Water Res.*, 2006, **40**, 2572–2582.
3 H. Koch, L. Gonzalez-Reche and J. Angerer, *J. Chromatogr. B: Anal. Technol. Biomed. Life Sci.*, 2003, **784**, 169–182.
4 C. P. Feás, M. B. Alonso, E. Pena-Vazquez, P. H. Hermelo and P. Bermejo-Barrera, *Talanta*, 2008, **75**, 1184–1189.
5 A. G. Oomen, C. H. M. Versantvoort, M. R. Duits, E. van de Kamp and K. van Twillert, RIVM report 320102003/2004, *Application of in vitro digestion models to assess release of lead and phthalate from toy matrices and azo dyes from textile*, National Institute for Public Health and the Environment (RIVM), Netherland, 2004.
6 M. Castillo and D. Barceló, *Anal. Chim. Acta*, 2001, **426**, 253–264.
7 J. A. Tickner, T. Schettler, T. Guidotti, M. McCally and M. Rossi, *Am. J. Ind. Med.*, 2001, **39**, 100–111.
8 M. Wagner and J. Oehlmann, *Environ. Sci. Pollut. Res.*, 2009, **16**, 278–286.
9 E. Tahmasebi, Y. Yamini, M. Moradi and A. Esrafili, *Anal. Chim. Acta*, 2013, **770**, 68–74.
10 H. Ohtani, I. Miura and Y. Ichikawa, *Environ. Health Perspect.*, 2000, **108**, 1189–1193.

11 G. Latini, A. Verrotti and C. De Felice, *Curr. Drug Targets: Immune, Endocr. Metab. Disord.*, 2004, **4**, 37–40.
12 P. Foster, *Int. J. Androl.*, 2006, **29**, 140–147.
13 P. Kajitvichyanukul and N. Suntronvipart, *J. Hazard. Mater.*, 2006, **138**, 384–391.
14 W. Chao, C. Lin, I. Shiung and Y. Kuo, *Chemosphere*, 2006, **63**, 1377–1383.
15 B. Chang, C. Yang, C. Cheng and S. Yuan, *Chemosphere*, 2004, **55**, 533–538.
16 P. Thebault, J. Cases and F. Fiessinger, *Water Res.*, 1981, **15**, 183–189.
17 W. Zhang, Z. Xu, B. Pan, L. Lv, Q. Zhang, Q. Zhang, W. Du, B. Pan and Q. Zhang, *J. Colloid Interface Sci.*, 2007, **311**, 382–390.
18 M. Julinová and R. Slavík, *J. Environ. Manage.*, 2012, **94**, 13–24.
19 S. Shahabuddin, N. Muhamad Sarih, S. Mohamad and s. n. a. baharin, *RSC Adv.*, 2016, DOI: 10.1039/c6ra04757b.
20 D. Xiao, C. Zhang, D. Yuan, J. He, J. Wu, K. Zhang, R. Lin and H. He, *RSC Adv.*, 2014, **4**, 64843–64854.
21 S. Shin and J. Jang, *Chem. Commun.*, 2007, 4230–4232.
22 J. Meng, J. Bu, C. Deng and X. Zhang, *J. Chromatogr. A*, 2011, **1218**, 1585–1591.
23 A. Mehdinia, F. Roohi and A. Jabbari, *J. Chromatogr. A*, 2011, **1218**, 4269–4274.
24 E. Tahmasebi and Y. Yamini, *Microchim. Acta*, 2014, **181**, 543–551.
25 M. Behpour, S. Ghoreishi, N. Soltani and M. Salavati-Niasari, *Corros. Sci.*, 2009, **51**, 1073–1082.
26 S. Issaadi, T. Douadi, A. Zouaoui, S. Chafaa, M. Khan and G. Bouet, *Corros. Sci.*, 2011, **53**, 1484–1488.
27 A. Yurt, A. Balaban, S. U. Kandemir, G. Bereket and B. Erk, *Mater. Chem. Phys.*, 2004, **85**, 420–426.
28 W. Chen, Y. Chen, F. Li, L. Chen, K. Yuan, K. Yao and P. Wang, *Sol. Energy Mater. Sol. Cells*, 2012, **96**, 266–275.
29 L. Shen, P. E. Laibinis and T. A. Hatton, *Langmuir*, 1999, **15**, 447–453.
30 B. J. Vasanthi and L. Ravikumar, *Open J. Polym. Chem.*, 2013, **3**, 70–77.
31 M. Aydın, Z. Durmus, H. Kavas, B. Esat, H. Sözeri, A. Baykal, F. Yılmaz and M. S. Toprak, *Polyhedron*, 2011, **30**, 1120–1126.
32 L. F. Cótica, I. A. Santos, E. M. Girotto, E. V. Ferri and A. A. Coelho, *J. Appl. Phys.*, 2010, **108**, 064325.
33 S. Giri, B. G. Trewyn, M. P. Stellmaker and V. S. Y. Lin, *Angew. Chem., Int. Ed.*, 2005, **44**, 5038–5044.
34 J. Jayabharathi, P. Ramanathan, V. Thanikachalam and C. Karunakaran, *New J. Chem.*, 2015, **39**, 3801–3812.
35 Z. Ma, Y. Guan and H. Liu, *J. Polym. Sci., Part A: Polym. Chem.*, 2005, **43**, 3433–3439.
36 M. Mahdavi, M. B. Ahmad, M. J. Haron, F. Namvar, B. Nadi, M. Z. A. Rahman and J. Amin, *Molecules*, 2013, **18**, 7533–7548.
37 K. S. W. Sing, *Journal*, 1985, **57**, 603.
38 Q. Wang, Y. F. Chen, M. Yang, X. F. Wu and Y. J. Tian, 2008.
39 J. G. Darab, J. C. Linehan and D. W. Matson, *Energy Fuels*, 1994, **8**, 1004–1005.
40 C. Moreno-Castilla, *Carbon*, 2004, **42**, 83–94.
41 S. V. Mohan, N. C. Rao, K. K. Prasad and J. Karthikeyan, *Waste Manag.*, 2002, **22**, 575–582.
42 Z. Fang and H. Huang, *Adsorpt. Sci. Technol.*, 2009, **27**, 685–700.
43 S. Memon, N. Memon, S. Memon and Y. Latif, *J. Hazard. Mater.*, 2011, **186**, 1696–1703.
44 B. Pan, B. Pan, W. Zhang, Q. Zhang, Q. Zhang and S. Zheng, *J. Hazard. Mater.*, 2008, **157**, 293–299.
45 J. Febrianto, A. N. Kosasih, J. Sunarso, Y.-H. Ju, N. Indraswati and S. Ismadji, *J. Hazard. Mater.*, 2009, **162**, 616–645.
46 Y.-S. Ho and G. McKay, *Water Res.*, 2000, **34**, 735–742.
47 W. J. Weber and R. R. Rumer, *Water Resour. Res.*, 1965, **1**, 361–373.
48 F. A. Pavan, S. L. Dias, E. C. Lima and E. V. Benvenutti, *Dyes Pigm.*, 2008, **76**, 64–69.
49 S. Venkata Mohan, S. Shailaja, M. Rama Krishna and P. N. Sarma, *J. Hazard. Mater.*, 2007, **146**, 278–282.
50 A. A. Jalil, S. Triwahyono, S. H. Adam, N. D. Rahim, M. A. A. Aziz, N. H. H. Hairom, N. A. M. Razali, M. A. Abidin and M. K. A. Mohamadiah, *J. Hazard. Mater.*, 2010, **181**, 755–762.
51 P. Tewari, A. Campbell and W. Lee, *Can. J. Chem.*, 1972, **50**, 1642–1648.
52 K. Yadava, B. Tyagi and V. Singh, *J. Environ. Sci. Health, Part A: Environ. Sci. Eng.*, 1989, **24**, 783–808.
53 G. Minling, M. Xiaojun, S. Wenhua, Q. Yun and W. Lin, *Int. J. Environ. Res.*, 2015, **9**, 605–612.
54 Y. A. Aydın and N. D. Aksoy, *Chem. Eng. J.*, 2009, **151**, 188–194.
55 N. Salleh, A. Jalil, S. Triwahyono, J. Efendi, R. Mukti and B. Hameed, *Appl. Surf. Sci.*, 2015, **349**, 485–495.
56 M. Kilic, E. Apaydin-Varol and A. E. Pütün, *J. Hazard. Mater.*, 2011, **189**, 397–403.
57 A. Zarrouk, B. Hammouti, H. Zarrok, S. Al-Deyab and M. Messali, *Int. J. Electrochem. Sci.*, 2011, **6**, 6261–6274.
58 P. Saha and S. Chowdhury, *Insight into adsorption thermodynamics*, INTECH Open Access Publisher, 2011.
59 V. C. Srivastava, M. M. Swamy, I. D. Mall, B. Prasad and I. M. Mishra, *Colloids Surf., A*, 2006, **272**, 89–104.
60 G. Mckay, H. Blair and J. Gardner, *J. Appl. Polym. Sci.*, 1982, **27**, 3043–3057.
61 M. I. Temkin and V. Pyzhev, *Acta Physicochim. URSS*, 1940, **12**(3), 217–222.
62 F. Wang, J. Yao, K. Sun and B. Xing, *Environ. Sci. Technol.*, 2010, **44**, 6985–6991.
63 H. Xu, L. Yang, P. Wang, Y. Liu and M. Peng, *J. Mater. Sci. Technol.*, 2007, **23**, 417.
64 L. Pelit, F. Ertaş, A. Eroğlu, T. Shahwan and H. Tural, *Bioresour. Technol.*, 2011, **102**, 8807–8813.
65 S. Lyubchik, A. Lyubchik, I. Fonseca, O. Lygina and S. Lyubchik, *Comparison of the thermodynamic parameters estimation for the adsorption process of the metals from liquid phase on activated carbons*, INTECH Open Access Publisher, 2011.
66 M. Cherian, M. S. Rao, W.-T. Yang, J.-M. Jehng, A. M. Hirt and G. Deo, *Appl. Catal., A*, 2002, **233**, 21–33.

67 H. Chan, T. Lau, P. Ang, M. Wu and P. Wong, *J. Appl. Phycol.*, 2004, **16**, 263–274.
68 C.-Y. Chen and Y.-C. Chung, *J. Environ. Sci. Health, Part A: Toxic/Hazard. Subst. Environ. Eng.*, 2006, **41**, 235–248.
69 C.-Y. Chen, C.-C. Chen and Y.-C. Chung, *Bioresour. Technol.*, 2007, **98**, 2578–2583.
70 S. Shailaja, S. Venkata Mohan, M. Rama Krishna and P. N. Sarma, *Int. Biodeterior. Biodegrad.*, 2008, **62**, 143–152.
71 X. Cao, X. Li and X. Meng, *Environ. Eng. Sci.*, 2014, **31**, 55–60.

polymers

MDPI

Article

Novel Functionalized Polythiophene-Coated Fe_3O_4 Nanoparticles for Magnetic Solid-Phase Extraction of Phthalates

Siti Nor Atika Baharin [1,2], Norazilawati Muhamad Sarih [1,*] and Sharifah Mohamad [1,3]

1 Department of Chemistry, Faculty of Science, University of Malaya, 50603 Kuala Lumpur, Malaysia; atikabaharin@gmail.com (S.N.A.B.); sharifahm@um.edu.my (S.M.)
2 Faculty of Applied Science, Universiti Teknologi MARA, 40450 Shah Alam, Malaysia
3 University of Malaya Centre for Ionic Liquids, University of Malaya, 50603 Kuala Lumpur, Malaysia
* Correspondence: nmsarih@um.edu.my; Tel.: +60-3-7967-7173

Academic Editor: Andreas Taubert
Received: 10 March 2016; Accepted: 24 March 2016; Published: 28 April 2016

Abstract: Poly(phenyl-(4-(6-thiophen-3-yl-hexyloxy)-benzylidene)-amine) (P3TArH) was successfully synthesized and coated on the surface of Fe_3O_4 magnetic nanoparticles (MNPs). The nanocomposites were characterized by Fourier transform infra-red (FTIR), X-ray diffractometry (XRD), Brunauer-Emmett-Teller (BET) surface area analysis, analyzer transmission electron microscopy (TEM) and vibrating sample magnetometry (VSM). P3TArH-coated MNPs (MNP@P3TArH) showed higher capabilities for the extraction of commonly-used phthalates and were optimized for the magnetic-solid phase extraction (MSPE) of environmental samples. Separation and determination of the extracted phthalates, namely dimethyl phthalate (DMP), diethyl phthalate (DEP), dipropyl phthalate (DPP), dibutyl phthalate (DBP), butyl benzyl phthalate (BBP), dicyclohexyl phthalate (DCP), di-ethylhexyl phthalate (DEHP) and di-*n*-octyl phthalate (DNOP), were conducted by a gas chromatography-flame ionization detector (GC-FID). The best working conditions were as follows; sample at pH 7, 30 min extraction time, ethyl acetate as the elution solvent, 500-µL elution solvent volumes, 10 min desorption time, 10-mg adsorbent dosage, 20-mL sample loading volume and 15 g· L^{-1} concentration of NaCl. Under the optimized conditions, the analytical performances were determined with a linear range of 0.1–50 µg· L^{-1} and a limit of detection at 0.08–0.468 µg· L^{-1} for all of the analytes studied. The intra-day (n = 7) and inter-day (n = 3) relative standard deviations (RSD%) of three replicates were each demonstrated in the range of 3.7–4.9 and 3.0–5.0, respectively. The steadiness and reusability studies suggested that the MNP@P3TArH could be used up to five cycles. The proposed method was executed for the analysis of real water samples, namely commercial bottled mineral water and bottled fresh milk, whereby recoveries in the range of 68%–101% and RSD% lower than 7.7 were attained.

Keywords: polythiophene; Fe_3O_4 magnetic nanoparticles; phthalates; magnetic solid-phase extraction

1. Introduction

Belonging to non-halogenated esters of phthalic acid, phthalates or phthalate esters are used as plasticizers for nitrocellulose, since it was first recognized in 1880, replacing camphor [1]. Nowadays, phthalates can be found in many different matrices in our environment and are widely utilized in the PVC industries as a plasticizer, from floors, hoses, cables (building materials), toys and medical appliances [2]. Other consumer-based products utilizing phthalates are as a component in inks, adhesive materials, lacquers, sealing and packing materials, materials for treating surfaces, solvents and fixing agents in fragrances, as well as additives in cosmetics [3–5]. They become emerging pollutants and harmful to humans, especially children, since they are not chemically bound in plastics

and could be leached out into the environment [4]. Thus, the usage of phthalates in the production of toys, baby bottles and pacifiers is banned in many countries [6]. Exposure to phthalates over long-term periods could result in health issues, for example potential carcinogenic effects or critical impact on the hormonal systems, since they own lipophilic properties, which make them easily stored in fatty tissues [7–10]. The higher molecular weight of phthalates, such as di(2-ethyl-hexyl) phthalate (DEHP), di-*n*-butyl phthalate (DBP) and di-*n*-octyl phthalate (DNOP) often leads to serious health illnesses and is alleged to be carcinogenic and lethal to liver and kidneys, as well as reproductive organs [11,12]. In Malaysia, due to the awareness of the migration of phthalates from food packaging, baby bottles and pacifiers, a regulation has been proposed, which in stated in Food Regulation 27(B) 1985, which regulated plastic materials, and articles shall be examined in agreement with Malaysia Standard MS 2234: "Plastic Materials and Articles Intended to Come into Contact with Food", which clarified the specific migration limits as follows; 1.5 mg· kg^{-1} for di(2-ethyl-hexyl) phthalate (DEHP), 0.3 mg· kg^{-1} for di-n-butyl phthalate (DBP), 30 mg· kg^{-1} for butyl benzyl phthalate (BBP) and 9.0 mg· kg^{-1} for diisodecyl phthalate (DIDP) [13,14]. Recently, phthalates have been found in polyethylene terephthalate (PET) bottles which may lead to many serious consequences, since the PET bottles are widely used as containers for mineral water, milk and soft drinks. The existence of phthalates in PET bottles may be explained through several possibilities: the type of raw materials, the chemicals or processes involved in bottle manufacturing, the practice of the use of PET bottles, as well as cross contamination in the bottling plant and cap resins [15–20]. Studies conducted by Plotan *et al.* and Wagner *et al.* reported that in most of the inspected PET-bottled water samples, endocrine disruptor activity was found [21,22].

Given the unlimited toxic effects arising from these materials, much research has been conducted to find a solution to eliminate its contamination of the environment [23,24]. However, the determination of phthalates in environmental samples is challenging due to their trace amounts and the intervention of an intricate matrix [25]. Therefore, a sample preparation step for the extraction and preconcentration of the analytes is required [26]. Solid phase extraction (SPE) is one of the established and popular methods for sample enrichment prior to analysis using high performance liquid chromatography (HPLC) and gas chromatography (GC) [27–29]. The advantages of SPE over liquid-liquid extraction (LLE) are its simplicity, rapidness, that the adsorbent is recyclable, the steadiness, low cost, high enrichment factors and low usage of organic solvents [30]. Numerous types of sorbents were synthesized and used for the determination of plasticizers, for example an octadecyl packed column (C18), α-cyclodextrin functionalized chitosan, poly(styrene–divinylbenzene) polymers and zeolitic imidazolate [31–34]. The selection of adsorbent plays an important role in SPE, since it can determine the efficiency, anti-interference ability and selectivity of the method for the targeted analytes [35].

Magnetic nanoparticles (MNPs), especially iron oxides, have become one of the most useful materials in numerous applications since their discovery, for example magnetic fluids, catalysis, magnetic resonance imaging and environmental disciplines [36–38]. In the application for the removal of pollutants from the environment, the nano-sized particles provide a high surface area to volume ratio, which enhances adsorption capacity and efficiency [39,40]. Moreover, the distinct feature of MNPs is their rapid response to an external magnetic field. This special property, called superparamagnetism, does not preserve magnetism after the elimination of an external field. Thus, it helps to isolate the adsorbents from an aqueous solution in a complex matrix without the need for centrifugation or filtration and can be referred to as magnetic solid-phase extraction (MSPE) [41,42]. Due to the simplicity of the technique, much research has been published on utilizing Fe_3O_4 as the adsorbent for MSPE in water samples, for example determining antimicrobial residue, heavy metals, non-steroidal anti-inflammatory drugs and pesticides [43–46].

However, the smaller the particle size, the more it becomes unstable, which initiates particle accumulation. Moreover, metal oxide may be oxidize easily and reduce its magnetism properties. Therefore, an appropriate surface functionalization can be done, which can be tailored to the specific targeted analyte. The strategy to protect the magnetic core can be either by organic or inorganic

compounds, for example Al_2O_3, SiO_2, surfactants, alkyl carboxylates and polymeric coatings [47–50]. Recently, research articles reported on the utilization of conducting polymers as a coating agent of the MNPs [51–53]. These nanocomposites have multifunctional and diverse properties, which may enhance the surface functionalization and protect the magnetic core from environmental agitation. Moreover, it may reduce aggregation and disperse the nanoparticles' core shell distribution within the suspension media [54]. Herein, we prepared a modified polythiophene containing an additional aromatic ring and aliphatic sides on the surface of Fe_3O_4 magnetic nanoparticles (MNPs) to investigate its performance as a magnetic solid-phase extraction of phthalates, as shown in Figure 1. Thus, in this work, the sorbent was further tested for real aqueous samples, including commercial mineral water and commercial fresh milk kept in a PET bottle.

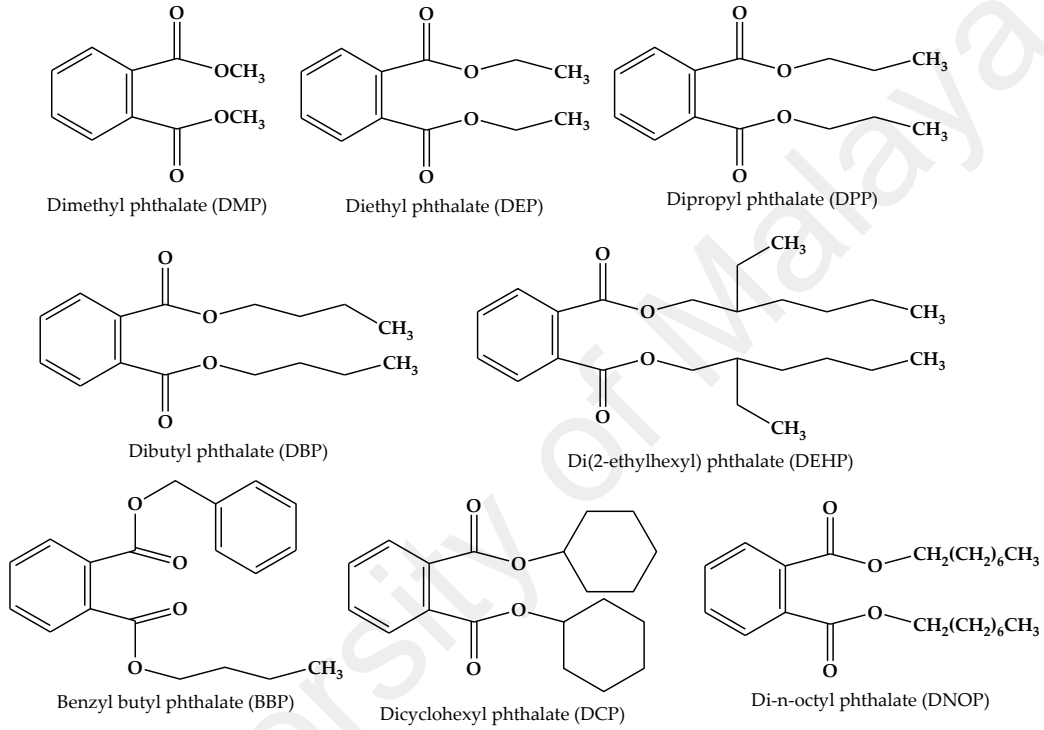

Figure 1. Phthalates used in this study.

2. Materials and Methods

2.1. Standard, Reagents and Chemicals

Analytical grade ferric chloride, ferrous chloride, ammonia solution (25 wt %), thiophene, 4-hydroxybenzaldehyde, acetonitrile, potassium permanganate, 4-aminophenol, 3-bromothiophene, 1,6-dibromohexane, *N*-bromosuccinimide, acetic acid, sodium hydrogen bicarbonate, potassium iodide, potassium carbonate, tetrahydrofuran, methanol, hydrochloric acid, acetone and ethyl acetate were purchased from Merck (Darmstadt, Germany). Acetone was procured from Fisher Scientific (Loughborough, UK). Thiophene carboxaldehyde, polyvinyl alcohol and *n*-butyllithium (2.0 M in cyclohexane) were obtained from Sigma Aldrich (Milwaukee, WI, USA). Magnesium sulfate anhydrous, ethanol denatured and hexane were received from J. Kollins (Parkwood, Australia), while dimethyl sulfoxide-d_6 (DMSO-d_6) and phthalate esters were purchased from Acros Organics (Geel, Belgium). Ultrapure water was prepared by a model Aqua Max-Ultra ultra-pure water purification system (Zef Scientific Inc., San Diego, CA, USA). Stock solutions of 1000 mg·L^{-1} of standards were prepared by dissolving appropriate amounts of compounds in methanol, which remain stable for three months if stored in a refrigerator at 4 °C. Working standard solutions were prepared daily by diluting the stock standard solution to the required concentrations.

2.2. Instruments

The Fourier transform infrared (FTIR) spectra were recorded on a Perkin–Elmer FTIR between 4000 and 400 cm^{-1}, with a resolution of 2 cm^{-1}. Structural elucidation was determined using ^1H NMR, JEOL 400 MHz. The pore diameter and surface area of Brunauer-Emmett-Teller (BET) analysis were determined from low-temperature nitrogen adsorption isotherms at 77.40 K using a Quantachrome Autosorb Automated Gas Sorption System (Quantachrome Instruments, Boynton Beach, FL, USA). X-ray powder diffraction (XRD) analysis was conducted with Panalytical model Empyrean (Panalytical, Almelo, Netherlands) at 40 kV and 35 mA using Cu Kα radiation (λ = 1.54059 Å). Morphological analyses of the synthesized products were conducted using transmission electron microscopy (TEM) analysis using an FEI Tecnai G2 spectra microscope (FEI, Hillsboro, OR, USA). The magnetic property was tested using a vibration sample magnetometer (VSM) Model 9600 (Quantum Design Inc., San Diego, CA, USA). Magnetization measurements were carried out in an external field of up to 15 kOe at room temperature.

Separation and detection of target analytes were performed by a Shimadzu 2010 gas chromatograph (Shimadzu, Kyoto, Japan) equipped with a split/splitless injector and a flame ionization detector (FID). A DB-5 Agilent fused-silica capillary column (Agilent, Santa Clara, CA, USA) (30 m × 0.32 mm i.d. × 0.25 μm film thickness) was applied for separation of analytes. Helium (with 99.999% purity) was used as the carrier gas at a constant flow rate of 4 mL· min^{-1}. Chromatographic conditions were controlled as described; the temperatures of the injector and detector were set at 260 and 280 °C, respectively. The injection port was operated at splitless mode. Oven temperature was held at 150 °C for 1 min and increased to 280 °C at 8 °C· min^{-1} for 3 min.

2.3. Synthesis of Adsorbents

2.3.1. Synthesis of (Phenyl-(4-(6-Thiophen-3-yl-Hexyloxy)-Benzylidene)-Amine) Monomer (**3**) (3TArH)

Synthesis of (**3**) consists of two steps (Scheme 1). The first step is to prepare the intermediates, which were 3-(6-bromohexyl)thiophene (**1**) and 4-((phenylimino)methyl)phenol (**2**). The second step was combining the two intermediates by the Williamson etherification method [55]. FT-IR spectrums of synthesized compounds were demonstrated in (Figure S1, Supplementary Material)

- 3-(6-bromohexyl)thiophene (**1**): 3-bromothiophene (2 mL, 21.3 mmol) was added to the dry, degassed hexane (50 mL). The reaction started by cooling the flask at −78 °C. *n*-Butyllithium in hexane (10.16 mL) was poured into the reaction flask and stirred for 10 min. THF (5 mL) was injected drop-wise for 15 min and continuously stirred for 1 h, which produced a white precipitate and clear supernatant liquid. The supernatant liquid was removed and changed with hexane/THF (10:1 *v*/*v*, 55 mL). 1,6-dibromohexanes (32.7 mL, 213 mmol) was added and stirred for 2 h. The reaction was stopped with the addition of saturated $NaHCO_3$ (50 mL) and diluted diethyl (100 mL). The organic layer was washed with water (100 mL), brine (100 mL), dried with magnesium sulfate anhydrous, treated with decolorizing charcoal, filtered and concentrated in a vacuum to give an oil with an orange color. Excess 1,6-dibromohexane was removed via vacuum distillation (0.04 torr, 55 °C) and purified by silica gel column chromatography (ethyl acetate/hexane, 1/99–5/95 *v*/*v*) to obtain an oily product. Yield: 52%. ^1H NMR (Figure S2, Supplementary Material) (400 MHz, DMSO-D_6) δ (ppm): 7.42–6.97, ($H_{a, b, c}$), 3.51 (H_i), 2.57 (H_d), 1.6–1.32 ($H_{e, f, g, h}$). FTIR (cm^{-1}): 3062.45 (C–H aromatic), 2983 and 2912 (C–H (sp^3)), 1589.22 and 1423.89 (C=C aromatic), 651.02 (C–Br).
- 4-((Phenylimino)methyl)phenol (**2**): 4-hydroxybenzaldehyde (122 mg, 10 mmol) was added to (112 mg, 10 mmol) 2-aminobenzenethiol in 50 mL ethanol. The mixture was refluxed for 3 h. A yellow crystal was obtained after recrystallization with ethanol. Yield: 95%. ^1H NMR (Figure S3, Supplementary Material) (400 MHz, DMSO-D_6) δ (ppm): 10.13 (H_a), 8.46 (H_d), 7.80–6.89 ($H_{b, c, f}$). FTIR (cm^{-1}): 3413.56 (O–H), 3100.34 (C–H aromatic), 1623.05 (C=N) 1589.45 and 1454.65.

- Phenyl-(4-(6-thiophen-3-yl-hexyloxy)-benzylidene)-amine) (**3**): A mixture of 4-((phenylimino) methyl)phenol (1.97 g, 10 mmol), anhydrous potassium carbonate (4.14 g, 30 mmol) and 18-Crown-6 (16.6 mg, 0.1 mmol) was stirred in dried acetone (50 mL) at room temperature. Then, compound 3-(6-bromohexylthiophene) (0.81 g, 2 mmol) was added. The reaction mixture was refluxed under nitrogen with stirring for 24 h. After cooling to room temperature, the reaction mixture was poured into the saturated solution of potassium carbonate. The organic phase was collected and washed by water (3 × 100 mL), dried by anhydrous sodium sulfate and filtered. The solvent was removed by reduced pressure, and the residue was dried by vacuum to produce the crude product. Purification was accomplished by column chromatography on silica with 25% hexane in chloroform to afford the monomer [56]. Yield: 67.6%. ^{1}H NMR (Figure S4, Supplementary Material) (400 MHz, DMSO-D$_6$) δ (ppm): 8.5 (H$_l$), 7.8 (H$_k$), 7.4–6.9 (H$_{j,\,m,\,n,\,o}$), 6.6–6.9 (H$_{a,\,b,\,c}$), 3.97 (H$_i$), 2.67 (H$_d$), 1.74–1.41 (H$_{e,\,f,\,g,\,h}$). FTIR (cm^{-1}): 2938.38, 1617, 1499.9, 1426.71, 1239.71, 1018.26.

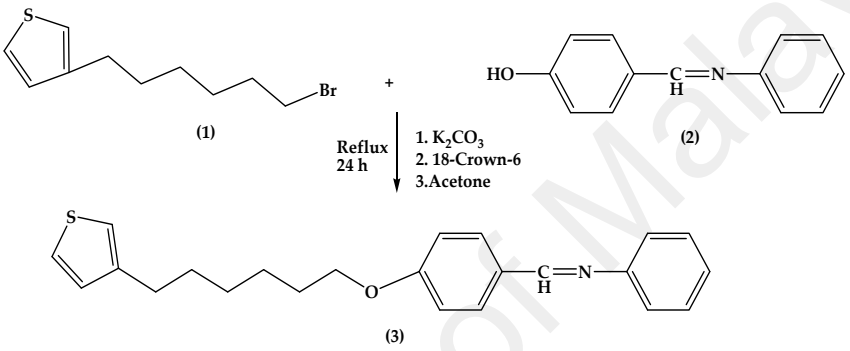

Scheme 1. Synthesis pathway for (phenyl-(4-(6-thiophen-3-yl-hexyloxy)-benzylidene)-amine) (3TArH).

2.3.2. Polymerization of 3TArH and Thiophene Monomers on the Surface of MNPs

The preparation of MNP@PTh and MNP@P3TArH NPs involves two steps. Briefly, Fe_3O_4 has been prepared by the co-precipitation method [57]. $FeCl_3 \cdot 6H_2O$ (8.48 g, 30 mmol) and $FeCl_2 \cdot 4H_2O$ (2.25 g, 11.3 mmol) were dissolved in 400 mL deionized water under nitrogen atmosphere via vigorous stirring (1000 rpm) at 80 °C. Then, a 20-mL ammonia solution 25% (*w*/*w*) was added to the solution. The color of the bulk solution immediately changed from orange to black. After stirring the mixture for 5 min, the Fe_3O_4 NP precipitates were obtained via magnetic decantation and washed three times with deionized water. Finally, the Fe_3O_4 NPs were dried in a vacuum oven at 70 °C for 12 h.

The surface of Fe_3O_4 NPs was modified by being coated with the newly-designed modified thiophene monomers via oxidation polymerization with the generation of ferric cations on the Fe_3O_4 NPs' surface [54]. Fe_3O_4 NPs (1 mmol, 0.235 g) were discrete in polyvinyl alcohol (PVA) aqueous solution (0.001 M). Later, 3TArH (3.64 g, 10 mmol) was added into the mixed solution with vigorous stirring. Subsequently, 30 mL of HCl (0.5 M) solution were introduced into the mixture. Then, the products obtained were dried in a vacuum oven at 70 °C for 12 h. Experiments were repeated using freshly-distilled thiophene monomer (10 mmol, 0.84 g).

2.4. Solid Phase Extraction Optimization and Reusability Studies

Factors affecting the extraction efficiency of the proposed method, such as type of adsorbents, pH, extraction time, sample volume, elution solvent, elution solvent volume, desorption time, adsorbent dosage and effect of NaCl, were studied. All of the experiments were performed in triplicate, and the means of the results were used in plotting the optimization curves.

The reusability of the adsorbent was determined with optimized conditions for up to five cycles. The adsorbent was recycled after being washed with methanol and water and dried in vacuum at 70 °C for 12 h.

2.5. Analytical Performances and Real Sample Analysis

In order to evaluate the figures of merit of the proposed technique, linearity, the limit of detection (LOD), the limit of quantitation (LOQ) and repeatability were investigated under optimized conditions. The linearity was analyzed through the standard curves ranging from 0.1–50 $\mu g \cdot L^{-1}$ by diluting appropriate amounts of phthalates stock solution (1000 $mg \cdot L^{-1}$) with methanol and prepared in triplicate. The calibration curves were prepared using 10 spiking levels of analytes. For each level, three replicate experiments were performed.

To evaluate the reliability of the proposed method for the extraction of the plasticizers from real samples, two real samples were selected, spiked and subjected to the MSPE-GC-FID analysis. The two real samples were commercial bottled mineral water and bottled fresh milk.

3. Results and Discussion

3.1. Characterization of the Samples

Figure 2 shows several additional peaks in the spectrum of nanocomposites, proportional to the MNP spectrum, which might be due to the surface functionalization. The strong absorption peaks in the range of ~3400 cm^{-1} for MNP and all nanocomposites indicated the presence of OH vibration, while the peak at 530–632 cm^{-1} corresponds to Fe–O stretching modes [58]. The C–H aromatic stretching peak was observed for all nanocomposites, which falls at 3000 cm^{-1} for MNP@PTh and 2980 cm^{-1} for MNP@P3TArH. C–H sp^3 stretching (hexyl aliphatic side) occurred at 2934 cm^{-1} for MNP@P3TArH. Schiff base peaks (C=N) were observed at 1674 and 1685 cm^{-1} for MNP@P3TArH [59]. C=C aromatic symmetric and asymmetric absorption bands demonstrated in the range of 1573–1461 cm^{-1} occurred for both nanocomposites. Two absorption band peaks at 1250 and 1072 cm^{-1} indicated the presence of C–O in MNP@P3TArH. Hence, the FTIR study clearly revealed that the MNPs prepared have been successfully functionalized.

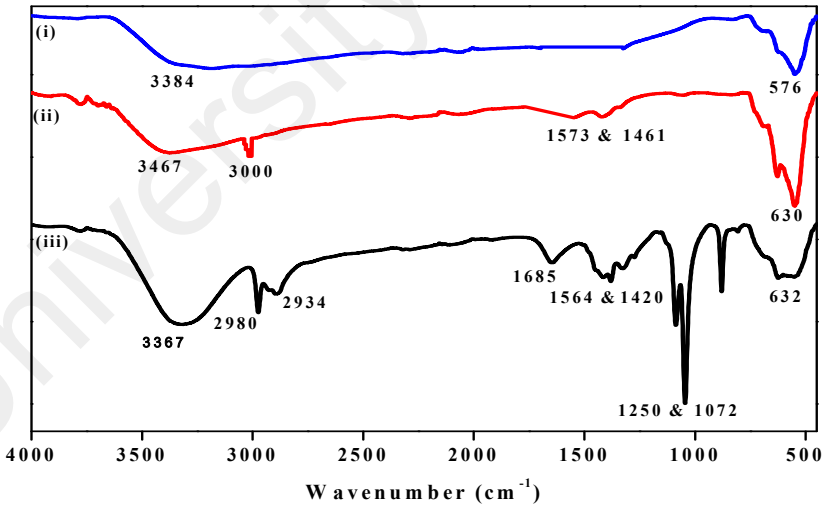

Figure 2. FTIR of: (**i**) MNP; (**ii**) MNP@PTh; (**iii**) MNP@P3TArH.

Figure 3 displayed the characteristic peaks observed for the MNPs and all nanocomposites. The peaks of the nanocomposites were slightly wider than unmodified MNP. This may be due to the presence of amorphous and polymeric materials, which coat the surfaces of the MNPs [60]. The characteristic peaks of all nanocomposites were observed at $2\theta = 30^\circ$, 35.7°, 43°, 53.4°, 57.0° and 62.6°, which are marked by their respective indices ((220), (311), (400), (422), (511) and (440)) [61]. This showed that the surface functionalization does not change the crystalline phase of MNPs [62].

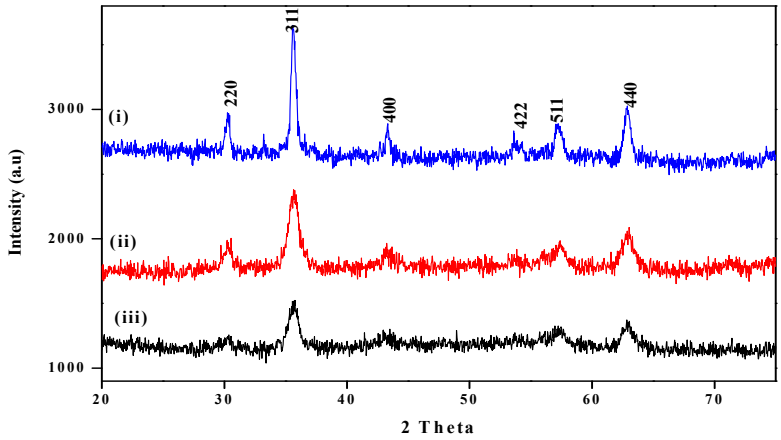

Figure 3. Diffractogram of: (**i**) MNP; (**ii**) MNP@PTh; (**iii**) MNP@P3TArH.

The BET surface area is measured using the multipoint BET method, within the relative pressure ($P/P0$) range of 0.05–1. As described in (Figure S5, Supplementary Material), the MNPs and all nanocomposites display an H3-type hysteresis loop, based on the Brunauer-Deming-Deming-Teller (BDDT) classification, demonstrating the existence of mesopores with pore diameters between 2 and 50 nm [63]. The pore size and BET surface area of MNPs and nanocomposites are tabulated in Table 1. The reduction in the pore size of nanocomposites is due to the addition of polymers on the surface. Meanwhile, escalation in the surface area could be because of the dispersity of particles that results from the enhancement of the spaces between them [64,65].

Table 1. BET pore size and surface area.

Sample	Pore size (nm)	Surface area ($m^2 \cdot g^{-1}$)
MNP	20.2	37.37
MNP@PTh	18.3	95.6
MNP@P3TArH	12.09	103.80

Morphological analysis of the synthesized products was performed using TEM techniques. As shown in Figure 4, TEM images of all materials demonstrated a sphere-shaped property. From the images, we could clearly observe the good dispersion of the functionalized nanoparticles (MNP@PTArH) in the TEM image. For instance, before polymerization, magnetic nanoparticles were highly agglomerated with each other. After polymerization of MNP with 3TArH, they showed lower agglomeration, and the nanocomposite became well dispersed. The dispersity of the nanocomposite influenced its surface area, as evidence by the BET result of MNP@P3TArH, which is higher compared to MNP@PTh and MNP, as tabulated in Table 1.

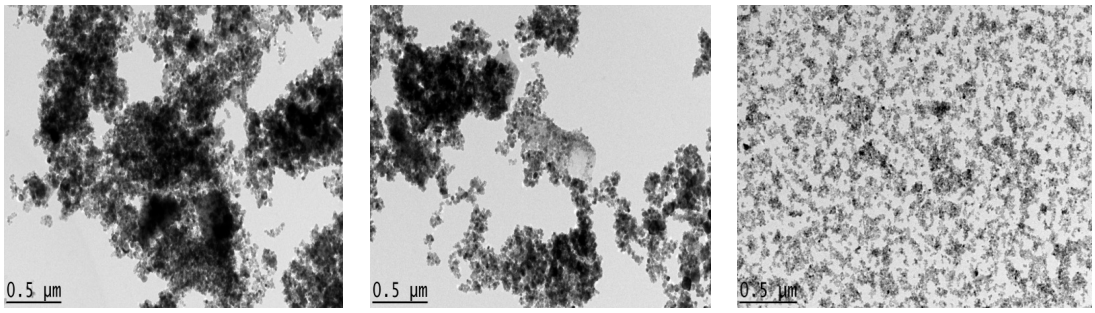

(**a**) (**b**) (**c**)

Figure 4. TEM images of: (**a**) MNP; (**b**) MNP@PTh; (**c**) MNP@PTArH.

The magnetic properties of the samples were recorded at room temperature with an external field of ±15 kOe. Important magnetic variables, such as saturation magnetization (M_S), were evaluated. The maximum saturation (M_S) of MNPs occurred at 69.2 emu·g^{-1}, respectively. After surface functionalization, the magnetization of MNP@PTh and MNP@P3TArH was reduced to 65.3 and 61.5 emu·g^{-1} respectively. The magnetization decrease signified the presence of a dead magnetic layer on the surface of the nanocomposites [58]. Although the magnetization has declined, the value is still within the acceptable range, which suggests that it can be applied as the MSPE sorbent [66].

3.2. Solid Phase Extraction Optimization and Reusability Studies

3.2.1. Type of Adsorbent

Hypothetically, the adsorption of phthalates is based on the hydrophobicity and π–π dispersion [67]. To prove that the structure architecture influences the adsorption studies of phthalates, three different types of sorbents, which are naked magnetic nanoparticles (MNP), MNP-PTh and MNP@P3TArH, were tested. As seen in Figure 5, MNP resulted in an insignificant peak area for all of the analytes studied. After the introduction of polythiophene derivatives on the surface of MNP, the peak area of phthalates increased. The presence of aliphatic and aromatic groups in the MNP@P3TArH enhances the dispersion of phthalates, which enhances the π–π dispersion and hydrophobic interaction. As evidenced, butyl benzyl phthalate (BBP) is more prone to the adsorbent with more aromatic sides, as in the MNP@PT3ArH, compared to the other adsorbents. Besides, the high surface area of MNP@P3TArH also contributes to the increase of extraction performance. Since the MNP@P3TArH has demonstrated the high peak area for all analytes studied, it was selected for further MSPE optimization.

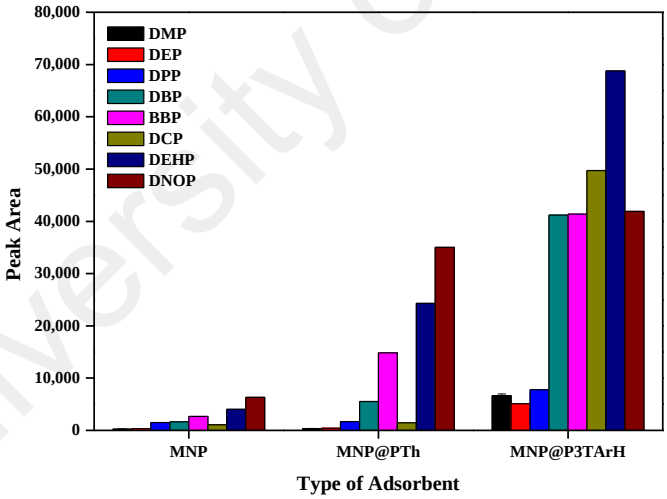

Figure 5. Comparison of MNP@P3TArH with naked MNP and MNP@PTh for the extraction of targeted phthalates.

3.2.2. Sample pH

To study the influence of the surface charge of adsorbent/adsorbate in the extraction process, experiments were performed under different pH conditions, ranging from pH 2–9. As shown from Figure 6a, the peak areas for phthalates increase when the pH rise from 2–7, but decline later from 8–9. At low pH, C=N, alkoxy in P3TArH was protonated, making the adsorbent surface positively charged. At pH < 7, phthalates hydrolyze to phthalic acid, thus making the carbonyl group nucleophilic, reacting with hydrogen ions in the aqueous solution, producing positive charges. Due to both the absorbate and adsorbent acquiring positive charges, the electrostatic repulsion occurred and retarded the adsorption performance [68]. At basic conditions, the surface adsorbent became negatively charged, while the

adsorbate hydrolyzes to phthalate anions, reducing the extraction efficiency [69]. Thus, in neutral pH, the extraction increased due to the absence of electrostatic repulsion that disturbed the extraction capability. As the optimum performance was demonstrated at pH 7, this pH was selected for all of the experiments.

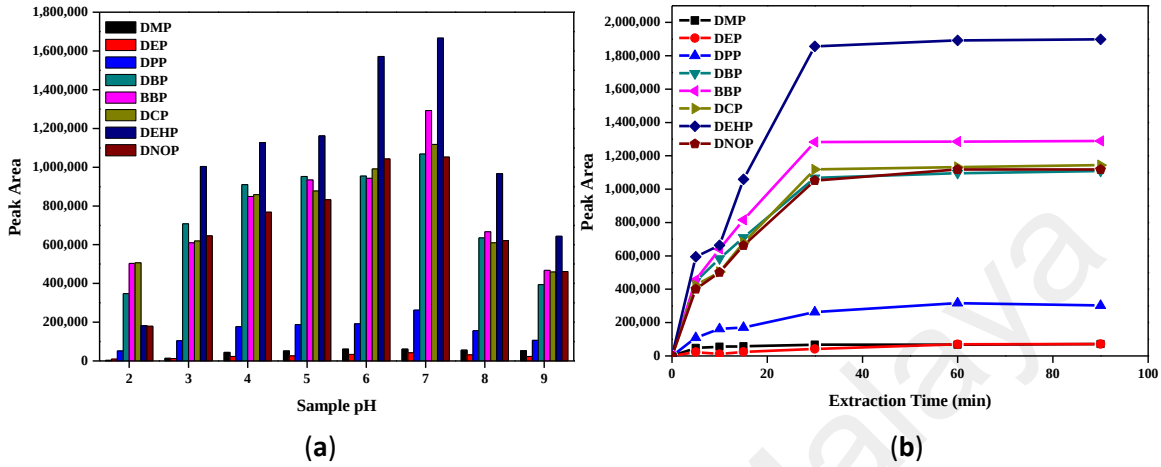

Figure 6. (**a**) Effect of sample pH; (**b**) effect of extraction time for the extraction of targeted phthalates.

3.2.3. Extraction Time

It has been understood that prolonged extraction time might increase the recovery of analytes. Thus, the influence of extraction time on the recoveries of the analyte has been investigated. As demonstrated in Figure 6b, the peak area increased rapidly for the first 20 min, since more adsorption sites were available and phthalates could easily interact with these sites. After 30 min, the peak area was almost persistent; therefore, 30 min was sufficient to extract the maximum of the target analytes. In order to ensure that the extraction time was satisfactory, further experiments were carried out until 90 min, and they were found to be constant.

3.2.4. Desorption Studies

The elution solvent is one of the crucial parameters to be considered. In order to determine the best elution solvent, the solvent must be able to elute all of the analytes that were retained from the adsorbent in a small volume [70]. Six eluting solvents with dissimilar polarities, namely hexane, toluene, diethyl ether, acetonitrile, methanol and ethyl acetate, were studied.

As evidenced in Figure 7a, polar solvents (acetonitrile, methanol and ethyl acetate) were the best solvents, with high peak areas compared to non-polar solvents (hexane, toluene and diethyl ether), since phthalates contain a polar carbonyl group [71]. Among the polar solvents, ethyl acetate showed high solvent strength, since it gave the maximum peak area for the phthalates studied and was thus selected to be the eluent.

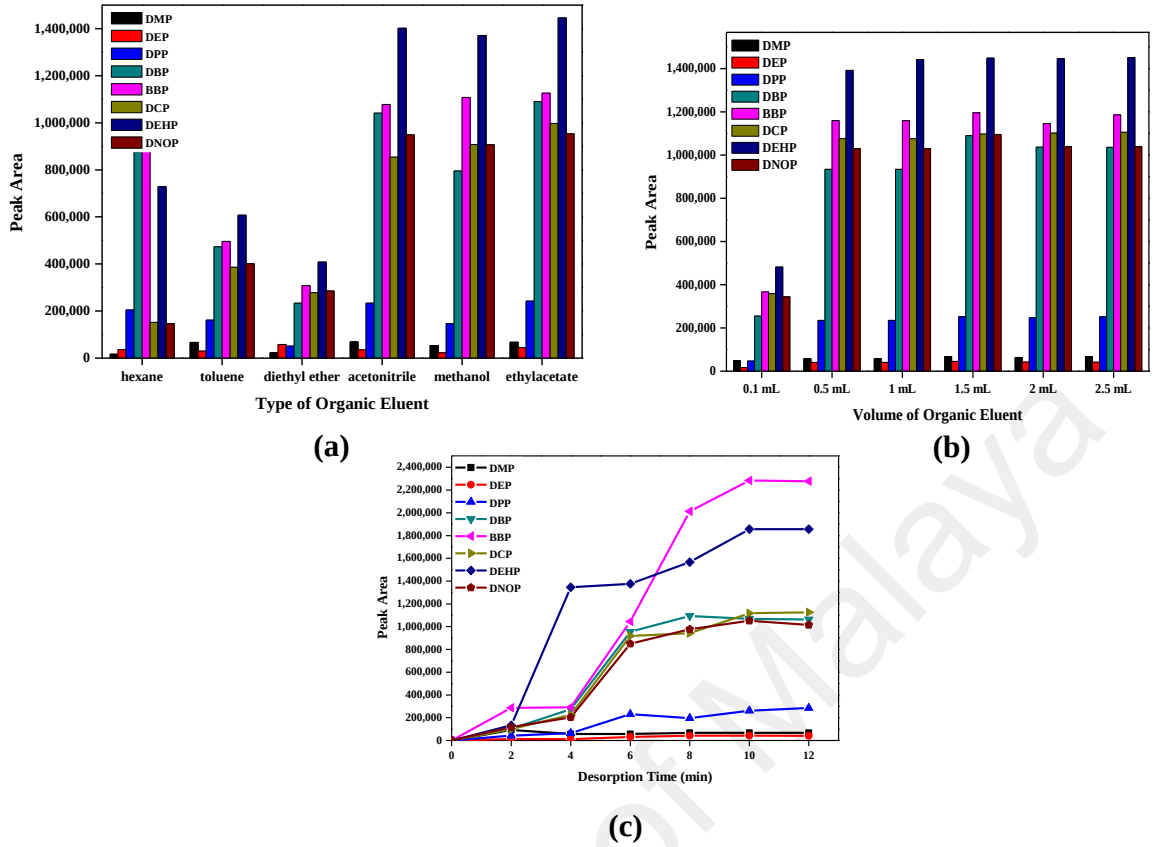

Figure 7. Desorption studies for the extraction of targeted phthalates: (**a**) effect of eluent type; (**b**) volume of organic eluent; (**c**) desorption time.

The volume of ethyl acetate was tested from 0.1 mL–2.5 mL. As observed in Figure 7b, the peak area increased from 0.1 mL and remained constant after 0.5 mL. This showed that 0.5 mL may accommodate the maximum phthalates extracted from the sorbent.

Further, desorption time was optimized to investigate the best time taken for the analytes to desorb from the sorbent ranging from 0–12 min. As revealed in Figure 7c, analytes were desorbed rapidly in the first 4 min and started to become linear after 10 min. This indicated that 10 min of time are sufficient to desorb back all of the analytes from the adsorbent. As for the case of BBP, desorption was found to be slower than other phthalates. This could be due to the presence of an additional aromatic ring in BBP, which makes it less polar to the eluent (ethyl acetate). After 6 min of desorption, most of the phthalates had reached near to equilibrium, whereas BBP was desorbed steeply after 6 min until it reached equilibrium at 10 min.

3.2.5. Mass of Adsorbent

Investigation of the adsorbent amount was executed in the range of 1–25 mg. As exposed in Figure 8a, the extraction peak area increased up to 10 mg, but decreased later with a further increase of the adsorbent. Increasing the adsorbent amount provides more active sites for the adsorption of target analytes. However, a high amount of adsorbent at a specific volume has weakened elution efficiency [30]. It is shown that this adsorbent only required a small amount of adsorbent to remove phthalates efficiently, which added the advantage of economic value. Therefore, for further experiments, the adsorbent amount of 10 mg was applied.

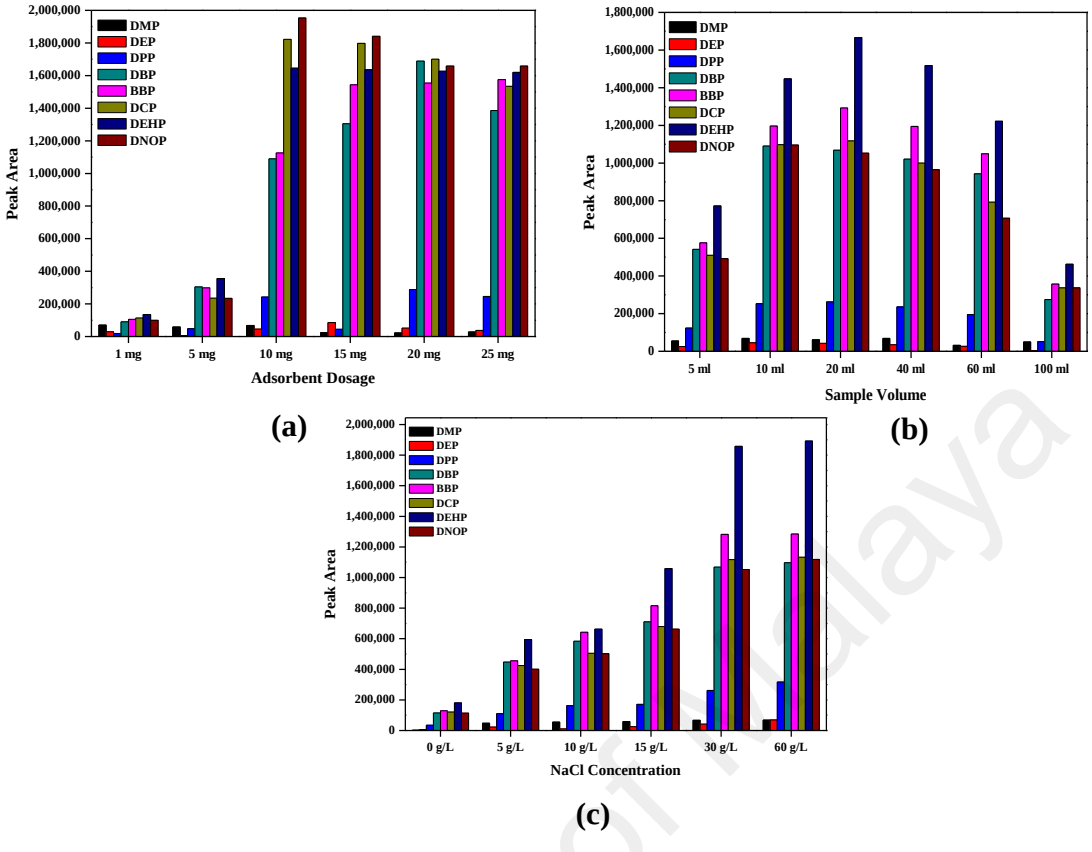

Figure 8. (**a**) Effect of adsorbent dosage; (**b**) effect of sample volume; (**c**) effect of NaCl concentration, for the extraction of targeted phthalates.

3.2.6. Sample Loading Volume

The effect of sample volume was investigated by the extraction of the phthalates ranging from 5–100 mL and shown in Figure 8b. Each sample was spiked with 10 mg· L^{-1} analytes and 10 mg adsorbent. As can be seen, peak area increased until 20 mL and further decreased till 100 mL. A 20-mL volume of sample demonstrated the most efficient extraction. An increase in sample volume could lead to a high distribution of adsorbent to the aqueous phase, which lowered the amount of adsorbent in the volume unit sample solution, and the extraction became less effective [72]. Thus, a 20-mL sample volume was chosen as the optimized sample volume.

3.2.7. Effect of NaCl

Indeed, the addition of salt in the sample matrices effects the extraction efficiency. Thus, studies on the concentration of NaCl ranging from 0–25 g· L^{-1} were conducted. As observed in Figure 8c, peak areas of the studied analytes increased from 0–15 g· L^{-1}, but decreased later from 20–25 g· L^{-1}. This can be due to the addition of salt, which increases the ionic strength and eventually decreases the solubility of the analytes in the media. However, as the concentration of salt increases, the diffusion rate of the analytes may reduce, since the solvation cage of the analytes is disturbed [51]. Since a 30 g· L^{-1} NaCl concentration gave a high peak area for all analytes studied, it was chosen for subsequent experiments.

3.2.8. Reusability Studies

To investigate the probability of reusing and regenerating the sorbent, a reusability test was designed and implemented for Fe_3O_4@P3TArH, which was recycled after being washed with methanol and water and was dried in a vacuum at 70 °C for 12 h. From Figure 9, it could be surmised that after five repeated experiments, the adsorbent was still active. This may be due to some of the particles

in the adsorbent accumulating due to the heat treatment after several cycles, which decreases the surface area.

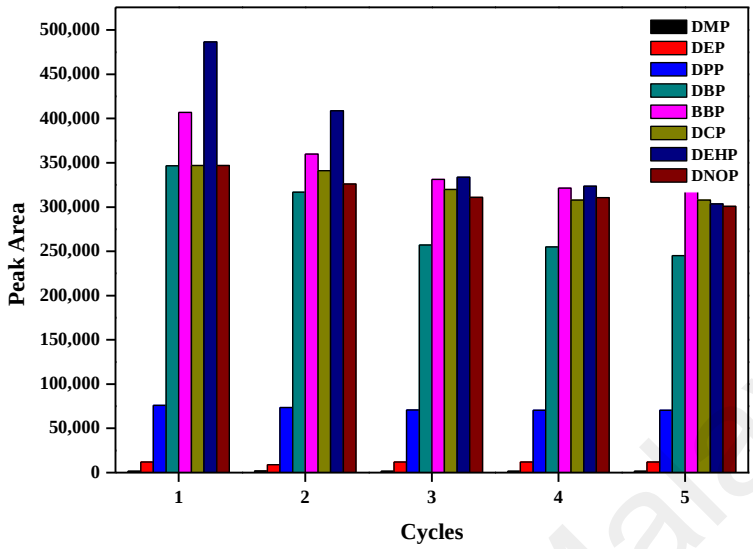

Figure 9. Reusability cycles.

3.3. Analytical Performances and Real Sample Analysis

The optimized method obtained for the extraction of phthalates using MNP@P3TARH involved the sample at pH 7, 30 min extraction time, ethyl acetate as the elution solvent, 500-µL elution solvent volumes, 10 min desorption time, 10 mg adsorbent dosage, 20-mL sample loading volume and a 15 g· L^{-1} concentration of NaCl. In order to assess the validation of the proposed method, linearity, the limit of detection, the limit of quantitation and repeatability were performed under optimum conditions. Analytical performance figures of merits are tabulated in Table 2.

Table 2. MNP@P3TArH (magnetic-solid phase extraction (MSPE)) analytical figures of merit.

Analytes	R^2	Linear range (µg· L^{-1})	LOD (µg· L^{-1})	LOQ (µg· L^{-1})	RSD (%) Interday n = 3	RSD (%) Intraday n = 7
DMP	0.992	0.5–50	0.462	1.539	3.4	4.8
DEP	0.992	0.5–50	0.468	1.562	5.0	4.3
DPP	0.997	0.5–50	0.286	0.954	4.6	3.7
DBP	0.998	0.1–50	0.063	0.213	4.5	4.5
BBP	0.996	0.1–50	0.080	0.268	4.8	4.3
DCP	0.993	0.5–50	0.332	1.106	4.7	4.0
DEHP	0.997	0.1–50	0.054	0.182	3.0	4.0
DNOP	0.997	0.1–50	0.073	0.244	3.6	4.9

Calibration curves obtained for the studied phthalates were linear over the range of 0.1–50 µg· L^{-1} with R^2 more than 0.99. As per the U.S. EPA standard, the screening of phthalates in drinking water must be done at a concentration above 0.6 µg· L^{-1} [4]. However, the LOD of our method lies within the range of 0.080–0.468, indicating the suitability of this method as an efficient phthalate detector.

Repeatability studies were conducted for inter-day (three consecutives replicates for three days) and intra-day (seven consecutives replicates on the same day). The results were expressed as relative standard deviations (RSD%). This method demonstrated good precision, since the RSD (%) values were in the range of 3%–5% [73]. Comparative studies on the analytical performance between the proposed methods with other developed methods are shown in Table 3. Obviously, the extraction of phthalates using MNP@P3TArH provides sensitivity and repeatability.

Table 3. Comparatives study of the proposed method with other MSPE adsorbents for the extraction of phthalates.

Analyte	Method	LOD ($\mu g \cdot L^{-1}$)	LDR ($\mu g \cdot L^{-1}$)	RSD (%)	Reference
DBP, DEHP, DOA	MNP@PTh-GC-FID	0.2–0.4	0.4–100	4–12.3	[72]
DPP, DBP, DCP, DNOP	MNP@Chitosan-C18-HPLC-UV	0.012–0.037	0.001–0.01	2.1–6.8	[73]
DBP, DEHP	MNP@Zeolite-GC-FID	2.80–3.2	10–1200	10%–13%	[74]
DMP, DEP, DBP, BBP, DNOP	MNP@ZIF-8-HPLC	0.08–0.24	1–100	<5.5	[75]
DMP, DPP, DEP, DBP, BBP, DCP, DEHP, DNOP	MNP@P3TArH- GC-FID	0.05–0.09	0.1–50	3.0–5.0	This study

To endorse the reliability of the method using MNP@P3TArH, it was applied to determine phthalates in the water from the mineral water bottle stored at room temperature and commercial fresh milk. Figure 10 shows the chromatogram of commercial fresh milk unspiked and spiked with phthalates. None of the targeted phthalates were found in the water samples under the optimized condition described. To evaluate the matrix effect, all of the samples were spiked with 50 $\mu g \cdot L^{-1}$ of the phthalates studied. Recoveries and RSD (%) for all of the water samples were determined and are shown in Table 4. From the optimization procedures until the real sample analyses, DMP, DEP and DPP demonstrated lower recoveries; this may be due to the lower molecular weight of phthalates being more prone to aqueous solution than to the adsorbent [76]. From the chromatogram of mineral bottle stored at room temperature as shown in (Figure S6, Supplementary Material), the recoveries obtained for water in the mineral bottle demonstrated higher values compared to the recovery for the milk sample. This might be caused by the matrix effect that holds the analyte in the milk sample to be higher compared to the water sample. RSD (%) values were found to be in the range of 1.3%–5.8%, which indicated a precise method.

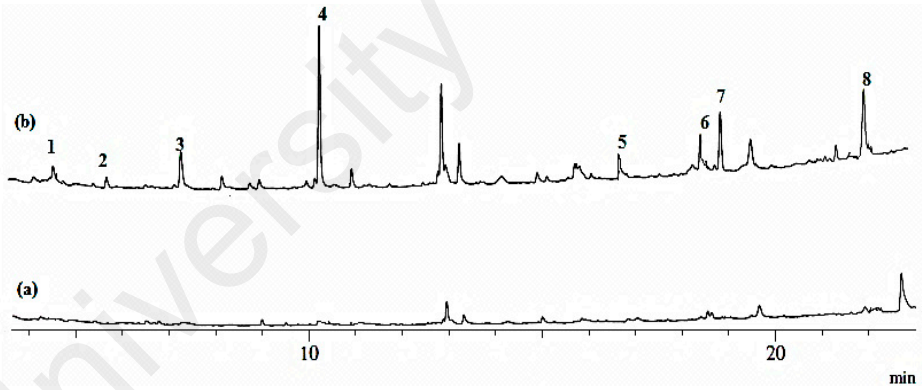

Figure 10. Chromatogram of commercial fresh milk: (**a**) unspiked; (**b**) spiked phthalates (50 $\mu g \cdot L^{-1}$). Peaks: (1) DMP; (2) DEP; (3) DPP; (4) DBP; (5) BBP; (6) DCP; (7) DEHP; (8) DNOP.

Table 4. Analysis of analytes in the real samples.

Analyte	MNP@P3TArH MSPE (±RSD%, n = 3)	
	Mineral water	Commercial fresh milk
DMP	85(5.8)	68(5.0)
DEP	85 (4.9)	67(3.0)
DPP	88(1.3)	72(7.7)
DBP	95(2.4)	85(3.3)
BBP	93(3.0)	82(3.8)
DCP	90(4.7)	77(5.8)
DEHP	99(1.3)	89(4.5)
DNOP	101(4.2)	91(3.3)

4. Conclusions

MNP@P3TArH has been successfully synthesized, characterized and utilized as a sorbent for the analysis of GC-FID in the determination of selected phthalates. The optimized conditions of MSPE were carefully selected as follows: sample at pH 7, 30 min extraction time, ethyl acetate as the elution solvent, 500-μL elution solvent volume, 10 min desorption time, 10 mg adsorbent dosage, 20-mL sample loading volume and a 15 g· L^{-1} concentration of NaCl. The steadiness and reusability studies suggested that the MNP@P3TArH could be used up to five cycles without significantly impacting its extraction capacity. The adsorbent covers a wide range of phthalates with a dynamic linear range of 0.1–50 μg· L^{-1} and a limit of detection at 0.08–0.468 μg· L^{-1}. The presence of new interfaces (π–π and hydrophobic interactions) among the sorbent and target analytes increased the adsorption capability. The application of MNP@P3TArH as the MSPE sorbent was successfully executed by the analysis of phthalate esters in the mineral water and commercial fresh milk.

Supplementary Materials: Supplementary Materials can be found at www.mdpi.com/2073-4360/8/5/117/s1.

Acknowledgments: We acknowledge the financial support granted by the Institute of Research Management and Monitoring (PG044-2012B), University of Malaya, and the Ministry of Higher Education for the High Impact Research grant (HIR/MOHE/SC/F0031). We also acknowledge the financial support of the Universiti of Teknologi MARA and the Ministry of Higher Education Malaysia (MOHE) for funding the PhD studies of Siti Nor Atika Baharin.

Author Contributions: All authors designed and contributed to this study. Siti Nor Atika Baharin executed the experiment and composed this paper. Norazilawati Muhamad Sarih edited the paper and gave final approval of the version to be submitted. Sharifah Mohamad contributed the analytical evaluation and tools. All authors participated in the discussion and commented on the paper.

Conflicts of Interest: The authors declare no conflict of interest.

References

1. Franck, H.-G.; Stadelhofer, J. Production and uses of xylene derivatives. In *Industrial Aromatic Chemistry*; Springer: Berlin, Germany/Heidelberg, Germany, 1988; pp. 265–290.
2. Jones-Lepp, T.; Gerlach, C.L.; Cooter, E.J. The power of analytical methods for measuring suspected endocrine disrupting compounds: A pilot field study. *TrAC Trends Anal. Chem.* **2000**, *19*, 286–291. [CrossRef]
3. Wypych, G. Effect of plasticizers on properties of plasticized materials. In *Handbook of Plasticizers*; Ontario, ChemTec Publishing: Toronto, ON, Canada, 2004; pp. 193–272.
4. Serôdio, P.; Nogueira, J. Considerations on ultra-trace analysis of phthalates in drinking water. *Water Res.* **2006**, *40*, 2572–2582. [CrossRef] [PubMed]
5. Yuan, B.-L.; Li, X.-Z.; Graham, N. Aqueous oxidation of dimethyl phthalate in a Fe(VI)-TiO_2-UV reaction system. *Water Res.* **2008**, *42*, 1413–1420. [CrossRef] [PubMed]
6. Sathyanarayana, S.; Karr, C.J.; Lozano, P.; Brown, E.; Calafat, A.M.; Liu, F.; Swan, S.H. Baby care products: Possible sources of infant phthalate exposure. *Pediatrics* **2008**, *121*, e260–e268. [CrossRef] [PubMed]
7. PnTER, P. *Hydrochemie [hydrochemistry]*, 4th ed.; Vydavatelstvi VSCHT: Prague, The Czech Republic, 2009.
8. Ohtani, H.; Miura, I.; Ichikawa, Y. Effects of dibutyl phthalate as an environmental endocrine disruptor on gonadal sex differentiation of genetic males of the frog rana rugosa. *Environ. Health Perspect.* **2000**, *108*, 1189–1193. [CrossRef] [PubMed]
9. Latini, G.; Verrotti, A.; de Felice, C. Di-2-ethylhexyl phthalate and endocrine disruption: A review. *Curr. Drug Targets Immune Endocr. Metab. Disord.* **2004**, *4*, 37–40. [CrossRef]
10. Foster, P. Disruption of reproductive development in male rat offspring following in utero exposure to phthalate esters. *Int. J. Androl.* **2006**, *29*, 140–147. [CrossRef] [PubMed]
11. Swan, S.H.; Main, K.M.; Liu, F.; Stewart, S.L.; Kruse, R.L.; Calafat, A.M.; Mao, C.S.; Redmon, J.B.; Ternand, C.L.; Sullivan, S. Decrease in anogenital distance among male infants with prenatal phthalate exposure. *Environ. Health Perspect.* **2005**, *113*, 1056–1061. [CrossRef] [PubMed]
12. Gomez-Hens, A.; Aguilar-Caballos, M. Social and economic interest in the control of phthalic acid esters. *TrAC Trends Anal. Chem.* **2003**, *22*, 847–857. [CrossRef]

13. Laws of Malaysia, Food Act 1983, Food Regulations 1985. Available online: http://www.asianfoodreg.com/dynamicAssets/regulationDoc/1412157254_Malaysian-Food-Regulations-19852014.pdf (accessed on 10 March 2016).
14. Ministry of Science, Technology and Innovation (MOSTI). *Plastic Materials and Articles Intended to Come into Contact with Food (First Revision)*; Ministry of Science, Technology and Innovation (MOSTI): Cyberjaya, Malaysia, 2014.
15. Amiridou, D.; Voutsa, D. Alkylphenols and phthalates in bottled waters. *J. Hazard. Mater.* **2011**, *185*, 281–286. [CrossRef] [PubMed]
16. Schmid, P.; Kohler, M.; Meierhofer, R.; Luzi, S.; Wegelin, M. Does the reuse of pet bottles during solar water disinfection pose a health risk due to the migration of plasticisers and other chemicals into the water? *Water Res.* **2008**, *42*, 5054–5060. [CrossRef] [PubMed]
17. Wu, M.-T.; Wu, C.-F.; Wu, J.-R.; Chen, B.-H.; Chen, E.K.; Chao, M.-C.; Liu, C.-K.; Ho, C.-K. The public health threat of phthalate-tainted foodstuffs in taiwan: The policies the government implemented and the lessons we learned. *Environ. Int.* **2012**, *44*, 75–79. [CrossRef] [PubMed]
18. Bach, C.; Dauchy, X.; Chagnon, M.-C.; Etienne, S. Chemical compounds and toxicological assessments of drinking water stored in polyethylene terephthalate (pet) bottles: A source of controversy reviewed. *Water Res.* **2012**, *46*, 571–583. [CrossRef] [PubMed]
19. Leivadara, S.V.; Nikolaou, A.D.; Lekkas, T.D. Determination of organic compounds in bottled waters. *Food Chem.* **2008**, *108*, 277–286. [CrossRef]
20. Liu, H.-C.; Den, W.; Chan, S.-F.; Kin, K.T. Analysis of trace contamination of phthalate esters in ultrapure water using a modified solid-phase extraction procedure and automated thermal desorption–gas chromatography/mass spectrometry. *J. Chromatogr. A* **2008**, *1188*, 286–294. [CrossRef] [PubMed]
21. Plotan, M.; Frizzell, C.; Robinson, V.; Elliott, C.T.; Connolly, L. Endocrine disruptor activity in bottled mineral and flavoured water. *Food Chem.* **2013**, *136*, 1590–1596. [CrossRef] [PubMed]
22. Wagner, M.; Oehlmann, J. Endocrine disruptors in bottled mineral water: Total estrogenic burden and migration from plastic bottles. *Environ. Sci. Pollut. Res.* **2009**, *16*, 278–286. [CrossRef] [PubMed]
23. Chen, C.-Y.; Chung, Y.-C. Removal of phthalate esters from aqueous solutions by chitosan bead. *J. Environ. Sci. Health Part. A* **2006**, *41*, 235–248. [CrossRef] [PubMed]
24. Julinová, M.; Slavík, R. Removal of phthalates from aqueous solution by different adsorbents: A short review. *J. Environ. Manag.* **2012**, *94*, 13–24. [CrossRef] [PubMed]
25. Yuan, S.; Liu, C.; Liao, C.; Chang, B. Occurrence and microbial degradation of phthalate esters in taiwan river sediments. *Chemosphere* **2002**, *49*, 1295–1299. [CrossRef]
26. López-Jiménez, F.J.; Rubio, S.; Pérez-Bendito, D. Determination of phthalate esters in sewage by hemimicelles-based solid-phase extraction and liquid chromatography–mass spectrometry. *Anal. Chim. Acta* **2005**, *551*, 142–149. [CrossRef]
27. Farahani, H.; Ganjali, M.R.; Dinarvand, R.; Norouzi, P. Screening method for phthalate esters in water using liquid-phase microextraction based on the solidification of a floating organic microdrop combined with gas chromatography–mass spectrometry. *Talanta* **2008**, *76*, 718–723. [CrossRef] [PubMed]
28. Ling, W.; Jiang, G.-B.; Cai, Y.-Q.; Bin, H.; Wang, Y.-W.; Shen, D.-Z. Cloud point extraction coupled with HPLC-UV for the determination of phthalate esters in environmental water samples. *J. Environ. Sci.* **2007**, *19*, 874–878.
29. Kerienė, I.; Maruška, A.; Sitonytė, J. Solid phase extraction and gas chromatographic-mass spectrometric analysis of phthalates in surface water: Method development and validation. *Chemija* **2011**, *22*, 204–209.
30. Tahmasebi, E.; Yamini, Y. Polythiophene-coated Fe_3O_4 nanoparticles as a selective adsorbent for magnetic solid-phase extraction of silver (I), gold (III), copper (II) and palladium (II). *Microchim. Acta* **2014**, *181*, 543–551. [CrossRef]
31. Kvistad, A.; Lundanes, E.; Greibrokk, T. Determination of alkylphenols in water samples by solid-phase extraction on to poly(styrene-divinylbenzene) and quantification by liquid chromatography with UV-detection. *Chromatographia* **1998**, *48*, 707–713. [CrossRef]
32. Holadova, K.; Hajšlová, J. A comparison of different ways of sample preparation for the determination of phthalic acid esters in water and plant matrices. *Int. J. Environ. Anal. Chem.* **1995**, *59*, 43–57. [CrossRef]
33. Chen, C.-Y.; Chen, C.-C.; Chung, Y.-C. Removal of phthalate esters by α-cyclodextrin-linked chitosan bead. *Bioresour. Technol.* **2007**, *98*, 2578–2583. [CrossRef] [PubMed]

34. Khan, N.A.; Jung, B.K.; Hasan, Z.; Jhung, S.H. Adsorption and removal of phthalic acid and diethyl phthalate from water with zeolitic imidazolate and metal–organic frameworks. *J. Hazard. Mater.* **2015**, *282*, 194–200. [CrossRef] [PubMed]
35. Raoov, M.; Mohamad, S.; bin Abas, M.R.; Surikumaran, H. New macroporous β-cyclodextrin functionalized ionic liquid polymer as an adsorbent for solid phase extraction with phenols. *Talanta* **2014**, *130*, 155–163. [CrossRef] [PubMed]
36. Li, Z.; Wei, L.; Gao, M.; Lei, H. One-pot reaction to synthesize biocompatible magnetite nanoparticles. *Adv. Mater.* **2005**, *17*, 1001–1005. [CrossRef]
37. Lin, P.-C.; Yu, C.-C.; Wu, H.-T.; Lu, Y.-W.; Han, C.-L.; Su, A.-K.; Chen, Y.-J.; Lin, C.-C. A chemically functionalized magnetic nanoplatform for rapid and specific biomolecular recognition and separation. *Biomacromolecules* **2012**, *14*, 160–168. [CrossRef] [PubMed]
38. Farrukh, A.; Akram, A.; Ghaffar, A.; Hanif, S.; Hamid, A.; Duran, H.; Yameen, B. Design of polymer-brush-grafted magnetic nanoparticles for highly efficient water remediation. *ACS Appl. Mater. Interf.* **2013**, *5*, 3784–3793. [CrossRef] [PubMed]
39. Shahabuddin, S.; Muhamad Sarih, N.; Mohamad, S.; Joon Ching, J. $SrTiO_3$ nanocube-doped polyaniline nanocomposites with enhanced photocatalytic degradation of methylene blue under visible light. *Polymers* **2016**, *8*, 27. [CrossRef]
40. Shahabuddin, S.; Sarih, N.M.; Ismail, F.H.; Shahid, M.M.; Huang, N.M. Synthesis of chitosan grafted-polyaniline/Co_3O_4 nanocube nanocomposites and their photocatalytic activity toward methylene blue dye degradation. *RSC Adv.* **2015**, *5*, 83857–83867. [CrossRef]
41. Xie, L.; Jiang, R.; Zhu, F.; Liu, H.; Ouyang, G. Application of functionalized magnetic nanoparticles in sample preparation. *Anal. Bioanal. Chem.* **2014**, *406*, 377–399. [CrossRef] [PubMed]
42. Li, Q.; Lam, M.H.; Wu, R.S.; Jiang, B. Rapid magnetic-mediated solid-phase extraction and pre-concentration of selected endocrine disrupting chemicals in natural waters by poly (divinylbenzene- *co*-methacrylic acid) coated Fe_3O_4 core–shell magnetite microspheres for their liquid chromatography–tandem mass spectrometry determination. *J. Chromatogr. A* **2010**, *1217*, 1219–1226. [PubMed]
43. Ibarra, I.S.; Miranda, J.M.; Rodriguez, J.A.; Nebot, C.; Cepeda, A. Magnetic solid phase extraction followed by high-performance liquid chromatography for the determination of sulphonamides in milk samples. *Food Chem.* **2014**, *157*, 511–517. [CrossRef] [PubMed]
44. Fayazi, M.; Taher, M.A.; Afzali, D.; Mostafavi, A. Fe_3O_4 and MnO_2 assembled on halloysite nanotubes: A highly efficient solid-phase extractant for electrochemical detection of mercury(II) ions. *Sens. Actuators B Chem.* **2016**, *228*, 1–9. [CrossRef]
45. Aguilar-Arteaga, K.; Rodriguez, J.; Miranda, J.; Medina, J.; Barrado, E. Determination of non-steroidal anti-inflammatory drugs in wastewaters by magnetic matrix solid phase dispersion–HPLC. *Talanta* **2010**, *80*, 1152–1157. [CrossRef] [PubMed]
46. Mehdinia, A.; Rouhani, S.; Mozaffari, S. Microwave-assisted synthesis of reduced graphene oxide decorated with magnetite and gold nanoparticles, and its application to solid-phase extraction of organochlorine pesticides. *Microchim. Acta* **2016**. [CrossRef]
47. Sun, L.; Sun, X.; Du, X.; Yue, Y.; Chen, L.; Xu, H.; Zeng, Q.; Wang, H.; Ding, L. Determination of sulfonamides in soil samples based on alumina-coated magnetite nanoparticles as adsorbents. *Anal. Chim. Acta* **2010**, *665*, 185–192. [CrossRef] [PubMed]
48. Zhai, Y.; He, Q.; Yang, X.; Han, Q. Solid phase extraction and preconcentration of trace mercury (ii) from aqueous solution using magnetic nanoparticles doped with 1,5-diphenylcarbazide. *Microchim. Acta* **2010**, *169*, 353–360. [CrossRef]
49. Faraji, M.; Yamini, Y.; Rezaee, M. Extraction of trace amounts of mercury with sodium dodecyle sulphate-coated magnetite nanoparticles and its determination by flow injection inductively coupled plasma-optical emission spectrometry. *Talanta* **2010**, *81*, 831–836. [CrossRef] [PubMed]
50. Ballesteros-Gómez, A.; Rubio, S. Hemimicelles of alkyl carboxylates chemisorbed onto magnetic nanoparticles: Study and application to the extraction of carcinogenic polycyclic aromatic hydrocarbons in environmental water samples. *Anal. Chem.* **2009**, *81*, 9012–9020. [CrossRef] [PubMed]
51. Tahmasebi, E.; Yamini, Y.; Mehdinia, A.; Rouhi, F. Polyaniline—Coated Fe_3O_4 nanoparticles: An anion exchange magnetic sorbent for solid—Phase extraction. *J. Sep. Sci.* **2012**, *35*, 2256–2265. [CrossRef] [PubMed]

52. Gao, Q.; Luo, D.; Bai, M.; Chen, Z.-W.; Feng, Y.-Q. Rapid determination of estrogens in milk samples based on magnetite nanoparticles/polypyrrole magnetic solid-phase extraction coupled with liquid chromatography–tandem mass spectrometry. *J. Agric. Food Chem.* **2011**, *59*, 8543–8549. [CrossRef] [PubMed]
53. Zhao, Q.; Lu, Q.; Feng, Y.-Q. Dispersive microextraction based on magnetic polypyrrole nanowires for the fast determination of pesticide residues in beverage and environmental water samples.*Anal. Bioanal. Chem.* **2013**, *405*, 4765–4776. [CrossRef] [PubMed]
54. Shin, S.; Jang, J. Thiol containing polymer encapsulated magnetic nanoparticles as reusable and efficiently separable adsorbent for heavy metal ions. *Chem. Commun.* **2007**. [CrossRef]
55. Williamson, A.W. XXII.—On etherification. *Q. J. Chem. Soc. Lond.* **1852**, *4*, 229–239. [CrossRef]
56. Chen, W.; Chen, Y.; Li, F.; Chen, L.; Yuan, K.; Yao, K.; Wang, P. Ordered microstructure induced by orientation behavior of liquid-crystal polythiophene for performance improvement of hybrid solar cells. *Sol. Energy Mater. Sol. Cells* **2012**, *96*, 266–275. [CrossRef]
57. Shen, L.; Laibinis, P.E.; Hatton, T.A. Bilayer surfactant stabilized magnetic fluids: Synthesis and interactions at interfaces. *Langmuir* **1999**, *15*, 447–453. [CrossRef]
58. Aydın, M.; Durmus, Z.; Kavas, H.; Esat, B.; Sözeri, H.; Baykal, A.; Yılmaz, F.; Toprak, M.S. Synthesis and characterization of poly(3-thiophene acetic acid)/Fe_3O_4 nanocomposite. *Polyhedron* **2011**, *30*, 1120–1126. [CrossRef]
59. Vasanthi, B.J.; Ravikumar, L. Synthesis and characterization of poly(azomethine ester) s with a pendent dimethoxy benzylidene group. *Open J. Polym. Chem.* **2013**, *3*, 70–77. [CrossRef]
60. Cótica, L.F.; Santos, I.A.; Girotto, E.M.; Ferri, E.V.; Coelho, A.A. Surface spin disorder effects in magnetite and poly(thiophene)-coated magnetite nanoparticles. *J. Appl. Phys.* **2010**, *108*, 064325. [CrossRef]
61. Giri, S.; Trewyn, B.G.; Stellmaker, M.P.; Lin, V.S.Y. Stimuli—Responsive controlled—Release delivery system based on mesoporous silica nanorods capped with magnetic nanoparticles. *Angew. Chem. Int. Ed.* **2005**, *44*, 5038–5044. [CrossRef] [PubMed]
62. Jayabharathi, J.; Ramanathan, P.; Thanikachalam, V.; Karunakaran, C. Optical and theoretical studies on Fe_3O_4–imidazole nanocomposite and clusters. *New J. Chem.* **2015**, *39*, 3801–3812. [CrossRef]
63. Sing, K.S.W. Reporting physisorption data for gas/solid systems with special reference to the determination of surface area and porosity (recommendations 1984). *Pure Appl. Chem.* **1985**, *57*, 603–619. [CrossRef]
64. Wang, Q.; Chen, Y.F.; Yang, M.; Wu, X.F.; Tian, Y.J. Key engineering materials. In *Synthesis of Low Agglomerating Spherical α-Fe_2O_3 Nanopowders*; Trans Tech Publisher: Pfaffikon, Switzerland, 2008; pp. 1568–1569.
65. Darab, J.G.; Linehan, J.C.; Matson, D.W. Effect of agglomerate size on the catalytic activity of an iron oxyhydroxide nanocrystalline powder toward carbon–carbon bond scission in naphthylbibenzylmethane. *Energy Fuels* **1994**, *8*, 1004–1005. [CrossRef]
66. Ma, Z.; Guan, Y.; Liu, H. Synthesis and characterization of micron—Sized monodisperse superparamagnetic polymer particles with amino groups. *J. Polym. Sci. Part A* **2005**, *43*, 3433–3439. [CrossRef]
67. Moreno-Castilla, C. Adsorption of organic molecules from aqueous solutions on carbon materials. *Carbon* **2004**, *42*, 83–94. [CrossRef]
68. Mohan, S.V.; Rao, N.C.; Prasad, K.K.; Karthikeyan, J. Treatment of simulated reactive yellow 22 (Azo) dye effluents using spirogyra species. *Waste Manag.* **2002**, *22*, 575–582. [CrossRef]
69. Fang, Z.; Huang, H. Adsorption of di-*n*-butyl phthalate onto nutshell-based activated carbon. Equilibrium, kinetics and thermodynamics. *Adsorpt. Sci. Technol.* **2009**, *27*, 685–700. [CrossRef]
70. Miskam, M.; Bakar, N.K.A.; Mohamad, S. Determination of polar aromatic amines using newly synthesized sol–gel titanium(IV) butoxide cyanopropyltriethoxysilane as solid phase extraction sorbent. *Talanta* **2014**, *120*, 450–455. [CrossRef] [PubMed]
71. Wade, L.G. *Organic Chemistry*; Prentice Hall: Upper Saddle River, NJ, USA, 2016.
72. Tahmasebi, E.; Yamini, Y.; Moradi, M.; Esrafili, A. Polythiophene-coated Fe_3O_4 superparamagnetic nanocomposite: Synthesis and application as a new sorbent for solid-phase extraction. *Anal. Chim. Acta* **2013**, *770*, 68–74. [CrossRef] [PubMed]
73. Le Zhang, X.; Niu, H.Y.; Zhang, S.X.; Cai, Y.Q. Preparation of a chitosan-coated C18-functionalized magnetite nanoparticle sorbent for extraction of phthalate ester compounds from environmental water samples. *Anal. Bioanal. Chem.* **2010**, *397*, 791–798. [CrossRef] [PubMed]

74. Mollahosseini, A.; Toghroli, M.; Kamankesh, M. Zeolite/Fe_3O_4 as a new sorbent in magnetic solid—Phase extraction followed by gas chromatography for determining phthalates in aqueous samples. *J. Sep. Sci.* **2015**, *38*, 3750–3757. [CrossRef] [PubMed]
75. Liu, X.; Sun, Z.; Chen, G.; Zhang, W.; Cai, Y.; Kong, R.; Wang, X.; Suo, Y.; You, J. Determination of phthalate esters in environmental water by magnetic zeolitic imidazolate framework-8 solid-phase extraction coupled with high-performance liquid chromatography. *J. Chromatogr. A* **2015**, *1409*, 46–52. [CrossRef] [PubMed]
76. Staples, C. *Phthalate Esters*; Springer Science and Business Media: Berlin, Germany, 2003.